Universidad Autónoma de Madrid

Departamento de Bioquímica

Regulatory role of calmodulin on systems relevant in tumor cells signaling

Silviya Raykova Stateva

Madrid, 2015

Departamento de Bioquímica

Facultad de Medicina

Universidad Autónoma de Madrid

Regulatory role of calmodulin on systems relevant in tumor cells signaling

Memoria de Tesis Doctoral presentada por:

Silviya Raykova Stateva

Licenciada y Máster en Biología Celular, para obtar al grado de Doctor

por la Universidad Autónoma de Madrid

Director de Tesis

Dr. Antonio Villalobo

Profesor de Investigación del CSIC

Profesor Honorario de la UAM

INSTITUTO DE INVESTIGACIONES BIOMÉDICAS “ALBERTO SOLS”

CONSEJO SUPERIOR DE INVESTIGACIONES CIENTÍFICAS

UNIVERSIDAD AUTÓNOMA DE MADRID

Antonio Villalobo, Profesor de Investigación del Consejo Superior de Investigaciones Científicas y Profesor Honorario de la Universidad Autónoma de Madrid, certifica que:

Silviya Raykova Stateva, Licenciada y Máster en Biología Celular por la Universidad "St. Kliment Ohridski" Sofia, Bulgaria, ha realizado bajo mi dirección el trabajo de investigación titulado: **"Regulatory role of calmodulin on systems relevant in tumor cells signaling"** en el Instituto de Investigaciones Biomédicas "Alberto Sols".

Considero que el mencionado trabajo es apto para poder optar al grado de Doctor por la Universidad Autónoma de Madrid.

Y para que así conste a todos los efectos, firmo el presente certificado en Madrid, a 2 de Junio de 2015.

Fdo.: Antonio Villalobo

Director de la Tesis

Profesor de Investigación, CSIC

Profesor Honorario, UAM

Vº Bº Tutor: Jaime Renart

Investigador Científico, CSIC

This work was done in the Department of Cancer Biology in the Institute of Biomedical Research “Alberto Sols” (CSIC, UAM), with the support of an European Commission Marie Curie ITN fellowship.

На майка ми!

To my mother!

“It's deeds we need, not words.”

Vasil Levski

ACKNOWLEDGMENTS

First, I would like to express my appreciation for my supervisor, Prof Antonio Villalobo, that he accepted me in his lab and gave me this great opportunity. His patience, endless optimism, and understanding have helped me and allowed me to learn many new things in science. He was always willing to take time to discuss any science, as well as any concerns I had during this time and this is deeply appreciated from my part.

I would like to thank to my academic tutor Jaime Renart for his constructive advices toward my work and his time spent in evaluating my results and progress for the Marie Curie reports. I would like also to thank to Prof. Martin Berchtold who helped me with the CaM part. Because of him I realized working with CaM is not that old-fashioned and I am really grateful that I had the chance to meet such a brilliant scientist.

I would also like to express my appreciation to our group members: Irene, Amparo, Karim, Ikram, Paola, Itziar, Ana, Alicia, Estefanía, Alejandro, Laura, Juan, David, Noemí, Olga, and Daniel. All of my research could not have been possible without each one of them and especially Itziar, Karim, Ikram, Pao, Alicia and Estefania, thank you for the good moments we have had. I do need to mention also all the IIBM “Alberto Sols” staff from the radioprotection, cell culture, media preparation, sterilization, imaging service, genomics unit, technical support unit, microscopy unit, IT service, and the purchasing department, to all the people at the administrative unit, and the women who clean the labs, the culturing: thank you for your help and your willingness to understand my broken Spanish.

Secondly I need to thank and express my heartfull appreciation to the Marie Curie foundation for supporting me throughout these three years and giving me the chance to be part of the DYNANO ITN group as early stage researcher. The network exposed us to a variety of disciplines from lectures/practice in companies such as Solvay and Attana, thought us management skills, writing skills, presentation skill and etc. I do need to mention the great variety of lecturers we have had from Björn O. Nilsson form the Royal Swedish Academy of Engineering Sciences to the Nobel Prize winner Prof. Jean-Marie Lehn. I would like also to thank to all of the DYNANO Group, the students: Romina, Alina, Madalina, Marta, Marion, Helene, Susanne, Calin, Ioanna, Andrea, Eva, Valentina, Xabier, Erol-Dan, Muhammet, Luca, Brian, Lars with which I had great moments during our meetings. I would like also to express my deepest appreciation to the supervisory panel of the DYNANO network, Prof. Mihai Barboiu, Prof. Nicolas

Giuseppone, Prof. Jean-Marie Lehn, Prof. Olof Ramstrom, Prof Edit Buzas, Prof. Stéphane Vincent, Prof. Jesús Jiménez-Barbero, Prof. Claudiu T. Supuran, Prof. Eugen Gheorghiu, Dr. Mihaela Gheorghiu, Nino Gaeta, and Teodor Aastrup for sharing their knowledge, and for their priceless advices toward my work. I would also like to express my appreciation to Dr. Dolores Solis, for her time sacrificed to help me with the CD experiments and all the good advices she had for me during our meetings with the DYNANO group. Her guidance and support is much appreciated. I also would like to thank to Dr. Margarita Menéndez for her help with the ITC experiments, her dedication and willingness to explain me everything about this technique was just amazing.

Finally, I would like to mention the support that I have received from my friends and family. Many friends have offered immense support throughout my PhD and it is much appreciated. I would like to thank my Mother, Milka Panayotova, for being a fantastic role model. She has been there each step of the way, always encouraging me to follow my dreams and try to be at first place a good human and then anything else. Without the unconditional love she has given me, none of this would have been possible.

Както винаги накрая идват тези, които най-много заслужават благодарности и признание. Много често в живота е така, онези, които са те формирали като човек и личност много често остават в сянка. Тях не ги споменаваме по имена и принос, защото техният принос остава зад завесите, той е незначителен в очите на науката, но всъщност са сърцето и душата ѝ. Това са семейството, приятелите и началните учители. Те са фундаментът и подправката на живота, неговият смисъл, който много често убягва на вглъбената и центрирана в себе си наука, науката, която се съзтезава и надбягва сама със себе си, която както и вселената, се разширява и се опитва да измести всяко кътче от животът ти, понякога центробежно и задушаващо поглъщане, друг път удобно място да избягаш от заобикалящия те свят. Това никога нямаше да е възможно без безпределната помощ на родителите ми Райко и Милка, на сестра ми Златомира, на племенниците ми Радомира и Петя, на бабите и дядовците ми, на цялото ми семейство и приятели, на всичките ми начални, гимназиални и университетски преподаватели. Над всички тях, обаче се извисява, тази, която беше и все още е винаги до мен, зад мен, подкрепяща, обичаща, безусловно отдадена и всеодайна- моята Майка. Малко ще е да кажа- Благодаря ти, Мамо...това е за теб!

INDEX

INDEX OF FIGURES AND TABLES

- **FIGURES**

- **TABLES**

1. ABSTRACT/RESUMEN

Calmodulin (CaM) phosphorylated at different serine/threonine and tyrosine residues is known to exert differential regulatory effects on diversity CaM-binding proteins as compared to non-phosphorylated CaM. In this work we describe the preparation and characterization of a series of phospho-(Y)-mimetic CaM mutants in which either one or the two tyrosine residues present in CaM (Y99 and Y138) were substituted to aspartic acid or glutamic acid. We demonstrated some biological properties of these CaM mutants, such as their differential phosphorylation by the tyrosine kinase c-Src, and their action as compared to wild type CaM, on the activity of two CaM-dependent enzymes: cyclic nucleotide phosphodiesterase 1 (PDE1), and endothelial nitric oxide synthase (eNOS), as well as c-Src and the epidermal growth factor receptor (EGFR). We demonstrated that CaM directly interacts with c-Src in both Ca^{2+}-dependent and Ca^{2+}-independent manners *in vitro*, and that in living cells the CaM antagonist W-7 inhibits this kinase induced by the upstream activation of EGFR, in human carcinoma epidermoide A431 cells, and by hydrogen peroxide-induced oxidative stress, in both A431 cells and human breast adenocarcinoma SK-BR-3 cells. Most relevant and for the first time, we demonstrated that Ca^{2+}-free CaM (apo-CaM) exerts a far higher activatory action on Src auto-phosphorylation. We also present experimental evidences suggesting that the EGFR from A431 cells is subjected to *O*-GlcNAcylation, and that CaM may be involved in the regulation of this process through binding to the *O*-GlcNAc transferase (OGT). We detected a positive *O*-GlcNAcylation signal in immunoprecipitated EGFR using immunoblot and two distinct specific anti-*O*-GlcNAc antibodies. Conversely, the presence of EGFR was detected by immunoblot among the *O*-GlcNAcylated proteins immunoprecipitated with an anti-*O*-GlcNAc antibody. These signals were enhanced when a highly specific *O*-linked β-N-acetylglucosaminidase (OGA) inhibitor was present. Most significantly, we detected a positive *O*-GlcNAcylation signal in immunoprecipitated and *N*-deglycosylated EGFR using peptide-*N*-glycosidase F (PNGase F), and from tunicamycin-treated cells when were metabolically labeled with GlcNAz. We also performed *O*-GlcNAcylation assay *in vitro* using immunoprecipitated EGFR and OGT, which resulted in the enhancement of the EGFR *O*-GlcNAcylation signal. We concluded that the EGFR from A431 tumor cells is subjected to *O*-GlcNAcylation. Furthermore, we present preliminary data using *in silico* studies, combined with binding assays such as Ca^{2+}-dependent CaM chromatography and co-immunoprecipitation experiments, showing that OGT is a putative CaM-binding protein.

La calmodulina (CaM) fosforilada en diferentes residuos de serina/treonina y tirosina se sabe que ejerce efectos reguladores diferenciales en una diversidad de proteínas de unión a CaM en comparación con CaM no fosforilada. En esta Tesis se describe la preparación y caracterización de una serie de mutantes fosfo-(Y)-miméticos de la CaM en el que uno o los dos residuos de tirosina presentes en la CaM (Y99 y Y138) fueron sustituidos por ácido aspártico o ácido glutámico. Hemos demostrado algunas propiedades biológicas de estos mutantes de la CaM, tales como su fosforilación diferencial por la tirosina quinasa c-Src y su acción, en comparación con CaM tipo salvaje, sobre la actividad de varios enzimas CaM-dependientes: la fosfodiesterasa de nucleótidos cíclicos 1 (PDE1), la óxido nítrico sintasa endotelial (eNOS), c-Src y el receptor del factor de crecimiento epidérmico (EGFR). Hemos demostrado que la CaM interactúa directamente con Src de forma dependiente e independiente de Ca^{2+} *in vitro*, y que en células vivas el antagonista de CaM W-7 inhibe esta quinasa inducida por la activación aguas arriba del EGFR, en células A431 de carcinoma epidermoide human, y por estrés oxidativo inducido por peróxido de hidrógeno, tanto en células A431 como en células de adenocarcinoma de mama humano SK-BR-3. De mayor relevencia y por primera vez, hemos demostrado que la CaM libre de Ca^{2+} (apo-CaM) ejerce una acción activadora mucho mayor que el complejo Ca^{2+}/CaM sobre la auto-fosforilación de Src. También presentamos evidencias experimentales que sugieren que el EGFR de células A431 está sometido a *O*-GlcNAcylatión, y que la CaM puede estar implicada en la regulación de este proceso mediante su unión a la *O*-GlcNAc transferasa (OGT). Hemos detectado una señal positiva de *O*-GlcNacylatión en la EGFR inmunoprecipitado usando inmunoblot y dos anticuerpos específicos anti-*O*-GlcNAc distintos. Adicionalmente, la presencia de EGFR se detectó por inmunoblot entre las proteínas *O*-GlcNacyladas e inmnoprecipitadas con un anticuerpo anti-*O*-GlcNAc. Estas señales se incrementaron cuando un inhibidor altamente específico de la O-ligado β-N-acetilglucosaminidasa (OGA) estuvo presente. Más significativamente, se detectó una señal de *O*-GlcNAcylatión positiva en el EGFR inmunoprecipitado y *N*-deglicosilado usando péptido-*N*-glicosidasa F (PNGasa F), y a partir de células tratadas con tunicamicina cuando se marcaron metabólicamente. También se realizaron ensayos de O-GlcNAcylatión *in vitro* utilizando EGFR y OGT inmunoprecipitados, lo que resultó en el incremento de la señal de *O*-GlcNAcylation en el EGFR. Llegamos a la conclusión de que el EGFR de las células tumorales A431 y A549 están sometidos a *O*-GlcNAcylation. Además, se presentan datos preliminares de estudios *in silico*, así como ensayos experimentales de unión, tales como cromatografía de afinidad de CaM dependiente de Ca^{2+} y co-inmunoprecupitación, demostrando que la enzima OGT es putativamente una proteína de unión a CaM.

2. ABBREVIATIONS & ACRONYMS

ABA: abscisic acid

AREG: amphiregulin

Apo-CaM: apocalmodulin

Akt: v-Akt murine thymoma viral oncogene homologue

BCA: bicinchoninic acid

BSA: bovine serum albumin

BTC: betacellulin

CaM: calmodulin

CaM-BD: CaM-binding domain

CaM-BP: CaM-binding protein

CaMK: CaM-dependent kinase

CaM KMT: Calmodulin-lysine N-methyltransferase

CDK: cyclin-dependent kinase

CID: collision-induced dissociation

DTT: dithiothreitol

ECL: enhanced chemiluminescence

EDTA: ethylenediaminetetraacetic acid

EGF: epidermal growth factor

EGFR: EGF receptor

EGTA: ethylene glycol-bis(2-aminoethylether)-N,N,N',N'-tetraacetic acid

eNOS: endothelial nitric oxide synthase

EPR: epiregulin

ErbB: erythroblastic leukemia viral oncogene homologue

ERK: extracellular signal-regulated kinase

ESI: electrospray ionization

ETD: electron-transfer dissociation

EV: empty vector

FBS: fetal bovine serum

GAPDH: glyceraldehyde-3-phosphate dehydrogenase

GFP: green fluorescent protein

Grb7: growth factor receptor-bound protein 7

HB-EGF: heparin-binding EGF-like growth factor

HEK: human embryonic kidney

HEPES: 4-(2-hydroxyethyl)-1-piperazineethanesulfonic acid

HER: human EGFR receptor

HRGβ1: heregulin β1

IGFR: insulin-like growth factor receptor

IGF-1R: insulin-like growth factor 1 receptor

IRS1: insulin receptor substrate 1

IRS2: insulin receptor substrate 2

IgG: immunoglobulin G

JD: juxtamembrane domain

JAK: Janus kinase

MAPK: mitogen-activated protein kinase

MEK: mitogen-activated protein kinase kinase

MLCK: myosin light chain kinase

MS: mass spectrometry

NLS: nuclear localization sequence/signal

NP-40: nonidet p-40

NT: non-transfected

OGA: *O*-linked β-*N*-acetylglucosaminidase

OGT: *O*-linked β-*N*-acetylglucosamine transferase

ORF: open reading frame

PBS: phosphate buffered saline

PDE: phosphodiesterase

PI3K: phosphatidylinositol 3-kinase

PLCγ1: phospholipase Cγ1

PMSF: phenylmethylsulfonyl fluoride

PNA: peanut agglutinin

PTB: phosphotyrosine binding

PTM: posttranslational modification

PVDF: polyvinylidene fluoride

RAF: v-Raf murine sarcoma viral oncogene homologue

Ras: rat sarcoma viral oncogene homologue

SDS: sodium dodecyl sulphate

SDS-PAGE: polyacrylamide gel electrophoresis in the presence of SDS

SH2: Src homology 2

SH3: Src homology 3

SHP-2: SH2 protein tyrosine-phosphatase

c-Src: proto-oncogene tyrosine-protein kinase cellular Src

SRY: sex determining region Y

STAT: signal transducer and activator of transcription

TK: tyrosine kinase

TCA: trichloroacetic acid

TRIS: tris(hydroxymethyl)aminomethane

v-Src: tyrosine-protein kinase viral transforming protein Src

W-7: *N*-(6-aminohexyl)-5-chloro-1-naphthalenesulfonamide

W-12: *N*-(4-aminobutyl)-2-naphthalenesulfonamide

W-13: N-(4-Aminobutyl)-5-chloro-2-naphthalenesulfonamide hydrochloride

WGA: wheat germ agglutinin

3. INTRODUCTION

Posttranslational modifications (PTMs) of the side chains of amino acids in proteins are playing pivotal roles in cell life. They are orchestrating the protein behavior, activity and interactions. Currently over 200 modifications has been described in the literature such as phosphorylation, acetylation, methylation, glycosylation just to mention a few (Walsh et al., 2005, Jensen, 2006). PTMs exhibit high diversity in terms of structure, stoichiometry, size, complexity and cellular localization (Garavelli, 2004, Walsh et al., 2005). Among the different PTMs, phosphorylation is one of the best characterized and consists of the addition of a phosphoryl group at serine, threonine, tyrosine and histidine residues of target proteins (Fischer, 2013, Puttick et al., 2008). The fact that 500 proteins encoded by the human genome are kinases is highlighting the importance of this PTM (Gomase and Tagore, 2008). Phosphorylation regulates almost all aspects of cell life; it is the driving force in transmitting the extracellular signals to the cell interior, protein degradation, protein interactions, and gene expression among many others (Fischer, 2013). Of central interest in this Thesis is to study the role of tyrosine (Tyr, Y) phosphorylation of CaM and how phosphorylation affects the functions exerted by this protein, and the role of CaM regulating c-Src activation. In addition other aspects of this Thesis will be to outline the possible *O*-GlcNAcylation on the EGFR, as it has been proposed to potentially occur at its CaM-binding site (Kaleem et al., 2009), and the interaction of CaM with OGT, the enzyme catalyzing the *O*-GlcNAcylation process.

3.1 Ca^{2+} as a messenger

Calcium ion (Ca^{2+}) is one of the major messengers in cell signaling playing pivotal roles in many cellular functions such as muscle contraction, synaptic transmission, gene transcription, cell proliferation, autophagy and apoptosis among many others (Clapham, 2007). In basal conditions free Ca^{2+} is at low concentrations within the cytosol (from 20 to 50 nM) and about 1 mM in the extracellular space (Barritt, 1999). Upon activating the cell by a variety of stimulus the cytosolic concentration of free Ca^{2+} increases to μM levels and this “jump” in Ca^{2+} concentration makes of Ca^{2+} a very powerful secondary messenger. Several transport systems are responsible for this regulation increasing or decreasing the cytosolic concentration of free Ca^{2+} such as $Na^{+}(H^{+})$/-Ca^{2+} exchangers, Ca^{2+} channels, and different Ca^{2+}-ATPases located at the plasma membrane, endoplasmic reticulum, mitochondria, and other intracellular organelles (Clapham, 2007, Barritt, 1999, Berridge et al., 2003).

3.2 The Ca^{2+} sensor protein CaM

3.2.1 Historical overview

In 1967 Cheung reported an activator of brain cyclic nucleotide phosphodiesterase (PDE) and that during purification it dissociates from the enzyme (Cheung, 1967). At the same time Kakiuchi and Yamazaki reported that a heat-stable protein factor along with Ca^{2+} was necessary for the activation of PDE (Kakiuchi and Yamazaki, 1970). Shortly after their discoveries these studies merged and gave birth to a new universe in cell signaling: they have found that this protein was responsible for the activation of PDE in a Ca^{2+}-dependent manner and in the next few years this crystallized in a few papers related to the newly found Ca^{2+} sensor protein that was named calmodulin (Teo and Wang, 1973, Wolff and Brostrom, 1974, Cheung et al., 1975, Cheung, 1980, Klee and Vanaman, 1982). Since then CaM has been isolated from many organisms and it is present in all eukaryotic cell types (Manalan and Klee, 1984, Smith et al., 1987). CaM is also a very conserved protein among different species. For example, there are just a few differences between mammalian and *Drosophila melanogaster* CaM, where only three amino acids are substituted at positions 99, 143 and 147 (Smith et al., 1987).

3.2.2 Structure of CaM

Since the discovery of CaM a large number of structural studies has accumulated. CaM is an acidic single polypeptide protein that contains 148 amino acid residues and has a molecular mass of 16.7 kDa (Means and Dedman, 1980). Its structure consists of two terminal globular domains connected by a flexible central linker. Each globular domain has two Ca^{2+}-binding sites known as EF hands (Means and Dedman, 1980, Chin and Means, 2000). When Ca^{2+} binds to apo-CaM (Ca^{2+}- free state) a transition occurs to the holo-state (Ca^{2+}/CaM complex), which causes the exposure of large hydrophobic patches of the protein (Figures 1A and 1B). The exposure of these hydrophobic patches is the critical event that drives CaM to bind its targets, as it is shown in Figure 1C representing a CaM-myosin light chain kinase (MLCK) peptide complex (Chin and Means, 2000). These hydrophobic patches are rich in methionine residues: which stabilize the open conformation of Ca^{2+}-loaded CaM and helps it in recognizing many different target proteins with various amino acid side chains (Bhattacharya et al., 2004). The different EF-hands have different affinity for its ligand, the EF hands at the C-terminal have a high Ca^{2+} affinity (K_d ~10^{-6}, M), which is 10-fold higher than the N-terminal EF hands affinity for Ca^{2+} (K_d ~10^{-5}, M) (Bhattacharya et al., 2004). Therefore, a different Ca^{2+} affinity of the four EF-hands allows CaM to adopt

many conformations and to be saturated to various degrees (Chin and Means, 2000, Bhattacharya et al., 2004). For example, for the activation of CaMK-II only two Ca^{2+} ions bound to the C-terminal sites are required (Shifman et al., 2006) while four Ca^{2+} are required for the activation of the EGF receptor (Dagher et al., 2011). Thus, the degree of saturation is the fundamental property that makes it dynamic and flexible, and also allows it to bind to several hundred different partners (Shifman et al., 2006, Crivici and Ikura, 1995).

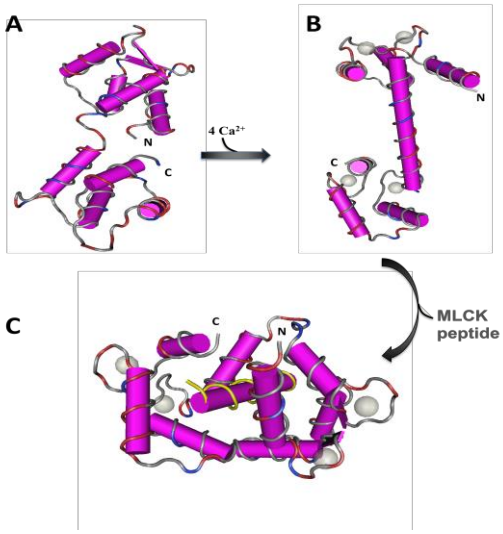

Figure 1: Three-dimensional structures of CaM in its different conformations: (A) Ca^{2+}-free CaM (pdb code: 1CFD); (B) CaM loaded with Ca^{2+} (pdb code: 1CLL) and (C) Ensemble of structures (PDB code: 2K0F) representing a CaM-myosin light chain kinase (MLCK) peptide complex. The ligand is shown in grey. The structures were drawn using the Cn3D program. The N-terminal (N) and the C-terminal (C) of the protein are also shown.

3.2.3 CaM binding domains

Based on the location of the hydrophobic groups, which serve as anchor points, CaM binding motifs have been classified in the following categories: 1–5–10, 1–8–14, 1–16, IQ, and the IQ-like motifs (Table 1) (Bhattacharya et al., 2004, Jurado et al., 1999). The key interaction occurs through hydrophobic residues such as Phe (F), Trp (W), Ile (I), Leu (L), or Val (V) and typically the C-terminal of CaM interacts with the first amino acids and the N-terminal with the hydrophobic residues at positions 10 and 14. In the case of 1-16 motifs the N-terminal of CaM binds the amino acid at first position and the C-terminal to the residue in position 16 (Bhattacharya et al., 2004). Although Ca^{2+} binding is necessary for CaM to bind to most of its target proteins, apo-CaM is also able to bind and regulate many proteins such as neurogranin, neuromodulin, IRS-1, myosin, and p68 helicase among others (Jurado et al., 1999, Wang et al., 2013).

CaM-BD	Motif sequence
1-5-10	(FILVW)xxxx(FAILVW)xxxx(FILVW)
1-8-14	(FILVW)xxxxxx(FAILVW)xxxxx(FILVW)
1-16	(FILVW)xxxxxxxxxxxxxx(FILVW)
IQ	(FILV)Qxxx(RK)Gxxx(RK)xx(FILVWY)
IQ-like	(FILV)Qxxx(RK)xxxxxxxx

Table 1: CaM-binding domains. The different CaM-binding domains (CaM-BD) including the IQ and IQ-like motifs sequences are shown.

CaM: functional implications

Since CaM is regulating a large number of proteins it is not of surprise that this Ca^{2+} sensor is involved in the regulation of many cellular processes, such as cell proliferation, apoptosis, muscle contraction, reproductive processes, cell motility, cytoskeleton architecture and function, autophagy, gene expression, osmotic control, ions transport, and protein folding among others (Chin and Means, 2000, Jurado et al., 1999, Berchtold and Villalobo, 2014).

3.2.4 Posttranslational modifications of CaM

The primary function of CaM is to transduce Ca^{2+} signaling in cells by binding hundreds of proteins including many kinases, it is not of surprise that CaM also undergoes posttranslational modifications. Up today CaM has been found to be subjected to acetylation, methylation, phosphorylation and glycation.

3.2.4.1 Acetylation

Watterson *et al.* in 1980 shortly after the discovery of CaM reported that the N-terminus of CaM undergoes acetylation (Watterson et al., 1980). In a later study it was reported that the acetylation of lysines 21 and 75 located in the central helix significantly reduces the affinity of CaM for MLCK and the acetylation of lysines 13, 30, 77, 94, or 148 had only a minor effect (Jackson et al., 1987). In general, not much has been done in studying the role of acetylation of CaM and the published data on the subject are quite poor.

3.2.4.2 Methylation

One of the noteworthy modification on CaM is the trimethylation of Lys115 a process driven by S-adenosyl-L-methionine: Calmodulin-lysine N-methyltransferase (CaM KMT) (Roberts et al., 1986, Rowe et al., 1986). The dimethylation of Lys13 in *Paramecium* has been described as well (Schaefer et al., 1987). The role of methylated CaM is still unclear, but it seems that the methylated form of the protein has differential effects on the activation of different CaM targets compared to the non-methylated protein. As for example, it has been reported that the replacement of Lys115 with alanine impairs its ability to activate plant NAD kinase and that the N-methylation of CaM prevents its degradation by ubiquitin-ATP-dependent proteolysis (Gregori et al., 1985). It was also reported that methylated and non-methylated CaM both can activate in the same extent PDE1 (Rowe et al., 1986). Moreover, non-methylated CaM was found in different mammalian tissues (Rowe et al., 1986), and CaM KMT has been found to be subjected to different developmental regulation in

plants (Oh et al., 1992). It has been also reported of a transgenic tobacco plant expressing the CaM mutant K117R, and this mutant plant had decreased growth, pollen viability and seed production (Roberts et al., 1992). In support to that study, recently it was demonstrated that the expression of CaM KMT in *Arabidopsis thaliana* was found to be at its highest levels during seed development, especially in tissues with active auxin signaling (Magnani et al., 2010). Moreover, this group reported that CaM KMT has a role in ABA signaling and auxin response to cold, heat and salt stress, and in return the enzyme is regulated by auxin and abiotic stresses. The authors using a microarray chip containing *Arabidopsis* proteins indentified that the methylated and non-methylated CaM have different binding partners, and that there are methylation-sensitive and methylation-insensitive partners of CaM (Magnani et al., 2010). It seems that N-methylation of CaM is involved in growth, body and seed development, and stress related functions in plants and gives rise to the possibility that it has similar role in animal cells. However, a Lys115 mutant CaM does not have a differential effect compared to wild type CaM on cell proliferation, and viability (Panina et al., 2012)

CaM can also undergo carboxyl methylation (Gagnon et al., 1981), the protein itself is very good substrate for protein-carboxyl methyltransferase, as it has many acidic and basic residues and low isoelectric point (Means and Dedman, 1980). CaM was also found to be carboxy methylated in living cells (Gagnon et al., 1981). The role of this modification is not clear, but it has been reported that carboxy methylated CaM has reduced ability to activate PDE1 *in vitro* and that this modification does not impair the Ca^{2+} binding, but most likely it affects the conformation of the Ca^{2+}/CaM complex (Weiss et al., 1980).

3.2.4.3 Phosphorylation

Reversible protein phosphorylation of threonine, serine, tyrosine or histidine residues is one of the most well studied posttranslational modifications and it is one of the most important in functional terms. Phosphorylation plays crucial roles in regulation of many cellular processes such as cell growth, cell cycle, apoptosis, cell metabolism, and signal transduction among many others (Fischer, 2013).

It has been demonstrated that CaM is phosphorylated both *in vitro* and *in vivo* (Plancke and Lazarides, 1983, Nakajo et al., 1986, Salas et al., 2005, Benaim and Villalobo, 2002). There are four serine and twelve threonine residues in CaM that could be subjected to phosphorylation by protein-Ser/Thr kinases and only two tyrosine residues that could be targeted for phosphorylation by different protein-tyrosine

kinases. Figure 2 shows the 3D structure of CaM from *Homo sapiens* where different amino acids known to be phosphorylated are highlighted.

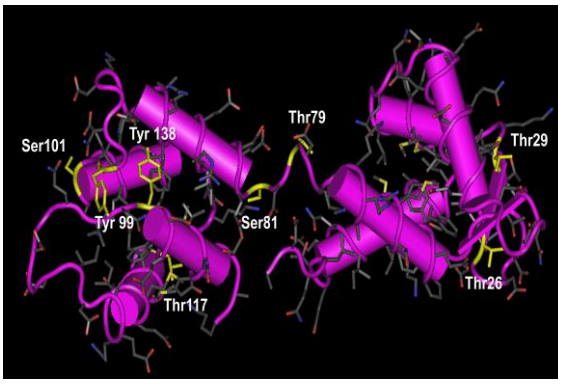

Figure 2: Serine, threonine and tyrosine residues in CaM phosphorylated by different kinases. The figure was prepared using the Cn3D 4.3.1 program and the amino acids phosphorylated by protein-serine/threonine kinases and protein-tyrosine kinases are highlighted in yellow. The CaM structure (pdb code: 1CFD_A) is presented as wire and the side-chains of the amino acids are shown with sticks.

Phosphorylation of CaM by protein Ser/Thr kinases

Four of the threonine residues have been reported to be subject to phosphorylation: Thr26, Thr29, Thr79 and Thr117 (Davis et al., 1996). The first two are phosphorylated by MLCK, the kinase phosphorylates mainly Thr29, while much lower phosphorylation of Thr26 was also detected. Interestingly, the MLCK was able to phosphorylate CaM in a Ca^{2+}-independent manner even when its canonical CaM-BD was mutated (Davis et al., 1996). Thr79 and Thr117 on the other hand are phosphorylated by casein kinase-II (CK-II), and this kinase is also responsible for the phosphorylation of Ser81 and Ser101 (Nakajo et al., 1986, Meggio et al., 1987, Nakajo et al., 1988, Quadroni et al., 1994). Thr79 and Ser81 are located in the central alpha helix of CaM, region with great importance for the binding of CaM-BPs (Figures 1B and 1C, Figure 2). The phosphorylation of Ser101, which is located in the III Ca^{2+}-binding pocket, may not only affect the binding of target proteins but also the binding of Ca^{2+}. Therefore, the effect of CK-II phosphorylation was investigated and two controversial finding were published (Aiuchi et al., 1991, Quadroni et al., 1998). The first one reported that CaM phosphorylated by CK-II has higher affinity for Ca^{2+} compared to non-phosphorylated CaM (Aiuchi et al., 1991). In reverse, the other group using flow dialysis reported that CK-II-phosphorylated CaM has lower affinity for Ca^{2+} (Quadroni et al., 1998). In fact Ca^{2+} at low concentrations stimulates the phosphorylation of CaM by CK-II and has inhibitory effect at higher concentration (Meggio et al., 1987, Sacks and McDonald, 1992).

Phosphorylation of CaM by receptor and non-receptor protein tyrosine kinases

Unlike Ser/Thr phosphorylation of CaM, where only two kinases are so far known to be involved: CK-II and MLCK, Tyr99 and Tyr138 are targeted by at least eight

different protein-tyrosine kinases (Figure 3). There are only two protein-tyrosine receptor kinases known so far, that are able to phosphorylate CaM: the InsR and the EGFR, and about six non-receptor tyrosine kinases, four of the Src family plus Syk and Jak2 kinases, that also are able to phosphorylate CaM.

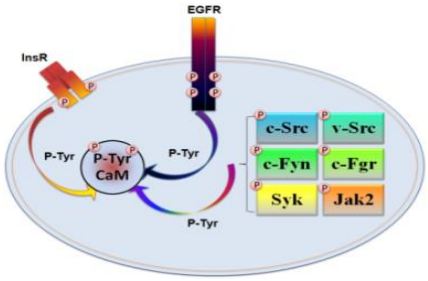

Figure 3: Receptor and non-receptor protein tyrosine kinases known to phosphorylate CaM. The receptor protein-tyrosine kinases EGFR and InsR are shown in their active conformation as well as the non-receptor tyrosine kinases of the Src family (c-Src, v-Src, Fyn and Fgr) plus Syk and Jak2.

Phosphorylation of CaM by InsR

In 1985 the group of McDonald for the first time reported that the InsR from rat adipocyte membranes is a CaM-BP, suggesting that Ca^{2+}/CaM has an important role in insulin-induced events (Graves et al., 1985). One year later the same group reported that CaM is not only binding to the InsR, but also enhances the receptor activity and in return the kinase phosphorylates CaM (Graves et al., 1986, Wong et al., 1988, Sacks and McDonald, 1988, Laurino et al., 1988, Sacks et al., 1989a). Shortly after this discovery a few additional papers were published on the subject, demonstrating that CaM is phosphorylated by the InsR in different tissues such as adipose tissues, skeletal muscle, liver and placenta (Graves et al., 1986, Wong et al., 1988, Sacks and McDonald, 1992, Sacks et al., 1989a). The *in vitro* phosphorylation of CaM by the InsR requires different polycations or basic proteins, such as poly-L-lysine or histones, as co-factors (Sacks and McDonald, 1988) and it has been suggested that in living cells this function could be exerted by the C-terminal of K-Ras. Indeed, a stimulatory effect on CaM phosphorylation by the InsR was demonstrated in an *in vitro* assay using a highly basic segment from K-Ras where the *in vitro* phosphorylation of CaM by InsR was also demonstrated (Fujita-Yamaguchi et al., 1989, Sacks et al., 1989b). Another interesting points on the subject are that low concentrations of Ca^{2+} have a highly stimulatory effect on the phosphorylation of CaM, while higher concentrations inhibits this process (Graves et al., 1986, Sacks and McDonald, 1992, Sacks et al., 1989a, Sacks, 1994), and that the InsR increased its potential to phosphorylate CaM that was previously phosphorylated by CK-II (Laurino et al., 1988). InsR is able to phosphorylated both Tyr99 and Tyr138, nevertheless, there is contradictory information published as some reports suggest that only Tyr99 is phosphorylated (Laurino et al., 1988, Saville and Houslay, 1993, 1994), while others demonstrate that both tyrosines are targeted by the InsR (Wong et al., 1988, Williams et al., 1994).

Phosphorylation of CaM by EGFR

In 1986 the group of Wharton detected phospho-Ser-CaM in EGF-stimulated A431 cells (Lin et al., 1988). However, this was an indirect effect mediated by an unknown Ser/Thr kinase. The direct tyrosine-phosphorylation of CaM by the EGFR was discovered and extensively studied by the group of Villalobo (San José et al., 1992, Benguría et al., 1994, 1995, De Frutos et al., 1997, Palomo-Jiménez et al., 1999, Benaim et al., 1998). It was reported that EGFR purified from rat liver by CaM-affinity chromatography was able to phosphorylate CaM at tyrosine (Benguría et al., 1994). The addition of poly-L-lysine or histones for the *in vitro* phosphorylation of CaM by EGFR, is an important requirement, as in the case with the InsR (Benguría et al., 1994). Interestingly, 1 μM of free Ca^{2+} was sufficient to profoundly inhibit CaM phosphorylation by EGFR (Benguría et al., 1994, De Frutos et al., 1997). Speaking of Ca^{2+} concentration and EGFR-CaM interaction it is of note that one of the consequences of the EGF-mediated activation of the receptor is the increase of cytosolic Ca^{2+} concentration and the extent of this increase maybe equivalent to a gradual decrease in the EGF-dependent phosphorylation of CaM (Villalobo et al., 2000). EGFR predominantly phosphorylates Tyr99, but it is also capable of phosphorylating Tyr138 (Palomo-Jiménez et al., 1999).

Phosphorylation of CaM by non-receptor tyrosine kinases

Several members of the Src family (c-Src, v-Src, Fyn and Fgr) have been shown to phosphorylate CaM as well as other tyrosine kinases such as Jak2 and Syk. It has been reported that CaM is phosphorylated in Rous sarcoma virus (RSV)-transformed chicken embryo fibroblasts but not in normal chicken embryo fibroblasts, and purified v-Src has been shown to phosphorylate CaM *in vitro* and that this phosphorylation was inhibited by Ca^{2+} (Ki= 30 μM) (Fukami et al., 1986). An interesting observation is that v-Src phosphorylated CaM had a slower electrophoretic mobility compared to non-phosphorylated CaM (Fukami et al., 1986). We have successfully phosphorylated CaM using recombinant c-Src and the presence of poly-L-lysine or histones strongly enhances the process (Salas et al., 2005, Stateva et al., 2015). However, the subsequent mutagenesis of Tyr99 and Tyr138 to Phe, Glu or Asp showed that when Tyr99 was mutated the efficiency of phosphorylation of Tyr138 was far greater as compared to the phosphorylation of Tyr99 when Tyr138 was mutated. This suggests that Tyr138 is the one preferred by the kinase (Salas et al., 2005, Stateva et al., 2015). Other non-receptor tyrosine kinases from the Src family capable of phosphorylate CaM are c-Fyn and c-Fgr, and both phosphorylate Tyr99 and Tyr138 (Corti et al., 1999).

The other two non-receptor tyrosine kinases known to phosphorylate CaM are Syk and Jak2. Syk kinase from spleen is able to tyrosine phosphorylates CaM at very low concentration of polycations (Meggio et al., 1987). As it is true for the Syk kinase, the information available for Jak2 CaM phosphorylation is scarce and there is only one report demonstrating that Jak2 is in fact capable of phosphorylate CaM (Mukhin et al., 2001).

3.3 CaM-dependent systems

As previously mentioned CaM is a ubiquitously expressed protein that has been found in all eukaryotic cells. Its subcellular localization may vary and it can be found in the cytoplasm, nucleus, attached to the plasma membrane or within organelles, regulating more than 300 different proteins with enzymatic or non-enzymatic functions (Crivici and Ikura, 1995, Shifman et al., 2006, Berchtold and Villalobo, 2014).

3.3.1 Cyclic nucleotide phosphodiesterase 1

PDEs form a large group of enzymes that specifically hydrolyze the second messengers cAMP and cGMP into the non-cyclic nucleotides 5'-AMP and 5'-GMP, respectively (Weishaar, 1986, Halpin, 2008, Keravis and Lugnier, 2012). Immediately after the discovery of cAMP the cyclic nucleotide PDE activity was described (Butcher and Sutherland, 1962). During the next two decades, research into the biochemical characterization and functional role of PDEs has grown exponentially and in this period around 1300 research articles have been published. More and more different PDE were found in different tissues and cell extracts. Interestingly the PDE activity as well as the distribution of PDE differed among different tissues and this led to a huge confusion in the nomenclature. Finally, the different PDEs were classified in 11 families based on the primary amino acid sequence as well as their kinetic and regulatory properties (Omori and Kotera, 2007). All of these 11 families of PDEs have a N-terminal regulatory domain (R-domain) and a C-terminal catalytic domain (C-domain). The N-terminal region of the PDEs differs the most among PDEs in size and structure, and contains sequences that are target for various regulators, and it also contain the binding site for cGMP and CaM, phosphorylation sites, and it is involved in membrane association and dimerization events (Lugnier, 2006).

CaM regulation of PDE1

The existence of Ca^{2+}-stimulated phosphodiesterase activity and that this is mediated by a heat stable protein activator was first demonstrated in the early ’70 of the last century (Cheung, 1970, Kakiuchi and Yamazaki, 1970). Since their discovery Ca^{2+}/CaM-dependent PDEs have been isolated from many mammalian tissues and the richest source of CaM-dependent isoenzyme (PDE1) is the bovine brain, but CaM-dependent PDEs have been isolated also from other tissues such as lung and heart (Sharma and Wang, 1986, Sharma and Kalra, 1994). CaM-dependent PDEs are named depending on their tissue distribution: brain (60 and 63 kDa isoforms), lung and heart, and these isoenzymes have different affinity for cGMP, cAMP and Ca^{2+}/CaM but what is common for all of them is that they have higher affinity for cGMP than for cAMP (Sharma and Kalra, 1994). Nevertheless, the K_m of the different isoenzymes of CaM-dependent PDEs for cAMP and cGMP may vary in a big range, for instance the K_m for cAMP of the enzyme in bovine brain has been shown in deferent studies to be in the range from 10 to 200 μM (Sharma and Kalra, 1994, Morrill et al., 1979, Klee et al., 1979, Tucker et al., 1981, Shenolikar et al., 1985).

The crucial role of Ca^{2+}/CaM in the activation of certain PDE isoenzymes is obvious, as Ca^{2+}/CaM is absolutely necessary for the maximal activation of these enzymes (Kakiuchi and Yamazaki, 1970, Sharma and Kalra, 1994), but this is only at first sight, since Ca^{2+}/CaM has much more to do in regulating this system. The activation of cells upon various stimulus leads to the activation of adenylate cyclase (AC), an enzyme able to convert ATP into cAMP, thus increasing the cellular concentration of cAMP. At the same time the cytosolic concentration of Ca^{2+} also rises and the increased levels of the Ca^{2+}/CaM complex and cAMP concentration activates the PDEs that starts to hydrolase cAMP to AMP. At that point the high levels of cAMP activate protein kinase A (PKA), which in turn phosphorylates PDE inactivating this enzyme. In fact, the inactivation of PDE by phosphorylation is not only due to PKA, the increase of the Ca^{2+} concentration leads to the activation of CaMKKs, which are also able to phosphorylate and inactivate the PDE. During these events the Ca^{2+} continues rising and finally achieves its pick and Ca^{2+}/CaM is now able to activate calcineurin (CaN), which is a ubiquitous phosphatase, that is able to dephosphorylate and activate PDE (Sharma et al., 2006). Taken all together it makes Ca^{2+} and the Ca^{2+}/CaM complex essential regulators of this processes, providing different mechanism for achieving a steady-state equilibrium between activation and inhibition of the main players in this signaling cascade.

Role of phospho-CaM on the regulation of PDE1

It has been reported that CaM phosphorylated by CK-II has lower affinity for bovine brain PDE1 compared to non-phosphorylated CaM, while the affinity of the enzyme for Ca^{2+} and the V_{max} remain the same (Sacks et al., 1992, Quadroni et al., 1998,). This observation was further proved by testing dansylated phospho-Ser/Thr-CaM with a peptide corresponding to the CaM-binding site of the same PDE1, as the phosphorylated peptide had lower affinity for PDE1 compared to the non-phosphorylated one (Leclerc et al., 1999).

The information published about the effect of phospho-Tyr-CaM is not that homogeneous, as some authors detected lower affinity of phospho-Tyr99/Tyr138-CaM (phosphorylated by the InsR) for PDE1 from bovine brain compared to the non-phosphorylated one (Williams et al., 1994), while purified phospho-Tyr99-CaM presented higher affinity (Corti et al., 1999) and in both cases the V_{max} was similar to the one presented by non-phosphorylated CaM. On the other hand, CaM phosphorylated by the EGFR was incapable of activating PDE1 from bovine heart (Palomo-Jiménez et al., 1999), while InsR-phosphorylated CaM has no effect when tested toward PDE1 isolated from rat hepatocytes (Saville and Houslay, 1994). The role of phospho-Tyr-CaM on PDE1 seems to fluctuate depending on the purity of the phospho-Tyr-CaM preparation, and the Tyr residues subject to phosphorylation, as well as the isoform of the enzyme.

3.3.2 Nitric oxide synthase

Nitric oxide (·NO) is a very important free radical second messenger molecule controlling process such as the immune response, blood pressure and neuronal activity among others (Kerwin et al., 1995, Bogdan, 2015, Das and Kumar, 1995, Luo and Zhu, 2011). ·NO is produced by the enzyme nitric oxide synthase (NOS) as product of the conversion of L-arginine into L-citrulline. For each L-citrulline and ·NO produced, 2 molecular oxygens and 1.5 NADPH are consumed (Kerwin et al., 1995).

NOS isoforms

There are three isoforms of mammalian NOS: endothelial (eNOS) expressed mainly in endothelial cells, neuronal (nNOS) expressed mainly in neuron cells and inducible (iNOS) expressed in macrophages, but can be induced in many other cell types (Griffith and Stuehr, 1995). The ·NO produced by eNOS controls vascular dilation and blood flow (Das and Kumar, 1995), nNOS-produced ·NO is responsible for

neurotransmission (Luo and Zhu, 2011) and the one produced by iNOS is used in the immune system as a defense mechanism (Bogdan, 2015). eNOS and nNOS are constitutively expressed and are classified as constitutive NOS (cNOS). Their enzymatic activity depends on increasing Ca^{2+} concentration in the cell, due to the Ca^{2+}-dependent binding of CaM to these isoforms (Govers and Rabelink, 2001). iNOS, on the other hand, is expressed only when required and as soon as it is transcribed, it can bind to CaM in the absence or presence of Ca^{2+}, and CaM is a constitutive subunit of the enzyme (Cho et al., 1992). The overall structure of the three isoforms is similar, with an oxygenase domain and a reductase domain separated by a CaM-BD. The oxygenase domain contains binding sites for tetrahydroxybiopterin (TH4), the catalytic heme and the active site, and the reductase domain accommodates the binding sites for NADPH, FAD and FMN. The NOS enzymes are found to be homo-dimeric proteins (Alderton et al., 2001).

CaM regulation of NOS

CaM is essential for the activation of the NOS isoforms. The binding affinity of CaM for each of the isoforms differs, with the highest binding affinity for iNOS, followed by nNOS and then eNOS (Aoyagi et al., 2003, Ghosh and Salerno, 2003). CaM binds to NOS at a 1-5-8-14 CaM-binding motif with the binding region consisting of residues 731-752 of nNOS, 491-512 of eNOS, and 501-531 of iNOS. It is believed that iNOS binds CaM in a Ca^{2+}-independent manner, however no IQ-motif within the protein has been identified so far. It is believed that CaM binds to iNOS in both Ca^{2+}-dependent and Ca^{2+}-independent manners (Aoyagi et al., 2003). A conformational change that is associated with CaM binding to NOS is required for electron transfer within these enzymes (Govers and Rabelink, 2001). The conformational change that CaM induces in the reductase domain of NOS allows for the FMN domain to interact with FAD to accept electrons and pass the electrons to the heme during catalysis. Exactly how CaM is able to initiate this process is still not fully understood. Clearly, these conformational changes caused by CaM are important for stimulating efficient electron transfer within the NOS enzymes (Daff et al., 2001).

Role of phospho-CaM on the regulation of NOS enzymes

Carafoli's group have demonstrated that phospho-(Tyr)-CaM and phospho-(Ser/Thr)-CaM both have stimulatory effects on the activation of NOS isolated from brain compared to the non-phosphorylated protein (Quadroni et al., 1994, Corti et al., 1999). Titration assay of dansyled CaM and dansyled phospho-(Ser/Thr)-CaM with a

peptide corresponding to the CaM-BD of NOS exhibited lower affinity for the phosphorylated than for the non-phosphorylated form (Leclerc et al., 1999). This observation was further confirmed and it was reported that CK-II-phosphorylated CaM has lower ability to activate eNOS and has two fold reduced V_{max} compared to non-phosphorylated CaM, while the affinity of the enzyme for CaM and Ca^{2+} was not changed (Greif et al., 2004).

In terms of phospho-(Tyr)-CaM and its effect on NOS activation not much has been done during the last few years. What we know is that in a displacement assay of a dansylated peptide corresponding to the CaM-BD of the Ca^{2+}-ATPase, which is bound to non-phosphorylated CaM or phospho-(Tyr99)-CaM by a peptide corresponding to the CaM-BD of NOS showed that the affinity of phospho-(Tyr99)-CaM for the CaM-BD of NOS was higher compared to non-phosphorylated CaM (Corti et al., 1999).

3.3.3 Tyrosine-protein kinase c-Src

c-Src kinase belongs to the Src family of non-receptor tyrosine kinases. Src family kinases are regulating processes such as cell differentiation, proliferation, motility and cell survival, stress response among other processes. It comprises Blk, Fgr, Fyn, Lck, Lyn, Hck, Yes, and c-Src itself. Fgr, Blk and Hck are found mainly within blood cells; Lyn and Lck in blood cells and brain, while Yes, Fyn and c-Src are ubiquitously expressed (Parsons and Parsons, 2004, Yeatman, 2004). The 3D structure of c-Src is well studied. c-Src is a 60 kDa modular protein formed by a N-terminal region containing a myristoyl-binding sequences, a SH4 domain, an Unique domain (UD), SH3 and SH2 domains followed by the protein-tyrosine kinase domain (SH1) and a short C-terminal tail (Xu et al., 1997). Src family members are attached to the cellular membrane through myristoylation in its N-terminal (Patwardhan and Resh, 2010). c-Src and oncoprotein v-Src play prominent roles in tumor progression and metastasis (Parsons and Parsons, 2004, Wheeler et al., 2009), thus they have been targeted by different inhibitors and strategies in thyroid, pancreas and breast cancers (Wheeler et al., 2009).

The non-receptor tyrosine kinase Src is subjected to complex regulatory mechanisms mediated by phosphorylation events that control its activation status (Okada and Nakagawa, 1989, Cooper and Howell, 1993, Parsons and Parsons, 2004, Irtegun et al., 2013). When inactive, c-Src is phosphorylated at Tyr530 (Tyr527 in chicken) by the tyrosine kinases Csk and Chk (Chong et al., 2005). Tyr530 is a highly conserved residue among all Src kinase family members and it is located at the C-

terminal tail of the protein. When Tyr530 is phosphorylated the C-tail interacts with the SH2 domain and the kinase is in its "closed" and inactive conformation (Ayrapetov et al., 2006, Roskoski, 2005). Dephosphorylation of Tyr530 by tyrosine phosphatases induce conformational changes and the subsequent auto-phosphorylation of Tyr419 opens up the kinase and stabilizes the catalytic domain in an active state (Roskoski, 2005).

CaM regulation of c-Src

Hayashi *et al.* demonstrated that a myristoylated peptide corresponding to the N-terminal of v-Src interacts with the Ca^{2+}/CaM complex, while the non-myristoylated peptide was not able to do so (Hayashi et al., 2004). It has been also proposed that upon Ca^{2+} entry in stimulated cells, CaM residing in lipid rafts interacts in a Ca^{2+}-dependent manner with c-Src, and in turn c-Src phosphorylates and inhibits PP2A, preventing in this manner its inhibitory action on Akt and henceforth promoting melanoma tumor growth (Fedida-Metula et al., 2012). The activation of c-Src by Ca^{2+}/CaM was also demonstrated in transfected neuroblastoma cells overexpressing α-synuclein, a cytotoxic protein abundant in Lewy bodies in Parkinson's disease, by a mechanism also implicating PP2A (Yang et al., 2013). The direct interaction of CaM with a recombinant GST-Src fusion protein was demonstrated to occur through both Ca^{2+}-dependent and Ca^{2+}-independent mechanisms, although mutation of the proposed CaM-binding site located at the SH2 domain of c-Src only partially prevented CaM binding (Yuan et al., 2011). The most recent evidence of CaM binding to Src surprisingly involves the unique domain of the kinase. Pérez *et al.* using NMR and peptides corresponding to the Unique and SH3 domains of Src have demonstrated that Ca^{2+}/CaM is able to bind to the Unique domain and thus modulating the binding of the kinase to the plasma membrane (Pérez et al., 2013). Additionally, Src was shown to co-immunoprecipitate with CaM but not with tyrosine-phosphorylated CaM in keratinocytes (Wu et al., 2015).

Nevertheless, these reports did not fully clarify the actual mechanism by which CaM interacts and activates c-Src, or if this process always occurs in the cell in a Ca^{2+}-dependent manner. This highlights the need for additional work to determine whether CaM controls the tyrosine kinase activity of c-Src in both Ca^{2+}-dependent and/or Ca^{2+}-independent manners. There is no information about the role of the phospho-CaM on c-Src functionality so far.

3.3.4 Epidermal growth factor receptor

The epidermal growth factor receptor (EGFR) is a transmembrane glycoprotein, and it belong to the ErbB receptor tyrosine kinase family formed by ErbB1/EGFR/Her1, ErbB2/Neu/Her2, ErbB3/Her3 and ErbB4/Her4. Its structure consists of an extracellular region which is responsible for the ligand-binding, a single transmembrane segment and a cytosolic region that contains a juxtamembrane domain (JD), a tyrosine kinase domain (TK) and a C-terminal tail (Figure 4) (Schlessinger, 2014, Olayioye et al., 2000, Yarden, 2001). A general accepted mechanism of EGFR activation is that upon binding of ligands, including EGF (epidermal growth factor), TGF-α (transforming growth factor-α), HB-EGF (heparin-binding EGF-like growth factor), BTC (betacellulin), AREG (amphiregulin) and EPR (epiregulin) causes structural changes of the domains, and induces dimerization of two receptor monomers (Olayioye et al., 2000, Yarden and Sliwkowski, 2001, Ferguson et al., 2003). EGFR can form homo-dimers or hetero-dimers with other ErbB family members (Olayioye et al., 2000, Gullick, 2001). The dimerization leads to activation of the intrinsic tyrosine kinase domain followed by auto-(trans)-phosphorylation at multiple Tyr residues located in the C-terminal tail: Y992, Y1045, Y1068, Y1086, Y1148 and Y1173 (Linggi and Carpenter, 2006). These auto-phosphorylation sites then are docking sites for different cytosolic proteins containing SH2 (Src homology 2) and PTB (phosphotyrosine binding) that are adaptors and signaling proteins forming transduction complexes to activate signaling pathways such as the RAF-RAS-MEK-ERK, the PI3K-Akt, the PLCγ-PKC, and the STATs pathways (Figure 4). The activation of these signaling pathways results in cell cycle progression, cell proliferation, migration, adhesion, survival, and differentiation (Schlessinger, 2014, Yarden, 2001, Wagner et al., 2013).

Ligand-induced EGFR internalization and degradation have been extensively studied (Wiley, et al., 1991, Kirisits et al., 2007, Zwang and Yarden, 2009). Following activation EGFR undergoes internalization through endocytosis where the receptor-ligand complex is sorted either for degradation or recycling back to the plasma membrane, or for nuclear translocation (Kirisits et al., 2007, Henriksen et al., 2013). After ligand binding, EGFR associates to coat adaptors such as adaptor protein 2 and Eps15 followed by endocytosis of the receptor through clathrin-coated pits, caveolae-mediated endocytosis, or through macropinocytosis (Zwang and Yarden, 2009). EGFR is frequently overexpressed, miss-regulated or mutated in many solid tumors contributing to cancerogenesis, thus the receptor has became an important target for cancer therapy (Yarden, 2001, Schlessinger, 2014, Lemmon et al., 2014, Dancey, 2004).

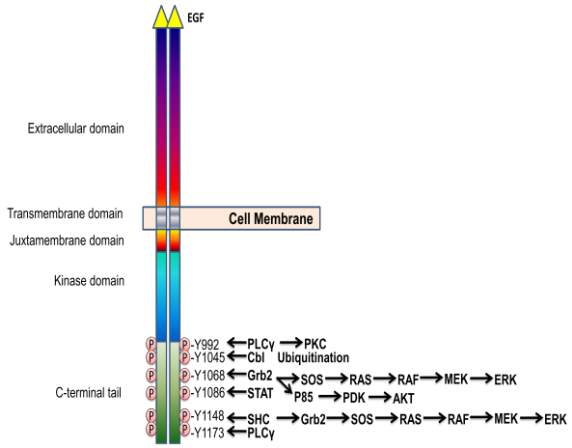

Figure 4: EGFR signaling pathways. Schematic representation of the functional domains of EGFR, the tyrosine phosphorylation residues induced by ligand (yellow triangle) stimulation and some downstream signaling cascades.

CaM regulation of the EGFR

The direct interaction of CaM with the EGFR was first reported in several studies done by our group (San José et al., 1992, Martín-Nieto and Villalobo, 1998, Li et al., 2004). The first evidence of direct binding between these two proteins was the identification of solubilized EGFR from rat liver bound to CaM-Sepharose in the presence of Ca^{2+} (San José et al., 1992). Later on the same was replicated using human EGFR, overexpressed in stably transfected murine fibroblasts (Martín-Nieto and Villalobo, 1998). In recent years the JM domain has been shown to play an important role in the regulation of the receptor and the specificity of its signaling (Hubbard, 2009, Red Brewer et al., 2009, Jura et al., 2009). In the JM region was identified a basic amphiphilic site comprising amino acids ^{645}RRRHIVRKRTLRRLLQ^{660} with CaM-binding properties (Martín-Nieto and Villalobo, 1998). Experiments using the CaM-BD of EGFR tagged with GST, determined that the interaction between CaM and the EGFR JM occurred in a Ca^{2+}- dependent manner and the formation of the complex was abolished in the presence of the Ca^{2+}-chelating agent EGTA (Martín-Nieto and Villalobo, 1998). In a more recent paper published by our group the role of CaM binding on EGFR functionality was further supported in living cells (Li et al., 2012). We used a conditional CaM-KO cell line in which all alleles of the genes encoding endogenous CaM were deleted and a construct encoding CaM from *Rattus norvegicus* was inserted. The latter one bearing a Tet-off cassette allowing the suppression of the expression of rat CaM in those cells by the addition of tetracycline (Panina et al., 2012). This cell line was stably transfected with the human EGFR and it was demonstrated that after the suppression of the expression of CaM the EGF-dependent activation of the receptor was significantly reduced highlighting the importance of CaM binding for EGFR functionality (Li et al., 2012).

Several models for how CaM mediates the regulation of the EGFR have been proposed (McLaughlin et al., 2005, Sánchez-González et al., 2010). McLaughlin et al. suggested that the basic amino acids that compose the cytosolic JM and the tyrosine kinase domain of the receptor is attached to the acidic lipids in the inner leaflet of the plasma membrane of the cell through electrostatic interaction and serves as an autoinhibitory mechanism of the receptor in the absence of ligand (McLaughlin et al., 2005). Ligand binding to the receptor leads to a rapid increase in the amount of the cytosolic Ca^{2+}, thus inducing the formation of the Ca^{2+}/CaM complex, which binds to the CaM-BD of the JM domain of the EGFR and detach it from the membrane. The detachment of the JM domain now allows the receptor to form an active homo-dimer (Figure 5) (McLaughlin et al., 2005, Sato et al., 2006).

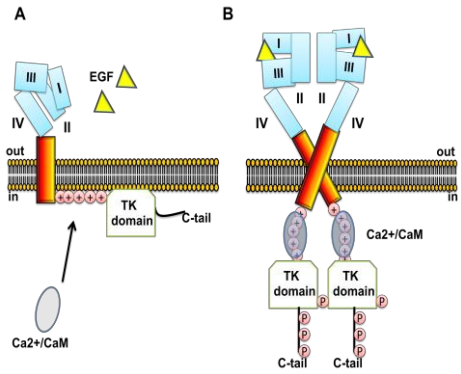

Figure 5: Model for the activation of the EGFR by the Ca^{2+}/CaM complex. (A) EGFR in an inactive state. The cytosolic JM is bound to the plasma membrane followed by the tyrosine kinase domain (TK) domain, which is also close to the negatively charged membrane. (B) EGF activated EGFR: Ca^{2+}/CaM binds to the CaM-BD in the JM and pull it out from the negatively charged bilayer. Adapted from (McLaughlin et al., 2005, Sato et al., 2006).

However, more recent NMR studies have suggested that the transmembrane domain dimerization is most likely enough to trigger the dissociation of the JM from the membrane (Matsushita et al., 2013). However, all of these models are based on the possibility that the membrane integrity is necessary to hold the receptor in an autoinhibited state in the absence of its ligand (Lemmon et al., 2014).

Phospho-CaM regulation of the EGFR

The effect of phospho-(Y)-CaM and phospho-(Ser/Thr)-CaM on the EGFR functionality is still not clear. To our knowledge nothing has been done with the phospho-(Ser/Thr)-CaM, while our group have shown that phospho-(Tyr)-CaM in both the absence and presence of Ca^{2+} have an activating role in the EGF-dependent EGFR activation of the solubilized receptor *in vitro*, while non-phosphorylated CaM had an inhibitory effect in the presence of EGF in this *in vitro* assay system (Stateva et al., 2015, manuscript in preparation).

3.4 *O*-GlcNAcylation

Protein *O*-GlcNAcylation is a posttranslational modification first identified by Hart group in 1984 in lymphocyte proteins (Torres and Hart, 1984). It consists in the reversible *O*-linked attachment of single β-D-*N*-acetylglucosamine moieties to serine/threonine residues in target proteins, but unlike the other types of glycosylation it is not further extended to more complex structures and occurs predominantly in intracellular proteins (Holt and Hart, 1986). It was shown that this modification has a short half-life and it can respond to different stimuli (ligand binding or different type of stress) within minutes (Zachara and Hart, 2004, Kneass and Marchase, 2004). Since then *O*-GlcNAcylation has been indentified in all higher eukaryotes from *Caenorhabditis elegans* to human and found to modify hundreds of different proteins, modifying their enzymatic activity, intracellular location, turnover, and/or exerting other functional roles (Hart, 2014). Altered *O*-GlcNAcylation has been proposed to contribute to the etiology of many illnesses such type-2 diabetes (Lefebvre et al., 2010, Hart et al., 2011, Ma and Hart, 2013, Vaidyanathan and Wells, 2014), cardiovascular ailments (Lefebvre et al., 2010, Marsh et al., 2014), neurodegeneration as in Alzheimer's disease (Gong et al., 2006, Zhu et al., 2014) and cancer (Li and Yi, 2014, Jozwiak et al., 2014, de Queiroz et al., 2014, Ma and Vosseller, 2014). The enzyme that transfers GlcNAc moieties to proteins is *O*-linked β-*N*-acetylglucosamine transferase (OGT) and unlike the rest of the enzymes involved in glycosylation is not restricted to the endoplasmic reticulum or Golgi (Janetzko and Walker, 2014). Three OGT isoforms are present in the cell, a canonical long form localized in the nucleus and cytosol (ncOGT), another one a bit shorter localized in the inner mitochondrial membrane (mOGT), and a third one, the shortest of them (sOGT), also localized in the nucleus and cytosol. These isoforms are basically differentiated by the number of tetratricopeptide (TRP) repeat motifs present in its N-terminal end (Janetzko and Walker, 2014). Although there is no consensus sequence for *O*-GlcNAcylation, OGT may modulate its substrate specificity through its TRP repeats (Iyer and Hart, 2003). It has been also shown that the TRP-rich domain of OGT is able to bind at the C-terminal of the transcriptional co-regulator host cell factor-1 (HCF-1) and subsequently to catalyze its proteolysis (Capotosti et al., 2011, Lazarus et al., 2013). In addition to OGT, an atypical EGF-like-repeat domain specific OGT (EOGT) was found to be also able to *O*-GlcNAcylate the side chain of Ser/Thr at the extracellular segment of different proteins such as Dumpy in *Drosophila* and the Notch receptor in mouse (Sakaidani et al., 2011, Sakaidani et al., 2012, Ogawa et al., 2014). Interestingly, the *O*-GlcNAcylation of the Notch receptor is followed by the addition of galactose, generating an *O*-LacNAc moiety (Sakaidani et al., 2012).

The enzyme that removes the *O*-GlcNAc from the protein backbone is the *O*-linked β-*N*-acetylglucosaminidase (OGA) that unlike the classical hexosaminidases that are resident in the lysosomes it has been found to be distributed in the nucleus and in the cytoplasm (Dong and Hart, 1994, Alonso et al., 2014). OGA shares significant sequence similarities with acetyltransferases, and appears to be a bifunctional enzyme. In fact in a recent study it has been shown to have acetytransferase activity *in vitro* (Toleman et al., 2004). It has been demonstrated that overexpression of OGA induces early mitotic exit and disruption of phosphorylation events during mitosis, while inhibiting it induces growth arrest (Slawson et al., 2005).

Protein *O*-GlcNAcylation is mainly intracellular, dynamic and it cycles on Ser/Thr residues in a manner very similar to protein phosphorylation. Interestingly the scientists have found out that there are extensive crosstalks between both PTMs, they either take place at the same site, or at distinct adjacent sites, competing or facilitating each other (Hart et al., 1995, Mishra et al., 2011, Zeidan and Hart, 2010). This crosstalk has been found to be involved in the regulation of multiple pathways implicated in the physiology of the cell, such as: metabolic control, stress response, epigenetic modification, gene transcription, translation of proteins, protein turnover, differentiation, apoptosis and cell cycle control among others (Wang et al., 2008, Zeidan and Hart, 2010, Hart et al., 2011, Lewis and Hanover, 2014). Interestingly, *O*-GlcNAcylation of some proteins can also affect its Tyr phosphorylation, as it is the case of prohibitin (Ande et al., 2009), a pleiotropic protein regulating many cellular functions including: proliferation, apoptosis, senescence, development, gene transcription, mitochondrial protein folding and also acting as a cell-surface receptor (Mishra et al., 2010, Theiss and Sitaraman, 2011, Whelan et al., 2010).

In recent years there was significant advancement in the field of *O*-GlcNAcylation and the identification of this process is becoming more available (Hart, 2014). Like for example, it was demonstrated using microarrays that a large set of serine/threonine- and tyrosine-kinases were good substrates for OGT and 42 of a total of 152 candidate kinases were found to be *O*-GlcNAcylated *in vitro* (Dias et al., 2012). Advances in the methodology of protein labeling and recent improvements in Mass Spectrometry (MS) techniques allowed scientists to detect and extensively investigate *O*-GlcNAcylation in many different proteins (Hahne and Kuster, 2011). Sprung *et al.* using high-throughput proteomic analysis and labeling proteins of *Drosophila melanogaster* with the GlcNAc analogue azido-GlcNAc indentified many proteins that are potentially *O*-GlcNAcylated, and interestingly the EGFR type III was among them, suggesting that it was susceptible to undergoes *O*-GlcNAcylation (Sprung et al., 2005). Thereafter, in an *in silico* study it

was proposed that the human EGFR could be subjected to *O*-GlcNAcylation at Thr654 and Ser1046/Ser1047 (Kaleem et al., 2009), phosphorylation sites of protein kinase C (PKC) (Hunter et al., 1984) and CaM-dependent protein kinase II (Countaway et al., 1992), respectively (Figure 6).

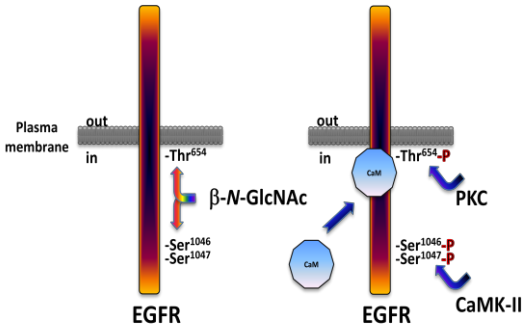

Figure 6: Potential *O*-GlcNAcylation sites in the EGFR based on *in silico* studies. Potential cross-talk between EGFR *O*-GlcNAcylation, and phosphorylation of Thr654 by PKC and Ser1046/Ser1047 by CaMK-II, and occlusion of Thr654 by CaM binding to the receptor at its cytosolic juxtamembrane region (Kaleem et al., 2009).

In fact, both residues Thr654 and Ser1046/1047 are very important control elements, regulating the functionality of the receptor. The generally accepted theory about the role of the phosphorylation of Thr654 by PKC is that this modification leads to the so-called desensitization or "shut-down" of the receptor followed by compartmentalization, internalization and recycling of the EGFR (Countaway et al., 1992, Llado et al., 2004). A more recent study, however, showed that c-Cbl-induced ubiquitination of EGFR and subsequent transfer of the receptor from the early to the late endosomes was inhibited by PKC-mediated phosphorylation and that receptor degradation and down-regulation were significantly reduced (Bao et al., 2000). Of note is to mention that CaM is not able to bind to the CaM-BD of the EGFR when the receptor is phosphorylated at Thr654 (Martin-Nieto and Villalobo, 1998), which let Kaleem *et al*. to speculated that the *O*-GlcNAcylation of Thr654 permit CaM to bind and prevents the PKC-mediated phosphorylation of that residue and thus allowing CaM and c-Cbl (multi-adaptor protein with E3-ubiquitin ligase) to guide the receptor degradation (Kaleem et al., 2009). Interestingly, the other two sites indentified as putative sites for *O*-GlcNAcylation, Ser1046/1047, and possible interplay with phosphorylation on the EGFR, are also under the control of Ca^{2+}/CaM, as they are phosphorylated by CaMK-II and this phosphorylation leads to the desensitization of the receptor (Countaway et al., 1992). Kaleem et al. suggested that the *O*-GlcNAcylation of these two sites could activate the receptor. Moreover, in another study it was demonstrated that the InsR, also a transmembrane protein-tyrosine kinase receptor was subjected to *O*-GlcNAcylation (Yang et al., 2008), highlighting that this modification is not restricted only to nuclear and cytosolic proteins. All taken together comes to show the necessity of studying the possible role of *O*-GlcNAcylation on human EGFR, and to explore the possible crosstalk between OGT, PKC, CaM and CaMKs.

4. OBJECTIVES

1. To study the possible differential role of phospho-(Y)-CaM and non-phosphorylated CaM on different CaM-dependent systems using phospho-(Y)-mimetic CaM mutants:

    - To generate and characterize phospho-(Y)-mimetic CaM mutants and to study their physicochemical properties.

    - To test the phospho-mimetic properties of these CaM mutants on different CaM-dependent systems: PDE1, eNOS, c-Src and EGFR.

2. To investigate the possible role of apo-CaM and Ca^{2+}/CaM on c-Src functionality *in vitro* and in living cells.

3. To study the potential *O*-GlcNAcylation of the EGFR as it has been suggested that it may occur at sites regulated either directly or indirectly by CaM.

4. To study whether *O*-linked β-*N*-acetylglucosamine transferase (OGT) is a CaM-binding protein.

5. Materials & Methods

5.1 Antibodies

Anti-mouse IgG (Fc specific) horseradish peroxidase (HRP)-conjugated secondary antibody, mouse monoclonal anti-tubulin-α (DM1A) antibody, purified mouse IgG (technical grade) and rabbit polyclonal anti-phospho-Src (Y418) (recognizing human phospho-Y416) were obtained from Sigma-Aldrich Co. (St. Louis, MO). Mouse monoclonal anti-phosphotyrosine antibody (4G10, isotype IgG2bκ), and rabbit monoclonal anti-EGFR (E235) antibody (recognizing the C-terminal domain of EGFR) were obtained from Millipore (Billerica, MA). Anti-rabbit IgG horseradish peroxidase-linked secondary antibody was purchased from Invitrogen (Eugene, OR). Rabbit monoclonal anti-Src (human) (clone 36D10, isotype IgG), rabbit polyclonal anti-phospho-Src family (Y416) and rabbit monoclonal anti-GAPDH (clone 14C10, isotype IgG) antibodies were obtained from Cell Signaling Company. Mouse monoclonal anti-*O*-GlcNAc monoclonal antibody (CTD110.6) and goat anti-mouse IgM (μ heavy chain) HRP-conjugated secondary antibody were obtained from Thermo Scientific-Pierce (Rockford, IL). The anti-*O*-GlcNAc antibody (RL2) was obtained from Novus Biologicals (Littleton, USA). Anti-OGT antibody (ab50271) was obtained from Abcam (Cambridge, UK).

5.2 Reagents and Materials

Phenyl-Sepharose 6 (fast flow), Sepharore 4B, (6R)-5,6,7,8-tetrahydrobiopterin dihydrochloride, FMN, FAD, cAMP, 3',5'-cyclic nucleotide PDE1 (from bovine brain), 5'-nucleotidase (from *Crotalus atrox* venom), recombinant GST-tagged human EGFR (695-end) expressed in baculovirus infected Sf9 cells, eNOS (bovine recombinant baculovirus-expressed in Sf9 cells), histone (type II-A), ATP (sodium salt), 4-amino-5-(methylphenyl)-7-(t-butyl)pyrazolo-(3,4-d)pyrimidine (PP1), benzyl 2-acetamido-2-deoxy−α−D-galactopyranoside (BADGP), O-(2-acetamido-2-deoxy-D-glucopyranosylidene)amino N-phenyl carbamate (PUGNAc), (3aR,5R,6S,7R,7aR)-2-(ethylamino)-3a,6,7,7a-tetrahydro-5-(hydroxymethyl)-5H-pyrano[3,2-d]thiazole-6,7-diol (Thiamet G), tunicamycin, tetracycline, biotin-labeled WGA and UDP-GlcNAc (sodium salt) were obtained from Sigma-Aldrich Co. (St. Louis, MO). The ultrasensitive colorimetric assay kit for eNOS was purchased from Oxford Biomedical Research (Rochester Hills, MI). The QuickChange® XL site-directed mutagenesis kit was acquired from Agilent Technology (Santa Clara, CA), and the QIAprep plasmid preparation kit from Quiagen Ltd. (Manchester, UK). The Slide-A-Lyzer dialysis cassettes and the Classic Magnetic IP/Co-IP kit were purchased from Thermo Scientific-Pierce (Rockford, IL). Competent *Escherichia coli* BL21(DE3)pLysS was purchased from Stratagene (La Jolla, CA), and BugBuster® Ni-NTA His•Bind®

purification kit and purified 6His-tagged recombinant human c-Src expressed by baculovirus in Sf21 insect cells were obtained from Merck/Millipore (Darmstadt, Germany). The ECL kits were obtained from GE Healthcare-Amersham.The PVDF membranes were obtained from Pall Corporation (Dreieich, Germany). Streptavidin peroxidase-conjugated tetraacetylated N-azidoacetylglucosamine (GlcNAz) and Click-iT®-protein reaction buffer kit were obtained from Invitrogen (Eugene, OR). Peptide-N-glycosidase F (PNGase F) (from *Flavobacterium meningosepticum*), *O*-glycosidase cloned from *Enterococcus faecalis* and expressed in *Escherichia coli* (*E. coli*) and neuraminidase cloned from *Clostridium perfringens* and overexpressed in *E. coli* were obtained from New England BioLabs (Herts, UK). Other chemicals used in this work were of analytical grade. The prokaryotic expression vector encoding full-length human OGT was a kind gift of Prof. Suzanne Walker (Harvard Medical School, Boston, MA). The pETCM vector encoding calmodulin was kindly provided by Prof. Nobuhiro Hayashi from the Institute for Comprehensive Medical Science, Fujita Health University, Japan.

5.3 Generation of calmodulin mutants

PCR-aided site-directed mutagenesis was performed in the pETCM vector containing the coding sequence of *Rattus norvegicus* CaM gene II (Hayashi et al., 1998) as template using the QuickChange® XL Site-Directed Mutagenesis kit and the following set of complementary oligos (Table 2).

Mutation	Primer Sequence (5'- 3')
Y99D	5'-GGCAATGGCGACATCAGTGCAGCA-3; 5'-TGCTGCACTGATGTCGCCATTGCC-3'
Y138D	5'-GGGGATGGTCAGGTAAACGACGAAGAGTTTGTACAAATG-3' 5'-CATTTGTACAAACTCTTCGTCGTCGTTTACCTGACCATCCCC-3'
Y99E	5'-GGCAATGGCGAGATCAGTGCAG-3'; 5'-CTGCACTGATCTCGCCATTGCC-3'
Y138E	5'-GGGGATGGTCAGGTAAACGAGGAAGAGTTTGTACAAATG-3' 5'-CATTTGTACAAACTCTTCCTCGTCGTTTACCTGACCATCCCC-3'

Table 2: Primers used in this study

Sequential mutagenesis was carried out to obtain the double substitutions Y99D/Y138D and Y99E/Y138E using the Y99D and Y99E mutated vectors, respectively, as template. *E. coli* DH5α was transformed with the pETCM, pETCM(Y99D), pETCM(Y138D), pETCM(Y99D/Y138D), pETCM(Y99E), pETCM(Y138E) or pETCM(Y99E/Y138E) vectors for their replication, and purification by the alkaline lysis method (Birnboim and Doly, 1979) using the QIAprep plasmid

preparation kit. The correctness of the mutagenesis procedures was ascertained by sequencing the vectors using an oligo annealing to the T7 promoter (Figure 7).

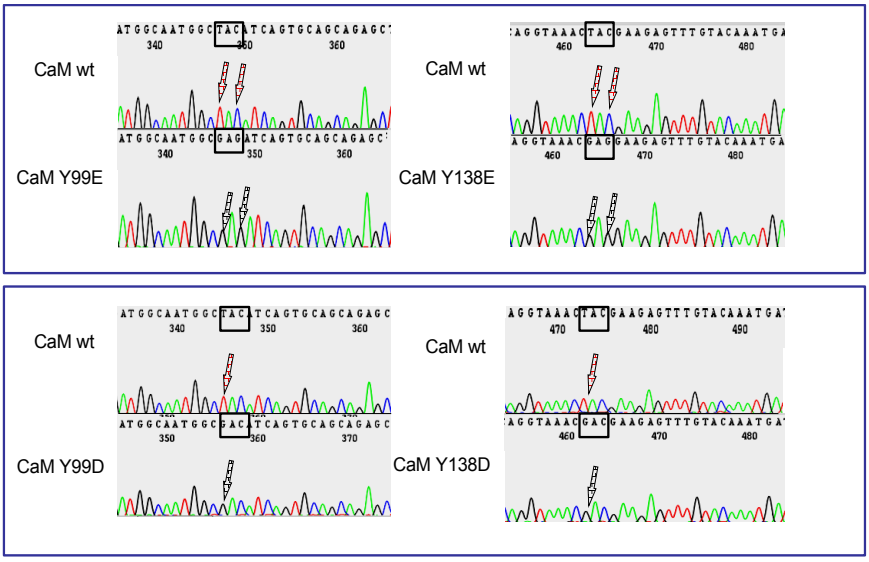

Figure 7: Sequence analysis of CaM(Y99E/D) and CaM(Y138E/D). The substitution of TAC (Tyr) to GAG (Glu) and TAC to GAC (Asp) codons are highlighted and arrows pointing the substitution are also shown. The alignment of the sequences was done with the CodonCode Aligner program.

5.4 Expression and purification of recombinant calmodulin mutants

E. coli BL21(DE3)pLysS was transformed with the vectors indicated above using a thermic-shock protocol. Single colonies grown in solid medium in the presence of 100 μg/ml ampicillin were collected and seeded in 5 ml of Luria´s broth containing the same concentration of ampicillin. Larger cultures (500 ml) were seeded with the pre-culture and grown in the same conditions until they reached an $OD_{600\ nm}$ = 0.7 ± 0.1. The expression of the recombinant proteins was induced with 0.5 mM IPTG during 4 hours at 37 ºC. Control cultures in the absence of IPTG were included. The bacteria were collected by centrifugation at 6,000 x g for 20 min and frozen at -70 °C until used. The bacteria were lysed using the BugBuster® protein extraction reagent kit, centrifuged at 11,000 x g during 10 min at 4 °C and the supernatant collected, heated at 95 °C for 5 min and centrifuged again as above. Heat-resistant CaM present in the new supernatant was purified as previously described (Hayashi et al., 1998). Briefly, phenyl-Sepharose 6 (fast flow) was packed in a column and equilibrated with a buffer containing 50 mM Tris-HCl (pH 7.5) and 1 mM $CaCl_2$. The sample was applied to the column and washed with four column volumes of a buffer containing 50 mM Tris-HCl (pH 7.5), 1 mM $CaCl_2$ and 100 mM NaCl. CaM was eluted with a buffer containing 50 mM Tris-HCl (pH 7.5) and 2 mM EGTA in fractions of 10 ml. The fractions containing CaM were desalted using Slide-A-Lyzer dialysis cassettes with membranes of 3.5 kDa

cut-off against a buffer containing 10 mM Hepes-NaOH (pH 7.5) or 20 mM Tris-HCl (pH 7.5) and kept at a concentration of 1-2 mg/ml at -70 °C. Protein concentration was determined by the BCA method (Stoscheck, 1990) using bovine serum albumin as standard. The purity of the samples was confirmed by SDS-PAGE (Laemmli, 1970) in a 5-20 % (w/v) polyacrylamide continuous gradient slab gel adding 5 mM EGTA or 1 mM $CaCl_2$ in the loading buffer to attain the characteristic Ca^{2+}-induced electrophoretic mobility shift of CaM (Burgess et al., 1980), and staining the gel with Coomassie Brilliant Blue R-250.

5.5 Absorption spectra

The absorption spectra in the range 240-340 nm of the different species of CaM (120 μM) were measured in 20 mM Tris-HCl (pH 7.5) using a CARY/1E/UV-Visible spectrophotometer (Varian) equipped with Cary winUV software.

5.6 Circular dichroism

Far-UV (200-260 nm) and near-UV (250-320 nm) circular dichroism spectra of the different CaM species were measured at 20 ºC in the presence of either 1 mM EGTA or 1 mM $CaCl_2$ in a buffer containing 20 mM Tris-HCl (pH 7.5) and 0.1 mM KCl using a JASCO J-810 spectropolarimeter (Cremelia, Italy) equipped with a Peltier type temperature control system (Model PTC-423S/L), a bandwidth of 0.2 nm and a response time of 4 s. Far-UV spectra were recorded in 0.1 cm path-length quartz cells at a protein concentration of 0.2 mg/ml, and near-UV spectra in 1 cm path-length cuvettes at a protein concentration of 2 mg/ml as previously described (Sun et al., 2001). The Spectra Manager software (JASCO, v 1.52.01) was used for data collection and analysis. Routinely, the corresponding buffer baseline was subtracted and the corrected data were normalized per mole of amino acid. Thermal denaturation experiments were carried out in the same system by increasing the temperature from 20 to 90 °C at a scanning rate of 0.66 °C/min. Variations in ellipticity at 222 nm were monitored at steps of 0.2 °C.

5.7 Tb^{3+} fluorescence

The emission fluorescence spectra of Tb^{3+} in the range 520-580 nm in the different species of CaM (10 μM) upon excitation of tyrosine (if present) at 280 nm were measured in 10 mM Pipes-HCl (pH 6.5), 100 mM KCl, and increasing concentrations of $TbCl_3$ (0-200 μM) using a Photon Technology International Inc. spectrofluorometer system (Birmingham, NJ). The Tb^{3+} emission fluorescence peak at 543 nm upon

tyrosine excitation at 280 nm was quantified as previously described (Wallace et al., 1982).

5.8 Phosphorylation of calmodulin

Phosphorylation of CaM was carried out at 37 °C for 30 min in a total volume of 0.1 ml in a buffer containing 15 mM Hepes-NaOH (pH 7.4), 5 mM $MgCl_2$, 1 mM EGTA, 1 mM DTT, 1.2 µM histone, 1.2 µM CaM (different species), and 0.02 µg of recombinant c-Src. The reaction was started upon addition of 2 mM ATP and stopped upon addition of Laemmli buffer and heating the sample at 100 °C for 5 min. Tyrosine-phosphorylated CaM and auto-phosphorylated c-Src were detected by standard Western blot technique using the anti-phospho-tyrosine 4G10 antibody. Membrane segments were stripped at 50 °C for 45 min in a buffer containing 2 % (w/v) SDS, 60 mM Tris-HCl (pH 6.8) and 0.1 % (v/v) β-mercaptoethanol, extensively washed with water, incubated in TBST buffer (0.1 % (w/v) Tween-20, 100 mM Tris-HCl (pH 8.8), 500 mM NaCl and 0.25 mM KCl) for 30 min and reprobed with either anti-Src or anti-CaM antibodies as loading controls. Alternatively, when larger amounts of phospho-(Y)-CaM was required to assay its action on target proteins, CaM (1 mg) was phosphorylated in a 1 ml reaction mixture containing 400 mM NaCl, 50 mM Tris-HCl (pH 7.5), 5 mM $MgCl_2$, 5 mM ATP, 2 mM EGTA, 1 mM DTT, 1 mg histone, and 8 µg c-Src at 37 ºC overnight as described (Corti et al., 1999). Tyrosine-phosphorylated CaM, free of non-phosphorylated CaM, was obtained by affinity-purification using an immobilized anti-phospho-tyrosine antibody as previously described (Palomo-Jiménez et al., 1999).

5.9 Phosphodiesterase assay

The CaM-dependent cyclic nucleotide PDE1 was assayed as previously described (Palomo-Jiménez et al., 1999) at 37 °C for 15 min in 250 µl of a medium containing 50 mM imidazole-HCl (pH 7.5), 10 mM Hepes-NaOH (pH 7.4), 0.2 M NaCl, 0.4 mM β-mercaptoethanol, 5 mM $MgCl_2$, 0.4 mM EGTA, 0.5 mM $CaCl_2$ (0.1 mM free Ca^{2+}), 2.5 mM cAMP, 0.01 units of cyclic nucleotide PDE1, 2 units of 5'-nucleotidase, and the concentrations of the different CaM species indicated in the legend to the figures. One unit of cyclic nucleotide PDE1 transforms 1 µmol of cAMP to AMP per min at 30 °C and pH 7.5. One unit of 5'-nucleotidase releases 1 µmol of inorganic phosphate from AMP per min at 37 °C and pH 9. The inorganic phosphate released from AMP was determined colorimetrically based in a described method (Fiske and Subbarow, 1925).

5.10 Isothermal titration calorimetry

Determination of the kinetics parameters of PDE1 in the absence and presence of wild type CaM and CaM(Y99D/Y138D) were done in a VP-ITC instrument (GE-Healthcare). The reaction cell (1.4619 ml) was filled with degassed protein solutions and equilibrated at 37 ºC. Stirring speed was 307 rpm and thermal power was registered every 2 seconds with an instrumental reference power of 20 µcal/s. Enzyme reaction rates were determined by measuring the change in the instrumental power supplied to the sample cell after addition of the substrate (Todd and Gomez, 2001). At least three independent measurements were carried out in each experimental condition. Serial injections of 4.7 mM cAMP were made every 2 min into the sample cell loaded with 0.01-0.04 U of PDE1 in the absence or presence of wild type CaM or the Y99D/Y138D mutant (3.8 µM) in the same reaction buffer as described in 5.9. To avoid distortions associated with dilution events, the power change associated with substrate addition at injection *i* was averaged over the 30 s immediately before the injection *i*+1. Reaction rates under steady-state conditions were then calculated dividing the power change for each injection, $(dQ/dt)_i$, by the cell volume and the apparent reaction enthalpy (ΔH_{app}) using the software provided by the manufacturer (Origin ITC 7.0). The complete enthalpy of the reaction was determined in separate experiments where 15 µl of 4.7 mM cAMP were injected into the cell filled with a solution containing 0.1 units PDE1 and 3.8 µM CaM wild type and the hydrolysis was monitored until initial baseline was recovered. Integration of the area under the peak gave the total heat of hydrolysis that was corrected by the heat of cAMP dilution, measured independently by injecting the substrate solution in the sample cell loaded with buffer. Very similar values of ΔH_{app} (-19.9 ± 0.5 kcal/mol) were obtained with subsequent injections, indicative of no product inhibition.

5.11 Nitric oxide synthase assay

Recombinant eNOS was assayed determining the accumulation of nitrite as by-product of NO oxidation using a nitrate reductase/colorimetric assay kit (Oxford Biomedical Research, UK) exogenously supplemented with 25 µM FAD, 25 µM FMN, 12 µM tetrahydrobiopterin and the concentrations of the different CaM species indicated in the legends to the figures following the recommendation of the supplier. One unit of eNOS produces 1 nmol/min of NO from arginine at 37 ºC and pH 7.4.

5.12 Determination of free Ca^{2+} concentrations

The concentrations of free Ca^{2+} in the PDE1 and eNOS assay systems were determined using established algorithms of the Maxchelator program. This program is freely available at http://maxchelator.stamford.edu.

5.13 Cell culture

Human epidermoid carcinoma A431 cells, human cervix adenocarcinoma HeLa cells, human lung carcinoma A549 cells, human breast adenocarcinoma SK-BR-3 cells and mouse EGFR-T17 fibroblasts, a stably transfected cell line overexpressing the human EGFR, were grown in DMEM supplemented with 10 % (v/v) fetal bovine serum, 2 mM L-glutamine and 40 µg/ml gentamicin in a humidified atmosphere of 5 % (v/v) CO_2 in air at 37°C. In case of activation of the EGFR or c-Src kinases the cells were maintained overnight or four hours in a fetal bovine serum-free medium before performing the experiments. DT40wt/EGFR cells clone G5, a chicken pre-B lymphoma cell line stably transfected with the human EGFR; and the ET1–55/EGFR clone H8, a conditional CaM-KO cell line stably transfected with the human EGFR, where the expression of recombinant rat CaM is negatively controlled by a tetracycline response element (Tet-Off system) (Panina et al., 2012), were grown in RPMI supplemented with 1 % (v/v) chicken serum, 10 % (v/v) fetal bovine serum, 2 mM L-glutamine and 40 µg/ml gentamicin. When CaM down-regulation was performed, the ET1-55/EGFR clone H8 and DT40wt EGFR clone G5 cells (negative control) were treated with 1 µg/ml tetracycline for the times indicated in the figure legends.

5.14 Preparation of cell membrane fraction

A431 cells were washed with PBS (137 mM NaCl, 2.7 mM KCl, 12 mM Na/K-phosphate, pH 7.4), gently scraped from the plates, harvested by centrifugation, and lysed in 3 ml of an ice-cold hypotonic buffer containing 15 mM Hepes-Na (pH 7.4), 1 mM EGTA, and a cocktail of protease inhibitors (0.5 mM AEBSF, 0.4 µM aprotinin, 25 µM bestatin, 7.5 µM E-64, 10 µM leupeptin, 5 µM pepstatin A, and freshly prepared 0.6 mM PMSF). The lysate was incubated 10 min on ice and centrifuged at 130,000 g for 30 min at 4 °C. The supernatant was discarded, and the pellet resuspended in the same buffer and centrifuged as above. This pellet corresponding to the membrane fraction was washed with the same buffer but without EGTA, centrifuged again, and resuspended in 3 ml of 25 mM Hepes-Na (pH 7.4) containing the protease inhibitors.

5.15 Electrophoresis and Western blots

Proteins were separated by slab SDS-PAGE in 5-20 % (w/v) linear gradient of polyacrylamide and 0.1 % (w/v) SDS at pH 8.3 according to a described method (Laemmli, 1970) at 6 mA during 16-17 h. After processing by SDS-PAGE, proteins were electro-transferred from the gel to a PVDF membrane or nitrocellulose in case we were testing for CaM for 2 h at 300 mA in a buffer containing 48 mM Tris-base, 36.6 mM L-glycine, 0.04 % (w/v) SDS and 20 % (v/v) methanol (TGSM buffer); fixed with 0.8

% (v/v) glutaraldehyde in T-TBS buffer (10 mM Tris-HCl pH 8, 150 mM NaCl, 0.1 % (v/v) Tween-20 for 10 minutes and transiently stained with 0.1 % Fast Green FCF (w/v) FCF, 50 % (v/v) methanol, 10 % (v/v) acetic acid to ascertain the regularity of the transfer procedure. The membranes were blocked with 5 % (w/v) bovine serum albumin, 3 or 5 % (w/v) fat-free powdered milk, as recommended by the antibodies supplier, in T-TBS or T-PBS buffer. This was followed by probing over-night at 4 ºC using a 1/2000 dilution of the corresponding primary antibody, and thereafter for 1 h at room temperature using a 1/5000 dilution of the appropriate secondary anti-IgG or anti-IgM antibodies coupled to horseradish peroxidase. The bands were visualized upon development with the ECL reagents. The intensity of the bands was quantified with a computer-assisted scanning densitometry using the ImageJ (1.47v) program.

5.16 *In vitro* EGFR phosphorylation assays

EGFR was assayed in a reaction mixture containing the detergent-solubilized receptor from a membrane fraction of A431 cells, 15 mM Hepes-NaO (pH 7.4), 2 mM $MgCl_2$, and 2 mM EGTA or 100 µM $CaCl_2$ were added depending on the condition tested, and 1 µg of each CaM species. The reaction mixture was then incubated on ice for 30 min in the absence or presence of 1 µM EGF. Thereafter, the reaction was started upon addition of 2 mM ATP at 37 °C for 5 min and stopped with the addition of loading buffer in a final volume of 50 or 100 µl. The samples were boiled at 100 °C for 5 min. centrifuged and analyze by SDS-PAGE and Western blot as detailed above. In case of using recombinant $EGFR_{cyt}$ for the *in vitro* phosphorylation of OGT, the reaction took place as follows: 250 ng of the recombinant $EGFR_{cyt}$ were assay in a buffer containing 15 mM Hepes-NaOH (pH 7.4), 5 mM $MgCl_2$, in the absence or presence of 500 ng ncOGT and in the absence or presence of 5 mM ATP. The reaction mixture was then incubated for 2 hours at 37 °C. The reaction was stopped by the addition of loading buffer, boiled for 5 min and processes by SDS-PAGE and Western blot as described above.

5.17 Activation of EGFR in living cells

Cells were grown to confluence in 6-well culture dishes containing 2 ml of DMEM supplemented with 10 % (v/v) FBS overnight, and deprived of FBS for 4 hours as mention above. In order to study the phosphorylation of EGFR induced by the EGF the following was done: 10 nM EGF was added to cells in 2 ml of serum-free culture medium and the incubation was continued for different periods of time (0, 2, 5, 10, 15 and 30 min). The reaction was arrested upon addition of ice-cold 10 % (w/v) trichloroacetic acid (TCA). The cells were scraped from the culture dish and centrifuged

at 16,060 g for 10 min. The supernatant was discarded and the proteins were resuspended in Laemmli buffer, boiled at 100°C for 10 min and centrifuged again for 1 min. The tyrosine phosphorylation level of EGFR and proper loading controls were determined by SDS-PAGE and Western blot analysis using an anti-phosphotyrosine and anti-GAPDH or anti-tubulin-α antibodies, respectively.

5.18 CaM-affinity chromatography and immobilized-CaM pull-down of Src

Cell membrane-anchored Src from A431 cells was detached from the membrane fraction upon incubation with 1 % (w/v) Triton X-100 and 5 % (w/v) glycerol at 0 °C for 10 min. The sample was centrifuged at 130,000 g for 30 min and the supernatant was used to isolate Src by CaM-affinity chromatography or pull-down using immobilized CaM. The isolation of Src by Ca^{2+}-dependent CaM-affinity chromatography was carried out loading the solubilized membrane fraction in a small column (1-2 ml bed volume) of CaM-Sepharose 4B equilibrated with a buffer containing 25 mM Hepes-NaOH (pH 7.4), 1 % (w/v) Triton X-100, 5 % (w/v) glycerol, 0.1 mM $CaCl_2$, and the protease inhibitors cocktail described above (Ca^{2+}-buffer). The column was washed with 25 volumes of the Ca^{2+}-buffer, and Src was eluted using the same buffer but containing 1 mM EGTA instead of $CaCl_2$ (EGTA-buffer). Proteins in the eluted fractions (0.6 ml) were precipitated with 10 % (w/v) TCA and processed by SDS-PAGE and Western blot for Src identification. The pull-down of Src was done using a slurry of CaM-Sepharose 4B beads (200 µl) in a buffer containing 25 mM Na-Hepes (pH 7.4), 1 % (w/v) Triton X-100 and 5 % (w/v) glycerol supplemented either with 0.1 mM $CaCl_2$ or 1 mM EGTA. We used naked Sepharose 4B beads as negative binding control. The beads were washed 10 times with the corresponding Ca^{2+} or EGTA buffers before processing the samples by SDS-PAGE and Western blot for Src identification as described above.

5.19 Co-immunoprecipitation assays

Immunoprecipitation of Src, EGFR and OGT from A431 cells (2 mg protein) was performed using the Pierce™ Classic Magnetic IP/Co-IP kit, and anti-Src, anti-EGFR or anti-OGT antibodies and protein-A/G following the manufacture instructions. The samples were processed for SDS-PAGE and Western blot using the appropriate antibodies as described above.

5.20 Src phosphorylation assays

The auto-phosphorylation of recombinant c-Src (0.1 µg) was assayed at 37 ºC in a medium containing 15 mM Tris-HCl (pH 7.5), 5 mM $MgCl_2$, 1 mM DTT, 1 mM EGTA, 1.2 mM $CaCl_2$ (when added), and 2.3 µM CaM wild type, or the phospho-mimetic CaM(Y99D/Y138D) and CaM(Y99E/Y138E) mutants, when added. The reaction was

started upon addition of 2 mM ATP and stopped by the addition of Laemmli buffer and boiled for 5 min. The samples were subjected to Western blot and probed with an anti-phospho-tyrosine antibody (4G10) or an anti-phospho-Y416-Src specific antibody to detect active phosphorylated Src, and an anti-Src (total) antibody and/or GAPDH antibody as loading controls.

5.21 Src activation assays in living cells

In the case of A431 cells, Src was activated either upon ligand-dependent activation of the EGFR, as an upstream signaling component of c-Src (Sato et al., 2001), adding 10 nM EGF during 2 min; and in the case of both A431 and SK-BR-3 cells, upon induction of oxidative stress by adding 1 mM H_2O_2 for 15 min, as described (Basuroy et al., 2010). The reaction was arrested upon addition of ice-cold 1 % (v/v) TCA, and the samples were processed by SDS-PAGE and Western blot. The PVDF membranes were probed with anti-phospho-tyrosine (4G10) or anti-phospho-Y416-Src specific antibodies to detect active phosphorylated Src, anti-phospho-tyrosine antibody to detect activated EGFR, and anti-Src (total), anti-EGFR (total) and/or anti-GAPDH antibodies as loading controls.

5.22 *O*-GlcNAc detection in EGFR

EGFR was immunoprecipitated from A431 cells using the Pierce Classic Magnetic IP/Co-IP kit following the manufacturer instructions. Briefly, a lysate of A431 cells (1-2 mg proteins) were incubated with anti-EGFR antibody (1:500 dilution) overnight at 4 ºC. The lysate containing the antigen-antibody complex was mixed with the magnetic beads and incubated for 1 hour at room temperature. The beads were extensively washed and the EGFR was released with the low pH (pH 2) elution buffer, resolved in SDS-PAGE and subjected to Western blot using appropriate anti-*O*-GlcNAc antibodies (RL2 or CTD110.6). Conversely, a lysate of A431 cells (1-2 mg proteins) were incubated as above with an anti-*O*-GlcNAc antibody (RL2) and the immunoprecipitated *O*-GlcNAcylated proteins were resolved in SDS-PAGE and subjected to Western blot using and anti-EGFR antibody.

5.23 *In vitro* EGFR *O*-GlcNAcylation

Immunoprecipitated EGFR was used for *in vitro* *O*-GlcNAcylation assay using immunoprecipitated OGT, both immunoprecipitated from A431 cells. The *O*-GlcNAcylation reaction took place in a buffer containing 50 mM Tris-HCl (pH 7.5), 1 mM DTT, 12.5 mM $MgCl_2$ and 1 mM UDP-GlcNAc, and incubated for 2.5 h at 30 ºC. The reaction was stopped by adding Laemmli buffer and boiled for 10 min at 100 ºC,

resolved in SDS-PAGE, transferred to a PVDF membrane, and probed with an anti-*O*-GlcNAc antibody (RL2).

5.24 Metabolic protein labeling with azido-GlcNAc

A431 cells were seeded in 150 cm^2 petri dishes and when ~ 70 % confluence was obtained 40 μM GlcNAz was added and incubated for 72 h. The cells were lysed in a buffer containing 25 mM Tris-HCl (pH 7.4), 150 mM NaCl, 1 mM EDTA, 1 % (v/v) NP-40, 5 % (v/v) glycerol supplemented with 20 μM PUGNAc to prevent deglycosylation and a cocktail of protease inhibitors (0.5 mM 4-(2-aminoethyl) benzenesulfonyl fluoride, 0.4 μM aprotinin, 25 μM bestatin, 7.5 μM [1-[N-[(L-3-trans-carboxyoxirane-2-carbonyl)-L-leucyl]amino]-4-guanidinobutane], 10 μM leupeptin, 5 μM pepstatin A, and freshly prepared 0.6 mM PMSF). The lysate was centrifuged at 16,000 g for 10 min and the supernatant used for EGFR immunoprecipitation. Biotinylation of the GlcNAz-labeled proteins was performed using Click-iT®-Protein Reaction Buffer kit following the manufacturer's instructions, the samples were subjected to SDS-PAGE, the proteins transferred to PVDF and overlaid with streptavidin-HRP (1:10,000 dilution).

5.25 *N*-deglycosylation of the EGFR

The immunoprecipitated EGFR was first denatured in a buffer containing 0.5 % (w/v) SDS and 40 mM DTT and boiled for 10 min at 100 °C. Thereafter, 10 % (v/v) NP-40, 50 mM sodium phosphate (pH 7.5) and 1,000 units of PNGase F were added, and the mixture was incubated for 2 h at 37 ºC. One unit of PNGase F is defined as the amount of enzyme required to remove > 95 % of the carbohydrates from 10 μg of denatured RNase B in 1 hour at 37 °C. The reaction was stopped by the addition of Laemmli buffer and boiled for 10 min at 100 ºC, resolved in SDS-PAGE, transferred to a PVDF membrane and probed with anti-*O*-GlcNAc antibodies (RL2 or CTD110.6). When tunicamycin was used as a deglycosylation agent A431 cells were cultured in complete DMEM supplemented with 1 μg/ml tunicamycin overnight where only newly synthetized EGFR molecules are expected to be fully N-deglycosylated. Higher concentrations of tunicamycin to attain more N-deglycosylated EGFR molecules was not possible as more drastic treatments result in extensive cell death.

5.26 *O*-deglycosylation of the EGFR

The immunoprecipitated EGFR was first denatured in a buffer containing 0.5 % (w/v) SDS and 40 mM DTT and boiled for 10 min at 100 °C. Thereafter, 10 % (v/v) NP-40, 50 mM sodium phosphate (pH 7.5) and 200,000 units of *O*-glycosidase and 100

units of neuraminidase were added, and the mixture was incubated for 2 h at 37 ºC. One unit of *O*-glycosidase is defined as the amount of enzyme required to remove 0.68 nmol of *O*-linked disaccharide from 5 mg of neuraminidase digested, non-denatured fetuin in 1 hour at 37°C in a total reaction volume of 100 µl. The reaction was stopped by the addition of Laemmli buffer and boiled for 10 min at 100 ºC, resolved in SDS-PAGE, transferred to a nitrocellulose membrane and overlaid with the lectins WGA and PNA.

5.27 Effect of OGT and OGA inhibitors on EGFR *O*-GlcNAcylation

A431 cells were grown to confluence in 6-well culture dishes containing 2 ml of DMEM supplemented with 10 % (v/v) FBS overnight in the absence and presence of the OGT inhibitor BADGP (2 mM), or the OGA inhibitor Thiamet G (20 µM). Thereafter, the EGFR was immunoprecipitated from a cell lysate using an anti-EGFR antibody and the immunocomplex was processed by SDS-PAGE and Western blot using an anti-*O*-GlcNAc antibody (RL2). The effect of 2 mM BADGP and increasing concentrations (0.5-20 µM) of Thiamet G was also tested on total proteins *O*-GlcNAcylation level from an A431 cell lysate as positive control.

5.28 Expression and purification of recombinant ncOGT

His-tagged full-length human OGT (ncOGT) recombinant protein was expressed and purified as previously described (Gross et al., 2005). Briefly, the plasmid containing the sequence encoding the ncOGT was expressed in *E. coli* BL21(DE3)pLysS cells. Single colonies grown in solid medium in the presence of 100 µg/ml kanamycin were collected and seeded in 5 ml of Luria´s broth containing the same concentration of kanamycin. Larger cultures (500 ml) were seeded with the pre-culture and grown in the same conditions until they reached an $OD_{600\ nm}$ = 1-1.2. The expression of the recombinant protein was induced with 0.1-0.2 mM IPTG overnight at 16 ºC. The purification of the His-tagged ncOGT was performed using the BugBuster® Ni-NTA His•Bind® Purification kit according to the manufacturer instructions.

5.29 Lectin overlay

The lectin overlay was performed according to the manufacturer protocol with small modifications. Briefly, the detergent-solubilized EGFR was immunoprecipitated from A431 cells and treated with PNGase F, *O*-glycosidase, and Neuraminidase separated in 5-20 % polyacrylamide gradient gel and transferred to nitrocellulose membranes as described above. The membranes were then washed in PBS (pH 7.5) and blocked for two minutes with PBS (pH 7.5) with 0.25 % (v/v) Tween-20 and rinsed with PBS (pH 7.5), 0.05 % (v/v) Tween-20, twice. Afterwards the membranes were

overlaid with 1 µg/ml biotin-labeled WGA or PNA for two hours at 20 °C in a buffer containing PBS (pH 7.5), 0.1 % (v/v) Tween-20, 1 mM $CaCl_2$, 1 mM $MnCl_2$ and 1 mM $MgCl_2$. Then the membranes were extensively washed with PBS (pH 7.5) 0.1 % (v/v) Tween-20 and incubated with streptavidin-HRP (1:10000) for 45 min in PBS (pH 7.5) 0.1 % (v/v) Tween-20, extensively washed with PBS with 0.05 % (v/v) Tween-20 and revealed with ECL.

5.30 Artificial wound-healing assays

Artificial wounds were done with a plastic pipette scratching a monolayer of confluent A431. The wounded monolayers were washed twice with fresh media to remove non-adherent cells before photographs were taken every hour for 72 hours using a Cell Observer system equipped with Zeiss Axiovert 200M Multi-stage Automated microscope with a 4x objective to follow the repopulation of the wounds. The cells were incubated in DMEM containing 1 % (v/v) FBS, in the absence or the presence of 10 nM EGF, 100 µM Thiamet G or 1 mM BADGP.

5.31 Ca^{2+}-dependent CaM-affinity chromatography of OGT

The isolation of recombinant ncOGT by Ca^{2+}-dependent CaM-affinity chromatography was carried out loading the purified recombinant ncOGT in a small column (1-2 ml bed volume) of CaM-Sepharose 4B equilibrated with a buffer containing 25 mM Hepes-NaOH (pH 7.4), 1 % (w/v) Triton X-100, 5 % (w/v) glycerol, 0.1 mM $CaCl_2$, and the protease inhibitors cocktail described above (Ca^{2+}-buffer). The column was washed with 20 volumes of the Ca^{2+}-buffer, and ncOGT was eluted using the same buffer but containing 1 mM EGTA instead of $CaCl_2$ (EGTA-buffer). Proteins in the eluted fractions were precipitated with 10 % (w/v) TCA and processed by SDS-PAGE and Western blot for OGT identification using an anti-OGT antibody.

5.32 Statistical analysis

The paired Student's t and the two-way ANOVA tests were performed using the Microsoft Excel (Microsoft Co., Redmon, WA) and GraphPad Prism (GraphPad Software Inc., La Jolla, CA) software programs. Data were expressed as the mean ± SEM or SD/range and differences were considered significant at $p \leq 0.05$ as indicated in the legends to the figures.

6. RESULTS

As CaM can be phosphorylated (Benaim and Villalobo, 2002), and in order to better understand its physiological functions in systems relevant for tumor cell biology, we decided to study the functionality of phospho-(Y)-CaM using a set of recombinant phospho-(Y)-mimetic CaM mutants by substituting either one or the two tyrosine residues to aspartic acid (Asp, D) or glutamic acid (Glu, E). Then we characterized their physicochemical properties and tested *in vitro* their action on the activity of several CaM-dependent enzymes: the 3',5'-cyclic nucleotide PDE1 (EC 3.1.4.17), eNOS (EC 1.14.13.39), c-Src (EC 2.7.10.2) and EGFR (EC 2.7.10.1).

6.1. Expression and purification of the phospho-(Y)-mimetic CaM mutants

In order to confirm if the generated mutants preserve the general structural and functional properties of wild type CaM and modulate CaM-dependent systems such as PDE1, eNOS, EGFR, and c-Src we performed an extensive physicochemical characterization of the generated CaM mutant species. The first step was to transform *E. coli* BL21(DE3)pLysS with the vectors containing the sequence of the whole panel of mutants: CaM(Y99D), CaM(Y138D), CaM(Y99D/Y138D), CaM(Y99E), CaM(Y138E) and CaM(Y99E/Y138E) and purify significant amount of each species. The expression of wild type and the different CaM mutants in *E.coli* BL21(DE3)pLysS was very efficient and their purification yielded an average ± SEM (n = 12) 13 ± 2 mg CaM per 500 ml of bacterial culture. Figure 8A shows an example of the expression of the mutants CaM(Y99E), CaM(Y138E), CaM(Y99E)/Y138E, CaM(Y99D), CaM(Y138D), and CaM(Y99D/Y138D) induced by IPTG addition, and the material obtained in the supernatant after heating the extracted proteins at 95 ºC for 5 min. It can be seen that CaM is the majoritarian heat-resistant protein. After Ca^{2+}-dependent phenyl-Sepharose chromatography all purified CaM species were homogeneous in SDS-PAGE (Figure 8B). The CaM variants presented a single band (~ 18 kDa) when electrophoretically separated in the presence of EGTA (absence of Ca^{2+}). In the presence of Ca^{2+}, however, wild type CaM and both CaM(Y99D) and CaM(Y99E) mutants presented the typical Ca^{2+}-induced electrophoretic mobility shift (Burgess et al., 1980), yielding a major band at ~ 15 kDa and a minor one with lower mobility. The electrophoretic mobility shift was less apparent in the single mutants CaM(Y138D) and CaM(Y138E), and in the double mutants CaM(Y99D/Y138D) and CaM(Y99E/Y138E) (Figure 8B).

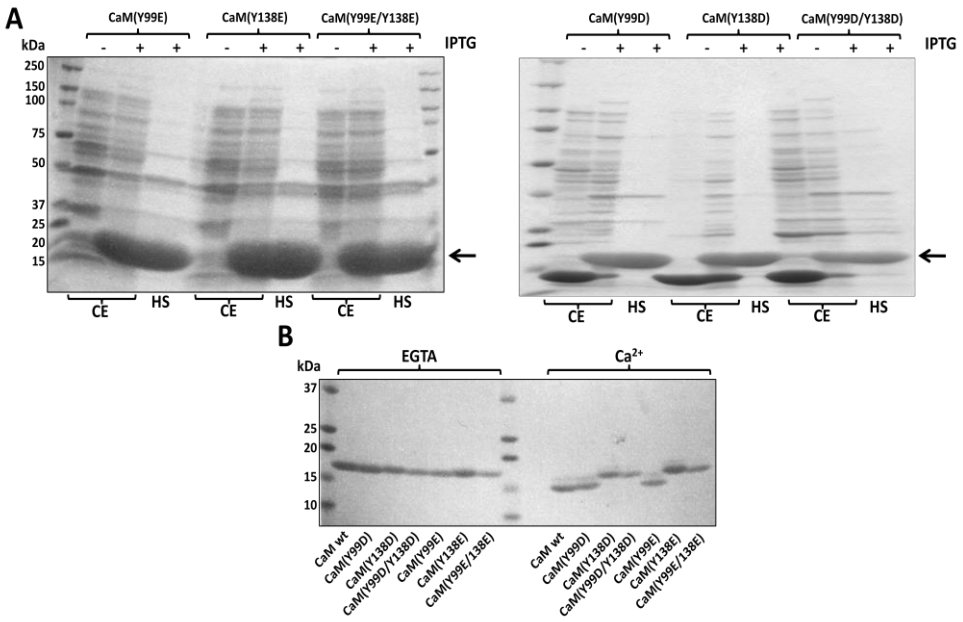

Figure 8: Expression and purification of the different CaM species. (*A*) The figure shows the pattern of proteins of the bacterial cell extract (CE) and the corresponding heated supernatant (HS) of CaM Y/E mutant species (*left panel*) and CaM Y/D mutant species (*right panel*) in the absence and presence of 0.5 mM IPTG for 4 h as described in Materials and Methods. (*B*) The different recombinant CaM species (~ 1-2 µg) purified as described in Materials and Methods were separated by SDS-PAGE in the presence of 5 mM EGTA or 1 mM $CaCl_2$ to observe the Ca^{2+}-induced mobility shift.

6.1.1 UV absorption spectra of the phospho-(Y)-mimetic CaM mutants

Since CaM has no tryptophan (W, Trp) to contribute to the UV-spectrum of the protein in the range of 280 nm, the tyrosine (Y, Tyr) absorption peak at 276 nm is very well defined, thus allowing us to detect the changes taking place in that region due to the subsequent removal of one or two Tyr residues. The UV absorption spectra (240-340 nm) of wild type CaM and the whole panel of Y/D and Y/E mutants are shown in Figure 9. As expected wild type CaM showed the characteristic absorption peaks at 252, 258, 265, 269 and 276 nm (Wolff et al., 1977), and the latest one due to the presence of tyrosine residues. As expected, the single Y/D and Y/E CaM mutants presented a significant reduction of the 276 nm peak, while this peak totally disappeared in the double mutants CaM(Y99D/Y138D) and CaM(Y99E/Y138E). The Y99D and Y99E substitutions presented a slightly higher decrease in the 270-285 nm region of the absorption spectrum than identical substitutions at Y138, pointing out a higher contribution of Y99 to the spectrum of wild type CaM. Moreover, no significant spectral differences between the respective Y/D and Y/E CaM mutants were found.

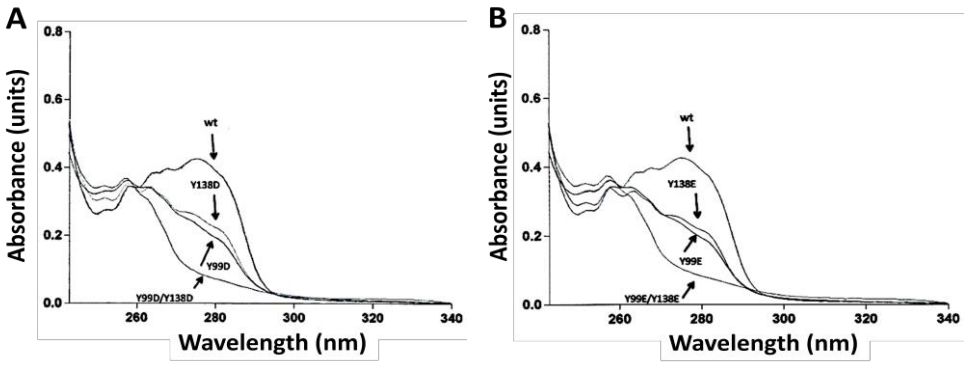

Figure 9: Absorption spectra of the different CaM species. The plots show UV-light absorption spectra of recombinant wild type (wt) and the indicated Y/D (A) and Y/E (B) CaM mutants (2 mg/ml) purified as described in Materials and Methods and dialyzed against 20 mM Tris-HCl (pH 7.5).

6.1.2 Circular dichroism studies of the phospho-(Y)-mimetic CaM mutants

Circular dichroism (CD) is a very powerful tool to study conformational features of proteins in solution (Kelly et al., 2005). In the absence of Ca^{2+}, the far-UV (200-260 nm) CD spectra of wild type and the full set of CaM mutants showed the characteristic negative maxima at 208 and 222 nm (Figure 10), typical of proteins with a high percentage of α-helical content. Ca^{2+} binding induces further deepening of the spectra due to an increase in the amount of α-helical structure (Martin & Bayley, 1986).

However, the ratio of molar ellipticity at 208 and 222 nm, a sensitive indicator of possible alterations in interactions between neighboring helices (Sun et al., 2001, Fasman, 1996), was slightly higher for the mutants (Table 3), pointing to subtle differences in helix packing compared to wild type CaM. For all the samples, there was a significant, mutant-specific, deepening of the far-UV signals in the presence of Ca^{2+} that may reflect a differential increase in α-helical content and/or reorientation of existing α-helices (Wang et al., 2011, Protasevich et al., 1997). Also, both CaM(Y99D/Y138D) and CaM(Y99E/Y138E) mutants presented a slight blue-shift of the 208 nm minimum in the absence of Ca^{2+} as compared to wild type CaM (Figure 10).

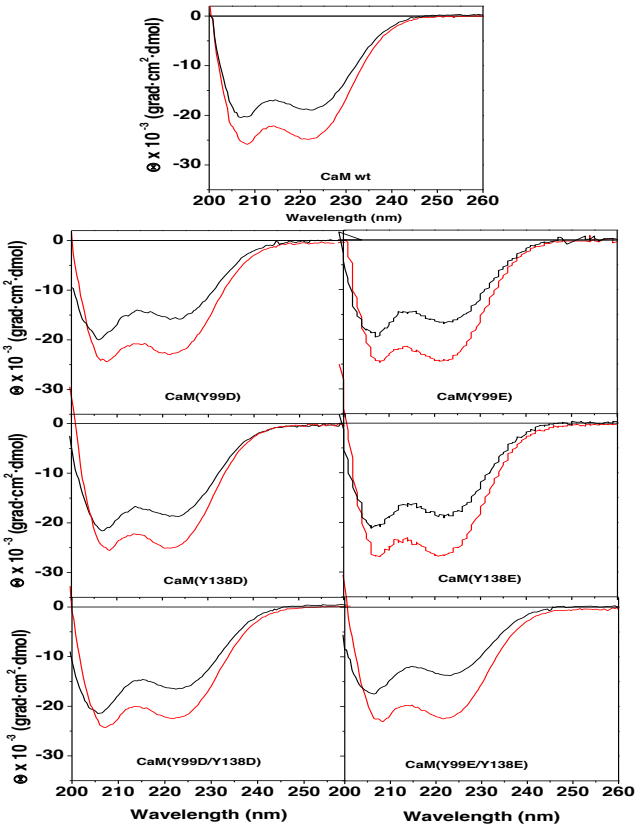

Figure 10: Ca^{2+}-induced changes in the Far-UV CD spectra of the different CaM species. Far-UV CD spectra of wild type (wt) and the Y/D and Y/E CaM mutants (12 μM) were recorded at 20 ºC in 20 mM Tris-HCl (pH 7.5), 0.1 M KCl, containing 1 mM EGTA (black lines) or 1 mM $CaCl_2$ (red lines).

As shown in Figure 11A, the ellipticity at 222 nm increased in the presence of Ca^{2+} 22 ± 3 % for wild type CaM, while for the Y138D and Y138E mutants the increase was of 32-35 %, and for the Y99D, Y99E, and double Y/E mutants it reached values of 50 % and above, the only exception being the CaM(Y99D/Y138D) mutant where no significant change was observed. Interestingly, the magnitude of the increase in ellipticity at 222 nm is directly correlated to the value of the $\Theta_{208}/\Theta_{222}$ ratio. On the other hand, percentage of Ca^{2+}-induced increases in ellipticity at 208 nm and variations among CaM species were noticeably smaller, going from 14 % to 29 % (Figure 11B).

As a result, no significant differences in the $\Theta_{208}/\Theta_{222}$ ratio were observed in the presence of Ca^{2+}, again with the only exception of the CaM(Y99D/Y138D) mutant (Table 1) revealing a similar overall structure of the holo forms. Above all, far-UV data clearly show that all the single and double Y/D and Y/E CaM mutants bind Ca^{2+}.

Sample	$\Theta_{208}/\Theta_{222}$		Θ_{208} Ca^{2+}/ Θ_{208} EGTA	Θ_{222} Ca^{2+}/ Θ_{222} EGTA
	EGTA	Ca^{2+}		
CaM wt	1.09 ± 0.01	1.01 ± 0.01	1.14 ± 0.05	1.22 ± 0.03
CaM(Y99D)	1.20 ± 0.01	1.01 ± 0.01	1.29 ± 0.01	1.52 ± 0.03
CaM(Y99E)	1.17 ± 0.01	1.00 ± 0.01	1.26 ± 0.01	1.48 ± 0.02
CaM(Y138D)	1.12 ± 0.01	1.01 ± 0.01	1.22 ± 0.02	1.35 ± 0.02
CaM(Y138E)	1.14 ± 0.02	1.02 ± 0.01	1.19 ± 0.06	1.32 ± 0.05
CaM(Y99D/Y138D)	1.23 ± 0.03	1.10 ± 0.01	1.15 ± 0.09	1.21 ± 0.05
CaM(Y99E/Y138E)	1.19 ± 0.02	1.03 ± 0.01	1.26 ± 0.03	1.55 ± 0.08

Table 3: $\Theta_{208}/\Theta_{222}$ ellipticity ratio in the absence and presence of Ca^{2+} of the different CaM species.

Ca^{2+}-binding also induces noticeable changes in the near-UV circular dichroism spectrum of wild type CaM (Sun et al., 2001, Wolff et al., 1977, Martin and Bayley, 1986), which is sensitive to the environment of the six phenylalanines and the two tyrosine residues in the molecule. As shown in Figure 12, in the presence of EGTA the spectrum is characterized by two well-defined negative bands at 262 and 269 nm, due to the phenylalanine residues, and a broad negative region centered at 280 nm due to the tyrosine residues.

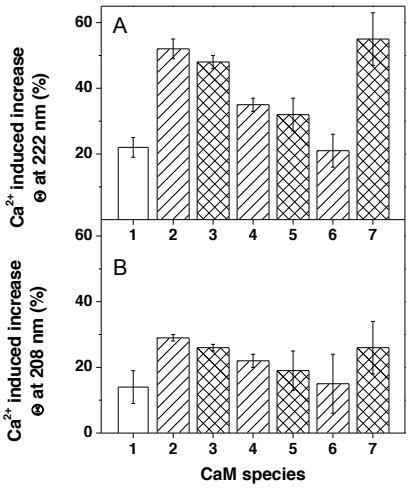

Figure 11: Percentage increase of ellipticity of the different CaM mutants in the presence of Ca^{2+} detected by CD at 222 and 208 nm. The mean ± SEM (n = 3) increase in ellipticity in the far-UV circular dichroism signals at 222 nm (A) and 208 nm (B) of the different CaM species 1, CaM wild type; 2, CaM(Y99D); 3, CaM(Y99E); 4, CaM(Y138D); 5, CaM(Y138E); 6, CaM(Y99D)/Y138D; and 7, CaM(Y99E)/Y138E) is represented as percentage taking as 100 % the ellipticity of each CaM species in the presence of EGTA. Measurements were carried out at 20 ºC in 20 mM Tris-HCl (pH 7.5), 0.1 M KCl, containing 1 mM EGTA or 1 mM $CaCl_2$. The concentration of CaM was 12 µM.

Addition of Ca^{2+} results in an increase of these ellipticity signals, what has been interpreted as a change in the environment of both phenylalanine and tyrosine residues. Having confirmed by far-UV CD experiment that all single and double Y/D and Y/E mutants bind Ca^{2+}, we also examined the near-UV CD spectra of their apo and holo forms. In the absence of Ca^{2+}, the ellipticity around 280 nm of the mutants diminished noticeably or even became positive (Figure 12), confirming a predominant contribution of the two tyrosine residues to this region. In addition, there was a significant decrease in the intensity of the bands at 262 and 269 nm compared to wild

type CaM, pointing to a partial contribution of both tyrosine residues to these signals. However, addition of Ca^{2+} induced different changes in the spectra depending on the mutant. While the Y99D/E mutants showed a small decrease in positive ellipticity at 280 nm, for the respective Y138 mutants the ellipticity change becames almost zero (Figure 12). Differences related to the 262/269 nm bands were even more apparent.

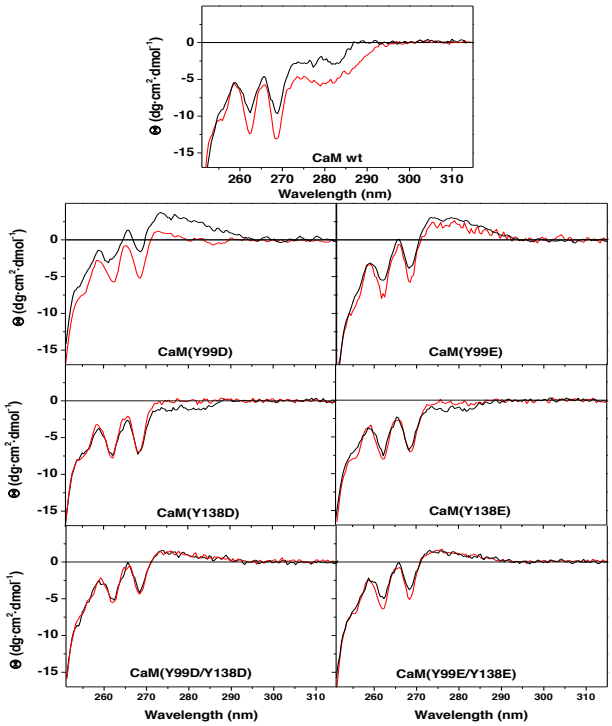

Figure 12: Ca^{2+}-induced changes in the near-UV circular dichroism spectra of the different CaM species. Near-UV CD spectra for wild type (*wt*) and the single and double Y/D and Y/E CaM mutants (118 µM) were recorded at 20 ºC in 20 mM Tris-HCl (pH 7.5), 0.1 M KCl, containing 1 mM EGTA (black lines) or 1 mM $CaCl_2$ (red lines). Ellipticity values were normalized per mole of residue.

There was a clear increase in ellipticity for the Y99D/E mutants upon Ca^{2+} binding, while little or no change was observed for the Y138D/E and double mutants (Figure 12), clearly revealing that the Ca^{2+}-induced alterations observed for wild type CaM in this region are mostly due to changes in the environment of Y138. This conclusion fully explains the small effect of Ca^{2+} on the near-UV CD spectrum of the separate CaM N-terminal half (residues 1-77) previously reported (Martin and Bayley, 1986), a result considered surprising by the authors in view of the similar distribution of phenylalanine residues in the N- and C-terminal halves of the protein. Indeed, the spectra with/without Ca^{2+} of the Y138D/E and double CaM mutants (Figure 12) are very similar to those published for the N-terminal half of CaM (Martin and Bayley, 1986).

It is known that Ca^{2+} binding induces a remarkable increase in the thermal stability of wild type CaM (Wang et al., 2011, Brzeska et al., 1983). In order to test whether the same was true for the single and double Y/D and Y/E mutants, we carried out thermal denaturation experiments by measuring changes in ellipticity at 222 nm (Supplementary Figure 1S) at increasing temperature. Figure 13 shows a quasi-sigmoidal decrease in ellipticity of wild type and all CaM mutants in the absence of Ca^{2+}, indicating the occurrence of at least one intermediate state, as previously described for wild type CaM (Sun et al., 2001, Wang et al., 2011). In the case of the CaM Y138D/E mutants, the temperature-dependent unfolding was clearly biphasic, showing a notable deviation of sigmoidicity at temperatures below 50 ºC.

Although fitting the data to a two- or three-state model did not yield acceptable clear-cut information, it is evident from the denaturation profiles that a major thermal unfolding for the different CaM species occurred at ~ 55 ºC, all of them being completely unfolded above 70 ºC. In addition, lower temperature transitions and/or discontinuities, also reported for wild type CaM (Brzeska et al., 1983, Martin and Bayley, 1986, Kilhoffer et al., 1981, Gangola and Pant, 1983) were observed in the ~ 20-40 ºC region, both in the absence and presence of Ca^{2+}. The binding of Ca^{2+} had a profound impact on the stability of wild type CaM and the mutants above 40 ºC. Therefore, the major unfolding transition occurring at ~ 55 ºC in the presence of EGTA was not observed when Ca^{2+} is present, and more than 54 % of the initial ellipticity signal was still preserved at 90 ºC (Figure 13), confirming that Ca^{2+} binding to the single and double Y/D and Y/E CaM mutants also causes remarkable thermal stabilization.

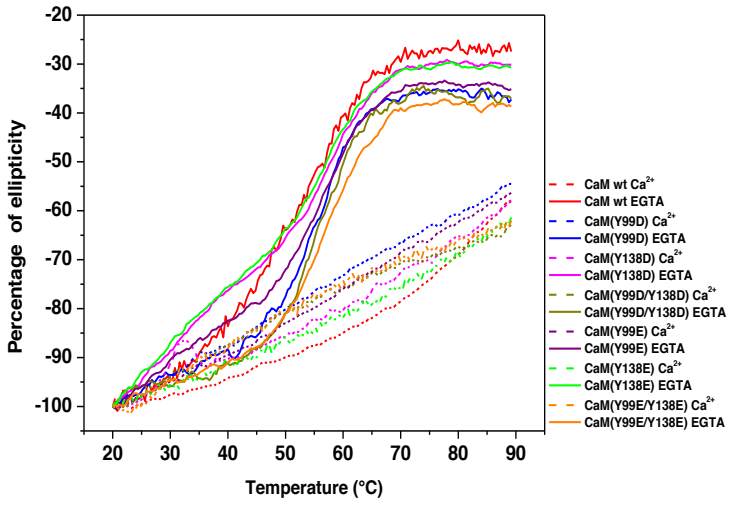

Figure 13: Thermal stability of the different CaM mutants in the absence and presence of Ca^{2+}. The plots present the decrease in the CD signal at 222 nm, expressed as percentage of the ellipticity at 20 ºC, for wild type (*wt*) and the single and double Y/D and Y/E CaM mutants (12 µM) in 20 mM Tris-HCl (pH 7.5), 0.1 M KCl, in the presence of 1 mM EGTA (*solid lines*) and 1 mM $CaCl_2$ (*dashed lines*) as described in Materials and Methods.

6.1.3 Fluorescence studies of the phospho-(Y)-mimetic CaM mutants

We also studied the fluorescence energy transfer from excited tyrosine residues to Tb^{3+}, a surrogate ion that binds CaM at the Ca^{2+}-binding sites, in wild type CaM and the different CaM mutant species by measuring the fluorescence emitted by Tb^{3+} in the 535-550 nm region upon exciting at 280 nm the tyrosine residues (when present) located at Ca^{2+}-binding sites III and IV of CaM. The spectrum obtained for wild type CaM presented a distinctive emission peak at 543 nm upon addition of increasing concentrations of Tb^{3+} to the medium (Figure 14A). Interestingly, the absence of Y99 induced an almost complete loss of the Tb^{3+} emission peak at 543 nm, whereas the absence of Y138 did not (Figure 14A). A similar behavior was observed for the Y/D and Y/E mutants. The Tb^{3+} titration curves shown in Figures 15B and 15C demonstrated that the apparent binding affinity of the Tb^{3+} ion to wild type CaM was slightly higher (K'_d ~ 20 μM) than for the CaM(Y138D) or CaM(Y138E) mutants (K'_d ~ 50 and 75 μM, respectively). Only trace fluorescence emission of Tb^{3+} was detected in the CaM Y99D/E mutants, and no significant fluorescence was detected in the double Y/D or Y/E mutants.

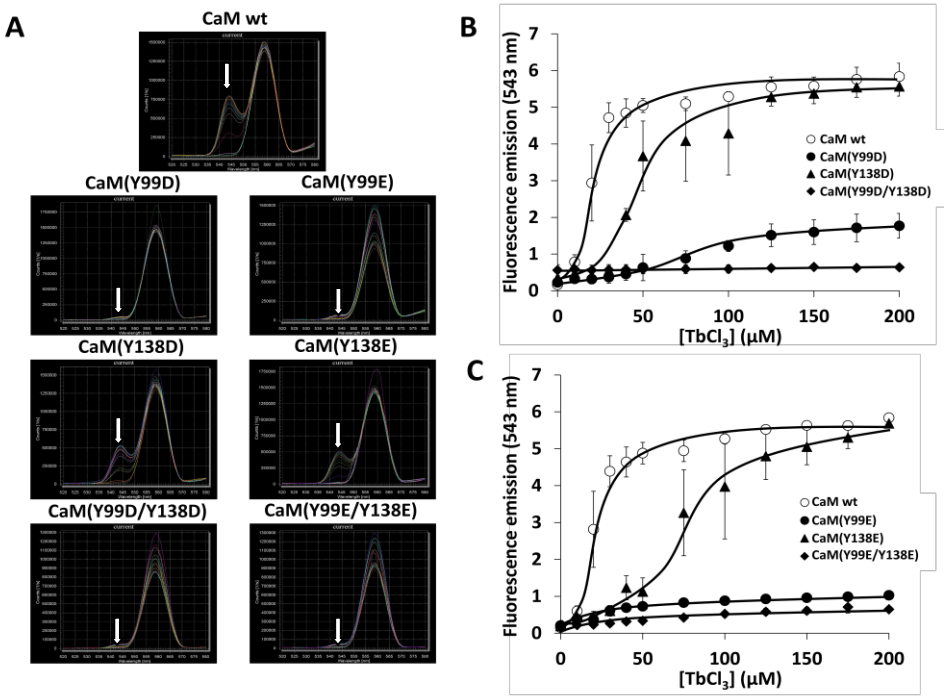

Figure 14: Tb^{3+}-induced fluorescence emission spectra of the different CaM species. (A) The fluorescence emission spectra (520-580 nm) of wild type (*wt*) CaM and the indicated CaM mutants (10 μM) was recorded in a buffer containing 10 mM Pipes-HCl (pH 6.5) and 100 mM KCl in the absence and presence of increasing concentrations of $TbCl_3$ (10-200 μM) as described in Materials an Methods. (B, C) The plots present the emission fluorescence at 543 nm of wild type (*wt*) CaM and the indicated CaM mutants (10 μM) at increasing concentrations of $TbCl_3$ in the conditions described in Materials and Methods.

6.2 Biological activity of the phospho-(Y)-mimetic CaM mutants

We first tested the capacity of c-Src to phosphorylate the different CaM species. Figure 15 shows that both CaM(Y99D) and CaM(Y99E) were phosphorylated *in vitro* by recombinant c-Src with similar efficiency than wild type CaM. However, the CaM Y138D/E mutants were phosphorylated with far lower efficiency than wild type CaM, suggesting that Y138 is preferrebly phosphorylated by the kinase. As expected, no phosphorylation of the double mutants was detected.

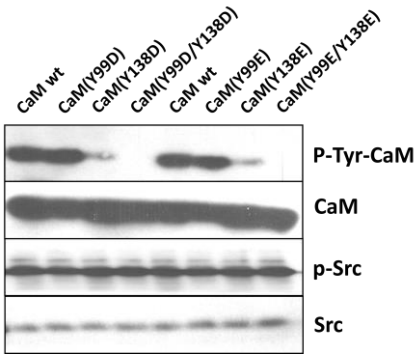

Figure 15: Phosphorylation of different CaM species by recombinant c-Src. The different CaM species (2 µg) were assayed for phosphorylation by recombinant c-Src as described in Materials and Methods. The samples were probed with an anti-phospho-tyrosine antibody to detect the tyrosine-phosphorylated CaM species (*P-(Y)-CaM*) and auto-phosphorylated c-Src (*p-Src*). The membranes were striped and reprobed with anti-CaM and anti-Src antibodies as loading controls.

6.2.1 Effect of the phospho-(Y)-mimetic CaM mutants on PDE1 activity

We next tested the effect of purified phospho-(Y)-CaM free of non-phosphorylated CaM on the CaM-dependent enzyme cyclic nucleotide PDE1. Figure 16A shows the slightly lower activatory effect of phospho-(Y)-CaM compared to non-phosphorylated CaM.

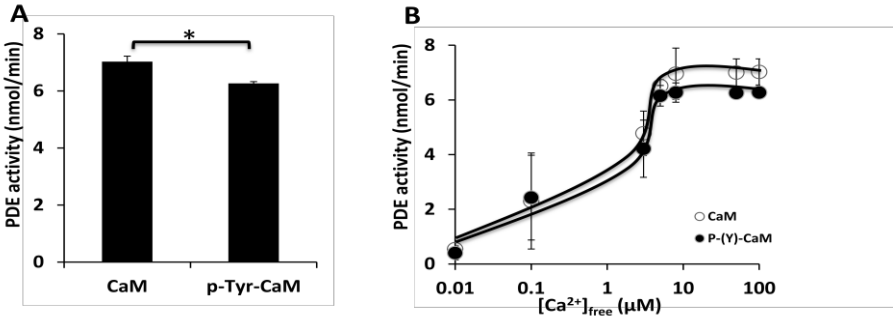

Figure 16: Effect of phospho-(Y)-CaM and non-phosphorylated CaM on the PDE1 activity. (A) The plot presents the average ± SEM PDE1 activity in the presence non-phosphorylated CaM or phospho-(Y)-CaM (0.97 µM) in three independent experiments (* p = 0.03 using the Student's t test) as described in Materials and Methods. (B) The plot presents the average ± range activity of PDE1 assayed in the presence of non-phosphorylated CaM (open symbols) and phospho-(Y)-CaM (filled symbols) (0.97 µM) in two independent experiments assayed at increasing concentrations of free Ca^{2+} as described in Materials and Methods.

In addition, an assay performed at increasing concentrations of free Ca^{2+} in the presence of phospho-(Y)-CaM and non-phosphorylated CaM showed no significant

differences in the apparent affinity for free Ca^{2+} and at saturating concentrations of Ca^{2+} a small decrease (~ 10 %) of PDE1 activity in the presence of phospho-(Y)-CaM compared to non-phosphorylated CaM was observed (Figure 16B).

We then tested the effect of the full set of mutants on the CaM-dependent activation of PDE1. Figure 17 shows that all the Y/D and Y/E CaM mutants were able to activate PDE1 in the presence of Ca^{2+} as it does wild type CaM. However, the CaM-dependent activity attained with CaM(Y99D/Y138D) was consistently lower (~ 20 %) than with the other CaM species, including the CaM(Y99E/Y138E) mutant.

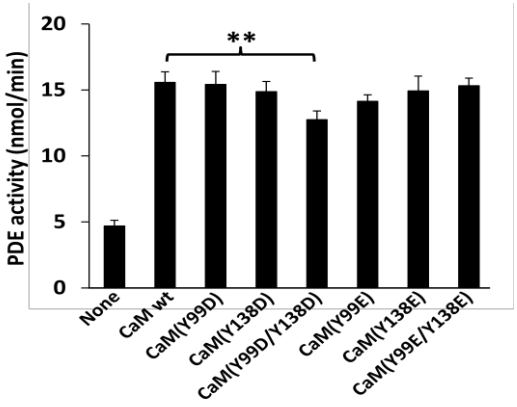

Figure 17: Effect of the different CaM species on the activity of PDE1. The cyclic nucleotide PDE1 activity was assayed in the absence (None) and presence of the indicated CaM species (1.9 μM) in the presence of 100 μM free Ca^{2+} as described in Materials and Methods. The plot presents the average ± SEM of triplicate samples from three separate experiments (** p = 0.02 using the Student's t test).

We also performed the PDE1 assay at increasing concentrations of the CaM mutant species, as compared to wild type CaM, and in agreement with the previous result CaM(Y99D/Y138D) showed no significant differences in the K_{act} (~ 5-10 nM), but a small decrease (~ 20 %) in the V_{max} of the enzyme (Figure 18A). The single CaM(Y99D) and CaM(Y138D) did not presented any differential effect on the PDE1 activation and they behaved as CaM wild type. No significant differences in the K_{act} and the V_{max} of the enzyme were detected when CaM Y/E mutants were tested in the same assay conditions, and all the Y/E mutants behaved as CaM wild type (Figure 18B).

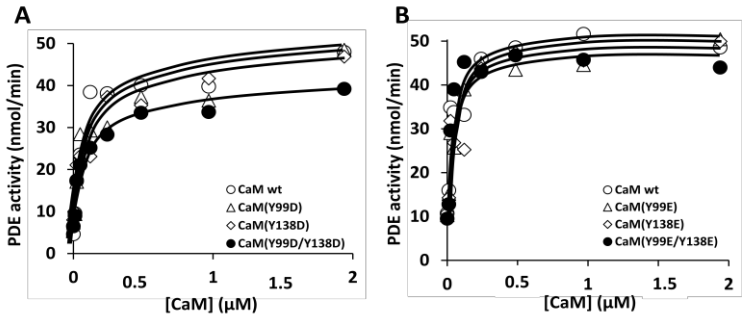

Figure 18: Effect of different concentrations of wild type CaM and the different CaM mutants on the activity of PDE1. The plots present the PDE1 activity assayed as in Figure 17 but using increasing concentrations of CaM Y/D (A) and CaM Y/E (B) mutants.

When the assays were performed at increasing concentrations of free Ca^{2+} no significant changes in the apparent affinity for free Ca^{2+} (~ 5 μM) between wild type and the double Y/D and the double Y/E CaM mutants was noticed (Figure 19). And again a decrease (~ 20-30 %) in the CaM-dependent activity of PDE1 at saturating concentrations of free Ca^{2+} was observed with CaM(Y99D/Y138D), unlike with CaM(Y99E/Y138E), who presented similar activatory effect as compared to the wild type CaM (Figure 19).

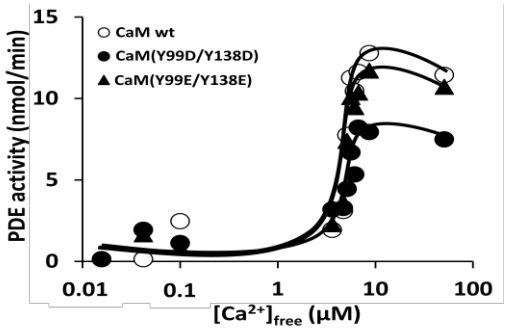

Figure 19: Effect of different Ca^{2+} concentrations on the CaM-dependent PDE1 activity. The plot presents the PDE1 activity assayed as in Figure 17 in the presence of the indicated CaM species (1.9 μM) at increasing concentrations of free Ca^{2+} using an EGTA/Ca^{2+} buffer as described in Materials and Methods.

We also performed PDE1 assays using isothermal titration calorimetry. Serial injections of cAMP were made into the sample cell loaded with PDE1, in the absence or presence of CaM wild type or the CaM(Y99D/Y138D) mutant (3.8 μM). Figure 20A shows heat production over time from serial injection of cAMP until the reaction reaches the plateau and the system was completely saturated. We determined the apparent enthalpy of the reaction ΔH_{app} to be -19.9 ± 0.5 kcal/moles, indicative of no product inhibition in experiments similar to the one shown in Figure 20A, but instead of injecting serial dilution we injected saturating conditions of cAMP. Knowing the enthalpy of the reaction we then performed the experiment in the absence or presence

of wild type CaM and CaM(CaMY99D/Y138D). Figure 20B shows a typical experiment where the presence of wild type CaM greatly enhanced PDE1 activity, while CaM(Y99D/Y138D) had a lesser effect.

We were able to determine from the data presented in Figure 20 the kinetic parameters of the reaction. We determined in a series of similar experiments that the PDE1 activity increased 2.61 ± 0.22 and 1.94 ± 0.09 ($p<0.03$) folds upon addition of wild type CaM and CaM(Y99D/Y138D), respectively.

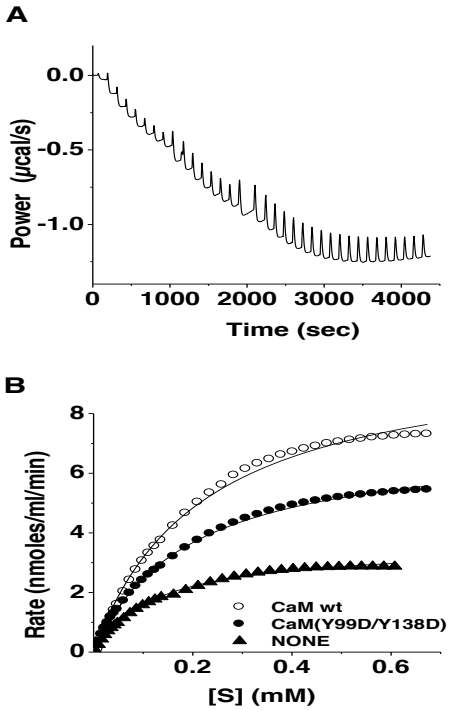

Figure 20: Effect of different CaM species on the kinetics of PDE1 determined by isothermal titration calorimetry. (A) The trace corresponds to a typical experiment showing the rate of heat produced by PDE1 over time after injections of different pulses of cAMP from which the activity of the enzyme can be derived as described in Materials and Methods. This particular trace corresponds to an experiment performed in the absence of CaM using 0.04 units of PDE1. (B) The plot presents the PDE1 activity (normalized for 0.04 units of enzyme) at increasing concentrations of cAMP in the absence (filled triangles) and presence of wild type CaM (open circles) or CaM(Y99D/Y138D) (filled circles) (3.8 µM) in a buffer containing 50 mM imidazol-HCl (pH 7.5), 200 mM NaCl, 5 mM $MgCl_2$, 0.4 mM EGTA, and 0.5 mM $CaCl_2$ using ITC as described in Materials and Methods setting the micro-calorimeter chamber 37 ºC.

Moreover, the V_{max} was determined to be 7.4 ± 2.8 and 5.5 ± 2.3* ($p<0.05$) nmols/s in the presence of wild type CaM and CaM(Y99D/Y138D), respectively, while the K_m of the enzyme for cAMP was the same (221 ± 27 µM) in the presence of both CaM species (Table 4).

CaM species	V_{max},(exp) (nmols/sec)	Km (fit) (µM)	V_{max} (fit) (nmols/sec)
None	1.8±1.1	170.3 ±94.5	2.4±1.5
CaM wt	5.3±2.1	221.6 ±17.6	7.4±2.8
CaM (Y99D/Y138D)	3.9±1.3	221 ±37.3	5.5±2.3*

Table 4: Kinetic values of PDE1 in the absence and presence of CaM wild type and CaM(Y99D/Y138D).

6.2.2 Effect of the phospho-(Y)-mimetic CaM mutants on eNOS activity

First we tested the comparative action of non-phosphorylated-CaM and phospho-(Y)-CaM on the activation of recombinant eNOS. Figure 21A shows that phospho-(Y)-CaM increased the activity of eNOS more efficiently (~ 30 %) than non-phosphorylated CaM, suggesting that phospho-(Y)-CaM have higher capacity to activate eNOS. When the assay was performed at increasing concentrations of free Ca^{2+} no significant changes in the apparent affinity for free Ca^{2+} (~ 4-6 μM) when compared non-phosphorylated CaM and phospho-(Y)-CaM was observed (Figure 21B).

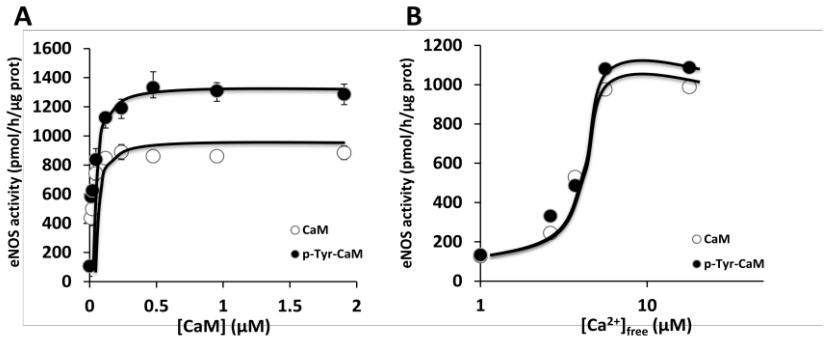

Figure 21: Effect of phospho-(Y)-CaM and non-phosphorylated CaM on the activity of eNOS. (*A*) The plot presents the average ± range activity of eNOS of two independent experiments assayed at increasing concentrations of non-phosphorylated CaM (*open symbols*) or phospho-(Y)-CaM (*filled symbols*) prepared as described in Materials and Methods. (B) The plot presents the activity of eNOS assayed at increasing concentrations of free Ca^{2+} in the presence of non-phosphorylated CaM (*open symbols*) or phospho-(Y)-CaM (*filled symbols*) prepared as described in Materials and Methods.

We tested the comparative action of wild type CaM, CaM(Y99D/Y138D) and CaM(Y99E/Y138E) on the activation of recombinant eNOS. Figure 22A shows that both double Y/D and Y/E CaM mutants strongly activate eNOS in assays performed in the presence of Ca^{2+}, and this activation was slightly more efficient than when wild type CaM was used. When eNOS was assayed at increasing concentrations of the different CaM species (Figure 22B), no significant differences in the K_{act} (~ 0.1 μM) were observed between wild type and the double Y/E CaM mutant. In contrast, a slight increment (~ 30 %) in the V_{max} compared to wild type CaM was noticeable with CaM(Y99E/Y138E). When we tested the effect of the CaM Y/D and Y/E double mutants on eNOS activity at increasing concentrations of free Ca^{2+} no significant changes in the apparent affinity for free Ca^{2+} (~ 4–6 μM) compared to wild type CaM was detected (Figure 22C).

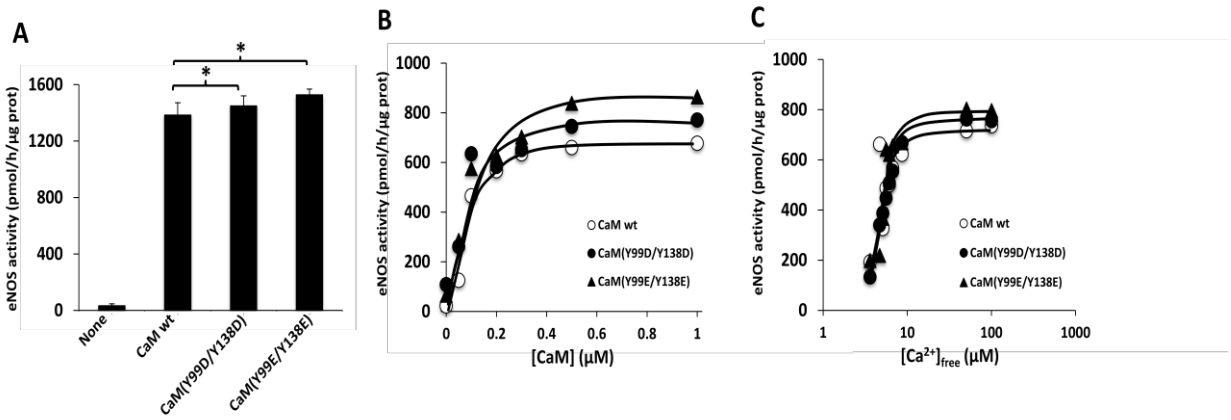

Figure 22: Effect of different CaM wild type and the double Y/D(E) CaM mutants on the activity of eNOS. (*A*) eNOS was assayed in the absence (*None*) and presence of the indicated CaM species (4.7 µM) in the presence of 1 mM free Ca^{2+} as described in Materials and Methods. The plot presents the average ± SEM of triplicate samples from three separate experiments ($p \leq 0.05$ using the Student's t test). (*B*) The plot presents the eNOS activity assayed as in *A* but using increasing concentrations of the indicated CaM species. (*C*) The plot presents the eNOS activity assayed as in *A* in the presence of the indicated CaM species (4.7 µM) at increasing concentrations of free Ca^{2+} using an EGTA/Ca^{2+} buffer as described in Materials and Methods.

6.3 CaM regulates c-Src in Ca^{2+}-dependent and Ca^{2+}-independent manners

The proto-oncogene product c-Src and its related oncoprotein v-Src play important roles in tumor progression and metastasis (Parsons and Parsons, 2004, Wheeler et al., 2009). Notable among the upstream receptors activating c-Src mediating strong metastatic responses are those coupled to G proteins (GPCR), and RTKs, such as EGFR (Parks and Ceresa, 2014) and ErbB2/Her2, as the later promotes the expression and stability of c-Src (Tan et al., 2005).

6.3.1 Apo-CaM and Ca^{2+}/CaM both interact with c-Src

We first performed a typical Ca^{2+}-dependent CaM-affinity chromatography using a detergent-solubilized membrane fraction from A431 tumor cells in order to determine whether Src binds CaM in a Ca^{2+}-dependent manner. Figure 23A shows that actually at least a fraction of the c-Src loaded in the column in the presence of Ca^{2+} can be eluted with a buffer containing EGTA.

As this technique does not show whether part of Src remained bound to CaM-Sepharose in the absence of Ca^{2+}, we performed pull-down experiments using Sepharose with immobilized CaM in the absence and presence of Ca^{2+}. Figure 23B shows that Src binds CaM, both in the presence of Ca^{2+} and its absence, while no significant binding of Src was detected using control CaM-free naked Sepharose beads. Furthermore, we demonstrated that CaM co-immunoprecipitated with Src

solubilized from A431 cells (Figure 23C). Overall, these experiments show most likely a direct interaction between CaM and Src and that this interaction occurs by both Ca^{2+}-dependent and Ca^{2+}-independent mechanisms, in agreement with previous findings (Yuan et al., 2011). We also performed CaM overlay and cross-linking experiments with biotinylated CaM to test whether CaM binds to a recombinant or membrane solubilized Src kinase from A431 cells. We were not able to detect, however, any binding neither in the overlay or the cross-linking assays.

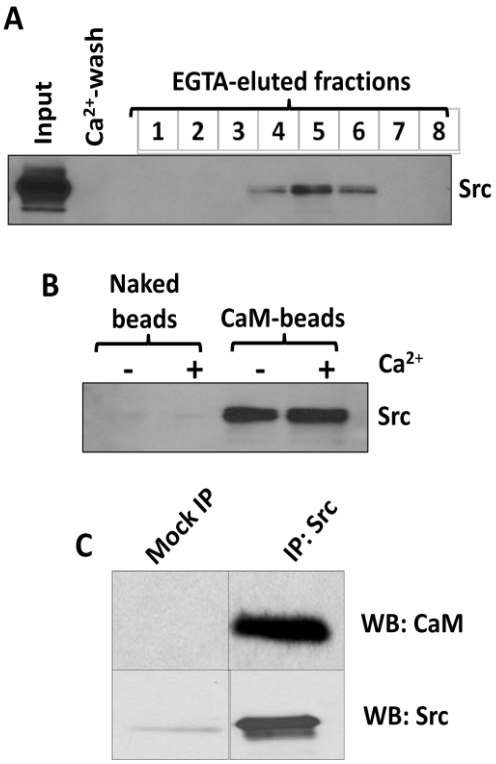

Figure 23: CaM interacts with Src in the absence and presence Ca^{2+}. (*A*) Ca^{2+}-dependent calmodulin-affinity chromatography of Src solubilized from A431 cells was performed as described in Materials and Methods. The input, the last fraction after washing with the Ca^{2+}-buffer (*Ca^{2+}-wash*), and the EGTA-eluted fractions were analyzed by Western blot using an anti-Src antibody. (*B*) Pull-down of Src solubilized from a membrane fraction of A431 cells was performed in the absence and presence of Ca^{2+} using CaM-Sepharose as described in Materials and Methods. Naked Sepharose 4B beads were used as negative binding control. (*C*) Src was solubilized from a membrane fraction of A431 cells (2 mg protein) and immunoprecipitated (IP) using an anti-Src antibody as described in Materials and Methods. The immunocomplex was processed by Western blot using anti-CaM and anti-Src antibodies. Mock IP using rabbit IgG was used as a negative control.

Significant evidence has been obtained on the activatory action of Ca^{2+}/CaM on the tyrosine kinase activity of Src (Fedida-Metula et al., 2012, Yang et al., 2013, Yuan et al., 2011). However, it was generally accepted that this process is always preceded by the generation of a Ca^{2+} signal upon cell activation required for the formation of the Ca^{2+}/CaM complex. Little is known, however, on the possible action of apo-CaM (Ca^{2+} free state) on the activation of c-Src. To solve this question, we tested the effect of CaM on the auto-phosphorylation (activation) of human Src in the absence and presence of Ca^{2+} using a full-length recombinant protein. Figures 24A and 24B show that little auto-phosphorylation of c-Src was observed in the absence of CaM and that the presence of this Ca^{2+} sensor strongly enhances c-Src activation in both absence and presence of Ca^{2+}. The activation of recombinant c-Src was stronger in the absence of Ca^{2+} than in its presence. And surprisingly, this effect was also observed

when the basal activity of c-Src was assayed in the absence of CaM. This may suggests a direct inhibitory action of Ca^{2+} on the Src kinase.

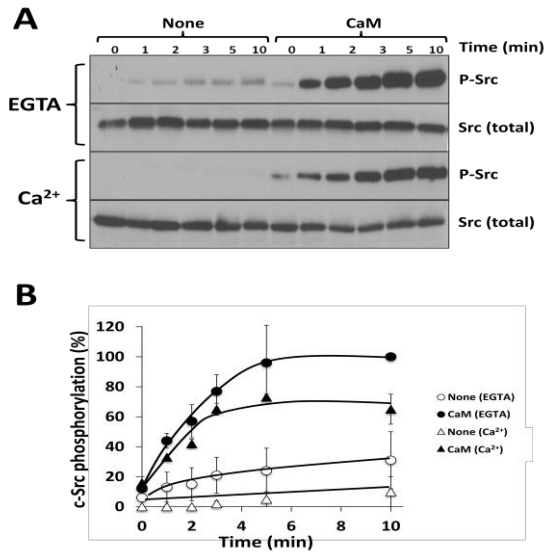

Figure 24: Apo-CaM and Ca^{2+}/CaM both activate recombinant c-Src. (*A*) The auto-phosphorylation assay of recombinant c-Src was performed in the absence and presence of CaM and in the absence and presence of Ca^{2+} for the indicated times as described in Materials and Methods. Duplicate samples were probed with an anti-Src (total) antibody as loading control. (*B*) The plot presents the mean ± range c-Src phosphorylation in the absence (*None*) and presence of CaM, and in the absence (*EGTA*) and presence of Ca^{2+} from two independent experiments similar to the one shown in *A*.

6.3.2 Effect of the phospho-(Y)-mimetic CaM mutants on c-Src activity.

As CaM is known to be phosphorylated by different Src family kinases (Benaim and Villalobo, 2002), we tested the action of phospho-(Y)-mimetic CaM mutants, on the auto-phosphorylation of recombinant c-Src. Figure 25 shows little if any differences in the activatory action of wild type CaM compared with the CaM(Y99D/Y138D) mutant both in the absence and presence of Ca^{2+}. Moreover, both CaM(Y99D/Y138D) and CaM(Y99E/Y138E) had the capacity to activate c-Src more strongly in the absence of Ca^{2+} (presence of EGTA) than in its presence (Figures 25 and 26).

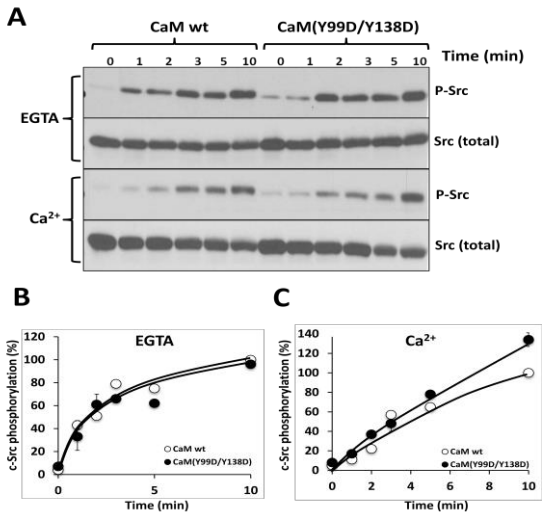

Figure 25: A phospho-(Y)-mimetic CaM mutant activates recombinant c-Src. (A) Auto-phosphorylation assays of recombinant c-Src (0.1 µg) was performed in a medium containing 15 mM Tris-HCl (pH 7.5), 5 mM $MgCl_2$, 1 mM DTT, 1 mM EGTA and where indicated 1.2 mM $CaCl_2$ (200 µM free Ca^{2+}) in the presence of either wild type CaM or CaM(Y99D/Y138D). The samples were processed for SDS-PAGE and Western blot using anti-phospho-tyrosine and anti-Src antibodies as described in Materials and Methods. (B, C) The plots present the mean ± SEM (n = 2) c-Src phosphorylation in the presence of wild type CaM or CaM(Y99D/Y138D) in the absence and presence of free Ca^{2+} from experiments similar to the ones shown in A.

These results suggest that phospho-(Y)-CaM may not have a distinct regulatory role than non-phosphorylated CaM on c-Src activation.

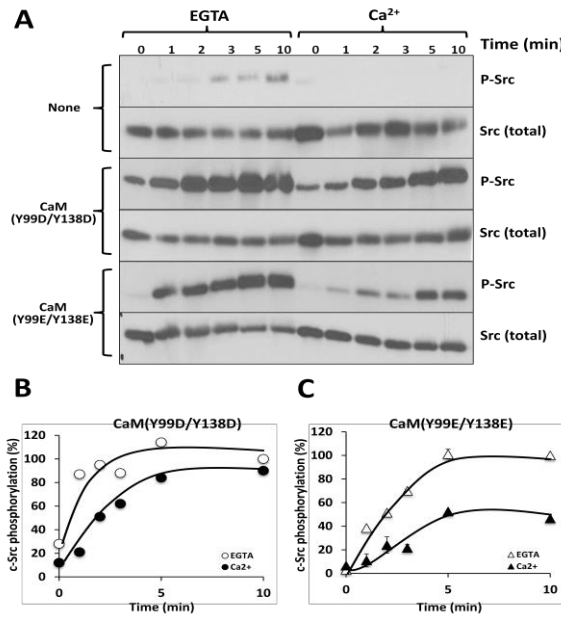

Figure 26: Phospho-(Y)-mimetic CaM mutants activate recombinant c-Src with better efficiency in the absence than in the presence of Ca^{2+}. (A) Auto-phosphorylation assays performed in conditions described in Figure 25 in the absence or presence of either CaM(Y99D/Y138D) or CaM(Y99E/Y138E). The samples were processed for SDS-PAGE and Western blot using anti-phospho-tyrosine and anti-Src antibodies as described in Materials and Methods. (B, C) The plots present the mean ± range c-Src phosphorylation in the presence of CaM(Y99D/Y138D) (n=1) or CaM(Y99E/Y138E) (n=2), and in the absence and presence of free Ca^{2+} from experiments similar to the ones shown in A.

6.3.3 The calmodulin antagonist W-7 inhibits Src activation in living cells.

Ligand-dependent activation of EGFR results in the down-stream activation of Src (Parks and Ceresa, 2014). To determine whether CaM is involved in EGFR-mediated Src activation in EGFR-overexpressing A431 cells, we performed experiments in the presence of the CaM antagonist W-7 and the less potent inhibitor W-12. Figures 27A (*left and center panels*), 27B and 27D show that activation of the EGFR by its ligand EGF also results in Src phosphorylation at Y416 as expected, and that increasing concentrations of W-7 progressively inhibit both phosphorylation processes. In contrast, high concentration (50 μM) of W-12, a chlorine-free analogue of W-7 with far lower affinity for CaM (IC_{50} of 260 μM versus 28 μM, inhibiting Ca^{2+}/CaM-dependent phosphodiesterase) (Hidaka et al., 1981, Hidaka and Tanaka, 1983), has a much lower inhibitory effects on EGFR activation than on Src activation (Figure 27D). It has been previously demonstrated that in living cells the ligand-dependent activation of the EGFR was aided by the Ca^{2+}/CaM complex, and that W-7 or W-13 inhibits this process (Martin-Nieto and Villalobo, 1998, Sengupta et al., 2007, Li et al., 2004, 2012). Nevertheless, as the inhibitory action of W-7 on Src phosphorylation was significantly stronger than that observed on ligand-dependent EGFR auto(trans)phosphorylation, this suggests a direct activatory effect of CaM on Src activity. Interestingly, W-7 itself had an activatory effect on the basal Src kinase activity, effect that may be due to the fact that this inhibitor may bind to the phospholipids on the inner leaflet of the plasma

membrane and thus change its electrostatic surface potential (Sengupta et al., 2007). The latter event may be accompanied of the detachment of a region in the Src structure that serves as an autoinhibitory mechanism. Similar effect of W-7/W-13 was also observed in EGFR, as treatment of a variety of cells lines expressing EGFR with this inhibitor led to the activation of the receptor in the absence of ligand (Sengupta et al., 2007).

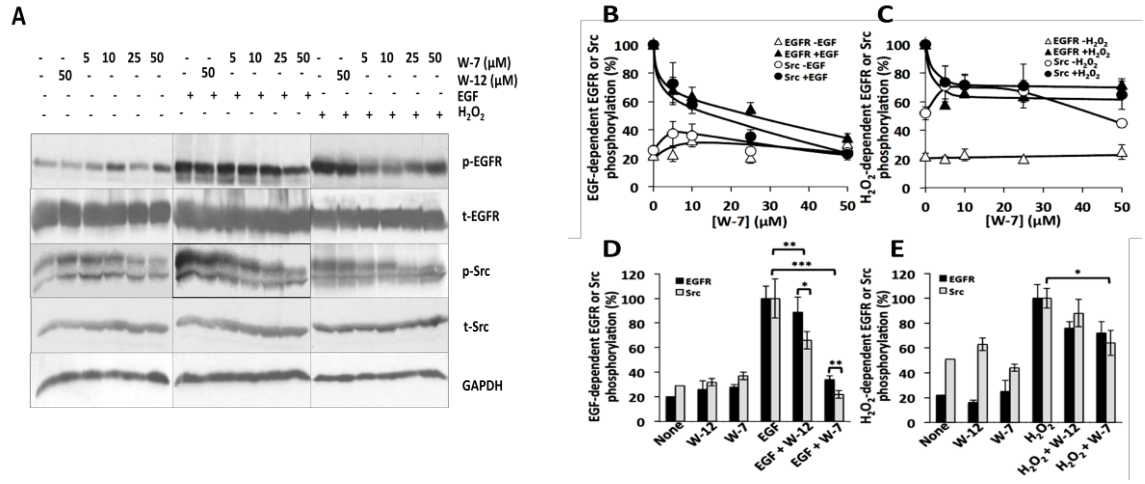

Figure 27: W-7 inhibits EGFR- and H_2O_2-mediated Src activation in A431 cells. (*A*) A431 cells were incubated in the absence and presence of the indicated concentrations of W-12 or W-7 during 15 min. Thereafter, the cells were stimulated either with 10 nM EGF for 2 min or 1 mM H_2O_2 for 15 min. The reaction was arrested and subjected to Western blot analysis as described in Materials and Methods, and probed with anti-phospho-tyrosine (4G10), anti-phospho-Src (Y416), and anti-EGFR (total), anti-Src (total) and anti-GAPDH antibodies as loading controls. (*B, C*) The plots present the mean ± SEM EGF-dependent (n = 6) and H_2O_2-dependent (n = 3) activation of Src at increasing concentrations of W-7 from experiments similar to those shown in *A*. (*D, E*) The plots present the mean ± SEM EGF-dependent (n = 6) and H_2O_2-dependent (n = 3) activation of Src in the absence (*None*) and presence of 50 μM W-12 or 50 μM W-7 from experiments similar to those shown in *A*. Statistically significant differences with $p < 0.05$ (*), $p < 0.005$ (**) and $p < 0.0001$ (***) using the Student's t-test are indicated.

The results discussed above do not represent a clear-cut evidence for a direct action of CaM on Src activation in living cells as EGFR is regulated by CaM (San José et al., 1992, Martin-Nieto and Villalobo, 1998, Sengupta et al., 2007, Li et al., 2004, 2012). Therefore, we searched for another way to activate Src without the involvement of EGFR to test the possible inhibitory effect of W-7. Figures 27A (*right panel*), 27C and 27E show that hydrogen peroxide, a known activator of Src (Sato et al., 2001, Basuroy et al., 2010), strongly enhances Src auto-phosphorylation (activation) in A431 cells as expected, and that W-7 indeed significantly inhibits this process in contrast to the lower effect of the low-affinity CaM inhibitor W-12 at identical concentrations (Figure 27E).

We also tested the inhibitory action of W-7 on H_2O_2-dependent activation of Src in a different cell line. Figure 28A show that H_2O_2 enhances the phosphorylation (activation) of Src in SK-BR-3 cells, and that the CaM antagonist W-7 inhibits the H_2O_2-

dependent activation of Src while W-12 does not. As W-7 appears to inhibit CaM in its Ca^{2+}-bound form (Okawa et. al, 1998) and may not affect apo-CaM, these results clearly suggest that Ca^{2+}/CaM regulates Src activity in living cells, although no information can be extracted from these experiments on the potential control that apo-CaM may exert on Src activation.

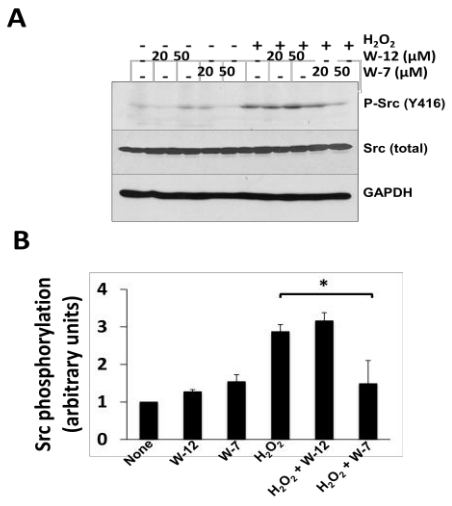

Figure 28: W-7 inhibits H_2O_2-mediated Src activation in SK-BR-3 cells. (*A*) SK-BR-3 cells were incubated in the absence and presence of the indicated concentrations of W-12 or W-7 during 15 min. Thereafter, the cells were stimulated with 1 mM H_2O_2 for 15 min. The reaction was arrested and subjected to Western blot analysis as described in Materials and Methods, and probed with anti-phospho-Src (Y416), and anti-Src (total) and anti-GAPDH antibodies as loading controls. (*B*) The plot presents the mean ± SEM (n = 5) H_2O_2-dependent activation of Src in the absence (*None*) and presence of either 50 μM W-12 or 50 μM W-7 from experiments similar to the one shown in *A*. Statistically significant differences with $p < 0.05$ (*) using the Student's t-test are indicated.

We tried to test the effect of CaM on the activity of Src family kinases espressed in ET1-55/EGFR cells, where the expression of CaM is down-modulated by tetracycline (Panina et al., 2012, Li et al., 2012), using as control cell line DT40/EGFR cells. After the antibiotic treatment for 48 hours we detected with a surprise an increase in the phosphorylation at Tyr416 of some unidentified member of the Src-family, but this was not due to the decrease of the expression of CaM, because this increased phosphorylation was also detected in the control cell line, suggesting that stress induced by tetracycline, but not the drop of CaM expression level, was the reason for the activation of the Src family kinase(s) (Supplementary Figure 2S).

6.4 Effect of CaM and phospho-(Y)-CaM on EGF-dependent EGFR activation

Overexpression, and/or truncated, site-mutated or segment-deleted hyperactive forms of EGFR are present in many solid tumors in human. The aberrant receptors significantly contribute to the oncogenic process (Kim and Muller, 1999, Roskoski, 2014). Thus, targeting overexpressed and/or aberrant hyperactive EGFR could be a valid therapeutic approach against cancer (Roskoski, 2014). In addition to anti-EGFR antibodies targeting the extracellular region of the receptor or small chemicals targeting the tyrosine kinase domain of EGFR have been developed. Another target site of

interest could be the CaM-BD located at the cytosolic JM region of the receptor (Villalobo et al., 2013).

6.4.1 Effect of CaM down-regulation in CaM-KO cells on EGF-dependent EGFR activation.

As CaM is implicated in EGF-dependent EGFR activation we used ET1-55/EGFR conditional CaM-KO cells stably transfected with the human EGFR (Panina et al., 2012, Li et al., 2012). Upon addition of tetracycline the expression level of CaM drops after 42-72 h of exposure of the antibiotic and we could barely detect the presence of CaM through immunoblot (Figure 29A). The activation of the EGFR was significantly reduced by the tetracycline addition in a time-dependent manner and the decrease of EGFR auto-phosphorylation follows the time-dependent down-regulation of CaM, showing that CaM is essential for EGF-dependent activation of the EGFR (Figures 29A and 29) as previously described by us (Panina et al., 2012, Li et al., 2012). Since CaM is vital for the cells, we used trypan blue exclusion test to determine the cell viability at the different times of tetracycline treatment, and at 72 h only 10 % drop in cell viability was observed compared to non-treated cells (Figure 29C).

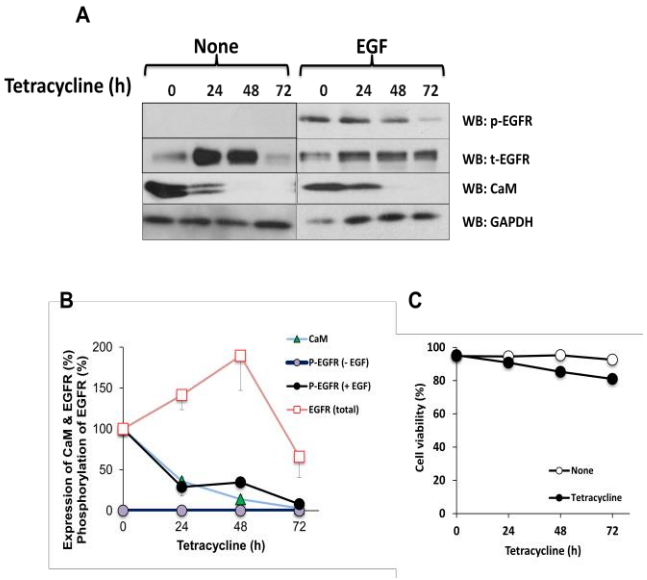

Figure 29: CaM down-regulation in conditional CaM-KO cells decreases EGF-dependent EGFR activation. (A) ET1-55/EGFR cells were incubated with 1 µg/ml tetracycline and stimulated with 10 nM EGF for 5 min for the indicated times. The expression of EGFR (t-EGFR), phospho-EGFR (p-EGFR) and CaM was determined using an anti-EGFR, anti-phosphotyrosine (4G10) and anti-CaM antibodies. GADPH is also shown as a loading control. (B) The plot presents the mean ± SEM (n=5 for total EGFR, n=3 for phospho-EGFR, and n=3 for total CaM) expression of total EGFR (*red squares*), non-stimulated EGFR (*purple circles*), EGF-stimulated EGFR (*black circles*) and total CaM (*green triangles*) in the presence of tetracycline for the indicated times. (C) The plot represents the mean ± SEM (n=3) of the cell viability measured by trypan blue exclusion test in the absence and presence of tetracycline for the indicated times.

6.4.2 Effect of the phospho-(Y)-mimetic CaM mutants on EGFR activation.

Then we wanted to test whether the double Y/D and Y/E CaM mutants have a differential regulatory effect on the EGF-dependent activation of the EGFR as compared to CaM wild type. Figure 30 shows the effect of the double Y/E and Y/D mutants on the EGF-dependent activation of EGFR solubilized from a membrane fraction of A431 cells *in vitro*. The results show that the receptor in the absence of its ligand has very low tyrosine kinase activity, and that upon addition of EGF leads to a strong activation of the EGFR. The effect of CaM wild type is in agreement with what has been already demonstrated by us, where in the presence of Ca^{2+}/CaM has an inhibitory effect on the EGF-dependent activation of EGFR *in vitro* (San José et al., 1992). Interestingly, CaM(Y99E/Y138E) and CaM(Y99D/Y138D) mutants had a differential effect on the activation of the receptor in the presence of Ca^{2+}. The glutamic acid double mutant had similar, if not stronger, inhibitory effect compared to the one exerted by wild type CaM. On the other hand, the aspartic acid mutant did not exhibit the same extend of inhibition on the EGF-dependent activation of EGFR in the presence of Ca^{2+}, compared to both wild type CaM and the double Y/E CaM mutant. In the presence of the chelating agent EGTA (Figures 30A and 30B) Y/D CaM mutants had a strong activatory effect on the EGF-dependent phosphorylation of EGFR as compared to wild type CaM (Figure 30).

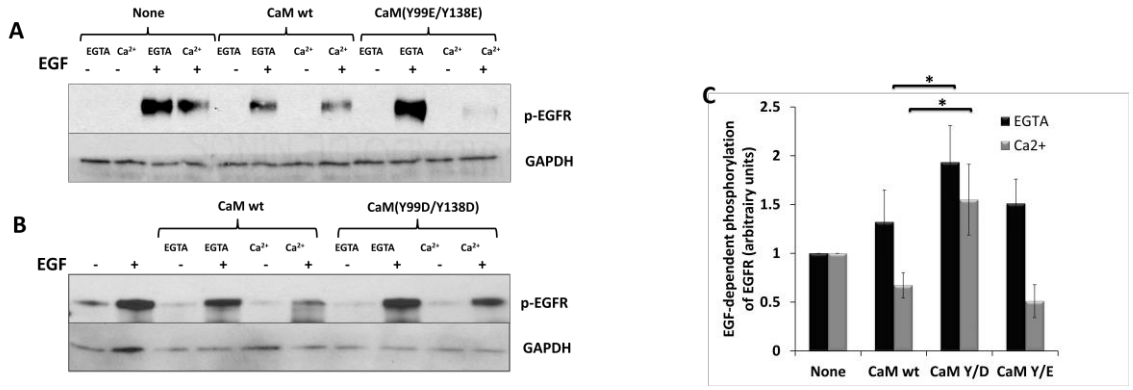

Figure 30: Effect of different CaM species on the EGF-dependent phosphorylation of the EGFR *in vitro*. (A, B) EGFR solubilized from membrane fraction from serum-starved A431 cells was incubated in the absence or presence of different recombinant CaM mutants (1 µg), in the absence of Ca^{2+} (presence of EGTA) or presence of Ca^{2+}, and in the absence or presence of 10 nM EGF as indicated. The samples were resolved in SDS-PAGE and processed by immunoblot using an anti-phosphotyrosine antibody to detect phosphorylated EGFR (p-EGFR). GAPDH is shown as a loading control. (C) The plot presents the mean ± SEM (n = 6) for wild type CaM and CaM (Y99D/Y138D), and (n=3) for CaM(Y99E/Y138E) of the EGF-dependent phosphorylation of EGFR in the absence (presence of EGTA) or in the presence of Ca^{2+} and the different CaM species as indicated.

6.5 *O*-GlcNAcylation in tumor cells

O-GlcNAcylation is the addition of β-D-N-acetylglucosamine moiety(ies) to serine or threonine of nuclear, cytoplasmic and mitochondrial proteins (Torres and Hart, 1984). Since 1984 when *O*-GlcNAcylation was found for the first time (Torres and Hart, 1984) significant amount of data revealing the function exerted by this non-typical glycosylation has been accumulated, and its involvement in diseases such as cancer has crystallized in recent years (Hart, 2014, de Queiroz et al., 2014, Jozwiak et al., 2014). It was found that EGFR type III in *Drosophila* is subjected to *O*-GlcNAcylation (Sprung et al., 2005) and it has been proposed based on *in silico* studies that Th654 and Ser1046/1047 in the EGFR are *O*-GlcNAcylated (Kaleem et al., 2009). The putative *O*-GlcNAcylation sites proposed for the EGFR are in fact directly or indirectly regulated by CaM as Thr654 is located in the CaM-BD of the receptor, and Ser1046/1047 are phosphorylated by CaMK-II. Thus we tried to peer whether the EGFR is in fact subjected to this PTM in tumor cells and whether CaM could have any role in this process.

6.5.1 EGFR *O*-GlcNAcylation in A431 and A549 cells

We first tested for the presence of *O*-GlcNAcylated proteins in whole cell lysates of A431 tumor cells by immunoblot using two distinct anti-*O*-GlcNAc specific antibodies (CTD110.6 and RL2) (Figure 31A). The presence of multiple strongly labeled bands of *O*-GlcNAcylated proteins in a range of > 250 kDa to < 50 kDa were detected presenting a similar distribution pattern when both antibodies were used. When cells were treated with Thiamet G, a highly specific inhibitor of *O*-GlcNAc hydrolase (OGA) to prevent *O*-GlcNAc deglycosylation (Goldberg et al., 2011), a significant two-fold increase in protein *O*-GlcNAcylation level was detected as expected (Figures 31B and 31D). Moreover, we also tested BADGP, a general *O*-glycosylation inhibitor not specific for *O*-GlcNAcylation but that also inhibits this process (Filhoulaud et al., 2009, Pantaleon et al., 2010, Onodera et al., 2014, Xu et al., 2014), and a small but significant decrease in protein *O*-GlcNAcylation was detected (Figures 31B and 31C).

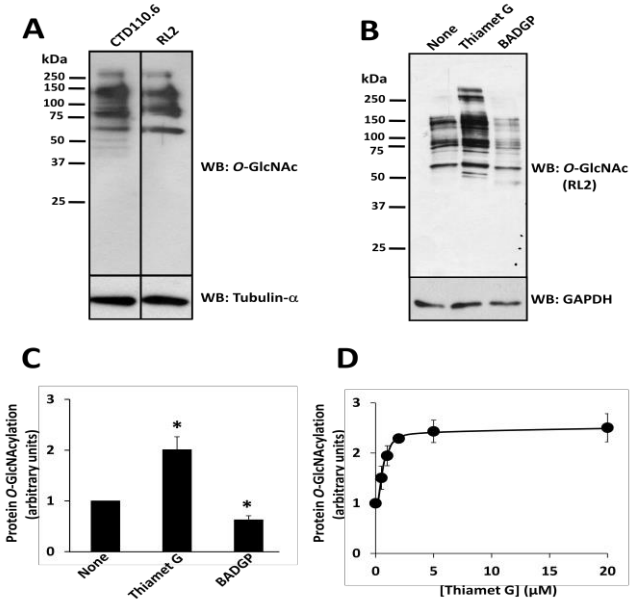

Figure 31: Effects of OGT and OGA inhibitors on protein *O*-GlcNAcylation. (A) A cell extract from A431 cells was processed by SDS-PAGE and Western blots (WB) and probed with the anti-*O*-GlcNAc antibodies CTD110.6 and RL2 as indicated. (B) A431 cells were incubated overnight in the absence (None) and presence of 20 μM Thiamet G or 2 mM BADGP as indicated and whole cell extracts probed with an anti-*O*-GlcNAc antibody (RL2). Anti-GAPDH antibody was used as loading control. (C) The plot presents the mean ± SEM (n = 4) of total protein *O*-GlcNAcylation. (*) $p < 0.05$ as determined by the Student's t test. (D) The plot presents the mean ± SEM (n = 3) protein *O*-GlcNAcylation using different concentrations of Thiamet G.

6.5.2 EGFR *O*-GlcNAcylation detected by immunoblot

To determine whether the EGFR from A431 tumor cells undergoes *O*-GlcNAcylation we treated the immunoprecipitated receptor in the absence and presence of PNGase F to remove *N*-glycans, and tested for *O*-GlcNAcylation using the same two distinct anti-*O*-GlcNAc antibodies mentioned above (Figures 32A and 32B). The results show that in both instances, not only the 170 kDa native EGFR, but most significantly and in greater extent the ~150 kDa *N*-deglycosylated receptor, yielded positive signals. To ascertain the specificity of the CTD110.6 anti-*O*-GlcNAc antibody, we competed its reactivity using an excess (20 mM) of free GlcNAc in the incubation medium (Figure 32C). Furthermore, we performed the experiment in reverse: immunoprecipitating first *O*-GlcNAcylated proteins from an A431 cell lysate and detecting the presence of EGFR in the immunoprecipitate (Figure 32D). When the cells were previously treated with the OGA inhibitor Thiamet G, the EGFR signal was slightly increased, and a decrease was detected when cells were treated with the *O*-glycosylation inhibitor BADGP, which also inhibits OGT (Figure 32D).

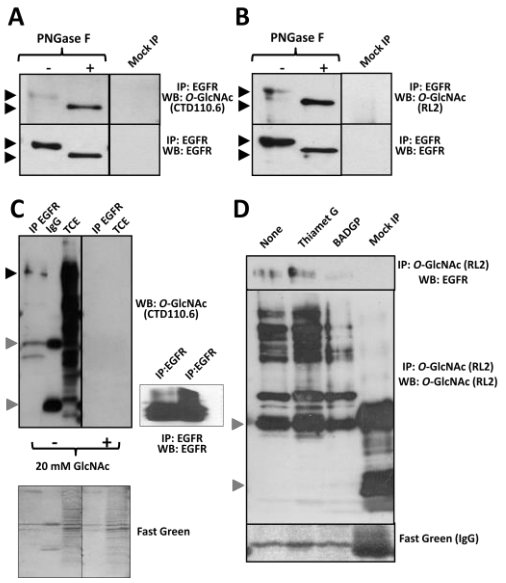

Figure 32: Detection of *O*-GlcNAcylation signal in immunoprecipitated EGFR by immunoblot. (*A, B*) The EGFR was immunoprecipitated (IP) from A431 cells using an anti-EGFR antibody and the immunocomplex was incubated in the absence and presence of PNGase F. The samples were blotted with the anti-*O*-GlcNAc antibodies CTD110.6 (*A*) and RL2 *(B*). The membranes were reprobed with an anti-EGFR antibody as loading controls. Mock IP were performed using a non-relevant IgG as negative controls. Arrowheads point the native and *N*-deglycosylated EGFR. (*C*) Immunoprecipitated (IP) EGFR, a non-relevant IgG fraction and an A431 cell extract were immunoblotted using an anti-*O*-GlcNAc antibody (CTD110.6) in the absence and presence 20 mM GlcNAc. (*D*) A431 cells were incubated overnight in the absence (*None*) and presence of 20 µM Thiamet G or 2 mM BADGP. The samples were immunoprecipitated (IP) using an anti-*O*-GlcNAc antibody (RL2) and the immunocomplex subjected to Western blots (WB) and probed with anti-EGFR and anti-*O*-GlcNAc antibodies. Mock IP was performed using a non-relevant IgG as negative control. The light chains of IgG were staining with Fast Green as loading control.

In agreement with the previous result, we also demonstrated that when A431 cells were treated with the OGA inhibitor Thiamet G the *O*-GlcNAcylation level of the immunoprecipitated native 170 kDa EGFR also increased, although little if any increment was detected in the ~150 kDa *N*-glycans-free EGFR band (Figures 33A and 33B).

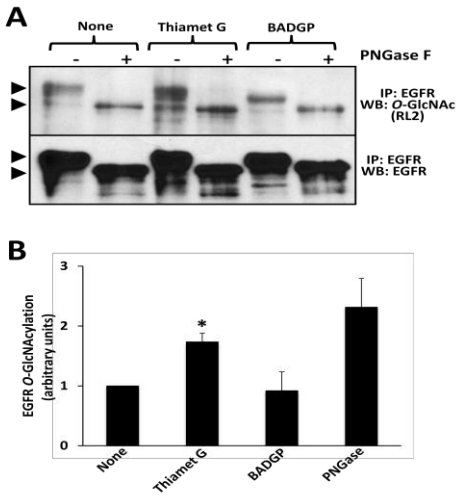

Figure 33: Effects of OGA and OGT inhibitors on the EGFR *O*-GlcNAcylation. (A) A431 cells were incubated overnight in the absence (None) and presence of 20 µM Thiamet G or 2 mM BADGP. The samples were processed as described in Materials and Methods and probed with an anti-*O*-GlcNAc antibody (RL2). The membrane was reprobed with an anti-EGFR antibody as loading control. Arrowheads point the native and *N*-deglycosylated EGFR. (B) The plot presents the mean ± SEM (n = 3) EGFR *O*-GlcNAcylation from a set of experiments similar to the one shown in A. (*) $p < 0.05$ as determined by the Student's t test.

We then tested whether EGFR activation with EGF has an effect on the *O*-GlcNAcylation of the receptor, and to the *O*-GlcNAcylation of proteins in A431 cells. Figures 34A and 34B show that when EGFR is activated by EGF there is a small, but not significant decrease in the *O*-GlcNAcylation, this may be partially due to the internalization and degradation of the receptor induced by its ligand (Wiley et al., 1991, Lamaze and Schmid, 1995, Oksvold et al., 2003, Henriksen et al., 2013) (see Figures 35C and 35B). Figure 34C shows that EGF-stimulated A431 cells have the same pattern of *O*-GlcNAcylated proteins compared to the non-treated ones, suggesting that EGFR signaling does not modulate this PTM in other proteins.

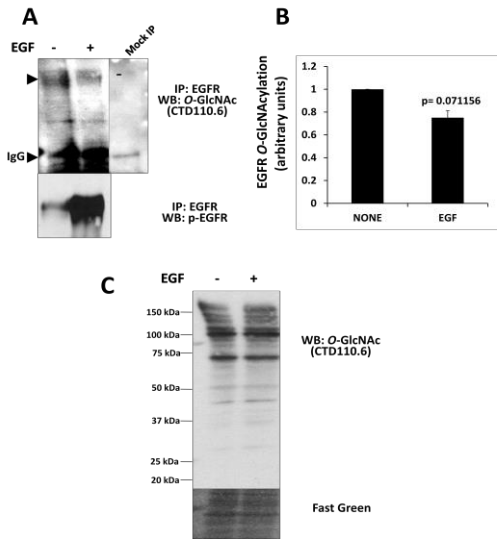

Figure 34: The effect of EGF-dependent activation on the *O*-GlcNAcylation of the EGFR. (A) Serum-starved A431 cells were incubated in the absence and presence of 10 nM EGF during 30 min. EGFR was immunoprecipitated and immunoblotted (WB) with the anti-*O*-GlcNAc antibody CTD110.6. (B) The plot presents the mean ± SEM (n = 3) EGFR *O*-GlcNAcylation. The p-value as determined by the Student's t test is also shown. (C) Cell extracts of serum-starved A431 cells were incubated in the absence and presence of 10 nM EGF for 30 min. The samples were then processed as described in Materials and Methods and probed with the anti-*O*-GlcNAc antibody.

6.5.3 EGFR *O*-GlcNAcylation detected by metabolic labeling with azido-GlcNAc

We next tried to detect *O*-GlcNAcylation of the EGFR by metabolically labeling cellular glycans from A431 cells with azido-GlcNAc. Figure 35A shows that after immunoprecipitation both the native 170 kDa EGFR and its ~150 kDa *N*-glycans-free form, obtained after PNGase F treatment, yielded a positive signal following biotinylation and overlay by streptavidin-HRP. The extent of the signal was lower in EGF-treated cells but this most likely represents degradation of the receptor after ligand-induced internalization, as this process has been well documented (Kirisits et al., 2007, Henriksen et al., 2013) and we further show this degradation in Figures 35B, 35C. We also treated A431 cells with tunicamycin to obtain EGFR devoid of *N*-glycans by a different method. Figure 34D shows that the native 170 kDa receptor and its ~150 kDa *N*-deglycosylated form both were metabolically labeled with azido-GlcNAc, the latter even after further treating the immunoprecipitated EGFR with PNGase F.

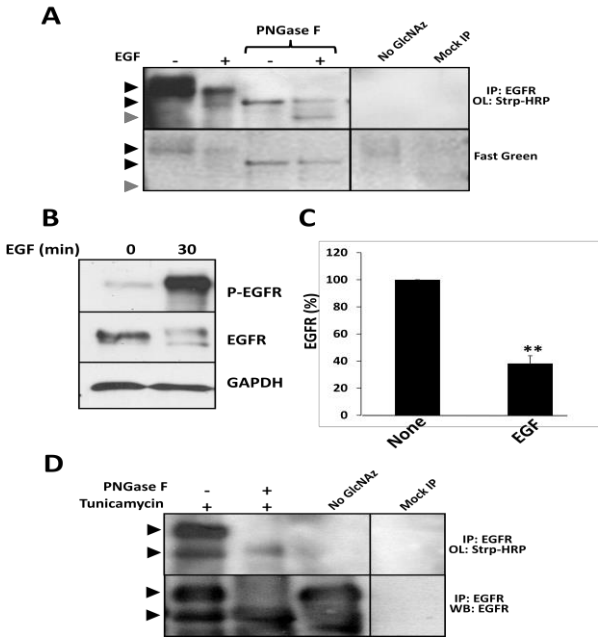

Figure 35: Detection of *O*-GlcNAcylation signal in EGFR by azido-GlcNAc labeling. (A) Serum-starved A431 cells were labeled with GlcNAz and incubated in the absence and presence of 10 nM EGF during 30 min. EGFR was then immunoprecipitated, biotinylated and N-deglycosylated as described in Materials and Methods. The detection of the biotin-GlcNAc complex was done by overlaid with streptavidin-HRP as described in Materials and Methods. Immunoprecipitated EGFR from cells non-treated with GlcNAz (No GlcNAz) and a mock IP are shown as negative controls. Fast Green staining is shown as loading control. (B) Serum-starved A431 cells were treated in the absence (-) and presence (+) of 10 nM EGFR for 30 min. The reaction was arrested with 10 % (w/v) TCA, and the samples were processed for SDS-PAGE and immunoblot using an anti-phospho-(Y) antibody to detect phosphorylated EGFR (P-EGFR) and an anti-EGFR antibody to detect total EGFR. GAPDH is shown as a loading control. (C) The plot presents the mean ± SEM (n = 3) of the densitometry of the EGFR/GAPDH signal ratio. (**) $p < 0.01$ as determined by the Student's t test. (D) A431 cells were treated overnight with 1 µg/ml tunicamycin, the EGFR was immunoprecipitated (IP) and where indicated treated with PNGase F. The samples were processed as in A. Duplicate samples were probed with an anti-EGFR antibody. Immunoprecipitated EGFR from cells non-treated with GlcNAz (No GlcNAz) and a mock IP are shown as negative controls. Arrowheads point the native and *N*-deglycosylated EGFR.

We tested different human tumor cell lines, with different levels of EGFR expression, and a mouse fibroblast stably transfected and overexpressing the human EGFR for *O*-GlcNAcylation of the receptor. Figure 36 shows a positive signal in human carcinoma epidermoid A431 cells, which were used as positive control. Also, a positive signal was detected in human lung carcinoma A549 cells. The double band observed in A549 cells may represent the presence of an unrelated *O*-GlcNAcylated protein associated to the EGFR and/or another ErbB receptor forming heterodimers with the EGFR. However, no *O*-GlcNAcylation of the EGFR was detected in human cervix adenocarcinoma HeLa cells or in the recombinant human EGFR expressed in mouse EGFR-T17 fibroblasts.

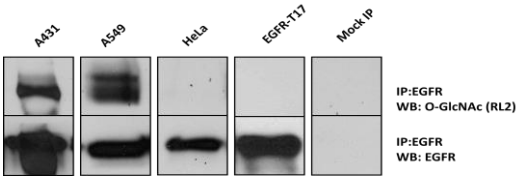

Figure 36: *O*-GlcNAcylation of EGFR in different cell lines. A431, A549, HeLa and EGFR-T17 cells were incubated overnight in the presence of the OGA inhibitor 20 µM Thiamet. The EGFR was immunoprecipitated (IP) using an anti-EGFR antibody and the immunocomplexes were processed by SDS-PAGE and immunoblot (WB) using anti-*O*-GlcNac (RL2) and anti-EGFR antibodies as described in Materials and Methods. A mock IP was performed using a non-relevant IgG as a negative control.

6.5.4 *In vitro* O-GlcNAcylation of EGFR

We first show that EGFR and OGT can be co-immunoprecipitated (Figure 37A), suggesting that the two proteins interact in living cells. Our results on the *in vitro* enzymatic assays show a significant increment in the *O*-GlcNAcylation level of the EGFR as detected by Western blot using an anti-*O*-GlcNAc antibody (RL2) (Figures 37B and 37C). Given the fact that the immunoprecipitated EGFR was already *O*-GlcNAcylated before starting the reaction catalyzed by OGT, this increment only reached ~1.8 ± 0.2 fold. This, however, strongly suggests that the EGFR undergoes this PTM.

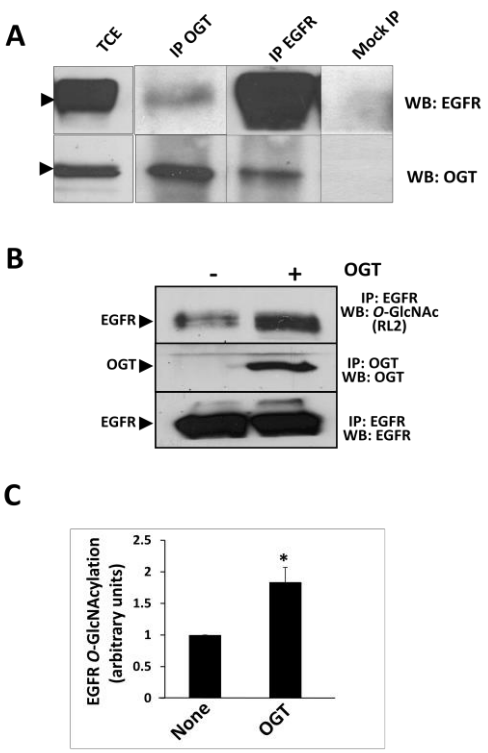

Figure 37: Enhanced *O*-GlcNAcylation of EGFR upon *in vitro* reaction catalyzed by OGT. (A) OGT and EGFR were immunoprecipitated from A431 cells and the samples were processed by immunoblot (WB) using anti-OGT and anti-EGFR antibodies to test for co-immunoprecipitation of both proteins. Mock IP were performed using a non-relevant IgG as negative controls. (B) OGT and EGFR were independently immunoprecipitated from A431 cells. Thereafter, the immunoprecipitated EGFR was incubated in the absence and presence of immunoprecipitated OGT and the *O*-GlcNAcylation was performed upon addition of UDP-GlcNAc as described in Materials and Methods. The samples were immunoblotted as indicated. OGT and EGFR were detected by WB using anti-OGT and anti-EGFR antibodies, respectively. (C) The plot presents the mean ± SEM EGFR O-GlcNAcylation in the absence (None) and presence of OGT from 3 independent experiments similar to the one shown in B measuring the densitometry of the O-GlcNAcylated EGFR band corrected by loading as determined by protein staining with Fast Green. (*) $p < 0.05$ as determined by the Student's t test.

6.5.5 Effect of OGA and OGT inhibitors on EGFR activation

We tested OGA and OGT inhibitors on the EGF-dependent activation of the EGFR in A431 tumor cells. Figure 38A shows that the presence of Thiamet G and BADGP, did not significantly change the time-dependent activation profile of the EGFR. The maximum EGFR phosphorylation was around 2 minutes of EGF stimulation followed by a subsequent decrease of the receptor auto-phosphorylation due to dephosphorylation (Figure 38B).

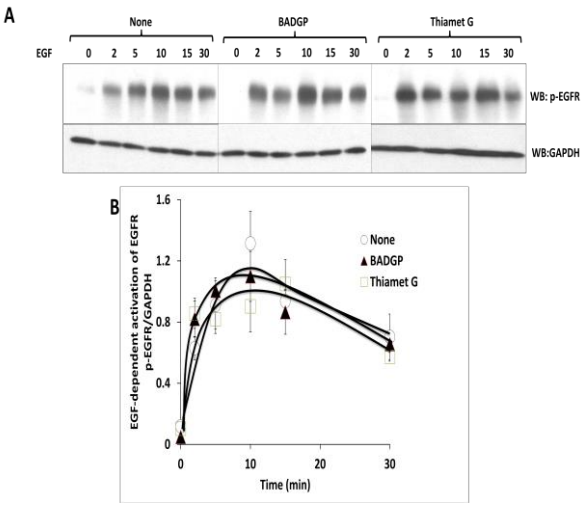

Figure 38: Effect of OGA and OGT inhibitors on the EGF-dependent activation of EGFR. (*A*) A431 cells were incubated in the absence (*None*) and presence of 20 µM Thiamet G or 2 mM BADGP overnight. Thereafter, the cells were stimulated with 10 nM EGF for the indicated times. The reaction was arrested and subjected to Western blot analysis as described in Materials and Methods, and probed with anti-phosphotyrosine antibody (p-EGFR), and anti-GAPDH antibody as a loading control. (*B*) The plot present the mean ± SEM (n=3) EGF-dependent activation of EGFR for the indicated times from experiments similar to those shown in *A*.

6.5.6 Possible role of CaM in protein *O*-GlcNAcylation

According to Kaleem *et al.* (2009) CaM could have a central role into the proposed interplay between *O*-GlcNAcylation and phosphorylation of the EGFR. We tried to study the possible role of CaM on OGT functionality in order to address this issue and clarify whether this Ca^{2+} modulator has anything to do with the *O*-GlcNAc modification. Figure 39 shows an *in silico* study proposing that OGT could be a CaM-BP. Using a CaM database *in silico* tool freely available at: http://calcium.uhnres.utoronto.ca/ctdb/ctdb/home.html we were able to find a sequence located in the C-terminal of the transferase that has great potential of being a CaM-BD (Figure 39A). Since we know that CaM-BD regions of a given protein are usually conserved among different species we tested whether the putative CaM-BD of OGT is also conserved, and the result of the alignment of this region is shown in Figure 39B. It is clear that this region is quite conserve is there is only one amino acid substitution, a valine at position 993 changed to isoleucine, both hydrophobic amino acids (Figure

39B). On the other hand, the putative CaM-binding site was identified as a canonical 1-5-10 class motif (see Table 1).

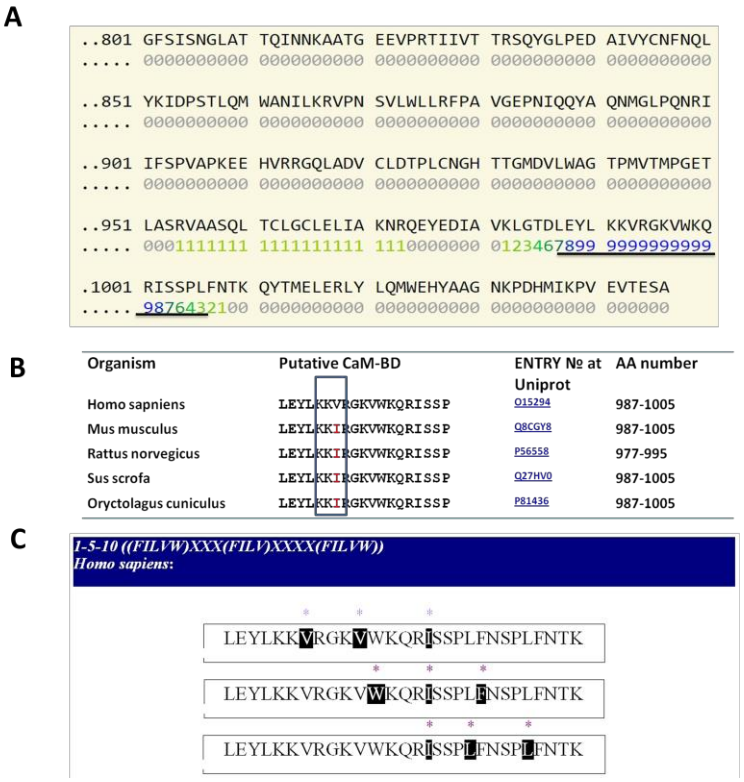

Figure 39: Putative CaM-binding domain in human ncOGT. (A) Presents the result from the *in silico* searching tool showing the amino acid sequence in the human ncOGT that have the highest potential to present CaM binding capacity (from 0 to 9). (B) Alignment of the selected region in different species. (C) The scheme represents the position of the conserved amino acids critical for CaM binding and several segments fitting to a CaM-binding domain of type 1-5-10.

We performed Ca^{2+}-dependent CaM-affinity chromatography using recombinant ncOGT in order to determine whether this enzyme binds CaM in a Ca^{2+}-dependent manner. Figure 40A shows that part of the OGT loaded in the column in the presence of Ca^{2+} can be eluted with a buffer containing EGTA. Furthermore, we demonstrated that CaM co-immunoprecipitated with OGT from A431 cells (Figure 40B). Overall, these experiments show possible direct interaction between CaM and OGT and that this interaction occurs by a Ca^{2+}-dependent mechanism.

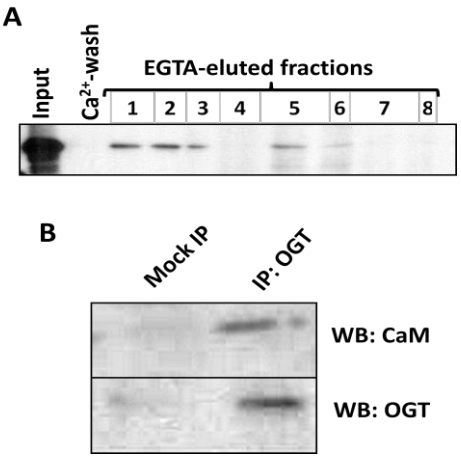

Figure 40: Calmodulin interacts with OGT. (*A*) Ca^{2+}-dependent CaM-affinity chromatography of recombinant ncOGT performed as described in Materials and Methods. The input, the last fraction after washing with the Ca^{2+}-buffer (*Ca^{2+}-wash*), and the EGTA-eluted fractions were analyzed by Western blot using an anti-OGT antibody. (*B*) OGT was immunoprecipitated (IP) from A431 cells using an anti-OGT antibody as described in Materials and Methods. The immunocomplex was processed by Western blot using anti-CaM and anti-OGT antibodies. A mock IP was used as a negative control.

We finally tested the effect of CaM inhibition and CaM down-regulation on the *O*-GlcNAcylation pattern of A431 cells and ET1-55/EGFR cells, respectively. Figures 41A and 41B show that neither the inhibition of CaM with W-7 in A431 cells nor the down-regulation of CaM in the conditional CaM-KO chicken lymphoma cell line has any effect on the general pattern of protein *O*-GlcNAcylation, suggesting that CaM may not regulate the enzymatic activity of OGT.

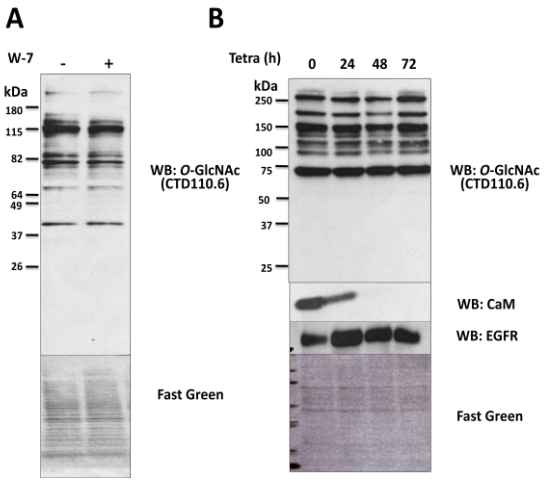

Figure 41: Effect of inhibition or down-regulation of CaM on the O-GlcNAcylation pattern. (A) A431 cells were treated in the absence or presence of 15 µM W-7 for 30 min. Total cell extracts samples were processed by SDS-PAGE and Western blot as described in Material and Methods, and the membrane was probed with anti-*O*-GlcNAc (CTD110.6) antibody. Protein stained with Fast Green is shown as a loading control. (B) ET1-55/EGFR cells were treated with tetracycline (1 µg/ml) for the indicated times. Total cell extracts were processed by SDS-PAGE and Western Blot as described in Material and Methods and the membranes probed with anti-*O*-GlcNAc antibody (CTD110.6), anti-CaM, anti-EGFR antibodies. Protein stained with Fast Green is shown as a loading control.

7. DISCUSSION

CaM is a modulator in eukaryotic cells transducing the Ca^{2+} signal generated upon activation by a variety of effectors, and regulates many cellular processes including: cell proliferation, apoptosis and autophagy, all of them playing a fundamental role in tumorigenesis and tumor progression (Chin and Means, 2000, Jurado et al., 1999, Berchtold and Villalobo, 2014). Understanding the different mechanisms by which CaM exerts its functions, regulating hundreds of proteins including PDE1, NOS, EGFR and c-Src, that also have been identified as important element of signaling pathways that control the invasive and metastatic capacities of various tumors (Kim and Muller, 1999, Roskoski, 2014, Tan et al.,2005) is of a highest interest. In this Thesis we focus on studing the effect of CaM on the functionality on systems important in tumorogenesis, particularly the EGFR and c-Src.

A broad range of Ser/Thr- and Tyr-protein kinases have been shown to phosphorylate CaM *in vitro* and in living cells and the different phospho-CaM species have different regulatory role on the activity of many target proteins as compared to non-phosphorylated CaM (Benaim and Villalobo, 2002). This suggests that this PTM in addition to Ca^{2+} binding could modulate the activity of CaM. The non-receptor tyrosine kinase Src (Fukami et al., 1986), the insulin receptor (Graves et al., 1986), and the EGFR (Benguría et al., 1994), are kinases implicated in the phosphorylation of CaM at both Y99 and Y138. The dynamic nature of this PTM and the distinct phosphorylated forms of CaM at a given time acting on specific target proteins could be difficult to observe in living cells due to the short half-life of phospho-(Y)-CaM. In this Thesis we show an alternative to explore these events by generation and characterization of recombinant phospho-(Y)-mimetic CaM mutants, where one or two of the two only Tyr present in CaM were substituted by glutamic acid (E) or aspartic acid (D), as this is a common approach used to mimic tyrosine phosphorylation (Potter et al., 2005, Lie et al., 2012, Fisslthaler et al., 2008). We generated and extensively characterized these phospho-mimetic potential of these CaM mutants.

7.1 The phospho-(Y)-mimetic CaM mutants binds Ca^{2+}

Our data showed, that in contrast to the homogeneous electrophoretic migration (~ 18 kDa) of the single or double Y/D and Y/E CaM mutants in the absence of Ca^{2+} (presence of EGTA), and the near absence of Ca^{2+}-induced electrophoretic mobility shift of the single or double CaM mutants where Y138 was substituted by acidic residues (D or E) described in this Thesis, the non-phosphorylatable Y/F CaM mutants previously described presented a different behavior (Salas et al., 2005). For instance, the CaM(Y138F) and CaM(Y99F/Y138F) mutants presented in the absence of Ca^{2+}

higher electrophoretic mobility than wild type CaM and CaM(Y99F), and even higher Ca^{2+}-induced mobility shift (Salas et al., 2005). This suggests that the substitution of Y138 by an acidic or a hydrophobic residue exerts distinct effects on the conformation of CaM and most likely have a great impact on the conformation of the protein. Our results are in agreement with previous findings in which a differential behavior was observed when Y138 or Y99 were substituted by diverse amino acids, suggesting that mutation of Y138 disrupts the structural coupling between the N and C globular halves of CaM potentially mimicking the collapse that CaM undergoes when binding to target proteins (Sun et al., 1999, Sun et al., 2001). The central position of Y138 in the Ca^{2+}-induced conformational change of CaM is also evidenced by the modification of the chiroptical properties of this residue, here revealed to be the culprit for the well-known changes in the near-UV CD spectrum of CaM. Of note, the spectrum of Ca^{2+}-bound rat CaM is very similar to that of *Drosophila melanogaster* CaM (Maune et al., 1992), which only contains the Y138 residue but not that at position 99, further substantiating this conclusion.

The far-UV CD spectra of the different phospho-mimetic CaM species as compared to the wild type in the absence or presence of Ca^{2+} suggest that the substitution of one or the two Tyr residues does not disrupt Ca^{2+} binding. Ca^{2+} binding induced similar conformational changes in the molecules of the whole panel of mutants. Nevertheless, the ratio of molar ellipticity at 208 and 222 nm, a sensitive criterion of possible alterations in interactions between neighboring helices (Sun et al., 2001, Fasman, 1996), was slightly higher for the mutants as compared to the wild type, pointing to slight differences in the helix packing of the mutants. Of note, the mutant-specific deepening of the signals in the presence of Ca^{2+} may be due to a differential increase in α-helical content and/or reorientation of existing α-helices (Wang et al., 2011, Protasevich et al., 1997). Interestingly, all CaM mutant species presented a slight blue-shift of the 208 nm minimum in the absence of Ca^{2+} as compared to wild type CaM. We could not differentiate if this blue-shift was due to a solvent-effect or because of a mechanism including the involvement of aromatic-side chains. However, the fact that the blue-shift was more noticeable in the spectra of the two double CaM mutants suggests that most likely this shift of 2-3 nm is due to a reorganization of the molecule, because of the lack of the two tyrosines.

On the other hand, the near-UV spectra of wild type CaM showed similar spectra as to what has been published so far (Sun et al., 2001, Wolff et al., 1977, Martin and Bayley, 1986). The spectrum consisted of two well-defined negative bands at 262 and 269 nm, attributed to the six phenylalanine residues presented in CaM, and a region

around 280 nm arising from the two Tyr residues. All the latter picks reacted to Ca^{2+} binding and presented the typical spectra deepening. Unlike the mutants, which presented the expected change in the region of 280 nm, the spectra in this region became in the case of Y99 mutants even positive, and in the case of Y138 mutants the ellipticity became almost zero. Our results clearly show that Ca^{2+}-induced alterations observed for wild type CaM in this region are mostly due to changes in the environment of Y138. Interestingly, this conclusion fully explains the small effect of Ca^{2+} on the near-UV CD spectrum of the separate N-terminal half (residues 1-77) of CaM reported by others (Martin and Bayley, 1986). They considered their result as a surprise, because of the equal distribution of the phenylalanine residues in the C- and N-terminal halves of the protein. Actually, the spectra with/without Ca^{2+} of the Y138 and double CaM mutants (Figure 19) are very similar to those published for the N-terminal half by the same group (Martin and Bayley, 1986).

In agreement with the previous reports showing that Ca^{2+} binding induces a notable increase in the thermal stability of wild type CaM (Wang et al., 2011, Brzeska et al., 1983), our results clearly showed that the full panel of mutants preserve this spectacular quality. All the CaM species showed quasisigmoidal decrease in ellipticity in the absence of Ca^{2+}, clearly indicating the occurrence of at least one intermediate state, as previously described for wild type CaM (Sun et al., 2001, Wang et al., 2011). In the case of the CaM Y138 mutants, the temperature-dependent unfolding was clearly biphasic, showing a notable deviation of sigmoidicity at temperatures below 50 ºC. The behavior of the Y138 mutant is remarkably similar to that reported for a CaM Y138Q mutant (Sun et al., 2001). Although, fitting the data to a two- or three-state model did not yield acceptable quality, it is clear from the denaturation profiles that a major thermal unfolding for the different CaM species occurred at ~ 55 ºC, and all of them were completely unfolded above 70 ºC. In addition, lower temperature transitions and/or discontinuities, also reported for wild type CaM (Brzeska et al., 1983, Martin and Bayley, 1986, Kilhoffer et al., 1981, Gangola and Pant, 1983), were observed in the lower temperature region (20-40 ºC), both in the absence and presence of Ca^{2+}. Most importantly, the binding of Ca^{2+} had a profound impact on the stability of wild type CaM and all of the mutants, they exhibited remarkably thermal stability in the presence of Ca^{2+}, showing that ion binding has a similar stabilizing effect on wild the type and the mutants. This conclusion, together with the far-UV CD spectrum is also supported by the fact that the full panel of CaM mutants required Ca^{2+} to stimulate the activities of PDE1 and eNOS, as it was the case for wild type CaM. Therefore, the absence of a

significant Ca^{2+}-induced electrophoretic mobility shift in the Y138D and Y138E CaM mutants is not a valid criterion to propose absence of Ca^{2+}-binding capability.

It has been previously reported that terbium ion binds to the four Ca^{2+}-binding pockets of CaM and that it can be excited indirectly by excitation of the tyrosine residues at 280 nm. The amount of energy transferred from the excited tyrosine to the terbium ion depends on how close the tyrosine and Tb^{3+} are. Thus, this indirect excitation of Tb^{3+} could be monitored at 545 nm (Wallace et al., 1982). This fact allowed us to study the binding and excitation of Tb^{3+} bound to the different CaM mutant species. The near loss of fluorescence emission by Tb^{3+} upon tyrosine excitation in the single mutant lacking Y99, but not the single mutant lacking Y138, suggests that Tb^{3+} is closer to tyrosine 99 located at the III Ca^{2+}-binding site of CaM, than to tyrosine 138 located at its IV Ca^{2+}-binding site. This is in full agreement with the crystallographic structure of CaM, where the carbonyl group of Y99 participates in the coordination of Ca^{2+}, while Y138 has a rather outward projecting conformation unable to coordinate Ca^{2+} (Strynadka and James, 1989).

In agreement with the distinct spatial projection and accessibility to kinases of the two tyrosine-residues of CaM, our c-Src phosphorylation experiments show that Y99 was phosphorylated with lower efficiency than Y138 by this kinase. The inward projection of Y99 within the III Ca^{2+}-binding pocket as compared to a more outward projection of Y138 within the IV Ca^{2+}-binding pocket (Strynadka and James, 1989) may explain these results. Although both tyrosine residues in CaM are phosphorylated by both c-Src and EGFR, as demonstrated using Y99F and Y138F CaM mutants (Salas et al., 2005), the substitution of the tyrosine residue at position 138 by a non-phosphorylatable amino acid somehow disturbs in part the accessibility of these kinases to Y99. This is remarkable as it was previously suggested that phosphorylation of Y99 by several tyrosine kinases was more efficient than the phosphorylation of Y138 (Benaim and Villalobo, 2002). Thus, the phosphorylation of single-tyrosine CaM mutants may not reflect the comparative efficiency of phosphorylation of both tyrosine residues of CaM in living cells. This may be related to the fact that substituting Y138 by other amino acids disrupts the structural coupling between the N- and C-globular domains of CaM (Sun et al., 2001), as previously mentioned.

7.2 All phospho-(Y)-mimetic CaM mutants are biologically active

Our results also show that the single and double Y/D and Y/E CaM mutants all retain biological activity, as they were able to activate distinct CaM-binding systems including PDE1, eNOS, EGFR, and c-Src. Moreover, we have shown a differential

action of wild type CaM and some of the phospho-(Y)-mimetic CaM mutants under study on the activity of PDE1, eNOS and EGFR.

The double mutant CaM(Y99D/Y138D), but not CaM(Y99E/Y138E), exerts a lower activatory effect on the V_{max} of the CaM-dependent cyclic nucleotide PDE1 isolated from bovine brain, as compared to wild type CaM. However, the aspartic acid mutant does not significantly change the apparent affinity for Ca^{2+} or the activation constant (K_{act}) of CaM for the enzyme. Of note is that other studies on the effect of phospho-(Y)-CaM versus non-phosphorylated CaM on the cyclic nucleotide phosphodiesterase of different origin yielded divergent results. Thus, both an increase (Williams et al., 1994) and a decrease (Corti et al., 1999) in the K_{act}, without affecting the V_{max}, has been reported for phospho-(Y)-CaM phosphorylated by the InsR and a phospho-(Y99)-CaM species, respectively, on the PDE1 from bovine brain in comparison to non-phosphorylated CaM. In contrast, InsR-phosphorylated CaM presented similar K_{act} and V_{max} than with non-phosphorylated CaM when assayed on the PDE1 from rat hepatocytes, although the phosphorylated form increased the IC_{50} of CaM antagonists inhibiting the PDE1 activity (Saville and Houslay, 1994). In radical contrast, phospho-(Y)-CaM phosphorylated by the EGFR inhibited by 90 % the activity of the PDE1 from bovine heart (Palomo-Jiménez et al., 1999). These conflicting data may be due to the fact that at least eleven families of distinct cyclic nucleotide PDEs, including different isoforms of the CaM-dependent PDE1 with distinct affinities for cAMP and/or cGMP and diverse regulatory properties may coexist and/or being differentially expressed at distinct ratios in various tissues and/or cell types in diverse organisms (Francis et al., 2011). Alternatively, distinct phospho-Y99/phospho-Y138 ratios in the sample of phospho-(Y)-CaM used may account for the observed discrepancies. Nevertheless, it is likely that the negative charges of the extra aspartic acids present in CaM(Y99D/Y138D) may exert a similar action that phospho-CaM in some PDE1 isoform(s). Furthermore, the absence of effect of the single Y/D mutants suggests that the phosphorylation of both tyrosine residues may be necessary for the lower activatory action of phospho-(Y)-CaM on PDE1. The absence of significant effect of the CaM(Y99E/Y138E) mutant also suggests that the length of the side chain of glutamic acid, longer than the one of aspartic acid (3.39 Å and 2.56 Å, respectively, from the carboxylic to the C-α) (Allen, 2002), may be unfitted to interact with the PDE1 site where phospho-(Y)-CaM exerts its regulatory action on the enzyme.

We show that the mutant CaM(Y99D/Y138D), and most prominently CaM(Y99E/Y138E), slightly increase (~ 20-30 %) the V_{max} of eNOS as compared to wild type CaM. Other studies, however, have shown that the single mutant CaM(Y99E)

slightly increase (16 %) the activity of recombinant iNOS, has no significant effect on nNOS, and significantly inhibited (40 %) the activity of eNOS (Piazza et al., 2012). This suggests that the different NOS isoforms may be regulated differently and that the phosphorylation of either one or the two tyrosine residues of CaM may exert significant differential effects on its activity. Nevertheless, our results are qualitatively, but not quantitatively, in agreement with the stimulatory action that phospho-(Y99)-CaM exerts on the V_{max} of nNOS, where a 3.4-fold higher V_{max} than with non-phosphorylated CaM was reported (Corti et al., 1999). These authors also reported a two-fold higher K_{act} of phospho-(Y99)-CaM with respect to non-phosphorylated CaM, and a 4-fold lower K_d for a peptide corresponding to the CaM-binding domain of nNOS (Corti et al., 1999). The different NOS isoforms used in these studies could explain the discrepancy with the lower phospho-mimetic capacity of CaM(Y99D/Y138D) and CaM(Y99E/Y138E) when compared to tyrosine-phosphorylated CaM observed by us.

We also tested the effect of CaM(Y99E/Y138E) on the eNOS activity determined by ITC technique using increasing concentration of L-arginine. However, we encountered huge difficulties with eNOS that made the result obtained uncertain. First of all, the calculated enthalpy of the reaction was very low (-1.4 ± 0.1 kcal/mol) and only a minute quantity of the heat produced during the reaction was detected. Secondly, the critical step of base-line stabilization was prolonged and took about ~1-2 hours for the base-line to stabilize, time that most likely had a negative impact on the enzyme activity. Moreover, during this stabilization period the enzyme was incubated in a complex medium containing a variety of cofactors; notably NADPH, as electron donor, and FAD/FMN that are essential cofactors and also electron acceptors, short-circuiting the electron flow due to the diaphorase activity of eNOS before L-arginine was added (Grozdanovic and Gossrau, 1995).

Our results with the phospho-mimetic CaM(Y99D/Y138D) and CaM(Y99E/Y138E) mutants suggest that phospho-(Y)-CaM may not have a differential action on c-Src activation as compared to non-phosphorylated CaM. Intriguingly, is has been shown in keratinocytes that phospho-(Y138)-CaM does not co-immunoprecipitate with Src, while non-phosphorylated CaM does (Wu et al., 2015). In contrast, our results using CaM(Y99D/Y138D) and CaM(Y99E/Y138E) suggest that CaM phosphorylated at both tyrosines may be able to interact with Src because increases its auto-phoshorylation, in contrast to what it was reported with CaM phosphorylated at Y138 (Wu et al., 2015). No information, however, is available on the possible action of CaM phosphorylated at Y99 on Src activity. This underscores, nevertheless, the potential importance of distinct phosphorylated tyrosine residues and/or variable phosphorylation stoichiometry in the

regulation of CaM-binding proteins, as it becomes apparent in other systems (Benaim and Villalobo, 2002).

It has been shown previously that the cytosolic JM region of the EGFR is essential for its activation (Hubbard, 2009, Red Brewer et al., 2009, Jura et al., 2009). In the generally accepted theory the JM domain as it contains many positively charged amino acids, serves as an auto-inhibitory mechanism by attaching this part of the protein to the negatively charged inner leaflet of the plasma membrane (McLaughlin et al., 2005). Our group has discovered that within the cytosolic juxtamembrane domain of the EGFR lays a region rich in basic amino acids that in fact are forming a CaM-BD (Martin-Nieto and Villalobo, 1998). Previous reports have demonstrated that when CaM binds to the CaM-BD of the EGFR *in vitro* it inhibits its tyrosine kinase activity in a Ca^{2+}-dependent manner as it mimics the negative charged acidic phospholipids in the plasma membrane (San José et al., 1992). In contrast to this, CaM has an activating role in the EGF-dependent activation of the EGFR in living cells (Li et al., 2004, 2012), as it helps to detach the JM from the plasma membrane (McLaughlin et al., 2005, Sato et al., 2006, Sengupta et al., 2007)

Our *in vitro* assays confirmed previous results showing that wild type CaM inhibits the EGF-dependent tyrosine activity of the EGFR in a detergent-solubilized preparation in a Ca^{2+}-dependent manner (San José et al., 1992). When no Ca^{2+} was present in the sample, CaM cannot bind to the receptor to inactivate it, thus we observed higher ligand-dependent activation of the receptor. Interestingly, as in the case of PDE1 and eNOS, here we also observed a differential role of the CaM mutants. CaM(Y99E/Y138E) behaved exactly as the wild type CaM inhibiting the EGF-dependent activation of the EGFR in the presence of Ca^{2+}, while CaM(Y99D/Y138D) exhibited far lower potential inhibiting the auto-phosphorylation of EGFR *in vitro*. The latter results, together with some yet unpublished results generated in our lab show that phospho-(Y)-CaM free of non-phosphorylated CaM has the ability to activate the EGFR instead of inhibiting it *in vitro*, similar to the one exerted by the CaM(Y99D/Y138D) mutant (Stateva et al., 2015, in preparation). All taken together comes to show that phospho-(Y)-CaM may have even more potential than non-phosphorylated CaM in activating the receptor in living cells.

It is intriguing that CaM(Y99D/Y138D), but not CaM(Y99E/Y138E), exerts a differential action on PDE1 and EGFR, as compared to wild type CaM; while in the case of eNOS both CaM(Y99D/Y138D) and CaM(Y99E/Y138E) exert similar effect, albeit the latter with better efficiency. This could be related to the different length of the

side chain of glutamic acid and aspartic acid as mentioned above. Thus, although the actual reason for these distinct effects is unknown, we could speculate that each enzyme or tyrosine kinase used in this study may have pockets or clefts of distinct depths where the negative charge of the carboxyl group of the acidic amino acid must adapt in a proper conformation in order to exert its differential action, and that this pocket/cleft may be deeper in PDE1 than in eNOS. Although the phospho-(Y)-mimetic CaM mutants described in this work exert small differential effects with respect to wild type CaM on the two CaM-binding enzymes tested, the observed effects are qualitative consistent with those exerted by phospho-(Y)-CaM. Therefore, these mutants might be useful tools to study the differential regulation exerted by phospho-(Y)-CaM in a wide variety of CaM-binding proteins with and without enzymatic activity in living cells. This could be achieved by the stable expression of these phospho-(Y)-mimetic CaM mutants in a conditional CaM knockout DT40 cell line recently describe (Panina et al., 2012), after the down-regulation of endogenous CaM by tetracycline, where the action of distinct Ca^{2+}-null and other CaM mutants on the viability and proliferation capacity of these cells was tested (Panina et al., 2012).

7.3 CaM interacts with and activates c-Src

In this work we also show that c-Src not only binds CaM in the absence and presence of Ca^{2+}, as others have previously demonstrated (Yuan et al., 2011, Fedida-Metula et al., 2012, Pérez et al., 2013), but that the Ca^{2+}/CaM complex, and more efficiently apo-CaM, both activate c-Src (Stateva et al., 2015 in press). Although the activation of Src by different signals appears to require Ca^{2+}, as demonstrated by the attenuation of Src activation in cells loaded with the Ca^{2+}-chelator BAPTA-AM (Bobe et al., 2003, Samak et al., 2011), the Ca^{2+}-independent action of CaM on Src activation advises for a partial revision of previous findings on the necessary involvement of an executor Ca^{2+} signal preceding the binding of CaM to Src (Fedida-Metula et al., 2012, Yang et al., 2013, Bobe et al., 2003, Samak et al., 2011, Pérez et al., 2013). The drastic reduction of the cytosolic concentration of free Ca^{2+} imposed in BAPTA-loaded cells may also affect other Ca^{2+}/CaM-dependent systems upstream of Src, as for example the EGFR (Martín-Nieto and Villalobo, 1998, Li et al., 2004, 2012), and not exclusively Src activation. Therefore, a transient Ca^{2+} rise may not be an obligatory step to attain activation of Src since apo-CaM exerts this role even more effectively than Ca^{2+}/CaM. One possibility, however, could be that oscillations in the cytosolic concentration of free Ca^{2+} indeed could act as a rate modulator of the activity of the Src/CaM complex, where CaM could be already tethered to Src, as it occurs in other CaM-binding proteins such as distinct Ca^{2+}-channels (Saucerman and Bers, 2012).

Thus, the kinase activity in the Src/CaM complex could decrease when the concentration of Ca^{2+} rises, by occupying the Ca^{2+}-binding sites of tethered CaM, and conversely increases when the concentration of Ca^{2+} falls and the cation is released from CaM. These events may not necessarily be a simple two-steps cycle (Ca^{2+}-free and Ca^{2+}-bound), as CaM has two high-affinity and two low-affinity Ca^{2+}-binding sites (Chin and Means, 2000). Thus, this process may occur as a multi-stage cycle where a variable number of Ca^{2+}-binding sites are free or occupied at a given time, what may result in a variable rate of Src activity and a more fine-tuned regulation of the kinase.

An alternative possibility is that distinct Ca^{2+}-dependent and Ca^{2+}-independent CaM-binding sites could exist in Src. Yuan and collaborators (Yuan et al., 2011) proposed as the CaM-binding site of human Src the sequence ^{199}KHYKIRKLDSGGF^{213}, located in the terminal part of the SH2 domain. However, mutation of this site substituting the sequence KHYKIRKLDS by alanine residues only partially prevented CaM binding (Yuan et al., 2011). This suggests the existence of additional CaM-binding sites in Src. We identified *in silico* in human Src two additional potential CaM-binding sites, that we denote atypical IQ-like motifs, corresponding to the sequences: ^{146}**IQ**AEEWYFG**K**^{155}, located in the proximal region of the SH2 domain, and ^{311}**LQ**EAQVM**KK**L**R**H^{322}, located in the proximal region of the tyrosine kinase domain (Figure 42). Of note, is to mention that the last sequence located at the proximal region of the kinase has a great potential to be a canonical CaM-BD as well (Figure 42). These sites may contribute to the binding of apo-CaM, as many IQ- and related IQ-like motifs are known to be receptor sites for Ca^{2+}-free CaM in different target proteins (Jurado et al., 1999, Rhoads and Friedberg, 1997).

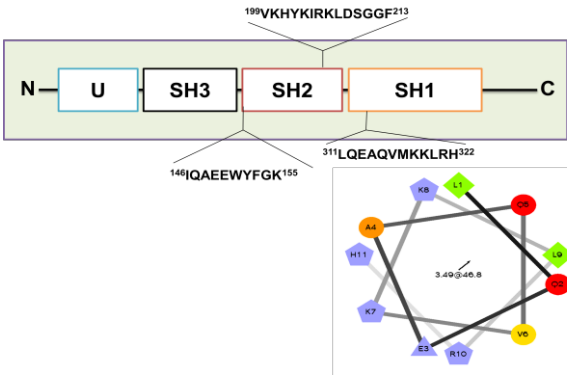

Figure 42: Putative CaM-binding domains in c-Src. The overall structure of Src family kinases is shown, as well as the two putative CaM-binding domains including the potential IQ-like motif. The alpha helical wheel projection of the ^{311}**LQ**EAQVM**KK**L**R**H^{322} sequence is shown.

The non-receptor tyrosine kinase Src is subjected to a complex regulatory mechanisms mediated by phosphorylation events which control its activation status (Okada and Nakagawa, 1989, Cooper and Howell, 1993, Parsons and Parsons, 2004, Irtegun et al., 2013). The stabilization of its activation loop induced by auto-

phosphorylation of Y416 maintains the kinase in an open conformation, allowing substrate binding and hence subsequent signal transmission by the resulting phosphorylated substrates (Cooper and Howell, 1993). On the other hand, the specific phosphorylation of its C-terminal tail at Y527 by Csk or Chk, maintains Src in a closed conformation repressing its activity (Okada and Nakagawa, 1989).

The identification of Src as a CaM-binding protein, and the proposed location of the CaM-binding site(s) at the SH2 and/or tyrosine kinase domains, suggests that CaM may mediate its action maintaining Src in its open activate conformation. We also observed that Ca^{2+} *per se* (absence of CaM) has a direct inhibitory action on Src auto-phosphorylation. This is unlikely to be mediated by an exogenous Ca^{2+}-dependent system, as for example PKC, because we used a purified preparation of recombinant Src and the assay was devoid of cofactors required for PKC activation. Although speculative, an interesting possibility is to search for potential EF-hand Ca^{2+}-binding pocket(s) in Src.

Another point of interest is the fact that the two partners in the well-known bidirectional activatory trans-phosphorylation between EGFR and Src, where Src phosphorylates the EGFR (Anderson et al., 1990, Lombardo et al., 1995, Sato et al., 1995, Biscardi et al., 1998, Gao et al., 2001), and the EGFR phosphorylates Src (Parks and Ceresa, 2014), are regulated by CaM, albeit in different manners. The regulation of EGFR by CaM is a Ca^{2+}-dependent process (Martín-Nieto and Villalobo, 1998, Li et al., 2004, 2012), while the regulation of Src by CaM appears to be a two-faced process, Ca^{2+}-dependent and Ca^{2+}-independent. This opens the door to explore in future work how physiological oscillations in the cytosolic concentration of free Ca^{2+}, upon cell stimulation by mitogenic and/or other factors, modifies this mechanism by affecting in different manner both interconnected partners, the EGFR and Src, and hence the proliferative response.

7.4 EGFR is subjected to *O*-GlcNAcylation in tumor cells

Overall our results show for the first time that human EGFR could be subjected to *O*-GlcNAcylation, as it is the case for the insulin receptor (Yang et al., 2008). We detected EGFR *O*-GlcNacylation in two distinct human tumor cell lines, A431 and A549 cells. A431 cells, derived from a tumor of epidermic origin, and A549 cells derived from a lung epithelial tumor. In contrast, no signal was detected in HeLa cells that are derived from a virus-induced cervical adenocarcinoma. This demonstrates that EGFR *O*-GlcNacylation may not occur in all tumor cells as this process could depend of its tissular and/or organ origin. Moreover, the absence of EGFR *O*-GlcNacylation signal in

EGFR-T17 mouse fibroblasts suggests that this post-translational modification may not be working in a non-physiological setting where a recombinant human EGFR is artificially expressed in cells of other species.

O-GlcNacylation normally is expected to take place in the cytosolic region of the EGFR. Nevertheless, it is noticeable that when the immunoprecipitated EGFR was treated with PNGase F the immunoreactivity of the ~150 kDa *N*-deglycosylated receptor to the two anti-*O*-GlcNAc antibodies used increased as compared with the native 170 kDa EGFR. This suggests that removal of *N*-glycans from the extracellular region of the EGFR could facilitate the exposure of occluded GlcNAc moieties linked to complex *O*-glycans, not related with *O*-GlcNAcylation events that could be non-specifically recognized by the two anti-*O*-GlcNAc antibodies used in this study. In fact, the presence of *O*-glycans in the extracellular region of the EGFR has been described (Wu et al., 2011). Other possibility could be that the removal of sialic acids distributed in the *N*-glycans by the PNGase F enzyme is the reason for both antibodies to have an increased reactivity with the deglycosylated receptor, as it has been already shown that desialation leads to a better binding of certain antibodies (Bolmstedt et al., 1992, Nguyen et al., 2006). Alternatively, the increased immunoreactivity of the anti-*O*-GlcNAc antibodies after the removal of the *N*-glycans by PNGase F, could be also related to the extracellular *O*-GlcNAcylation of the receptor, modification driven by EOGT (Sakaidani et al., 2011, Sakaidani et al., 2012, Ogawa et al., 2014). We were able to find in the extracellular region of the EGFR three sites (^{215}**C**AQQC**SG**R**C**^{223}, ^{236}**C**AA**G**C**TG**PRE^{245} and ^{506}**C**HALC**S**PE**GC**^{515}) that contain key amino acids (cysteine, glycine and serine/threonine) that are also present in the EGF-like domain consensus sequence **C**XX**G**X**S**/**TG**XX**C** recognized by EOGT (Alfaro et al., 2012), particularly the second one. These sites are in the S1 and S2 cysteine-rich regions of the receptor, and the cysteine residues located in the proposed sequences are involved in the formation of disulfide bridges (Abe et al., 1998). Moreover, the strict specificity of some of the anti-*O*-GlcNAc antibodies has been questioned, as for example the CTD110.6 antibody that also recognizes terminal β-GlcNac in complex *N*-glycans (Tashima and Stanley, 2014).

PNGase F is extensively used to remove *N*-glycans from glycoproteins (Maley et al., 1989), but this endoglycosidase is unable to work if a α1-3 bond links fucose to the innermost GlcNAc attached to asparagine (Tretter et al., 1991). Although α1-3-linked fucose to the innermost GlcNAc residues attached to asparagine is common in plant and insect glycoproteins, it appears to be absent in mammalian cells, where α1-6-

linked fucosylation of core GlcNAc catalyzed by fucosyl transferase 8 (FUT8) appears to be the norm (Ma et al., 2006). Nevertheless, to bypass the possible existence of an unrecognized aberrant α1-3-linked fucosylation of the innermost GlcNAc attached to asparagine in tumor cells we used tunicamycin treatment. Our results with tunicamycin also supports absence of α1-3-linked fucosylation of core *O*-GlcNAc in the EGFR from A431 cells, as GlcNAz labeling was clearly detected in the ~150 kDa *N*-deglycosylated EGFR.

The apparent lower level of *O*-GlcNAcylation on the EGFR when the receptor was exposed to EGF stimulation could be explained by the EGF-driven internalization and degradation of the receptor, as this is one of the major consequences of the ligand-dependent activation of the EGFR (Kirisits et al., 2007, Henriksen et al., 2013). In fact, we could not detect any difference in the pattern of the *O*-GlcNacylation in the whole cell protein extract of A431 cells stimulated with EGF. It seems that EGF-induced activation of the EGFR of these cells does not involve changes in the *O*-GlcNAcylation status of other proteins. The lack of effect of EGF-activated A431 cells on protein *O*-GlcNAcylation supports the idea that EGFR signaling is not modulating the *O*-GlcNAc machinery. Moreover, we expected that EGFR may be able to phosphorylate OGT as proposed by others (Kaleem et al., 2009). However, by the *in vitro* phosphorylation assay that we performed gave negative results and most likely OGT is not a substrate for EGFR (Supplementary figure 3S).

Besides the fact that lectins have limited binding affinity and specificity they have been extensively used in studying protein glycosylation (Yang and Hancock, 2005, Etxebarria et al., 2012, Rosenfeld et al., 2007, Fry et al., 2012). WGA is a lectin recognizing GlcNAc moieties located at any glycan structure (De Hoff et al., 2009, Gallagher et al., 1985), we tried to address the question on whether WGA may be able to bind to PNGase F-deglycosylated EGFR (Supplementary figure 4SA). The lectin was able to bind to the *N*-deglycosylated receptor, suggesting that GlcNAc moiety(ies) recognized by the WGA could be located at Ser/Thr residue (Supplementary figure 4SA). Moreover, in order to find out whether EGFR has more complex *O*-glycan structures in its extracellular part as suggested previously, that may be recognized by the anti-*O*-GlcNAc antibodies we have used in our study (CTD110.6 and RL2) or with WGA and thus giving false positive for EGFR *O*-GlcNAcylation, we probed the immunoprecipitated receptor with PNA, a lectin that has preferences in binding to Ser/Thr attached mucin type *O*-glycans (Tajima et al., 2005) (Supplementary figure 4SB). These glycans were found to be present in EGFR expressed in hepatocellular carcinoma cell (HCC) line (Wu et al., 2011). In fact, it has been shown that by

knocking-down the enzyme responsible for the transfer of this mucin type *O*-glycans on target proteins, GALNT2, the malignancy of HCC cells was significantly reduced through mechanism involving EGFR. However, the fact that PNA was not able to bind to the receptor immunoprecipitated from A431 cells (Supplementary figure 4S), strongly suggests that this mucin type *O*-glycosylation is not taking place in these cells. Therefore, we can exclude the possibility of cross-reaction of the two antibodies or WGA with any mucin type *O*-glycans of the receptor expressed in A431 tumor cells.

The suggestion that the EGFR could be subjected to *O*-GlcNAcylation at Thr654 and Ser1046/Ser1047 based on *in silico* modeling as proposed before (Kaleem et al., 2009) is pending experimental confirmation, as many predicting software programs are prone to both false-positive and false-negative predictions (Jochmann et al., 2014). We attempted some experiments using mass spectrometry (MS) to detect EGFR *O*-GlcNAcylation. However, the lack of peptides corresponding to the cytosolic juxtamembrane region of the EGFR, where Thr654 is located, prevents us attaining meaningful results. Nevertheless, we accumulated significant amount of data suggesting that the receptor is subjected to this PTM (Stateva et al., 2015 submitted). We believe that the identification in human EGFR of *O*-linked GlcNAc moiety/ies and the specific Ser and/or Thr residue(s) where it may be attached using a suitable MS method or another technology could be, if positive, the ultimate proof of EGFR *O*-GlcNAcylation. If Thr654 were to be confirmed as an *O*-GlcNAcylation site in EGFR, an interesting subject to study would be to elucidate the possible tripartite crosstalk that may be established between the phosphorylation of this site by PKC (Hunter et al., 1984), the binding of CaM to the cytosolic juxtamembrane region of the receptor where Thr654 residue is located (Martín-Nieto and Villalobo, 1998), and its *O*-GlcNAcylation. Our group demonstrated that phosphorylation of Thr654 by PKC prevents CaM binding to this region, and conversely binding of CaM prevents Thr654 phosphorylation by PKC (Martín-Nieto and Villalobo, 1998). Thus, it is expected that if Thr654 were targeted by OGT a more complex functional picture could emerge by the presence of this *O*-GlcNAcylated residue. Particularly, since phosphorylation of Thr654 appears to inhibit ligand-dependent EGFR activation maintaining the receptor in stand-by at the plasma membrane slowing its internalization (Sánchez-González et al., 2010), and CaM binding appears to contribute to ligand-dependent EGFR activation in living cells (Li et al., 2012).

Another important issue to study is the potential impact that *O*-GlcNAcylation has on EGFR functionality. Since, the OGA inhibitor Thiamet G will block the de-*O*-GlcNAcylation, and most likely will lead to the accumulation of *O*-GlcNAcylated proteins

including EGFR, we hypothesized that this could result in increased receptor activity upon EGF stimulation, of course in the scenario in which Thr654 were targeted by OGT. However, our results using the OGA inhibitor shows little, if any, changes in the time-dependent activation of the receptor by EGF in A431 cells, suggesting perhaps that the proposed cross-talk (Kaleem et al., 2009) is not correct. Both OGA and OGT inhibitors used in this study showed small effect on the EGF-dependent wound closing assay, both accelerating the ligand-driven closure (Supplementary Figure 5S). However, when using the OGT inhibitor (BADGP) and no stimulation present, we were able to observe significant delay in the artificial wound closing in A431 cells (Supplementary Figure 5S). Nevertheless, this observation strongly suggests that *O*-glycosylation is essential for tumor migration and invasion, but since BADGP is not a specific inhibitor of OGT it does not mean necessarily that the delay we observed is due to the inhibition specifically of this transferase.

We were able to locate in the C-terminal sequence of human ncOGT an amino acid sequence comprising of the amino acids ^{987}LEYLKKVRGKVWKQRISSP^{1005} that have great potential to be a CaM-BD. The latter sequence not only exhibit the necessary 1-5-10 CaM canonical biding motif, but contains a sequence ^{991}KKVRGK^{996} with high potential of being a monopartite nuclear localization signal (NLS) K(K/R)X(K/R) (Hodel et al., 2001). The possibility this sequence being a CaM-BD and a NLS at the same time is not surprising. In fact, there are many example of proteins such as the adaptor protein Grb7 (García-Palmero and Villalobo, 2012), the transcriptional factors SRY and SOX9 (Hanover et al., 2009), and nuclear myosin I (Dzijak et al., 2012) among others, where the CaM-BD overlaps the NLS. Moreover, the results from the Ca^{2+}-dependent CaM-affinity chromatography and the co-immunoprecipitation assays, indeed, confirmed that both OGT and CaM are possible binding partners. Generating deletion or substitution mutants lacking the proposed CaM-BD in ncOGT would give the ultimate answer if this is true or not. However, it is noteworthy to mention that we were not able to detect any effect using the CaM inhibitor W-7 on the *O*-GlcNAcylation status of A431 cell proteins and no apparent differences on the *O*-GlcNAcylation of the ET1-55/ EGFR cells was observed when CaM was down-regulated. We believe that the latter observation is most likely due to the possibility that CaM could regulate other function such as the shuttling of the transferase from the nucleus to the cytoplasm, as it does with Grb7 (García-Palmero and Villalobo, 2012) rather than affecting its activity.

With this Thesis we establish the foundation for three new lines of investigation that may reveal new regulatory mechanisms and pathways that could be of help in

understanding and targeting diseases such as cancer. We demonstrated that, indeed tyrosine-phosphorylated CaM and the generated phospho-(Tyr) mutant CaM exert differential roles compared to non-phosphorylated CaM. The generated mutants presented the typical characteristics of the wild type CaM and appeared to be fully functional. The whole panel of mutants was able to activate CaM-dependent systems such as EGFR, c-Src, PDE1 and eNOS *in vitro*, and therefore these mutants could be useful to study as well the role of phospho-(Y)-CaM in living cells. The latter can be achieved by expressing the phospho-mimetic CaM mutants in conditional CaM-KO cells (Panina et al., 2012) and allow to study in detail the role of phospho-(Y)-CaM in living cells. We also demonstrate novel data on the CaM/c-Src axis, showing that CaM can activate c-Src in a Ca^{2+}-dependent and more efficiently in a Ca^{2+}-independent manner *in vitro* (Stateva et al., 2015), and we strongly believe that these findings should bring back CaM/c-Src back on the "track", as CaM may regulates c-Src in a more complex manner in living cells than previously thought. Finally, we demonstrated for the first time that EGFR is subjected to *O*-GlcNAcylation in two distinct cancer cell lines: human carcinoma epidermoide A431 cells and human lung carcinoma A549 cells. Elevated *O*-GlcNAcylation and OGT levels has been found to correlate with higher breast cancer malignancy (Krzeslak et al., 2012), and the same observation has been done for lung and colon cancers (Mi et al., 2011), and prostate cancer (Lynch et al., 2012, Kamigaito et al., 2014) among others (reviewed in de Queiroz et al., 2014). Evidently both *O*-GlcNAcylation and EGFR are hallmarks of these severe pathological processes. It is of great interest to investigate the putative action of *O*-GlcNAc on EGFR functionality including EGF-independent activation, membrane location, nuclear translocation, internalization, intracellular traffic and/or degradation via the lysosomal and/or the ubiquitin-proteasome pathways. How these events may affect important EGFR-mediated cellular functions, such as cell proliferation, differentiation, cell survival, and programmed cell death warrant also special attention. Further investigation on this subject as well as the elucidation of the functional role exerted by CaM on OGT functionality would make a valuable contribution to the field of *O*-GlcNAcylation.

8. CONCLUSIONS

1. The generated Y/D and Y/E phospho-mimetic CaM mutants are functional and biologically active:
    - All of the CaM species bind Ca^{2+} as shown by circular dichroism, Tb^{3+} fluorescence and thermal stability experiments
    - All of the CaM species are able to activate specific the CaM-dependent enzymes PDE1 and eNOS in a Ca^{2+}-dependent manner.

2. CaM(Y99D/Y138D), but not CaM(Y99E/Y138E), has lower potential to activate PDE1 and exhibit effect similar to phospho-(Y)-CaM.

3. CaM(Y99E/Y138E) has higher potential to activate eNOS than wild type CaM and shows effect similar to phospho-(Y)-CaM.

4. Both double Y/D and Y/E CaM mutants do not have any differential effects on the activation of c-Src.

5. CaM(Y99D/Y138D) has significantly higher ability to activate EGF-dependent activation of purified EGFR in the absence and presence of Ca^{2+} than Ca^{2+}/ CaM.

6. Apo-CaM has higher activatory effect on the auto-phosphorylation of c-Src suggesting that c-Src has more than one CaM-BD.

7. The highly specific calmodulin inhibitor W-7 blocked the EGF and H_2O_2 driven activation of c-Src in A431 and/or SK-BR-3 cells, pointing out that CaM is actively involved in the regulation of Src *in vivo*.

8. Human EGFR is subjected to *O*-GlcNAcylation in A431 and A549 cells but not in HeLa cells and mouse EGFR-T17 fibroblast.

9. The highly specific OGA inhibitor Thiamet G increased significantly the *O*-GlcNAcylation of the receptor, but did not have any effect on its EGF-dependent activation in living cells.

10. OGT is a putative CaM-binding protein.

9. REFERENCES

ABE, Y., ODAKA, M., INAGAKI, F., LAX, I., SCHLESSINGER, J. & KOHDA, D. 1998. Disulfide bond structure of human epidermal growth factor receptor. *J Biol Chem,* 273**,** 11150-7.

AIFA, S., AYDIN, J., NORDVALL, G., LUNDSTROM, I., SVENSSON, S. P. & HERMANSON, O. 2005. A basic peptide within the juxtamembrane region is required for EGF receptor dimerization. *Exp Cell Res,* 302**,** 108-14.

AIUCHI, T., HAGIWARA, T., OMATA, K., NAKAYA, K. & NAKAMURA, Y. 1991. Effect of phosphorylation of calmodulin on calcium binding affinity as estimated by terbium fluorescence. *Biochem Int,* 23**,** 145-9.

ALDERTON, W. K., COOPER, C. E. & KNOWLES, R. G. 2001. Nitric oxide synthases: structure, function and inhibition. *Biochem J,* 357**,** 593-615.

ALFARO, J. F., GONG, C. X., MONROE, M. E., ALDRICH, J. T., CLAUSS, T. R., PURVINE, S. O., WANG, Z., CAMP, D. G., 2ND, SHABANOWITZ, J., STANLEY, P., HART, G. W., HUNT, D. F., YANG, F. & SMITH, R. D. 2012. Tandem mass spectrometry identifies many mouse brain O-GlcNAcylated proteins including EGF domain-specific O-GlcNAc transferase targets. *Proc Natl Acad Sci U S A,* 109**,** 7280-5.

ALLEN, F. H. 2002. The Cambridge Structural Database: a quarter of a million crystal structures and rising. *Acta Crystallogr B,* 58**,** 380-8.

ALONSO, J., SCHIMPL, M. & VAN AALTEN, D. M. 2014. O-GlcNAcase: promiscuous hexosaminidase or key regulator of O-GlcNAc signaling? *J Biol Chem,* 289**,** 34433-9.

ANDE, S. R., MOULIK, S. & MISHRA, S. 2009. Interaction between O-GlcNAc modification and tyrosine phosphorylation of prohibitin: implication for a novel binary switch. *PLoS One,* 4**,** e4586.

ANDERSON, D., KOCH, C. A., GREY, L., ELLIS, C., MORAN, M. F. & PAWSON, T. 1990. Binding of SH2 domains of phospholipase Cγ1, GAP, and Src to activated growth factor receptors. *Science,* 250**,** 979-82.

AOYAGI, M., ARVAI, A. S., TAINER, J. A. & GETZOFF, E. D. 2003. Structural basis for endothelial nitric oxide synthase binding to calmodulin. *EMBO J,* 22**,** 766-75.

AYRAPETOV, M. K., WANG, Y. H., LIN, X., GU, X., PARANG, K. & SUN, G. 2006. Conformational basis for SH2-Tyr(P)527 binding in Src inactivation. *J Biol Chem,* 281**,** 23776-84.

BAO, J., ALROY, I., WATERMAN, H., SCHEJTER, E. D., BRODIE, C., GRUENBERG, J. & YARDEN, Y. 2000. Threonine phosphorylation diverts internalized epidermal growth factor receptors from a degradative pathway to the recycling endosome. *J Biol Chem,* 275**,** 26178-86.

BARRITT, G. J. 1999. Receptor-activated Ca^{2+} inflow in animal cells: a variety of pathways tailored to meet different intracellular Ca^{2+} signalling requirements. *Biochem J,* 337 (Pt 2)**,** 153-69.

BASUROY, S., DUNAGAN, M., SHETH, P., SETH, A. & RAO, R. K. 2010. Hydrogen peroxide activates focal adhesion kinase and c-Src by a phosphatidylinositol 3 kinase-dependent mechanism and promotes cell migration in Caco-2 cell monolayers. *Am J Physiol Gastrointest Liver Physiol,* 299**,** G186-95.

BENAIM, G., CERVINO, V. & VILLALOBO, A. 1998. Comparative phosphorylation of calmodulin from trypanosomatids and bovine brain by calmodulin-binding protein kinases. *Comp Biochem Physiol C Pharmacol Toxicol Endocrinol,* 120**,** 57-65.

BENAIM, G. & VILLALOBO, A. 2002. Phosphorylation of calmodulin. Functional implications. *Eur J Biochem,* 269**,** 3619-31.

BENGURÍA, A., HERNÁNDEZ-PERERA, O., MARTÍNEZ-PASTOR, M. T., SACKS, D. B. & VILLALOBO, A. 1994. Phosphorylation of calmodulin by the epidermal-growth-factor-receptor tyrosine kinase. *Eur J Biochem,* 224**,** 909-16.

BENGURÍA, A., MARTÍN-NIETO, J., BENAIM, G. & VILLALOBO, A. 1995. Regulatory interaction between calmodulin and the epidermal growth factor receptor. *Ann N Y Acad Sci,* 766**,** 472-6.

BERCHTOLD, M. W. & VILLALOBO, A. 2014. The many faces of calmodulin in cell proliferation, programmed cell death, autophagy, and cancer. *Biochim Biophys Acta,* 1843**,** 398-435.

BERRIDGE, M. J., BOOTMAN, M. D. & RODERICK, H. L. 2003. Calcium signalling: dynamics, homeostasis and remodelling. *Nat Rev Mol Cell Biol,* 4**,** 517-29.

BHATTACHARYA, S., BUNICK, C. G. & CHAZIN, W. J. 2004. Target selectivity in EF-hand calcium binding proteins. *Biochim Biophys Acta,* 1742**,** 69-79.

BIRNBOIM, H. C. & DOLY, J. 1979. A rapid alkaline extraction procedure for screening recombinant plasmid DNA. *Nucleic Acids Res,* 7**,** 1513-23.

BISCARDI, J. S., BELSCHES, A. P. & PARSONS, S. J. 1998. Characterization of human epidermal growth factor receptor and c-Src interactions in human breast tumor cells. *Mol Carcinog,* 21**,** 261-72.

BOBE, R., YIN, X., ROUSSANNE, M. C., STEPIEN, O., POLIDANO, E., FAVERDIN, C. & MARCHE, P. 2003. Evidence for ERK1/2 activation by thrombin that is independent of EGFR transactivation. *Am J Physiol Heart Circ Physiol,* 285**,** H745-54.

BOGDAN, C. 2015. Nitric oxide synthase in innate and adaptive immunity: an update. *Trends Immunol,* 36**,** 161-178.

BOLMSTEDT, A., OLOFSSON, S., SJOGREN-JANSSON, E., JEANSSON, S., SJOBLOM, I., AKERBLOM, L., HANSEN, J. E. & HU, S. L. 1992. Carbohydrate determinant NeuAc-Gal β (1-4) of N-linked glycans modulates the antigenic activity of human immunodeficiency virus type 1 glycoprotein gp120. *J Gen Virol,* 73 (Pt 12)**,** 3099-105.

BRZESKA, H., VENYAMINOV, S., GRABAREK, Z. & DRABIKOWSKI, W. 1983. Comparative studies on thermostability of calmodulin, skeletal muscle troponin C and their tryptic fragments. *FEBS Lett,* 153**,** 169-73.

BURGESS, W. H., JEMIOLO, D. K. & KRETSINGER, R. H. 1980. Interaction of calcium and calmodulin in the presence of sodium dodecyl sulfate. *Biochim Biophys Acta,* 623**,** 257-70.

BUTCHER, R. W. & SUTHERLAND, E. W. 1962. Adenosine 3',5'-phosphate in biological materials. I. Purification and properties of cyclic 3',5'-nucleotide phosphodiesterase and use of this enzyme to characterize adenosine 3',5'-phosphate in human urine. *J Biol Chem,* 237**,** 1244-50.

CAPOTOSTI, F., GUERNIER, S., LAMMERS, F., WARIDEL, P., CAI, Y., JIN, J., CONAWAY, J. W., CONAWAY, R. C. & HERR, W. 2011. O-GlcNAc transferase catalyzes site-specific proteolysis of HCF-1. *Cell,* 144**,** 376-88.

CHEUNG, W. Y. 1967. Cyclic 3',5'-nucleotide phosphodiesterase: pronounced stimulation by snake venom. *Biochem Biophys Res Commun,* 29**,** 478-82.

CHEUNG, W. Y. 1970. Cyclic 3',5'-nucleotide phosphodiesterase. Demonstration of an activator. *Biochem Biophys Res Commun,* 38**,** 533-8.

CHEUNG, W. Y. 1980. Calmodulin plays a pivotal role in cellular regulation. *Science,* 207**,** 19-27.

CHEUNG, W. Y., BRADHAM, L. S., LYNCH, T. J., LIN, Y. M. & TALLANT, E. A. 1975. Protein activator of cyclic 3':5'-nucleotide phosphodiesterase of bovine or rat brain also activates its adenylate cyclase. *Biochem Biophys Res Commun,* 66**,** 1055-62.

CHIN, D. & MEANS, A. R. 2000. Calmodulin: a prototypical calcium sensor. *Trends Cell Biol,* 10**,** 322-8.

CHO, H. J., XIE, Q. W., CALAYCAY, J., MUMFORD, R. A., SWIDEREK, K. M., LEE, T. D. & NATHAN, C. 1992. Calmodulin is a subunit of nitric oxide synthase from macrophages. *J Exp Med,* 176**,** 599-604.

CHONG, Y. P., MULHERN, T. D. & CHENG, H. C. 2005. C-terminal Src kinase (CSK) and CSK-homologous kinase (CHK)-endogenous negative regulators of Src-family protein kinases. *Growth Factors,* 23**,** 233-44.

CLAPHAM, D. E. 2007. Calcium signaling. *Cell,* 131**,** 1047-58.

COOPER, J. A. & HOWELL, B. 1993. The when and how of Src regulation. *Cell,* 73**,** 1051-4.

CORTI, C., LECLERC L'HOSTIS, E., QUADRONI, M., SCHMID, H., DURUSSEL, I., COX, J., DAINESE HATT, P., JAMES, P. & CARAFOLI, E. 1999. Tyrosine phosphorylation modulates the interaction of calmodulin with its target proteins. *Eur J Biochem,* 262**,** 790-802.

COUNTAWAY, J. L., NAIRN, A. C. & DAVIS, R. J. 1992. Mechanism of desensitization of the epidermal growth factor receptor protein-tyrosine kinase. *J Biol Chem,* 267**,** 1129-40.

CRIVICI, A. & IKURA, M. 1995. Molecular and structural basis of target recognition by calmodulin. *Annu Rev Biophys Biomol Struct,* 24**,** 85-116.

DAFF, S., NOBLE, M. A., CRAIG, D. H., RIVERS, S. L., CHAPMAN, S. K., MUNRO, A. W., FUJIWARA, S., ROZHKOVA, E., SAGAMI, I. & SHIMIZU, T. 2001. Control of electron transfer in neuronal NO synthase. *Biochem Soc Trans,* 29**,** 147-52.

DAGHER, R., PENG, S., GIORIA, S., FEVE, M., ZENIOU, M., ZIMMERMANN, M., PIGAULT, C., HAIECH, J. & KILHOFFER, M. C. 2011. A general strategy to characterize calmodulin-calcium complexes involved in CaM-target recognition: DAPK and EGFR calmodulin binding domains interact with different calmodulin-calcium complexes. *Biochim Biophys Acta,* 1813**,** 1059-67.

DANCEY, J. E. 2004. Predictive factors for epidermal growth factor receptor inhibitors--the bull's-eye hits the arrow. *Cancer Cell,* 5**,** 411-5.

DAS, S. & KUMAR, K. N. 1995. Nitric oxide: its identity and role in blood pressure control. *Life Sci,* 57**,** 1547-56.

DAVIS, H. W., CRIMMINS, D. L., THOMA, R. S. & GARCIA, J. G. 1996. Phosphorylation of calmodulin in the first calcium-binding pocket by myosin light chain kinase. *Arch Biochem Biophys,* 332**,** 101-9.

DE FRUTOS, T., MARTÍN-NIETO, J. & VILLALOBO, A. 1997. Phosphorylation of calmodulin by permeabilized fibroblasts overexpressing the human epidermal growth factor receptor. *Biol Chem,* 378**,** 31-7.

DE HOFF, P. L., BRILL, L. M. & HIRSCH, A. M. 2009. Plant lectins: the ties that bind in root symbiosis and plant defense. *Mol Genet Genomics,* 282**,** 1-15.

DE QUEIROZ, R. M., CARVALHO, E. & DIAS, W. B. 2014. O-GlcNAcylation: The Sweet Side of the Cancer. *Front Oncol,* 4**,** 132.

DIAS, W. B., CHEUNG, W. D. & HART, G. W. 2012. O-GlcNAcylation of kinases. *Biochem Biophys Res Commun,* 422**,** 224-8.

DONG, D. L. & HART, G. W. 1994. Purification and characterization of an O-GlcNAc selective N-acetyl-β-D-glucosaminidase from rat spleen cytosol. *J Biol Chem,* 269**,** 19321-30.

DZIJAK, R., YILDIRIM, S., KAHLE, M., NOVAK, P., HNILICOVA, J., VENIT, T. & HOZAK, P. 2012. Specific nuclear localizing sequence directs two myosin isoforms to the cell nucleus in calmodulin-sensitive manner. *PLoS One,* 7**,** e30529.

ETXEBARRIA, J., CALVO, J., MARTIN-LOMAS, M. & REICHARDT, N. C. 2012. Lectin-array blotting: profiling protein glycosylation in complex mixtures. *ACS Chem Biol,* 7**,** 1729-37.

FASMAN, G. D. 1996. Differentiation between transmembrane helices and peripheral helices by the deconvolution of circular dichroism spectra of membrane proteins. In: Circular Dichroism and the Conformational Analysis of Biomolecules (G. D. Fasman, Ed.), Plenum Press, New York. 381-412.

FEDIDA-METULA, S., FELDMAN, B., KOSHELEV, V., LEVIN-GROMIKO, U., VORONOV, E. & FISHMAN, D. 2012. Lipid rafts couple store-operated Ca^{2+} entry to constitutive activation of PKB/Akt in a Ca^{2+}/calmodulin-, Src- and PP2A-mediated pathway and promote melanoma tumor growth. *Carcinogenesis,* 33**,** 740-50.

FERGUSON, K. M., BERGER, M. B., MENDROLA, J. M., CHO, H. S., LEAHY, D. J. & LEMMON, M. A. 2003. EGF activates its receptor by removing interactions that autoinhibit ectodomain dimerization. *Mol Cell,* 11**,** 507-17.

FILHOULAUD, G., GUILLEMAIN, G. & SCHARFMANN, R. 2009. The hexosamine biosynthesis pathway is essential for pancreatic beta cell development. *J Biol Chem,* 284**,** 24583-94.

FISCHER, E. H. 2013. Cellular regulation by protein phosphorylation. *Biochem Biophys Res Commun,* 430**,** 865-7.

FISKE, C. H. & SUBBAROW, Y. 1925. The colorimetric determination of phosphorus. *J Biol Chem,* 66**,** 375-400.

FISSLTHALER, B., LOOT, A. E., MOHAMED, A., BUSSE, R. & FLEMING, I. 2008. Inhibition of endothelial nitric oxide synthase activity by proline-rich tyrosine kinase 2 in response to fluid shear stress and insulin. *Circ Res,* 102**,** 1520-8.

FRANCIS, S. H., BLOUNT, M. A. & CORBIN, J. D. 2011. Mammalian cyclic nucleotide phosphodiesterases: molecular mechanisms and physiological functions. *Physiol Rev,* 91**,** 651-90.

FRY, S., AFROUGH, B., LEATHEM, A. & DWEK, M. 2012. Lectin array-based strategies for identifying metastasis-associated changes in glycosylation. *Methods Mol Biol,* 878**,** 267-72.

FUJITA-YAMAGUCHI, Y., KATHURIA, S., XU, Q. Y., MCDONALD, J. M., NAKANO, H. & KAMATA, T. 1989. *In vitro* tyrosine phosphorylation studies on RAS proteins and calmodulin suggest that polylysine-like basic peptides or domains may be involved in interactions between insulin receptor kinase and its substrate. *Proc Natl Acad Sci U S A,* 86**,** 7306-10.

FUKAMI, Y., NAKAMURA, T., NAKAYAMA, A. & KANEHISA, T. 1986. Phosphorylation of tyrosine residues of calmodulin in Rous sarcoma virus-transformed cells. *Proc Natl Acad Sci U S A,* 83**,** 4190-3.

GAGNON, C., KELLY, S., MANGANIELLO, V., VAUGHAN, M., ODYA, C., STRITTMATTER, W., HOFFMAN, A. & HIRATA, F. 1981. Modification of calmodulin function by enzymatic carboxylic methylation. *Nature,* 291**,** 515-6.

GALLAGHER, J. T., MORRIS, A. & DEXTER, T. M. 1985. Identification of two binding sites for wheat-germ agglutinin on polylactosamine-type oligosaccharides. *Biochem J,* 231**,** 115-22.

GANGOLA, P. & PANT, H. C. 1983. Temperature dependent conformational changes in calmodulin. *Biochem Biophys Res Commun,* 111**,** 301-5.

GAO, Y., TANG, S., ZHOU, S. & WARE, J. A. 2001. The thromboxane A2 receptor activates mitogen-activated protein kinase via protein kinase C-dependent G_i coupling and Src-dependent phosphorylation of the epidermal growth factor receptor. *J Pharmacol Exp Ther,* 296**,** 426-33.

GARAVELLI, J. S. 2004. The RESID Database of Protein Modifications as a resource and annotation tool. *Proteomics,* 4**,** 1527-33.

GARCÍA-PALMERO, I. & VILLALOBO, A. 2012. Calmodulin regulates the translocation of Grb7 into the nucleus. *FEBS Lett,* 586**,** 1533-9.

GHOSH, D. K. & SALERNO, J. C. 2003. Nitric oxide synthases: domain structure and alignment in enzyme function and control. *Front Biosci,* 8**,** d193-209.

GOLDBERG, H., WHITESIDE, C. & FANTUS, I. G. 2011. O-linked beta-N-acetylglucosamine supports p38 MAPK activation by high glucose in glomerular mesangial cells. *Am J Physiol Endocrinol Metab,* 301**,** E713-26.

GOMASE, V. S. & TAGORE, S. 2008. Kinomics. *Curr Drug Metab,* 9**,** 255-8.

GONG, C. X., LIU, F., GRUNDKE-IQBAL, I. & IQBAL, K. 2006. Impaired brain glucose metabolism leads to Alzheimer neurofibrillary degeneration through a decrease in tau O-GlcNAcylation. *J Alzheimers Dis,* 9**,** 1-12.

GOVERS, R. & RABELINK, T. J. 2001. Cellular regulation of endothelial nitric oxide synthase. *Am J Physiol Renal Physiol,* 280**,** F193-206.

GRAVES, C. B., GALE, R. D., LAURINO, J. P. & McDONALD, J. M. 1986. The insulin receptor and calmodulin. Calmodulin enhances insulin-mediated receptor kinase activity and insulin stimulates phosphorylation of calmodulin. *J Biol Chem,* 261**,** 10429-38.

GRAVES, C. B., GOEWERT, R. R. & McDONALD, J. M. 1985. The insulin receptor contains a calmodulin-binding domain. *Science,* 230**,** 827-9.

GREGORI, L., MARRIOTT, D., WEST, C. M. & CHAU, V. 1985. Specific recognition of calmodulin from *Dictyostelium discoideum* by the ATP, ubiquitin-dependent degradative pathway. *J Biol Chem,* 260**,** 5232-5.

GREIF, D. M., SACKS, D. B. & MICHEL, T. 2004. Calmodulin phosphorylation and modulation of endothelial nitric oxide synthase catalysis. *Proc Natl Acad Sci U S A,* 101**,** 1165-70.

GRIFFITH, O. W. & STUEHR, D. J. 1995. Nitric oxide synthases: properties and catalytic mechanism. *Annu Rev Physiol,* 57**,** 707-36.

GROSS, B. J., KRAYBILL, B. C. & WALKER, S. 2005. Discovery of O-GlcNAc transferase inhibitors. *J Am Chem Soc,* 127**,** 14588-9.

GROZDANOVIC, Z. & GOSSRAU, R. 1995. α-NADPH appears to be primarily oxidized by the NADPH-diaphorase activity of nitric oxide synthase (NOS). *Acta Histochem,* 97**,** 313-20.

GULLICK, W. J. 2001. The Type 1 growth factor receptors and their ligands considered as a complex system. *Endocr Relat Cancer,* 8**,** 75-82.

HAHNE, H. & KUSTER, B. 2011. A novel two-stage tandem mass spectrometry approach and scoring scheme for the identification of O-GlcNAc modified peptides. *J Am Soc Mass Spectrom,* 22**,** 931-42.

HALPIN, D. M. 2008. ABCD of the phosphodiesterase family: interaction and differential activity in COPD. *Int J Chron Obstruct Pulmon Dis,* 3**,** 543-61.

HANOVER, J. A., LOVE, D. C. & PRINZ, W. A. 2009. Calmodulin-driven nuclear entry: trigger for sex determination and terminal differentiation. *J Biol Chem,* 284**,** 12593-7.

HART, G. W. 2014. Minireview series on the thirtieth anniversary of research on O-GlcNAcylation of nuclear and cytoplasmic proteins: Nutrient regulation of cellular metabolism and physiology by O-GlcNAcylation. *J Biol Chem,* 289**,** 34422-3.

HART, G. W., GREIS, K. D., DONG, L. Y., BLOMBERG, M. A., CHOU, T. Y., JIANG, M. S., ROQUEMORE, E. P., SNOW, D. M., KREPPEL, L. K., COLE, R. N. & ET AL. 1995. O-linked N-acetylglucosamine: the "yin-yang" of Ser/Thr phosphorylation? Nuclear and cytoplasmic glycosylation. *Adv Exp Med Biol,* 376**,** 115-23.

HART, G. W., SLAWSON, C., RAMIREZ-CORREA, G. & LAGERLOF, O. 2011. Cross talk between O-GlcNAcylation and phosphorylation: roles in signaling, transcription, and chronic disease. *Annu Rev Biochem,* 80**,** 825-58.

HAYASHI, N., MATSUBARA, M., TAKASAKI, A., TITANI, K. & TANIGUCHI, H. 1998. An expression system of rat calmodulin using T7 phage promoter in Escherichia coli. *Protein Expr Purif,* 12**,** 25-8.

HAYASHI, N., NAKAGAWA, C., ITO, Y., TAKASAKI, A., JINBO, Y., YAMAKAWA, Y., TITANI, K., HASHIMOTO, K., IZUMI, Y. & MATSUSHIMA, N. 2004. Myristoylation-regulated direct interaction between calcium-bound calmodulin and N-terminal region of $pp60^{v\text{-}src}$. *J Mol Biol,* 338**,** 169-80.

HENRIKSEN, L., GRANDAL, M. V., KNUDSEN, S. L., VAN DEURS, B. & GROVDAL, L. M. 2013. Internalization mechanisms of the epidermal growth factor receptor after activation with different ligands. *PLoS One,* 8**,** e58148.

HIDAKA, H., SASAKI, Y., TANAKA, T., ENDO, T., OHNO, S., FUJII, Y. & NAGATA, T. 1981. N-(6-aminohexyl)-5-chloro-1-naphthalenesulfonamide, a calmodulin antagonist, inhibits cell proliferation. *Proc Natl Acad Sci U S A,* 78**,** 4354-7.

HIDAKA, H. & TANAKA, T. 1983. Naphthalenesulfonamides as calmodulin antagonists. *Methods Enzymol,* 102**,** 185-94.

HODEL, M. R., CORBETT, A. H. & HODEL, A. E. 2001. Dissection of a nuclear localization signal. *J Biol Chem,* 276**,** 1317-25.

HOLT, G. D. & HART, G. W. 1986. The subcellular distribution of terminal N-acetylglucosamine moieties. Localization of a novel protein-saccharide linkage, O-linked GlcNAc. *J Biol Chem,* 261**,** 8049-57.

HUBBARD, S. R. 2009. The juxtamembrane region of EGFR takes center stage. *Cell,* 137**,** 1181-3.

HUNTER, T., LING, N. & COOPER, J. A. 1984. Protein kinase C phosphorylation of the EGF receptor at a threonine residue close to the cytoplasmic face of the plasma membrane. *Nature,* 311**,** 480-3.

IRTEGUN, S., WOOD, R. J., ORMSBY, A. R., MULHERN, T. D. & HATTERS, D. M. 2013. Tyrosine 416 is phosphorylated in the closed, repressed conformation of c-Src. *PLoS One,* 8**,** e71035.

IYER, S. P. & HART, G. W. 2003. Roles of the tetratricopeptide repeat domain in O-GlcNAc transferase targeting and protein substrate specificity. *J Biol Chem,* 278**,** 24608-16.

JACKSON, A. E., CARRAWAY, K. L., 3RD, PAYNE, M. E., MEANS, A. R., PUETT, D. & BREW, K. 1987. Association of calmodulin and smooth muscle myosin light chain kinase: application of a label selection technique with trace acetylated calmodulin. *Proteins,* 2**,** 202-9.

JANETZKO, J. & WALKER, S. 2014. The making of a sweet modification: structure and function of O-GlcNAc transferase. *J Biol Chem,* 289**,** 34424-32.

JENSEN, O. N. 2006. Interpreting the protein language using proteomics. *Nat Rev Mol Cell Biol,* 7**,** 391-403.

JOCHMANN, R., HOLZ, P., STICHT, H. & STURZL, M. 2014. Validation of the reliability of computational O-GlcNAc prediction. *Biochim Biophys Acta,* 1844**,** 416-21.

JOZWIAK, P., FORMA, E., BRYS, M. & KRZESLAK, A. 2014. O-GlcNAcylation and Metabolic Reprograming in Cancer. *Front Endocrinol (Lausanne),* 5**,** 145.

JURA, N., ENDRES, N. F., ENGEL, K., DEINDL, S., DAS, R., LAMERS, M. H., WEMMER, D. E., ZHANG, X. & KURIYAN, J. 2009. Mechanism for activation of the EGF receptor catalytic domain by the juxtamembrane segment. *Cell,* 137**,** 1293-307.

JURADO, L. A., CHOCKALINGAM, P. S. & JARRETT, H. W. 1999. Apocalmodulin. *Physiol Rev,* 79**,** 661-82.

KAKIUCHI, S. & YAMAZAKI, R. 1970. Calcium dependent phosphodiesterase activity and its activating factor (PAF) from brain studies on cyclic 3',5'-nucleotide phosphodiesterase (3). *Biochem Biophys Res Commun,* 41**,** 1104-10.

KALEEM, A., AHMAD, I., HOESSLI, D. C., WALKER-NASIR, E., SALEEM, M., SHAKOORI, A. R. & NASIR UD, D. 2009. Epidermal growth factor receptors: function modulation by phosphorylation and glycosylation interplay. *Mol Biol Rep,* 36**,** 631-9.

KAMIGAITO, T., OKANEYA, T., KAWAKUBO, M., SHIMOJO, H., NISHIZAWA, O. & NAKAYAMA, J. 2014. Overexpression of O-GlcNAc by prostate cancer cells is significantly associated with poor prognosis of patients. *Prostate Cancer Prostatic Dis,* 17**,** 18-22.

KELLY, S. M., JESS, T. J. & PRICE, N. C. 2005. How to study proteins by circular dichroism. *Biochim. Biophys. Acta,* 1751**,** 19-139.

KERAVIS, T. & LUGNIER, C. 2012. Cyclic nucleotide phosphodiesterase (PDE) isozymes as targets of the intracellular signalling network: benefits of PDE inhibitors in various diseases and perspectives for future therapeutic developments. *Br J Pharmacol,* 165**,** 1288-305.

KERWIN, J. F., JR., LANCASTER, J. R., JR. & FELDMAN, P. L. 1995. Nitric oxide: a new paradigm for second messengers. *J Med Chem,* 38**,** 4343-62.

KILHOFFER, M. C., DEMAILLE, J. G. & GERARD, D. 1981. Tyrosine fluorescence of ram testis and octopus calmodulins. Effects of calcium, magnesium, and ionic strength. *Biochemistry,* 20**,** 4407-14.

KIM, H. & MULLER, W. J. 1999. The role of the epidermal growth factor receptor family in mammary tumorigenesis and metastasis. *Exp Cell Res,* 253**,** 78-87.

KIRISITS, A., PILS, D. & KRAINER, M. 2007. Epidermal growth factor receptor degradation: an alternative view of oncogenic pathways. *Int J Biochem Cell Biol,* 39**,** 2173-82.

KLEE, C. B., CROUCH, T. H. & KRINKS, M. H. 1979. Subunit structure and catalytic properties of bovine brain Ca^{2+}-dependent cyclic nucleotide phosphodiesterase. *Biochemistry,* 18**,** 722-9.

KLEE, C. B. & VANAMAN, T. C. 1982. Calmodulin. *Adv Protein Chem,* 35**,** 213-321.

KNEASS, Z. T. & MARCHASE, R. B. 2004. Neutrophils exhibit rapid agonist-induced increases in protein-associated O-GlcNAc. *J Biol Chem,* 279**,** 45759-65.

KRZESLAK, A., FORMA, E., BERNACIAK, M., ROMANOWICZ, H. & BRYS, M. 2012. Gene expression of O-GlcNAc cycling enzymes in human breast cancers. *Clin Exp Med,* 12**,** 61-5.

LAEMMLI, U. K. 1970. Cleavage of structural proteins during the assembly of the head of bacteriophage T4. *Nature,* 227**,** 680-5.

LAMAZE, C. & SCHMID, S. L. 1995. Recruitment of epidermal growth factor receptors into coated pits requires their activated tyrosine kinase. *J Cell Biol,* 129**,** 47-54.

LAURINO, J. P., COLCA, J. R., PEARSON, J. D., DEWALD, D. B. & McDONALD, J. M. 1988. The in vitro phosphorylation of calmodulin by the insulin receptor tyrosine kinase. *Arch Biochem Biophys,* 265**,** 8-21.

LAZARUS, M. B., JIANG, J., KAPURIA, V., BHUIYAN, T., JANETZKO, J., ZANDBERG, W. F., VOCADLO, D. J., HERR, W. & WALKER, S. 2013. HCF-1 is cleaved in the active site of O-GlcNAc transferase. *Science,* 342**,** 1235-9.

LECLERC, E., CORTI, C., SCHMID, H., VETTER, S., JAMES, P. & CARAFOLI, E. 1999. Serine/threonine phosphorylation of calmodulin modulates its interaction with the binding domains of target enzymes. *Biochem J,* 344 Pt 2**,** 403-11.

LEFEBVRE, T., DEHENNAUT, V., GUINEZ, C., OLIVIER, S., DROUGAT, L., MIR, A. M., MORTUAIRE, M., VERCOUTTER-EDOUART, A. S. & MICHALSKI, J. C. 2010. Dysregulation of the nutrient/stress sensor O-GlcNAcylation is involved in the etiology of cardiovascular disorders, type-2 diabetes and Alzheimer's disease. *Biochim Biophys Acta,* 1800**,** 67-79.

LEMMON, M. A., SCHLESSINGER, J. & FERGUSON, K. M. 2014. The EGFR family: not so prototypical receptor tyrosine kinases. *Cold Spring Harb Perspect Biol,* 6**,** a020768.

LEWIS, B. A. & HANOVER, J. A. 2014. O-GlcNAc and the epigenetic regulation of gene expression. *J Biol Chem,* 289**,** 34440-8.

LI, H., PANINA, S., KAUR, A., RUANO, M. J., SÁNCHEZ-GONZÁLEZ, P., LA COUR, J. M., STEPHAN, A., OLESEN, U. H., BERCHTOLD, M. W. & VILLALOBO, A. 2012. Regulation of the ligand-dependent activation of the epidermal growth factor receptor by calmodulin. *J Biol Chem,* 287**,** 3273-81.

LI, H., RUANO, M. J. & VILLALOBO, A. 2004. Endogenous calmodulin interacts with the epidermal growth factor receptor in living cells. *FEBS Lett,* 559**,** 175-80.

LI, Z. & YI, W. 2014. Regulation of cancer metabolism by O-GlcNAcylation. *Glycoconj J,* 31**,** 185-91.

LIE, P. P., MRUK, D. D., MOK, K. W., SU, L., LEE, W. M. & CHENG, C. Y. 2012. Focal adhesion kinase-Tyr407 and -Tyr397 exhibit antagonistic effects on blood-testis barrier dynamics in the rat. *Proc Natl Acad Sci U S A,* 109**,** 12562-7.

LIN, P. H., SELINFREUND, R. H., WAKSHULL, E. & WHARTON, W. 1988. Rapid isolation of plasmalemma from cultured A431 cells: characterization of epidermal growth factor receptors. *Anal Biochem,* 168**,** 300-5.

LINGGI, B. & CARPENTER, G. 2006. ErbB receptors: new insights on mechanisms and biology. *Trends Cell Biol,* 16**,** 649-56.

LLADO, A., TEBAR, F., CALVO, M., MORETO, J., SORKIN, A. & ENRICH, C. 2004. Protein kinaseCdelta-calmodulin crosstalk regulates epidermal growth factor receptor exit from early endosomes. *Mol Biol Cell,* 15**,** 4877-91.

LOMBARDO, C. R., CONSLER, T. G. & KASSEL, D. B. 1995. *In vitro* phosphorylation of the epidermal growth factor receptor autophosphorylation domain by c-Src: identification

of phosphorylation sites and c-Src SH2 domain binding sites. *Biochemistry,* 34**,** 16456-66.

LUGNIER, C. 2006. Cyclic nucleotide phosphodiesterase (PDE) superfamily: a new target for the development of specific therapeutic agents. *Pharmacol Ther,* 109**,** 366-98.

LUO, C. X. & ZHU, D. Y. 2011. Research progress on neurobiology of neuronal nitric oxide synthase. *Neurosci Bull,* 27**,** 23-35.

LYNCH, T. P., FERRER, C. M., JACKSON, S. R., SHAHRIARI, K. S., VOSSELLER, K. & REGINATO, M. J. 2012. Critical role of O-Linked beta-N-acetylglucosamine transferase in prostate cancer invasion, angiogenesis, and metastasis. *J Biol Chem,* 287**,** 11070-81.

MA, B., SIMALA-GRANT, J. L. & TAYLOR, D. E. 2006. Fucosylation in prokaryotes and eukaryotes. *Glycobiology,* 16**,** 158R-184R.

MA, J. & HART, G. W. 2013. Protein O-GlcNAcylation in diabetes and diabetic complications. *Expert Rev Proteomics,* 10**,** 365-80.

MA, Z. & VOSSELLER, K. 2014. Cancer metabolism and elevated O-GlcNAc in oncogenic signaling. *J Biol Chem,* 289**,** 34457-65.

MAGNANI, R., DIRK, L. M., TRIEVEL, R. C. & HOUTZ, R. L. 2010. Calmodulin methyltransferase is an evolutionarily conserved enzyme that trimethylates Lys-115 in calmodulin. *Nat Commun,* 1**,** 43.

MALEY, F., TRIMBLE, R. B., TARENTINO, A. L. & PLUMMER, T. H., JR. 1989. Characterization of glycoproteins and their associated oligosaccharides through the use of endoglycosidases. *Anal Biochem,* 180**,** 195-204.

MANALAN, A. S. & KLEE, C. B. 1984. Calmodulin. *Adv Cyclic Nucleotide Protein Phosphorylation Res,* 18**,** 227-78.

MARSH, S. A., COLLINS, H. E. & CHATHAM, J. C. 2014. Protein O-GlcNAcylation and cardiovascular (patho)physiology. *J Biol Chem,* 289**,** 34449-56.

MARTÍN-NIETO, J., CUSIDÓ-HITA, D. M., LI, H., BENGURÍA, A. & VILLALOBO, A. 2002. Regulation of ErbB receptors by calmodulin. *in Recent Research Developments in Biochemistry (Pandalai S. G., editor. , ed),* 3**,** p. 41–58 Research Signpost, Trivandrum.

MARTIN-NIETO, J. & VILLALOBO, A. 1998. The human epidermal growth factor receptor contains a juxtamembrane calmodulin-binding site. *Biochemistry,* 37**,** 227-36.

MARTIN, S. R. & BAYLEY, P. M. 1986. The effects of Ca^{2+} and Cd^{2+} on the secondary and tertiary structure of bovine testis calmodulin. A circular-dichroism study. *Biochem J,* 238**,** 485-90.

MATSUSHITA, C., TAMAGAKI, H., MIYAZAWA, Y., AIMOTO, S., SMITH, S. O. & SATO, T. 2013. Transmembrane helix orientation influences membrane binding of the intracellular juxtamembrane domain in Neu receptor peptides. *Proc Natl Acad Sci U S A,* 110**,** 1646-51.

MAUNE, J. F., BECKINGHAM, K., MARTIN, S. R. & BAYLEY, P. M. 1992. Circular dichroism studies on calcium binding to two series of Ca^{2+} binding site mutants of *Drosophila melanogaster* calmodulin. *Biochemistry,* 31**,** 7779-86.

McLAUGHLIN, S., SMITH, S. O., HAYMAN, M. J. & MURRAY, D. 2005. An electrostatic engine model for autoinhibition and activation of the epidermal growth factor receptor (EGFR/ErbB) family. *J Gen Physiol,* 126**,** 41-53.

MEANS, A. R. & DEDMAN, J. R. 1980. Calmodulin--an intracellular calcium receptor. *Nature,* 285**,** 73-7.

MEGGIO, F., BRUNATI, A. M. & PINNA, L. A. 1987. Polycation-dependent, Ca^{2+}-antagonized phosphorylation of calmodulin by casein kinase-2 and a spleen tyrosine protein kinase. *FEBS Lett,* 215**,** 241-6.

MI, W., GU, Y., HAN, C., LIU, H., FAN, Q., ZHANG, X., CONG, Q. & YU, W. 2011. O-GlcNAcylation is a novel regulator of lung and colon cancer malignancy. *Biochim Biophys Acta,* 1812**,** 514-9.

MISHRA, S., ANDE, S. R. & NYOMBA, B. L. 2010. The role of prohibitin in cell signaling. *Febs j,* 277**,** 3937-46.

MISHRA, S., ANDE, S. R. & SALTER, N. W. 2011. O-GlcNAc modification: why so intimately associated with phosphorylation? *Cell Commun Signal,* 9**,** 1.

MORRILL, M. E., THOMPSON, S. T. & STELLWAGEN, E. 1979. Purification of a cyclic nucleotide phosphodiesterase from bovine brain using blue dextran-Sepharose chromatography. *J Biol Chem,* 254**,** 4371-4.

MUKHIN, Y. V., VLASOVA, T., JAFFA, A. A., COLLINSWORTH, G., BELL, J. L., THOLANIKUNNEL, B. G., PETTUS, T., FITZGIBBON, W., PLOTH, D. W., RAYMOND, J. R. & GARNOVSKAYA, M. N. 2001. Bradykinin B2 receptors activate Na^+/H^+ exchange in mIMCD-3 cells via Janus kinase 2 and Ca^{2+}/calmodulin. *J Biol Chem,* 276**,** 17339-46.

NAKAJO, S., HAYASHI, K., DAIMATSU, T., TANAKA, M., NAKAYA, K. & NAKAMURA, Y. 1986. Phosphorylation of rat brain calmodulin *in vivo* and *in vitro*. *Biochem Int,* 13**,** 687-93.

NAKAJO, S., MASUDA, Y., NAKAYA, K. & NAKAMURA, Y. 1988. Determination of the phosphorylation sites of calmodulin catalyzed by casein kinase 2. *J Biochem,* 104**,** 946-51.

NGUYEN, D. H., BALL, E. D. & VARKI, A. 2006. Myeloid precursors and acute myeloid leukemia cells express multiple CD33-related Siglecs. *Exp Hematol,* 34**,** 728-35.

OGAWA, M., FURUKAWA, K. & OKAJIMA, T. 2014. Extracellular O-linked β-N-acetylglucosamine: Its biology and relationship to human disease. *World J Biol Chem,* 5**,** 224-30.

OH, S. H., STEINER, H. Y., DOUGALL, D. K. & ROBERTS, D. M. 1992. Modulation of calmodulin levels, calmodulin methylation, and calmodulin binding proteins during carrot cell growth and embryogenesis. *Arch Biochem Biophys,* 297**,** 28-34.

OKADA, M. & NAKAGAWA, H. 1989. A protein tyrosine kinase involved in regulation of $pp60^{c\text{-}src}$ function. *J Biol Chem,* 264**,** 20886-93.

OSAWA, M., SWINDELLS, M. B., TANIKAWA, J., TANAKA, T., MASE, T., FURUYA, T. & IKURA, M. 1998. Solution structure of calmodulin-W-7 complex: the basis of diversity in molecular recognition. *J Mol Biol,* 276**,** 165-76.

OLAYIOYE, M. A., NEVE, R. M., LANE, H. A. & HYNES, N. E. 2000. The ErbB signaling network: receptor heterodimerization in development and cancer. *Embo j,* 19**,** 3159-67.

OMORI, K. & KOTERA, J. 2007. Overview of PDEs and their regulation. *Circ Res,* 100**,** 309-27.

ONODERA, Y., NAM, J. M. & BISSELL, M. J. 2014. Increased sugar uptake promotes oncogenesis via EPAC/RAP1 and O-GlcNAc pathways. *J Clin Invest,* 124**,** 367-84.

PALOMO-JIMÈNEZ, P. I., HERNÁNDEZ-HERNANDO, S., GARCIA-NIETO, R. M. & VILLALOBO, A. 1999. A method for the purification of phospho(Tyr)calmodulin free of nonphosphorylated calmodulin. *Protein Expr Purif,* 16**,** 388-95.

PANINA, S., STEPHAN, A., LA COUR, J. M., JACOBSEN, K., KALLERUP, L. K., BUMBULEVICIUTE, R., KNUDSEN, K. V., SÁNCHEZ-GONZALEZ, P., VILLALOBO, A., OLESEN, U. H. & BERCHTOLD, M. W. 2012. Significance of calcium binding, tyrosine phosphorylation, and lysine trimethylation for the essential function of calmodulin in vertebrate cells analyzed in a novel gene replacement system. *J Biol Chem,* 287**,** 18173-81.

PANTALEON, M., TAN, H. Y., KAFER, G. R. & KAYE, P. L. 2010. Toxic effects of hyperglycemia are mediated by the hexosamine signaling pathway and *O*-linked glycosylation in early mouse embryos. *Biol Reprod,* 82**,** 751-8.

PARKS, E. E. & CERESA, B. P. 2014. Cell surface epidermal growth factor receptors increase Src and c-Cbl activity and receptor ubiquitylation. *J Biol Chem,* 289**,** 25537-45.

PARSONS, S. J. & PARSONS, J. T. 2004. Src family kinases, key regulators of signal transduction. *Oncogene,* 23**,** 7906-9.

PATWARDHAN, P. & RESH, M. D. 2010. Myristoylation and membrane binding regulate c-Src stability and kinase activity. *Mol Cell Biol,* 30**,** 4094-107.

PÈREZ, Y., MAFFEI, M., IGEA, A., AMATA, I., GAIRI, M., NEBREDA, A. R., BERNADO, P. & PONS, M. 2013. Lipid binding by the Unique and SH3 domains of c-Src suggests a new regulatory mechanism. *Sci Rep,* 3**,** 1295.

PIAZZA, M., FUTREGA, K., SPRATT, D. E., DIECKMANN, T. & GUILLEMETTE, J. G. 2012. Structure and dynamics of calmodulin (CaM) bound to nitric oxide synthase peptides: effects of a phosphomimetic CaM mutation. *Biochemistry,* 51**,** 3651-61.

PLANCKE, Y. D. & LAZARIDES, E. 1983. Evidence for a phosphorylated form of calmodulin in chicken brain and muscle. *Mol Cell Biol,* 3**,** 1412-20.

POTTER, M. D., BARBERO, S. & CHERESH, D. A. 2005. Tyrosine phosphorylation of VE-cadherin prevents binding of p120- and β-catenin and maintains the cellular mesenchymal state. *J Biol Chem,* 280**,** 31906-12.

PROTASEVICH, I., RANJBAR, B., LOBACHOV, V., MAKAROV, A., GILLI, R., BRIAND, C., LAFITTE, D. & HAIECH, J. 1997. Conformation and thermal denaturation of apocalmodulin: role of electrostatic mutations. *Biochemistry,* 36**,** 2017-24.

PUTTICK, J., BAKER, E. N. & DELBAERE, L. T. 2008. Histidine phosphorylation in biological systems. *Biochim Biophys Acta,* 1784**,** 100-5.

QUADRONI, M., JAMES, P. & CARAFOLI, E. 1994. Isolation of phosphorylated calmodulin from rat liver and identification of the *in vivo* phosphorylation sites. *J Biol Chem,* 269**,** 16116-22.

QUADRONI, M., L'HOSTIS, E. L., CORTI, C., MYAGKIKH, I., DURUSSEL, I., COX, J., JAMES, P. & CARAFOLI, E. 1998. Phosphorylation of calmodulin alters its potency as an activator of target enzymes. *Biochemistry,* 37**,** 6523-32.

RED BREWER, M., CHOI, S. H., ALVARADO, D., MORAVCEVIC, K., POZZI, A., LEMMON, M. A. & CARPENTER, G. 2009. The juxtamembrane region of the EGF receptor functions as an activation domain. *Mol Cell,* 34**,** 641-51.

RHOADS, A. R. & FRIEDBERG, F. 1997. Sequence motifs for calmodulin recognition. *FASEB J,* 11**,** 331-40.

ROBERTS, D. M., BESL, L., OH, S. H., MASTERSON, R. V., SCHELL, J. & STACEY, G. 1992. Expression of a calmodulin methylation mutant affects the growth and development of transgenic tobacco plants. *Proc Natl Acad Sci U S A,* 89**,** 8394-8.

ROBERTS, D. M., ROWE, P. M., SIEGEL, F. L., LUKAS, T. J. & WATTERSON, D. M. 1986. Trimethyllysine and protein function. Effect of methylation and mutagenesis of lysine 115 of calmodulin on NAD kinase activation. *J Biol Chem,* 261**,** 1491-4.

ROSENFELD, R., BANGIO, H., GERWIG, G. J., ROSENBERG, R., ALONI, R., COHEN, Y., AMOR, Y., PLASCHKES, I., KAMERLING, J. P. & MAYA, R. B. 2007. A lectin array-based methodology for the analysis of protein glycosylation. *J Biochem Biophys Methods,* 70**,** 415-26.

ROSKOSKI, R., JR. 2005. Src kinase regulation by phosphorylation and dephosphorylation. *Biochem Biophys Res Commun,* 331**,** 1-14.

ROSKOSKI, R., JR. 2014. The ErbB/HER family of protein-tyrosine kinases and cancer. *Pharmacol Res,* 79**,** 34-74.

ROWE, P. M., WRIGHT, L. S. & SIEGEL, F. L. 1986. Calmodulin N-methyltransferase. Partial purification and characterization. *J Biol Chem,* 261**,** 7060-9.

SACKS, D. B. 1994. Alteration of calmodulin-protein interactions by a monoclonal antibody to calmodulin. *Biochim Biophys Acta,* 1206**,** 120-8.

SACKS, D. B., DAVIS, H. W., WILLIAMS, J. P., SHEEHAN, E. L., GARCIA, J. G. & McDONALD, J. M. 1992. Phosphorylation by casein kinase II alters the biological activity of calmodulin. *Biochem J,* 283 (Pt 1)**,** 21-4.

SACKS, D. B., FUJITA-YAMAGUCHI, Y., GALE, R. D. & McDONALD, J. M. 1989a. Tyrosine-specific phosphorylation of calmodulin by the insulin receptor kinase purified from human placenta. *Biochem J,* 263**,** 803-12.

SACKS, D. B., GLENN, K. C. & McDONALD, J. M. 1989b. The carboxyl terminal segment of the c-Ki-ras 2 gene product mediates insulin-stimulated phosphorylation of calmodulin and stimulates insulin-independent autophosphorylation of the insulin receptor. *Biochem Biophys Res Commun,* 161**,** 399-405.

SACKS, D. B. & MCDONALD, J. M. 1988. Insulin-stimulated phosphorylation of calmodulin by rat liver insulin receptor preparations. *J Biol Chem,* 263**,** 2377-83.

SACKS, D. B. & MCDONALD, J. M. 1992. Effects of cationic polypeptides on the activity, substrate interaction, and autophosphorylation of casein kinase II: a study with calmodulin. *Arch Biochem Biophys,* 299**,** 275-80.

SAKAIDANI, Y., ICHIYANAGI, N., SAITO, C., NOMURA, T., ITO, M., NISHIO, Y., NADANO, D., MATSUDA, T., FURUKAWA, K. & OKAJIMA, T. 2012. O-linked-N-acetylglucosamine modification of mammalian Notch receptors by an atypical O-GlcNAc transferase Eogt1. *Biochem Biophys Res Commun,* 419**,** 14-9.

SAKAIDANI, Y., NOMURA, T., MATSUURA, A., ITO, M., SUZUKI, E., MURAKAMI, K., NADANO, D., MATSUDA, T., FURUKAWA, K. & OKAJIMA, T. 2011. O-linked-N-acetylglucosamine on extracellular protein domains mediates epithelial cell-matrix interactions. *Nat Commun,* 2**,** 583.

SALAS, V., SÁNCHEZ-TORRES, J., CUSIDÓ-HITA, D. M., GARCÍA-MARCHAN, Y., SOJO, F., BENAIM, G. & VILLALOBO, A. 2005. Characterisation of tyrosine-phosphorylation-defective calmodulin mutants. *Protein Expr Purif,* 41**,** 384-92.

SAMAK, G., NARAYANAN, D., JAGGAR, J. H. & RAO, R. 2011. CaV1.3 channels and intracellular calcium mediate osmotic stress-induced N-terminal c-Jun kinase activation and disruption of tight junctions in Caco-2 CELL MONOLAYERS. *J Biol Chem,* 286**,** 30232-43.

SAN JOSE, E., BENGURIA, A., GELLER, P. & VILLALOBO, A. 1992. Calmodulin inhibits the epidermal growth factor receptor tyrosine kinase. *J Biol Chem,* 267**,** 15237-45.

SÁNCHEZ-GONZÁLEZ, P., JELLALI, K. & VILLALOBO, A. 2010. Calmodulin-mediated regulation of the epidermal growth factor receptor. *FEBS J,* 277**,** 327-42.

SATO, K., OGAWA, K., TOKMAKOV, A. A., IWASAKI, T. & FUKAMI, Y. 2001. Hydrogen peroxide induces Src family tyrosine kinase-dependent activation of *Xenopus* eggs. *Dev Growth Differ,* 43**,** 55-72.

SATO, K., SATO, A., AOTO, M. & FUKAMI, Y. 1995. Site-specific association of c-Src with epidermal growth factor receptor in A431 cells. *Biochem Biophys Res Commun,* 210**,** 844-51.

SATO, T., PALLAVI, P., GOLEBIEWSKA, U., MCLAUGHLIN, S. & SMITH, S. O. 2006. Structure of the membrane reconstituted transmembrane-juxtamembrane peptide EGFR(622-660) and its interaction with Ca^{2+}/calmodulin. *Biochemistry,* 45**,** 12704-14.

SAUCERMAN, J. J. & BERS, D. M. 2012. Calmodulin binding proteins provide domains of local Ca^{2+} signaling in cardiac myocytes. *J Mol Cell Cardiol,* 52**,** 312-6.

SAVILLE, M. K. & HOUSLAY, M. D. 1993. The role of polybasic compounds in determining the tyrosyl phosphorylation of calmodulin by the human insulin receptor. *Cell Signal,* 5**,** 709-25.

SAVILLE, M. K. & HOUSLAY, M. D. 1994. Phosphorylation of calmodulin on Tyr99 selectively attenuates the action of calmodulin antagonists on type-I cyclic nucleotide phosphodiesterase activity. *Biochem J,* 299 (Pt 3)**,** 863-8.

SCHAEFER, W. H., LUKAS, T. J., BLAIR, I. A., SCHULTZ, J. E. & WATTERSON, D. M. 1987. Amino acid sequence of a novel calmodulin from *Paramecium tetraurelia* that contains dimethyllysine in the first domain. *J Biol Chem,* 262**,** 1025-9.

SCHLESSINGER, J. 2014. Receptor tyrosine kinases: legacy of the first two decades. *Cold Spring Harb Perspect Biol,* 6.

SENGUPTA, P., RUANO, M. J., TEBAR, F., GOLEBIEWSKA, U., ZAITSEVA, I., ENRICH, C., MCLAUGHLIN, S. & VILLALOBO, A. 2007. Membrane-permeable calmodulin inhibitors (e.g. W-7/W-13) bind to membranes, changing the electrostatic surface potential: dual

effect of W-13 on epidermal growth factor receptor activation. *J Biol Chem,* 282**,** 8474-86.

SHARMA, R. K., DAS, S. B., LAKSHMIKUTTYAMMA, A., SELVAKUMAR, P. & SHRIVASTAV, A. 2006. Regulation of calmodulin-stimulated cyclic nucleotide phosphodiesterase (PDE1): review. *Int J Mol Med,* 18**,** 95-105.

SHARMA, R. K. & KALRA, J. 1994. Characterization of calmodulin-dependent cyclic nucleotide phosphodiesterase isoenzymes. *Biochem J,* 299 (Pt 1)**,** 97-100.

SHARMA, R. K. & WANG, J. H. 1986. Purification and characterization of bovine lung calmodulin-dependent cyclic nucleotide phosphodiesterase. An enzyme containing calmodulin as a subunit. *J Biol Chem,* 261**,** 14160-6.

SHENOLIKAR, S., THOMPSON, W. J. & STRADA, S. J. 1985. Characterization of a Ca^{2+}-calmodulin-stimulated cyclic GMP phosphodiesterase from bovine brain. *Biochemistry,* 24**,** 672-8.

SHIFMAN, J. M., CHOI, M. H., MIHALAS, S., MAYO, S. L. & KENNEDY, M. B. 2006. Ca^{2+}/calmodulin-dependent protein kinase II (CaMKII) is activated by calmodulin with two bound calciums. *Proc Natl Acad Sci U S A,* 103**,** 13968-73.

SLAWSON, C., ZACHARA, N. E., VOSSELLER, K., CHEUNG, W. D., LANE, M. D. & HART, G. W. 2005. Perturbations in O-linked β-N-acetylglucosamine protein modification cause severe defects in mitotic progression and cytokinesis. *J Biol Chem,* 280**,** 32944-56.

SMITH, V. L., DOYLE, K. E., MAUNE, J. F., MUNJAAL, R. P. & BECKINGHAM, K. 1987. Structure and sequence of the *Drosophila melanogaster* calmodulin gene. *J Mol Biol,* 196**,** 471-85.

SPRUNG, R., NANDI, A., CHEN, Y., KIM, S. C., BARMA, D., FALCK, J. R. & ZHAO, Y. 2005. Tagging-via-substrate strategy for probing O-GlcNAc modified proteins. *J Proteome Res,* 4**,** 950-7.

STATEVA, S. R., SALAS, V., BENAIM, G., MENENDEZ, M., SOLIS, D. & VILLALOBO, A. 2015. Characterization of phospho-(Tyrosine)-mimetic calmodulin mutants. *PLoS One,* 10**,** e0120798.

STATEVA, S. R., SALAS, V., ANGUITA, E., BENAIM, G., & VILLALOBO, A.: Ca^{2+}/calmodulin and apo-calmodulin both bind to and enhance the tyrosine kinase activity of c-Src. PLoS ONE. In press, doi:10.1371/journal.pone.01028783 (2015).

STOSCHECK, C. M. 1990. Quantitation of protein. *Methods Enzymol,* 182**,** 50-68.

STRYNADKA, N. C. & JAMES, M. N. 1989. Crystal structures of the helix-loop-helix calcium-binding proteins. *Annu Rev Biochem,* 58**,** 951-98.

SUN, H., YIN, D., COFFEEN, L. A., SHEA, M. A. & SQUIER, T. C. 2001. Mutation of Tyr138 disrupts the structural coupling between the opposing domains in vertebrate calmodulin. *Biochemistry,* 40**,** 9605-17.

SUN, H., YIN, D. & SQUIER, T. C. 1999. Calcium-dependent structural coupling between opposing globular domains of calmodulin involves the central helix. *Biochemistry,* 38**,** 12266-79.

TAJIMA, Y., UYAMA, E., GO, S., SATO, C., TAO, N., KOTANI, M., HINO, H., SUZUKI, A., SANAI, Y., KITAJIMA, K. & SAKURABA, H. 2005. Distal myopathy with rimmed vacuoles: impaired O-glycan formation in muscular glycoproteins. *Am J Pathol,* 166**,** 1121-30.

TAN, M., LI, P., KLOS, K. S., LU, J., LAN, K. H., NAGATA, Y., FANG, D., JING, T. & YU, D. 2005. ErbB2 promotes Src synthesis and stability: novel mechanisms of Src activation that confer breast cancer metastasis. *Cancer Res,* 65**,** 1858-67.

TASHIMA, Y. & STANLEY, P. 2014. Antibodies that detect O-linked β-D-N-acetylglucosamine on the extracellular domain of cell surface glycoproteins. *J Biol Chem,* 289**,** 11132-42.

TEO, T. S. & WANG, J. H. 1973. Mechanism of activation of a cyclic adenosine 3':5'-monophosphate phosphodiesterase from bovine heart by calcium ions. Identification of the protein activator as a Ca^{2+} binding protein. *J Biol Chem,* 248**,** 5950-5.

THEISS, A. L. & SITARAMAN, S. V. 2011. The role and therapeutic potential of prohibitin in disease. *Biochim Biophys Acta,* 1813**,** 1137-43.

TODD, M. J. & GOMEZ, J. 2001. Enzyme kinetics determined using calorimetry: a general assay for enzyme activity? *Anal Biochem,* 296**,** 179-87.

TOLEMAN, C., PATERSON, A. J., WHISENHUNT, T. R. & KUDLOW, J. E. 2004. Characterization of the histone acetyltransferase (HAT) domain of a bifunctional protein with activable O-GlcNAcase and HAT activities. *J Biol Chem,* 279**,** 53665-73.

TORRES, C. R. & HART, G. W. 1984. Topography and polypeptide distribution of terminal N-acetylglucosamine residues on the surfaces of intact lymphocytes. Evidence for O-linked GlcNAc. *J Biol Chem,* 259**,** 3308-17.

TRETTER, V., ALTMANN, F. & MARZ, L. 1991. Peptide-N4-(N-acetyl-beta-glucosaminyl)asparagine amidase F cannot release glycans with fucose attached alpha 1----3 to the asparagine-linked N-acetylglucosamine residue. *Eur J Biochem,* 199**,** 647-52.

TUCKER, M. M., ROBINSON, J. B., JR. & STELLWAGEN, E. 1981. The effect of proteolysis on the calmodulin activation of cyclic nucleotide phosphodiesterase. *J Biol Chem,* 256**,** 9051-8.

VAIDYANATHAN, K. & WELLS, L. 2014. Multiple tissue-specific roles for the O-GlcNAc post-translational modification in the induction of and complications arising from type II diabetes. *J Biol Chem,* 289**,** 34466-71.

VILLALOBO, A., GARCÍA-PALMERO, I., STATEVA, S. R. & JELLALI, K. 2013. Targeting the calmodulin-regulated ErbB/Grb7 signaling axis in cancer therapy. *J Pharm Pharm Sci,* 16**,** 177-89.

VILLALOBO, A., RUANO, M. J., PALOMO-JIMÈNEZ, P. I., LI, H. & MARTÍN-NIETO 2000. The epidermal growth factor receptor and the calcium signal. In Calcium: the Molecular Basis of Calcium Action in Biology and Medicine (Pochet, R., Donato, R., Haiech, J., Heizmann, C. & Gerke, V., eds). *Kluwer Academic Publishers, Boston, MA, USA.,* pp. 287–303

WAGNER, M. J., STACEY, M. M., LIU, B. A. & PAWSON, T. 2013. Molecular mechanisms of SH2- and PTB-domain-containing proteins in receptor tyrosine kinase signaling. *Cold Spring Harb Perspect Biol,* 5**,** a008987.

WALLACE, R. W., TALLANT, E. A., DOCKTER, M. E. & CHEUNG, W. Y. 1982. Calcium binding domains of calmodulin. Sequence of fill as determined with terbium luminescence. *J Biol Chem,* 257**,** 1845-54.

WALSH, C. T., GARNEAU-TSODIKOVA, S. & GATTO, G. J., JR. 2005. Protein posttranslational modifications: the chemistry of proteome diversifications. *Angew Chem Int Ed Engl,* 44**,** 7342-72.

WANG, H., GAO, X., YANG, J. J. & LIU, Z. R. 2013. Interaction between p68 RNA helicase and Ca^{2+}-calmodulin promotes cell migration and metastasis. *Nat Commun,* 4**,** 1354.

WANG, Q., LIANG, K. C., CZADER, A., WAXHAM, M. N. & CHEUNG, M. S. 2011. The effect of macromolecular crowding, ionic strength and calcium binding on calmodulin dynamics. *PLoS Comput Biol,* 7**,** e1002114.

WANG, Z., GUCEK, M. & HART, G. W. 2008. Cross-talk between GlcNAcylation and phosphorylation: site-specific phosphorylation dynamics in response to globally elevated O-GlcNAc. *Proc Natl Acad Sci U S A,* 105**,** 13793-8.

WATTERSON, D. M., SHARIEF, F. & VANAMAN, T. C. 1980. The complete amino acid sequence of the Ca^{2+}-dependent modulator protein (calmodulin) of bovine brain. *J Biol Chem,* 255**,** 962-75.

WEISHAAR, R. E. 1986. Multiple molecular forms of phosphodiesterase: an overview. *J Cyclic Nucleotide Protein Phosphor Res,* 11**,** 463-72.

WEISS, B., PROZIALECK, W., CIMINO, M., BARNETTE, M. S. & WALLACE, T. L. 1980. Pharmacological regulation of calmodulin. *Ann N Y Acad Sci,* 356**,** 319-45.

WHEELER, D. L., IIDA, M. & DUNN, E. F. 2009. The role of Src in solid tumors. *Oncologist,* 14**,** 667-78.

WHELAN, S. A., DIAS, W. B., THIRUNEELAKANTAPILLAI, L., LANE, M. D. & HART, G. W. 2010. Regulation of insulin receptor substrate 1 (IRS-1)/AKT kinase-mediated insulin signaling by O-Linked β-N-acetylglucosamine in 3T3-L1 adipocytes. *J Biol Chem,* 285**,** 5204-11.

WILEY, H. S., HERBST, J. J., WALSH, B. J., LAUFFENBURGER, D. A., ROSENFELD, M. G. & GILL, G. N. 1991. The role of tyrosine kinase activity in endocytosis, compartmentation, and down-regulation of the epidermal growth factor receptor. *J Biol Chem,* 266**,** 11083-94.

WILLIAMS, J. P., JO, H., SACKS, D. B., CRIMMINS, D. L., THOMA, R. S., HUNNICUTT, R. E., RADDING, W., SHARMA, R. K. & MCDONALD, J. M. 1994. Tyrosine-phosphorylated calmodulin has reduced biological activity. *Arch Biochem Biophys,* 315**,** 119-26.

WOLFF, D. J. & BROSTROM, C. O. 1974. Calcium-binding phosphoprotein from pig brain: identification as a calcium-dependent regulator of brain cyclic nucleotide phosphodiesterase. *Arch Biochem Biophys,* 163**,** 349-58.

WOLFF, D. J., POIRIER, P. G., BROSTROM, C. O. & BROSTROM, M. A. 1977. Divalent cation binding properties of bovine brain Ca^{2+}-dependent regulator protein. *J Biol Chem,* 252**,** 4108-17.

WONG, E. C., SACKS, D. B., LAURINO, J. P. & McDONALD, J. M. 1988. Characteristics of calmodulin phosphorylation by the insulin receptor kinase. *Endocrinology,* 123**,** 1830-6.

WU, J., MASCI, P. P., CHEN, C., CHEN, J., LAVIN, M. F. & ZHAO, K. N. 2015. β-Adducin siRNA disruption of the spectrin-based cytoskeleton in differentiating keratinocytes prevented by calcium acting through calmodulin/epidermal growth factor receptor/cadherin pathway. *Cell Signal,* 27**,** 15-25.

WU, Y. M., LIU, C. H., HU, R. H., HUANG, M. J., LEE, J. J., CHEN, C. H., HUANG, J., LAI, H. S., LEE, P. H., HSU, W. M., HUANG, H. C. & HUANG, M. C. 2011. Mucin glycosylating enzyme GALNT2 regulates the malignant character of hepatocellular carcinoma by modifying the EGF receptor. *Cancer Res,* 71**,** 7270-9.

XU, Q., YANG, C., DU, Y., CHEN, Y., LIU, H., DENG, M., ZHANG, H., ZHANG, L., LIU, T., LIU, Q., WANG, L., LOU, Z. & PEI, H. 2014. AMPK regulates histone H2B O-GlcNAcylation. *Nucleic Acids Res,* 42**,** 5594-604.

XU, W., HARRISON, S. C. & ECK, M. J. 1997. Three-dimensional structure of the tyrosine kinase c-Src. *Nature,* 385**,** 595-602.

YANG, W., WANG, X., DUAN, C., LU, L. & YANG, H. 2013. α-synuclein overexpression increases phospho-protein phosphatase 2A levels via formation of calmodulin/Src complex. *Neurochem Int,* 63**,** 180-94.

YANG, X., ONGUSAHA, P. P., MILES, P. D., HAVSTAD, J. C., ZHANG, F., SO, W. V., KUDLOW, J. E., MICHELL, R. H., OLEFSKY, J. M., FIELD, S. J. & EVANS, R. M. 2008. Phosphoinositide signalling links O-GlcNAc transferase to insulin resistance. *Nature,* 451**,** 964-9.

YANG, Z. & HANCOCK, W. S. 2005. Monitoring glycosylation pattern changes of glycoproteins using multi-lectin affinity chromatography. *J Chromatogr A,* 1070**,** 57-64.

YARDEN, Y. 2001. The EGFR family and its ligands in human cancer. signalling mechanisms and therapeutic opportunities. *Eur J Cancer,* 37 Suppl 4**,** S3-8.

YARDEN, Y. & SLIWKOWSKI, M. X. 2001. Untangling the ErbB signalling network. *Nat Rev Mol Cell Biol,* 2**,** 127-37.

YEATMAN, T. J. 2004. A renaissance for SRC. *Nat Rev Cancer,* 4**,** 470-80.

YUAN, K., JING, G., CHEN, J., LIU, H., ZHANG, K., LI, Y., WU, H., MCDONALD, J. M. & CHEN, Y. 2011. Calmodulin mediates Fas-induced FADD-independent survival signaling in

pancreatic cancer cells via activation of Src-extracellular signal-regulated kinase (ERK). *J Biol Chem,* 286**,** 24776-84.

ZACHARA, N. E. & HART, G. W. 2004. O-GlcNAc a sensor of cellular state: the role of nucleocytoplasmic glycosylation in modulating cellular function in response to nutrition and stress. *Biochim Biophys Acta,* 1673**,** 13-28.

ZEIDAN, Q. & HART, G. W. 2010. The intersections between O-GlcNAcylation and phosphorylation: implications for multiple signaling pathways. *J Cell Sci,* 123**,** 13-22.

ZHU, Y., SHAN, X., YUZWA, S. A. & VOCADLO, D. J. 2014. The emerging link between O-GlcNAc and Alzheimer disease. *J Biol Chem,* 289**,** 34472-81.

ZWANG, Y. & YARDEN, Y. 2009. Systems biology of growth factor-induced receptor endocytosis. *Traffic,* 10**,** 349-63.

10. APPENDIX

10.1 Supplementary material:

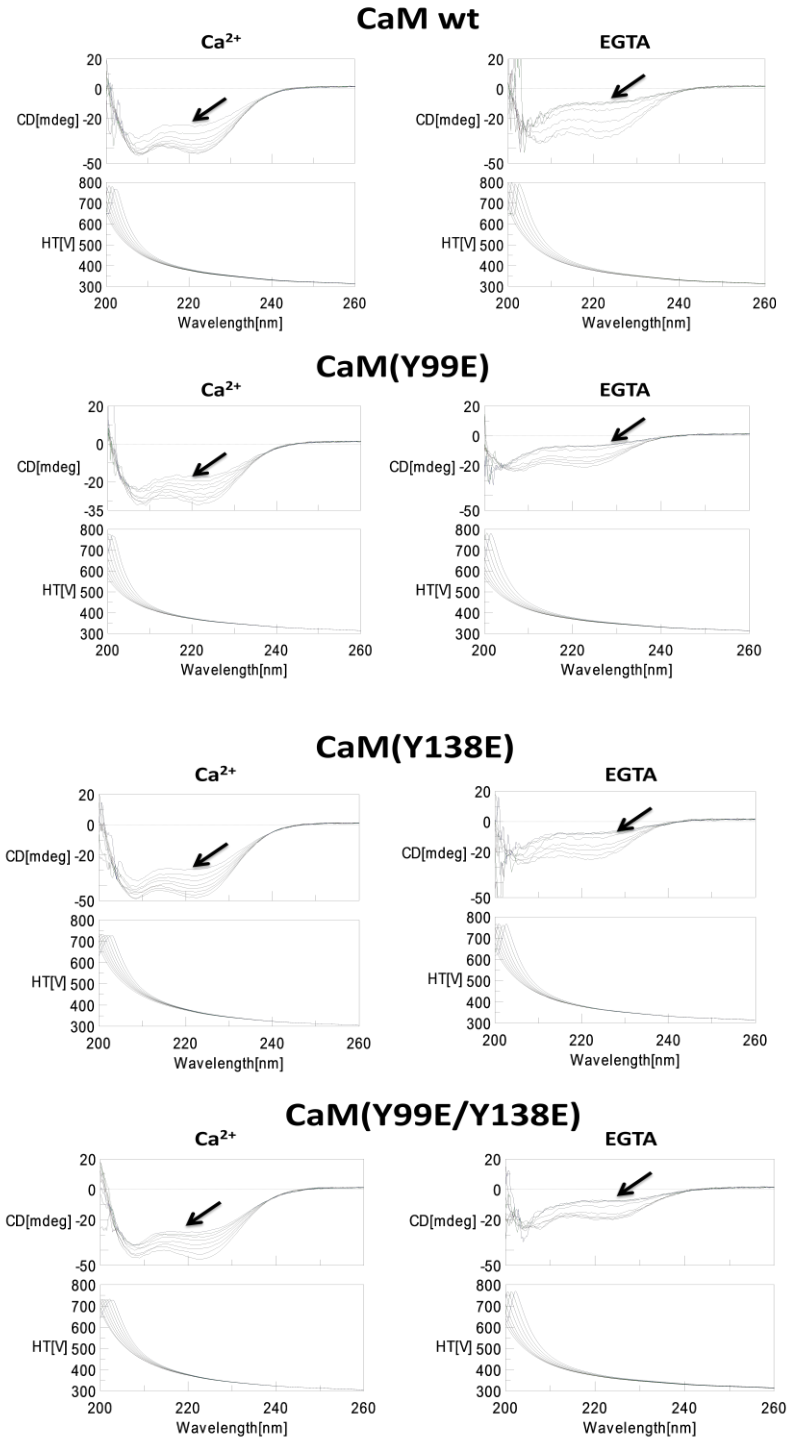

Supplementary Figure 1S: Ca^{2+}-induced thermal stability detected in the Far-UV CD spectra of the different CaM species. Far-UV CD spectra for wild type (wt) and the Y/E CaM mutants (12 μM) were recorded at increasing temperatures (20-90 ºC) in 20 mM Tris-HCl (pH 7.5), 0.1 M KCl, containing 1 mM $CaCl_2$ (*left panels*) or 1 mM EGTA (*right panels*). Similar spectra were recorded for the CaM Y/D mutants. The arrows are pointing the temperature dependent change of the CaM spectra in the absence of Ca^{2+} (presence of EGTA) or presence of Ca^{2+}.

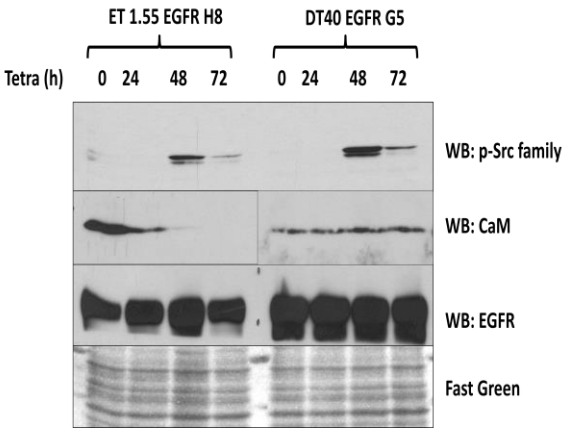

Supplementary Figure 2S: Testing CaM down-regulation in conditional CaM-KO cells on the activation status of Src family kinase(s). The ET1-55/EGFR and DT40/EGFR cells were treated with 1 µg/ml tetracycline for the indicated times, then the proteins were extracted and subjected to SDS-PAGE and Western blot as described under Material and Method. The membranes were probed with anti-phospho-Y416 Src family, anti-CaM and anti-EGFR antibodies. Protein staining with Fast Green is shown as a loading control.

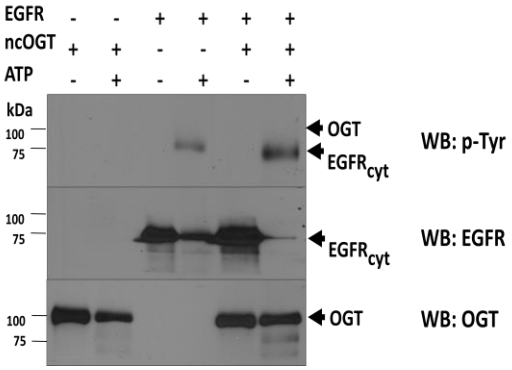

Supplementary Figure 3S: EGFR fails to phosphorylate OGT *in vitro*. Recombinant $EGFR_{cyt}$, that contain only the cytosolic part of the EGFR, was incubated in the absence or presence of ATP and OGT as indicated. The samples were then subjected to Western Blot using anti-phospho-Tyr antibody (clone 4G10). After striping the membrane was reprobed with anti-EGFR and anti-OGT antibodies to confirm the presence of the indicated proteins.

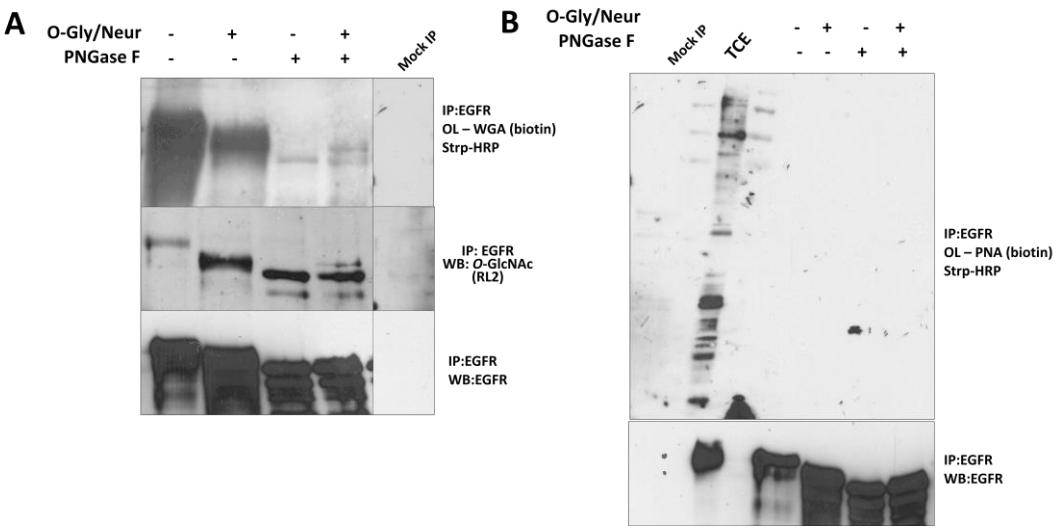

Supplementary Figure 4S: Lectin overlay of the immunoprecipitated EGFR. EGFR was immunoprecipitated (IP) from A431 cells treated with 100 μM PUGNAc (OGA inhibitor). After the immunoprecipitation the receptor was subjected to PNGase F and *O*-glycosidase plus neuraminidase (*O*-Gly/Neur) treatments as indicated and processed by SDS-PAGE and Western blots (WB) and overlaid (OL) with WGA (A) or PNA (B) as described in Materials and Methods. The membranes were then stripped and reprobed with an anti-*O*-GlcNAc antibody (RL2) (A) antibody and anti-EGFR antibody as a loading control.

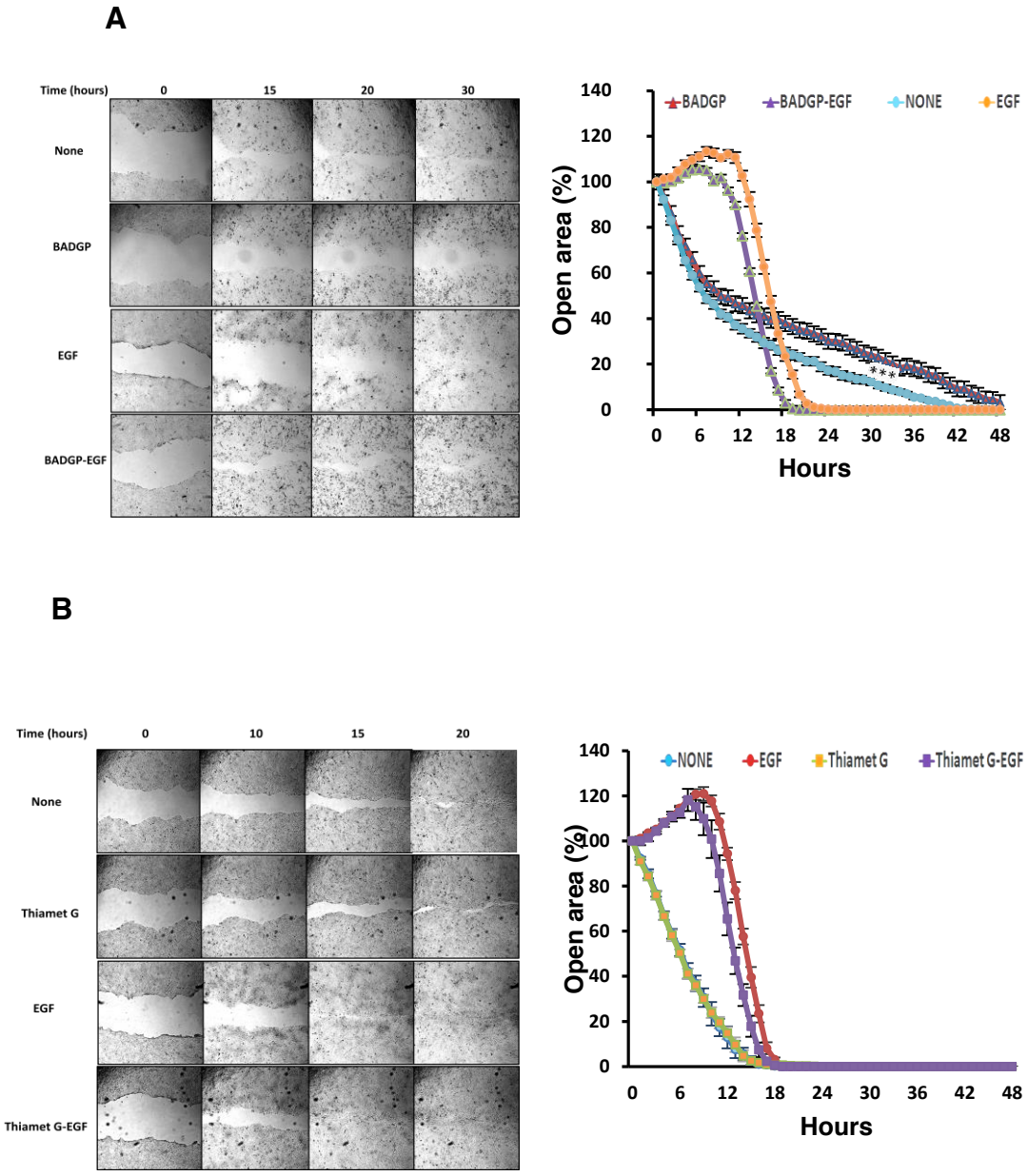

Supplementary Figure 5S: Effect of OGA and OGT inhibitors on the healing of an artificial wound. (A) Artificial wounds were performed in confluent monolayers of A431 cells in the absence (None) or in the presence of 1 mM BADGP (OGT inhibitor), and 10 nM EGF as indicated. Photographs were taken at different times in order to follow the closure of the different wounds using a Zeiss Axiovert 200M Multi-stage Automated microscope with 4x objectives to follow the repopulation of the wounds. The plot represents the mean ± SEM (n=8) for non-stimulated and (n=4) for the EGF-stimulated samples of opening of the wound in the different conditions as indicated. Significant differences versus controls are presented (ANOVA; *** $p<0.0001$). (B) Artificial wounds were performed in confluent monolayers of A431 cells in the absence (None) or in the presence of 100 µM Thiamet-G (OGA inhibitor) and 10 nM EGF as indicated. Photographs were taken as described in (A). The plot represents the mean ± SEM (n=4) of the opening of the wound in the different conditions as indicated.

10.2 Publication list:

1. VILLALOBO, A., GARCÍA-PALMERO, I**.,** **STATEVA, S. R.**, & JELLALI, K.: Targeting the calmodulin-regulated ErbB/Grb7 signaling axis in cancer therapy. J. Pharm. Pharmaceut. Sci. *16,* 52-64 (2013).

2. **STATEVA, R. S.,** SALAS, V., BENAIM, G., MENÉNDEZ, M., SOLIS, D., & VILLALOBO, A.: Characterization of phospho-(tyrosine)-mimetic calmodulin mutants. PLoS One 10(4): e0120798. doi:10.1371/journal.pone.0120798 (2015).

3. **STATEVA, S. R.**, SALAS, V., ANGUITA, E., BENAIM, G., & VILLALOBO, A.: Ca^{2+}/calmodulin and apo-calmodulin both bind to and enhance the tyrosine kinase activity of c-Src. PLoS One. Doi:10.1371/journal.pone.0128783 (2015). (accepted in press)

4. **STATEVA, S. R.**, & VILLALOBO, A.: *O*-GlcNAcylation of the human epidermal growth factor receptor. Org. Biomol. Chem. (2015). (*submitted*)

5. **STATEVA, S. R.**, COSSIO-CUARTERO, I. SALAS, V., BENGURÍA, A., BENAIM, G., & VILLALOBO, A.: The activating role of phospho-(Tyr)-calmodulin on the epidermal growth factor receptor. (2015). (*in preparation*)

J Pharm Pharmaceut Sci (www.cspsCanada.org) 16(2) 177 - 189, 2013

Targeting the Calmodulin-Regulated ErbB/Grb7 Signaling Axis in Cancer Therapy

Antonio Villalobo[1], Irene García-Palmero[1], Silviya R. Stateva[1], and Karim Jellali[2]

[1]Department of Cancer Biology, Instituto de Investigaciones Biomédicas, Consejo Superior de Investigaciones Científicas and Universidad Autónoma de Madrid. c/ Arturo Duperier 4, Madrid, Spain.
[2] Centre of Biotechnology of Sfax, Sidi Mansour Road Km 6, Sfax, Tunisia

Received, March 5, 2013; Revised, March 30, 2013; Accepted, April 7, 2013; Published, April 8, 2013.

ABSTRACT - Signal transduction pathways essential for the survival and viability of the cell and that frequently present aberrant expression or function in tumors are attractive targets for pharmacological intervention in human cancers. In this short review we will describe the regulation exerted by the calcium-receptor protein calmodulin (CaM) on signaling routes involving the family of ErbB receptors - highlighting the epidermal growth factor receptor (EGFR/ErbB1) and ErbB2 - and the adaptor protein Grb7, a downstream signaling component of these receptors. The signaling mechanism of the ErbB/Grb7 axis and the regulation exerted by CaM on this pathway will be described. We will present a brief overview of the current efforts to inhibit the hyperactivity of ErbB receptors and Grb7 in tumors. The currently available information on targeting the CaM-binding site of these signaling proteins will be analyzed, and the pros and cons of directly targeting CaM versus the CaM-binding domain of the ErbB receptors and Grb7 as potential anti-cancer therapy will be discussed.

INTRODUCTION

The ErbB receptors form a subfamily of RTKs that includes four members: EGFR/ErbB1/HER1, ErbB2/neu/HER2, ErbB3/HER3 and ErbB4/HER4. These receptors present three distinct zones: an extracellular region with two cysteine-rich domains and containing the ligand-bind site; a single membrane-spanning segment; and an intracellular region composed by a JM domain that plays an essential role in receptor activation, the tyrosine kinase catalytic domain, and a C-terminal tail containing a set of tyrosine residues that are auto-phosphorylated upon receptor activation (1-4).

The ErbB receptors share an extensive family of polypeptide ligands that are either very promiscuous or have relative or absolute preference for specific receptor subtypes, orchestrating in this manner a variety of signaling events to accomplish differentiated cellular responses (5, 6). These receptors form homo- or hetero-dimers upon ligand binding. This process induces a series of conformational changes that result in the activation of their intrinsic tyrosine kinase followed by the auto(trans)-phosphorylation of tyrosine residues (1-4). The most likely mechanism for the ligand-dependent activation of these receptors is the formation of an asymmetric dimer involving the allosteric interaction of the proximal and terminal regions of two apposed tyrosine kinase domains (7). Although ErbB2 does not have ligand-binding capacity and ErbB3 presents a non-functional tyrosine kinase domain, they form active ErbB2/ErbB3 hetero-dimers (8).

The phospho-tyrosine residues in the active receptors act as docking sites for adaptor proteins or transducing enzymes harboring SH2 or PTB domains, initiating in this manner complex networks of signaling events (2, 4, 9, 10). Thereafter, the ligand/receptor complexes at the plasma membrane are internalized in clathrin-coated pits. The receptors are subjected to ubiquitination by the E3 ubiquitin-protein ligase c-Cbl and sorted in endosomal vesicles where they continue generating signals. Afterwards they are proteolytically degraded via the lysosomal pathway, previous de-ubiquitination at the proteasome, or directly processed via this pathway. Alternatively, the receptors are recycled back to the plasma membrane (11-13).

The ErbB receptors participate in the control of an extensive variety of cellular functions, most prominently stimulating cell proliferation, but in

Correspondence Author: Prof. Antonio Villalobo, Instituto de Investigaciones Biomédicas CSIC-UAM, c/ Arturo Duperier 4, E-28029 Madrid, Spain;
E-mail: antonio.villalobo@iib.uam.es

J Pharm Pharmaceut Sci (www.cspsCanada.org) 16(2) 177 - 189, 2013

addition they control differentiation, cell polarity, cell survival mechanisms, the prevention or induction of apoptosis, and cell motility (14-19). These processes are frequently altered in neoplastic cells leading to cancerogenesis, tumor progression and the development of metastasis (18).

Grb7 is an adaptor protein that participates in signal transduction events initiated from many active RTKs located at the plasma membrane, including the ErbB receptors, or from cytosolic tyrosine kinases such as FAK. Grb7 forms part of a mammalian family of adaptors that also includes Grb10 and Grb14 (20-24). These proteins are phylogenetically related to the Mig10 protein from *Caenorhabditis elegans* that is involved in the regulation of embryonic neural cell migration (25, 26).

The human *GRB7* gene maps at the 17q12-q21.1 locus in the large arm of chromosome 17 and encodes a 532 amino acids modular protein. This protein harbors an N-terminal PR domain; a central GM region (for Grb and Mig10) that includes a RA domain, a PH domain, and a BPS domain (for between PH and SH2); and a SH2 domain located in its C-terminal segment (20-24). In human tumor cells Grb7 is frequently co-amplified with ErbB2 and other neighbor genes forming the *ERBB2* amplicon (24).

Similar to other adaptor proteins, Grb7 does not have intrinsic enzymatic activity but plays important roles participating in many signaling pathways. Grb7 docks via its SH2 domain at phospho-tyrosine residues in active RTKs, FAK, and other phospho-proteins. Upon recruitment by FAK or the EphB1 receptor Grb7 is phosphorylated and signals to control cell migration processes (27, 28). In human cancers - including for example breast, stomach, esophagus and ovary - the overexpression of Grb7, its co-amplification with ErbB2, and/or the expression of an aberrant truncated variant denoted Grb7V is known to contribute to the invasiveness and spread of metastatic tumor cells (29-33).

In addition to its well-known implication in cell migration, Grb7 plays additional roles in signaling pathways controlling other important physiological functions. This includes the control of cell proliferation, as demonstrated by disrupting Grb7 expression with siRNA or shRNA (34-36), treating cells with a cell-permeable inhibitory peptide targeting Grb7 (37), mutating the FAK-mediated Grb7 phosphorylation sites (34), or deleting the CaM binding site of Grb7 (38). On the other hand, Grb7 is also an RNA-binding protein that interacts via its PR domain with the 5'-UTR of mRNAs regulating translational processes with the intervention of netrin-1 and FAK, and participating as well in the storage of mRNAs in stress granules under a variety of environmental conditions unsuitable for appropriate protein translation (39, 40). Additionally, we have demonstrated that Grb7 participates in the control of angiogenesis *in vitro* (41), and *in vivo* determining the extent and functional performance of the tumor-associated vasculature using an experimental model of glioma and MRI (38).

CALMODULIN

Many Ca^{2+}-regulated cellular functions are controlled by CaM, a small Ca^{2+}-binding sensor protein harboring four Ca^{2+}-binding sites that is ubiquitously present in all known eukaryotic cells and is highly conserved across vertebrate species - albeit CaMs from some lower eukaryotes only have three functional Ca^{2+}-binding sites (42, 43). The transient increase in the cytosolic concentration of free Ca^{2+} induced by many agonists, including mitogenic growth factors, results in the progressive formation of the Ca^{2+}/CaM complex at increasing Ca^{2+} levels in living cells (44). Upon Ca^{2+} binding CaM changes its conformation exposing hydrophobic amino acids that favor its interaction with more than one hundred target proteins modulating their activities (42, 43). The central helical segment of CaM appears to wrap around the CaM-BD of some target proteins upon Ca^{2+} binding. The number of calcium ions bound to CaM required for efficient interaction with distinct targets varies for each protein, as experimentally demonstrated using peptides corresponding to the CaM-BDs of distinct proteins (45). For example, only two Ca^{2+} bound to CaM at their high affinity C-terminal sites are enough to activate CaMK-II (46). Nevertheless, Ca^{2+}-free CaM (apo-CaM) is also able to bind and regulate many target proteins (47). The CaM-BDs of diverse target proteins often correspond to an amphipathic α-helix with positively charged and hydrophobic amino acid residues usually distributed at opposite sides of the helix, or Ca^{2+}-independent and Ca^{2+}-dependent IQ motifs (47-49). Diverse molecular mechanisms for recognizing distinct CaM-dependent target proteins by CaM have been described (50).

Targeting calmodulin in cancer

Inhibition of CaM has been thought to have potential therapeutic effects in cancer (49, 50) because of its suppressing action on cell

J Pharm Pharmaceut Sci (www.cspsCanada.org) 16(2) 177 - 189, 2013

proliferation and/or their capacity to revert the multi-drug resistance tendency of many tumor cells (51-54). A great variety of CaM antagonists have been described and their mechanisms of action established (55-59). This includes CaM inhibitors isolated from plant and animal products (60). CaM antagonists, however, negatively affect the proliferation of both normal and tumor cells, and to complicate matters in some instances these compounds have been reported to be less effective in transformed than in normal cells because of alterations in some CaM-dependent pathways in the former (61). Thus, as CaM is essential in all eukaryote cells for the regulation of a myriad of vital cellular functions, the widespread use of CaM antagonists as chemotherapeutic agents against cancer in a clinical setting is expected to be problematic.

Therefore, it could be of interest to explore alternative strategies, such as the potential efficacy of targeting the CaM-binding region(s) of selected CaM-binding proteins relevant for the proliferation of tumor cells or other essential functions for tumor progression and metastatic spread. In the following sections, we shall discuss how targeting the CaM-dependent ErbB/Grb7 axis at the CaM-BD of ErbB receptors and/or Grb7 could facilitate new therapeutic approaches to fight cancer.

ErbB RECEPTORS AND CALMODULIN

The Ca^{2+}/CaM complex controls the functionality of ErbB receptors - particularly the EGFR and ErbB2 - by a dual mechanism, either implicating CaM-dependent kinases that phosphorylate and indirectly control their activity, down-regulation, trafficking and fate; or by directly binding to the cytosolic JM region of the receptor regulating in this manner its ligand-dependent activation (62).

Our group obtained the first experimental evidence for CaM binding to the EGFR in a Ca^{2+}-dependent manner in rat liver more than twenty years ago (63). The CaM-BD (residues 645-660) was subsequently located at the cytosolic JM region of human EGFR (64, 65) (see Figure 1a). Furthermore, the occurrence of CaM/EGFR complexes in living cells was established, and the possible functional implication of this interaction for ligand-dependent activation of the receptor was determined (66-71). The recent engineering of vertebrate conditional CaM-knockout cell lines (72) has been an important breakthrough to obtain further evidence of the positive regulatory action that the Ca^{2+}/CaM complex exerts on the ligand-dependent activation of the EGFR in living cells without the need to use CaM antagonists, as these compounds could have unwanted off-target side effects (73).

The CaM-BD appears to be highly conserved in all ErbB receptor family members except in ErbB3 that lacks intrinsic tyrosine kinase activity (74), underscoring the relevance of this domain for its activation. High affinity binding of Ca^{2+}/CaM to peptides corresponding to the sequences of the proposed CaM-BD of all the ErbB receptors has been determined, except for the ErbB3 peptide that presented lower affinity (68). In the ligand-free EGFR the CaM-BD appears to play an auto-inhibitory role because of the electrostatic interaction of this region with the inner leaflet of the plasma membrane, preventing in this manner the ligand-independent constitutive activation of the receptor (68, 71).

It has been experimentally established that CaM also binds to ErbB2 in a Ca^{2+}-dependent manner modulating its tyrosine kinase activity, the downstream signaling pathways of the receptor and cell growth (75, 76). Nevertheless, it appears that Ca^{2+}/CaM and apo-CaM interact with ErbB2, as CaM binds to ErbB2 not in one but in two near-by sites, respectively located at the cytosolic JM region (residues 676-689) and at a more distally located segment (residues 714-732) (76). The 676-689 segment was proposed to be the site of interaction for apo-CaM, while both the 676-689 and 714-732 segments contribute to the Ca^{2+}-dependent binding (76).

In addition to the canonical signaling functions exerted by ErbB receptors when located at the plasma membrane and/or after internalization from intracellular vesicles, these receptors are known to translocate to the nucleus after ligand-induced activation where they appear to control transcriptional events relevant for cell proliferation and other functions (77-79). Although it is well established that ErbB4 is proteolytically processed before nuclear translocation and only the cytosolic segment moves to the nucleus, the full-length EGFR has been proposed to undergo nuclear translocation by a not fully understood mechanism (80). This has opened a strong controversy because it was argued that the experimental evidence for its location in the nucleoplasm was not as strong as suggested (81). Most significantly, it is not clear how the full-length receptor harboring a hydrophobic transmembrane segment undergoes its passage through a nuclear pore. Because the endoplasmic reticulum and the nuclear membrane form a network this could result in the

J Pharm Pharmaceut Sci (www.cspsCanada.org) 16(2) 177 - 189, 2013

misidentification of the compartment where the full-length receptor is indeed located.

Targeting ErbB receptors in cancer

Overexpression and/or the occurrence of truncated, site-mutated or segment-deleted hyperactive forms of EGFR and ErbB2 are common findings in many solid tumors in humans. These aberrant receptors significantly contribute to the oncogenic process and they have been studied in great detail (82-92). Additionally, oncogenic mutations are also found in a variety of proteins involved in the downstream signaling pathways of the ErbB receptors, as for example in those of the EGFR (93).

Consequently, targeting overexpressed and/or aberrant hyperactive ErbB receptors in anaplastic cells could be a valid therapeutic approach against cancer. In this context, a variety of EGFR and ErbB2 inhibitors have been developed, some of which are under test in clinical trials or are currently used in the clinic. These agents fall into two major categories: tyrosine kinase antagonists and inhibitory antibodies. Small molecules that bind to the tyrosine kinase domain of the receptor inhibiting its intrinsic tyrosine kinase activity form the first group. These compounds may specifically act on a single type of ErbB receptor, may have dual action inhibiting two receptor types (for example EGFR and ErbB2), or may have anti-pan-ErbB activity (94-100). Some of these compounds were identified from a database of traditional medicinal plants by virtually screening their potential inhibitory action on the tyrosine kinase activity of the EGFR (101). The second category of inhibitors includes chimeric, humanized or human monoclonal antibodies targeting the EGFR or ErbB2 (98, 102-107). Emerging techniques such as those using the minimum antigen-recognizing segment of the immunoglobulin against the receptor and/or fusing cytotoxic effector molecules - for example a toxin or an RNase - to a small segment of the anti-ErbB immunoglobulin have been developed to increase the efficacy of these immunodrugs (104, 108, 109).

As is common with other chemotherapeutic compounds, the use of anti-ErbB receptor agents may have important drawbacks that diminish or totally prevent their efficacy. This could be due to the occurrence of primary resistance of the tumor cells because of the expression of mutant receptors insensitive to the drug; or the establishment of acquired resistance induced by a variety of mechanisms including the appearance of secondary mutations (110-113). Another important problem when dispensing these antibodies to patients is the appearance of systemic or organ-selective toxic effects, for example cardiotoxicity (114, 115).

In addition to anti-ErbB receptor drugs targeting either the tyrosine kinase domain or the extracellular region of the receptor preventing ligand binding, activation, internalization, trafficking and/or signaling, there are other important functional sites in these receptors that could be targeted to inhibit their activity. An emerging target site of interest could be the CaM-BD located at the cytosolic JM region of the receptor, as we will describe in the next section.

Targeting the calmodulin-binding domain of the EGFR

The proximal segment of the cytosolic JM region of the human EGFR (residues 645-663, coded by exon 17), comprising the CaM-BD (residues 645-660) plays an important role in the functionality of the receptor, as its impairment results in the loss of most of its intrinsic tyrosine kinase activity without affecting ligand binding. This has been demonstrated either by deletion of this region (69, 116); substitution of critical positively-charged amino acids using site-directed mutagenesis, as for example replacing several arginine/lysine by neutral asparagine or alanine (73, 116, 117); or replacing the JM (amino acids 650-680) with an unstructured $(GGS)_{10}$ sequence (118). The R646 and R647 residues in the proximal part of the cytosolic JM region plus additional residues in the distal JM segment (residues 664-682, coded by exon 18) appear to be most relevant to preserve EGFR activity (117). The importance of the JM region for the activity of the receptor appears to rest in its participation in helping to form an asymmetric dimer involving two apposed tyrosine kinase domains stabilizing the dimer upon ligand binding (117, 119). A mutation (V665M) in the distal part of the cytosolic JM region has been shown to constitutively activate the EGFR in human non-small cell lung cancer (NSCLC) (117). However, two small-scale screenings for potential mutations in the JM of the four ErbB receptors gave negative results in a series of 200 human NSCLC samples (120) and 86/89 human astrocytic glioma samples (87, 121), suggesting that perhaps mutations in the JM segment are rare as it is required for receptor activity.

Targeting the cytosolic JM region of the EGFR, where the CaM-BD is located, could be an efficient new strategy to inhibit the overexpressed and/or constitutively active mutant receptor present

J Pharm Pharmaceut Sci (www.cspsCanada.org) 16(2) 177 - 189, 2013

in many tumor cells. Some exciting results have recently been obtained in this context. Thus, it has been demonstrated that a peptide corresponding to the proximal part of the cytosolic JM region (residues 645-662), tagged with a segment corresponding to the transactivation of transcription (Tat) sequence of HIV to allow its entry in the cell, induces non-apoptotic cell death after several hours of treatment, and caspase-3-mediated apoptosis after longer exposure in a variety of tumor cells expressing EGFR, but having reduced action on non-tumor cells and tumor cells not expressing EGFR (122). This peptide also decreases tumor growth *in vivo*, and increases the survival rate of experimental animals implanted with the tumor cells (122). The mechanism of action of the peptide appears mediated by its binds to the EGFR preventing receptor dimerization and favoring its down-regulation (122).

A peptide corresponding to the sequence R651-L658 of the EGFR in which threonine 654 has been substituted by a cysteine (RKRCLRRL, abbreviated T654C) (see Figure 1b) has been shown to inhibit PKC in an irreversible fashion because forms a disulfide bridge with a cysteine located in the catalytic site of the kinase (123). PKC is known to phosphorylate the EGFR at T654 (124), and to test whether this peptide was able as well to inhibit ligand-dependent activation of the EGFR in intact cells it was tagged with the membrane-permeable carrier sequence AAVALLPAVLLALAP (see Figure 1b). This sequence comprises the hydrophobic (h)-region of the signal sequence of the Kaposi fibroblast growth factor and is unlikely to produce by itself toxic effects, as it is a physiological signal peptide facilitating protein secretion (125). Moreover, this specific carrier sequence has been previously used to introduce several effector peptides inside living cells in order to disrupt the functionality of a variety of signaling pathways (126, 127).

We have demonstrated in murine EGFR-T17 fibroblasts overexpressing the EGFR that the T654C peptide tagged with the cell-permeable sequence inhibits both the ligand-dependent phosphorylation (activation) of the EGFR (see Figure 1c), and cell proliferation as determined by [methyl-^{3}H]thymidine incorporation into DNA (see Figure 1d), in contrast to the short T654C peptide lacking the carrier sequence and therefore unable to enter into the cells, at least with significant efficiency. The treatment of cells with the long T654C cell-permeable peptide eventually leads to cell death (Ruano and Villalobo, *unpublished*). The inhibitory effect of this peptide was also demonstrated in human epidermoid carcinoma A431 cells that also overexpress the EGFR (Ruano and Villalobo, *unpublished*). It is likely that the overexpression of the EGFR might facilitate the drastic inhibitory effects observed in these cells. The long T654C cell-permeable peptide might have a complex mechanism of action since it is an inhibitor of PKC (123), and it has not been tested if the cysteine prevents CaM binding. Nevertheless, our results are in agreement with those recently published using a distinct, though overlapping, peptide that binds to the EGFR preventing dimerization (122). Because of their related sequences, it is likely that both peptides have EGFR-interacting capacity.

This demonstrates that peptides based on the CaM-BD of the EGFR could be potential therapeutic agents against tumors expressing this receptor. Similarly, it could be important to explore in future studies the potential inhibitory action of cell-permeable peptides corresponding to the two CaM-BDs of ErbB2 in tumor cells expressing this receptor, as for example and most significant in some subtypes of human breast cancer.

Interestingly, the proposed NLS of the EGFR (128) overlaps with its CaM-BD (77) (see Figure 1a). This underscores the potential implication of CaM in the regulation of the nuclear translocation of the EGFR, even if only the cytosolic portion but not the full-length receptor moves to the nucleus. Nuclear EGFR associates to the catalytic subunit of DNA-PK inducing DNA repair. Mutation or deletion of the overlapping CaM-BD/NLS, however, prevents the nuclear localization of the EGFR and its association to DNA-PK, thus dampening the activity of this enzyme and subsequently reducing the DNA repairing activity (129). This may decrease the efficiency to the treatment of patients undergoing chemotherapy or ionizing radiation, highlighting the potential usefulness of targeting this region of the EGFR to additionally reduce the occurrence of resistance to these treatments in cancer patients.

Grb7 AND CALMODULIN

Our laboratory has also described the presence of a CaM-BD in the proximal region of the PH domain of human Grb7 comprising the sequence ^{243}RKLWKRFFCFLRRS^{256} that is predicted to form a basic amphipathic α-helix (see Figure 2a) (41). Sequence homology analysis shows that the CaM-BD of human, rat and mouse Grb7 are

J Pharm Pharmaceut Sci (www.cspsCanada.org) 16(2) 177 - 189, 2013

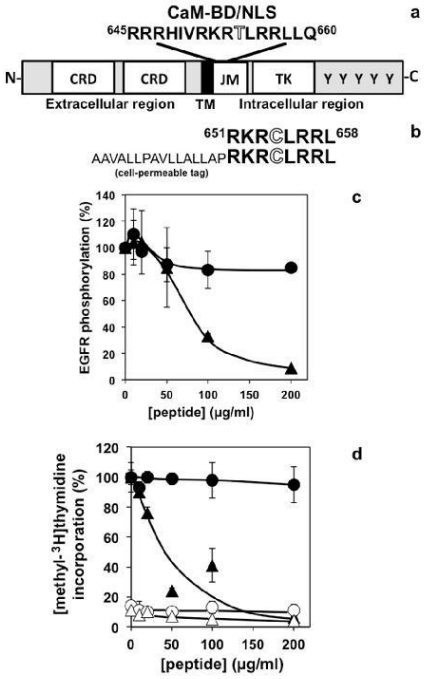

Figure. 1. Inhibitory effects of a modified cell-permeable EGFR peptide. a) Schematic representation of the EGFR structure showing the extracellular region containing two cysteine-rich domains (CRD); the transmembrane segment (TM); and the intracellular region comprising the cytosolic juxtamembrane segment (JM), the tyrosine kinase domain (TK), and the C-terminal tail with auto-phosphorylatable tyrosine residues (Y). The calmodulin-binding domain (CaM-BD), which overlaps the nuclear localization sequence (NLS), located in the proximal region of the cytosolic JM segment is indicated. The PKC-phosphorylatable residue T654 is highlighted. b) Amino acid sequences of the short and long (cell-permeable) T654C peptides. The N-terminal hydrophobic tag (*plain font*) and the substituted residue C654 are highlighted. c) The plot presents the mean ± range (n = 2) ligand-dependent phosphorylation of the EGFR in the presence of increasing concentrations of the short (*circles*) and long cell-permeable (*triangles*) peptides added to EGFR-T17 fibroblasts. d) The plot presents the mean ± SEM (n = 4) incorporation of [methyl-^{3}H]thymidine into DNA of EGFR-T17 fibroblasts in the absence (*open symbols*) and presence (*filled symbols*) of serum at increasing concentrations of the short (*circles*) and long cell-permeable (*triangles*) peptides (Ruano and Villalobo, *unpublished*).

identical, and that this region is highly conserved in Grb10 and Grb14 (23, 41). The truncated splice variant Grb7V lacking the C-terminal SH2 domain and expressed in certain adenocarcinomas (29) also maintains intact its CaM-BD (23, 41).

We have demonstrated that CaM binds to Grb7 and Grb7V in a Ca^{2+}-dependent manner *in vitro* and in living cells, and that the deletion mutants Grb7Δ and Grb7VΔ lacking the sequence corresponding to the proposed CaM-BD result in the near full loss of their capacity to bind CaM (41). Grb7Δ and Grb7VΔ have less ability to bind to membranes although they retain in part their capacity to bind to phosphoinositides (41). Moreover, the CaM antagonist W-7 - but not the CaMK-II inhibitor KN93 - prevents the translocation of Grb7 from the membrane to the cytosol upon activation of ErbB2 induced by heregulin ß1 in live cells, and a cell-permeable CaM sequestering peptide corresponding to the CaM-BD of MLCK decreases the association of Grb7 to cell membranes (41). Also, we have demonstrated that wild type Grb7 is translocated to the nucleus and that W-7 enhances this process, while Grb7Δ lacks this capacity (130). As the NLS and CaM-BD of Grb7 share superimposed sequences (see Figure 2a), our results suggest that CaM binding to Grb7 could occlude its NLS preventing in this manner the translocation of the protein to the nucleus and downstream signaling events occurring at this location (130).

Targeting Grb7 in cancer

Grb7 has been proposed to be a promising new target for anti-cancer therapy, as disrupting its functionality could inhibit the migratory capacity of tumor cells, their invasiveness and metastatic potential, and/or cell proliferation. As an example, it has been proposed that targeting the Grb7/ERK pathway and the downstream transcription factor FOXM1 could be a useful strategy to inhibit the growth, cell migratory capacity and invasiveness of ovarian tumor cells, as demonstrated *in vitro* and *in vivo* (131).

The SH2 domain of Grb7 has been suggested as a key target to inhibit this adaptor protein, most prominently using mimetic peptides (132). The cyclic structure of a small synthetic non-phosphorylated peptide containing an YXN motif, where X represents any amino acid, was shown to bind to the SH2 domain of Grb7 disrupting the interaction between Grb7 and ErbB receptors (133), and Grb7 and FAK (134). The peptide denoted G7-18NATE, with the sequence

J Pharm Pharmaceut Sci (www.cspsCanada.org) 16(2) 177 - 189, 2013

WFEGYDNTFPC, that cyclizes forming a thioether bond, inhibits the proliferation of a series of human breast cancer cells expressing Grb7 when tagged with a cell-permeable carrier sequence (37), and attenuates as well cell migration and the development of peritoneal metastasis from a primary pancreatic tumor in a mouse model (134). Furthermore, the G7-18NATE peptide presents a synergistic effect with other classical chemotherapeutic agents, such as the DNA-intercalating agent Doxorubicin, and the monoclonal antibody against ErbB2 denoted Trastuzumab (Herceptin) (37).

Moreover, a series of eleven benzopyrazine derivatives (135) and nine phenylbenzamine derivatives (136) targeting the SH2 domain of Grb7 have also been tested as potential antagonists of this adaptor protein. The leading compounds in the two series inhibited in culture the viability of a human breast cancer cell line overexpressing Grb7 (135, 136). These compounds were most effective at concentrations in the medium µmolar range (135, 136). Nevertheless, their efficacy, if any, against tumors *in vivo* remains to be tested.

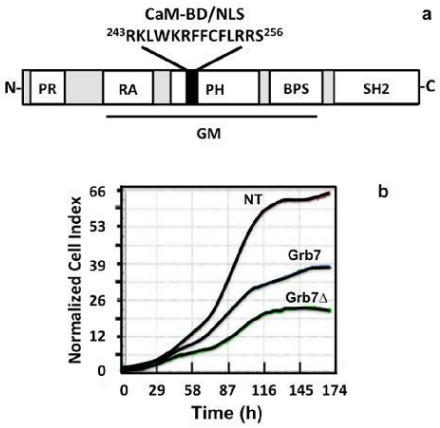

Figure. 2. Deletion of the CaM-BD of Grb7 decreases cell proliferation. a) Schematic representation of the Grb7 structure showing the PR, RA, PH, BPS and SH2 domains and highlighting the central GM region (see text for details). The calmodulin-binding domain (CaM-BD), overlapping the nuclear localization sequence (NLS), located in the proximal region of the PH domain is indicated. b) The plot shows the proliferation of non-transfected (NT) and stably transfected HEK-293 cells expressing Grb7 or Grb7Δ growing in the presence of serum and monitored in an xCELLigence RTCA system (García-Palmero and Villalobo, *unpublished*).

Targeting the calmodulin-binding domain of Grb7

To the best of our knowledge there is no information available on inhibitory compounds specifically targeting the CaM-BD of Grb7. However, this region of the protein could be a potential target for therapeutic intervention. This is based on interesting inhibitory effects observed in cells expressing the deletion mutant EYFP-Grb7Δ that lacks the CaM-BD, as compared to cells expressing EYFP-Grb7 (wild type) or EYFP alone. Thus, we have shown that rat glioma C6 cells expressing the mutant protein presented lower proliferation rate and diminished migratory capacity than the control cells (38). As an additional example, the inhibitory action of Grb7Δ on the proliferation of HEK-293 cells, as compared to wild type Grb7 or non-transfected cells is documented in Figure 2b. Although overexpression of Grb7 in tumors induces cell growth, the observed inhibitory effect of wild type Grb7 as compared to non-expressing cells (Figure 2b and Ref. 38), suggests that Grb7 may have a biphasic action when controlling cell proliferation. Expression of Grb7Δ also inhibits the migration of HEK-293 cells as compared to control cells (García-Palmero and Villalobo, *unpublished results*). Most relevant, these inhibitory effects were also observed *in vivo* measuring the growth of brain tumors derived from implanted C6 cells expressing the wild type and mutant proteins as determined by MRI (38).

Conditioned media from cells expressing Grb7Δ or Grb7VΔ also present strong anti-angiogenic activity, as compared to media from cells expressing their respective wild type counterparts, when tested on human vascular endothelial cells forming tubular structures in an *in vitro* assay system (41). The anti-angiogenic effect of Grb7Δ was also corroborated *in vivo*, as tumors derived from glioma C6 cells stably expressing the chimera EYFP-Grb7Δ and stereotaxically implanted in rat brain presented lower vascular performance and were less angiogenic that tumors derived from C6 cells stably expressing EYFP-Grb7 or EYFP alone, as determined by MRI perfusion techniques (38). This opens the possibility that targeting the CaM-BD of Grb7 with selective cell-permeable peptides or other compounds in tumors naturally expressing this adaptor protein could be an additional strategy to inhibit tumor-associated angiogenesis and tumor growth.

J Pharm Pharmaceut Sci (www.cspsCanada.org) 16(2) 177 - 189, 2013

FUTURE PERSPECTIVES

Many studies mostly performed *in vitro* point to a potential benefit of treating cancers with CaM antagonists. However, the therapeutic benefit of this strategy in patients has yet to be demonstrated because of the noxious side effects expected, even using sub-optimal doses. An alternative strategy that should be explored is targeting the site(s) of action of CaM in specific CaM-dependent systems that are upregulated and/or overexpressed in tumor cells, as we have proposed in this review with the CaM-BD of ErbB receptors and Grb7. Combinatory therapy targeting several systems at once could be a way to minimize the appearance of resistance to the drugs. Efforts are needed to discover specific biomarkers for the selective delivery of the intended drugs to the tumor, particularly targeting the tumor stem-cells, avoiding as much as possible the normal tissues.

Acknowledgements: The work in the authors laboratory was funded in part by grants (to AV) from the *Secretaría de Estado de Investigación Desarrollo e Innovación - SEIDEI* (SAF2011-23494), the *Consejería de Educación de la Comunidad de Madrid* (S2010/BMD-2349), the *Agencia Española de Cooperación Internacional para el Desarrollo - AECID* (AP/040803/11), and the European Commission (contract PITN-GA-2011-289033). IG-P, SRS and KJ were respectively supported by a fellowship from the *Ministerio de Educación Cultura y Deporte*, a Madame Curie contract from the European Commission, and a grant from the *AECID*. We thank Dr. Catherine A. O'Brian (University of Texas - MD Anderson Cancer Center) for generously donating the peptides.

Abbreviations: 5'-UTR, 5'-untranslated region; CaM, calmodulin; CaM-BD, CaM-binding domain; CaMK-II, CaM-dependent protein kinase II; c-Cbl, cellular Casitas B-lineage lymphoma proto-oncogene; DNA-PK, DNA-dependent protein kinase; EGFR, epidermal growth factor receptor; ErbB1/2/3/4, erythroblastic leukemia viral oncogene homologues 1 to 4; EYFP, enhanced yellow fluorescence protein; FAK, focal adhesion kinase; FOXM1, forkhead box M1; Grb7/10/14, growth factor receptor bound proteins 7/10/14; HER1/2/3/4, human EGFR 1 to 4; HIV, human immunodeficiency virus; JM, juxtamembrane; KN-93, 2-[*N*-(2-hydroxyethyl)]-*N*-(4-methoxybenzenesulfonyl)]amino-*N*-(4-chlorocinnamyl)-*N*-methylbenzylamine; MLCK, myosin light-chain kinase; MRI, magnetic resonance imaging; NLS, nuclear localization sequence; PH, pleckstrin homology; PKC, protein kinase C; PR, proline-rich; PTB, phospho-tyrosine-binding; RA, Ras-associating; SH2, Src homology 2; RTK, receptor tyrosine kinase; shRNA, small hairpin RNA; siRNA, small interfering RNA; W-7, *N*-(6-aminohexyl)-5-chloro-1-naphthalenesulfonamide.

REFERENCES

1. Downward J, Parker P, Waterfield MD. Autophosphorylation sites on the epidermal growth factor receptor. Nature, 1984; 311:483-485.
2. Carpenter G. Receptors for epidermal growth factor and other polypeptide mitogens. Annu Rev Biochem, 1987; 56:881-914.
3. Margolis BL, Lax I, Kris R, Dombalagian M, Honegger AM, Howk R, Givol D, Ullrich A, Schlessinger J. All autophosphorylation sites of epidermal growth factor (EGF) receptor and HER2/neu are located in their carboxyl-terminal tails: identification of a novel site in EGF receptor. J Biol Chem, 1989; 264:10667-10671.
4. Jorissen RN, Walker F, Pouliot N, Garrett TPJ, Ward CW, Burgess AW. Epidermal growth factor receptor: mechanisms of activation and signalling. Exp Cell Res, 2003; 284:31-53.
5. Alroy I, Yarden Y. The ErbB signaling network in embryogenesis and oncogenesis: signal diversification through combinatorial ligand-receptor interactions. FEBS Lett, 1997; 410:83-86.
6. Harris RC, Chung E, Coffey RJ. EGF receptor ligands. Exp Cell Res, 2003; 284:2-13.
7. Zhang X, Gureasko J, Shen K, Cole PA, Kuriyan J. An allosteric mechanism for activation of the kinase domain of epidermal growth factor receptor. Cell, 2006; 125:1137-1149.
8. Citri A, Skaria KB, Yarden Y. The deaf and the dumb: the biology of ErbB-2 and ErbB-3. Exp Cell Res, 2003; 284:54-65.
9. Citri A, Yarden Y. EGF-ERBB signalling: towards the systems level. Nat Rev Mol Cell Biol, 2006; 7:505-515.
10. Warren CM, Landgraf R. Signaling through ERBB receptors: multiple layers of diversity and control. Cell Signal, 2006; 18:923-933.
11. Alwan HAJ, van Zoelen EJJ, van Leeuwen JEM. Ligand-induced lysosomal epidermal growth factor receptor (EGFR) degradation is preceded by proteasome-dependent EGFR de-ubiquitination. J Biol Chem, 2003; 278:35781-35790.
12. Wiley HS. Trafficking of the ErbB receptors and its influence on signaling. Exp Cell Res, 2003; 284:78-88.
13. Kirisits A, Pils D, Krainer M. Epidermal growth factor receptor degradation: an alternative view of

oncogenic pathways. Int J Biochem Cell Biol, 2007; 39:2173-2182.
14. Cohen BD, Siegall CB, Bacus S, Foy L, Green JM, Hellström I, Hellström KE, Fell HP. Role of epidermal growth factor receptor family members in growth and differentiation of breast carcinoma. Biochem Soc Symp, 1998; 63:199-210.
15. Linggi B, Carpenter G. ErbB receptors: new insights on mechanisms and biology. Trends Cell Biol, 2006; 16:649-656.
16. Reinehr R, Häussinger D. Epidermal growth factor receptor signaling in liver cell proliferation and apoptosis. Biol Chem, 2009; 390:1033-1037.
17. Feigin ME, Muthuswamy SK. ErbB receptors and cell polarity: new pathways and paradigms for understanding cell migration and invasion. Exp Cell Res, 2009; 315:707-716.
18. Hynes NE, MacDonald G. ErbB receptors and signaling pathways in cancer. Curr Opi Cell Biol, 2009; 21:177-184.
19. Rush JS, Quinalty LM, Engelman L, Sherry DM, Ceresa BP. Endosomal accumulation of the activated epidermal growth factor receptor (EGFR) induces apoptosis. J Biol Chem, 2012; 287:712-722.
20. Margolis B. The GRB family of SH2 domain proteins. Prog Biophys Mol Biol, 1994; 62:223-244.
21. Daly RJ. The Grb7 family of signalling proteins. Cell Signal, 1998; 10:613-618.
22. Han DC, Shen T-L, Guan J-L. The Grb7 family proteins: structure, interactions with other signaling molecules and potential cellular functions. Oncogene, 2001; 20:6315-6321.
23. Villalobo A, Li H, Sánchez-Torres J. The Grb7 protein family. Curr Top Biochem Res, 2003; 5:105-114.
24. Lucas-Fernández E, García-Palmero I, Villalobo A. Genomic organization and control of the Grb7 gene family. Curr Genomics, 2008; 9:60-68.
25. Manser J, Wood WB. Mutations affecting embryonic cell migrations in *Caenorhabditis elegans*. Dev Genet, 1990; 11:49-64.
26. Manser J, Roonprapunt C, Margolis B. *C. elegans* cell migration gene mig-10 shares similarities with a family of SH2 domain proteins and acts cell nonautonomously in excretory canal development. Dev Biol, 1997; 184:150-164.
27. Han DC, Guan J-L. Association of focal adhesion kinase with Grb7 and its role in cell migration. J Biol Chem, 1999; 274:24425-24430.
28. Han DC, Shen T-L, Miao H, Wang B, Guan J-L. EphB1 associates with Grb7 and regulates cell migration. J Biol Chem, 2002; 277:45655-45661.
29. Tanaka S, Mori M, Akiyoshi T, Tanaka Y, Mafune K, Wands JR, Sugimachi K. A novel variant of human Grb7 is associated with invasive esophaheal carcinoma. J Clin Invest, 1998; 102:821-827.
30. Tanaka S, Sugimachi K, Kawaguchi H, Saeki H, Ohno S, Wands JR, Sugimachi K. Grb7 signal transduction protein mediates metastatic progression of esophageal carcinoma. J Cell Physiol, 2000; 183:411-415.
31. Wang Y, Chan DW, Liu VWS, Chu PM, Ngan HYS. Differential functions of growth factor receptor-bound protein 7 (GRB7) and its variant GRB7v in ovarian carcinogenesis. Clin Cancer Res, 2010; 16:2529-2539.
32. Ramsey B, Bai T, Newell AH, Troxell M, Park B, Olson S, Keenan E, Luoh S-W. GRB7 protein over-expression and clinical outcome in breast cancer. Breast Cancer Res Treat, 2011; 127:659-669.
33. Giricz O, Calvo V, Pero SC, Krag DN, Sparano JA, Kenny PA. GRB7 is required for triple-negative breast cancer cell invasion and survival. Breast Cancer Res Treat, 2012; 133:607-615.
34. Chu P-Y, Huang L-Y, Hsu C-H, Liang C-C, Guan J-L, Hung T-H, Shen T-L. Tyrosine phosphorylation of growth factor receptor-bound protein-7 by focal adhesion kinase in the regulation of cell migration, proliferation, and tumorigenesis. J Biol Chem, 2009; 284:20215-20226.
35. Chu P-Y, Li T-K, Ding S-T, Lai I-R Shen T-L. EGF-induced Grb7 recruits and promotes Ras activity essential for the tumorigenicity of Sk-Br3 breast cancer cells. J Biol Chem, 2010; 285:29279-29285.
36. Kao J, Pollack J-R. RNA interference-based functional dissection of the 17q12 amplicon in breast cancer reveals contribution of coamplified genes. Genes Chrom Cancer, 2006; 45:761-769.
37. Pero SC, Shukla GS, Cookson MM, Flemer S Jr, Krag DN. Combination treatment with Grb7 peptide and Doxorubicin or Trastuzumab (Herceptin) results in cooperative cell growth inhibition in breast cancer cells. Br J Cancer, 2007; 96:1520-1525.
38. García-Palmero I, López-Larrubia P, Cerdán S, Villalobo A. Nuclear magnetic resonance imaging of tumour growth and neovasculature performance *in vivo* reveals Grb7 as a novel antiangiogenic target. NMR Biomed, 2013; doi: 10.1002/nbm.2918.
39. Tsai N-P, Bi J, Wei L-N. The adaptor Grb7 links netrin-1 signaling to regulation of mRNA translation. EMBO J, 2007; 26:1522-1531.
40. Tsai N-P, Ho P-C, Wei L-N. Regulation of stress granule dynamics by Grb7 and FAK signaling pathway. EMBO J, 2008; 27:715-726.
41. Li H, Sánchez-Torres J, del Carpio AF, Nogales-González A, Molina-Ortiz P, Moreno MJ, Török K, Villalobo A. The adaptor Grb7 is a new calmodulin-binding protein: functional implications of the interaction of calmodulin with Grb7. Oncogene, 2005; 24:4206-4219.
42. Klee CB, Crouch TH, Richman PG. Calmodulin. Ann Rev Biochem, 1980; 49:489-515.

43. Chin D, Means AR. Calmodulin: a prototypical calcium sensor. Trends Cell Biol, 2000; 10:322-328.
44. Persechini A, Cronk B. The relationship between the free concentrations of Ca^{2+} and Ca^{2+}-calmodulin in intact cells. J Biol Chem, 1999; 274:6827-6830.
45. Dagher R, Peng S, Gioria S, Fève M, Zeniou M, Zimmermann M, Pigault C, Haiech J, Kilhoffer M-C. A general strategy to characterize calmodulin-calcium complexes in CaM-target recognition: DAPK and EGFR calmodulin binding domains interact with different calmodulin-calcium complexes. Biochim Biophys Acta, 2011; 1813:1059-1067.
46. Shifman JM, Choi MH, Mihalas S, Mayo SL, Kennedy MB. Ca^{2+}/calmodulin-dependent protein kinase II (CaMKII) is activated by calmodulin with two bound calciums. Proc Natl Acad Sci USA, 2006; 103:13968-13973.
47. Jurado LA, Chockalingam PS, Jarrett HW. Apocalmodulin. Physiol Rev, 1999; 79:661-682.
48. O'Neil KT, DeGrado WF. How calmodulin binds its targets: sequence independent recognition of amphiphilic □-helices. Trends Biochem Sci, 1990; 15:59-64.
49. Rhoads AR, Friedberg F. Sequence motifs for calmodulin recognition. FASEB J, 1997; 11:331-340.
50. Hoeflich KP, Ikura M. Calmodulin in action: diversity in target recognition and activation mechanisms. Cell, 2002; 108:739-742.
51. Wei JW, Hickie RZ, Klaassen DJ. Inhibition of human breast cancer colony formation by anticalmodulin agents: trifluoperazine, W-7, and W-13. Cancer Chemother Pharmacol, 1983; 11:86-90.
52. Hait WN, Lazo JS. Calmodulin: a potential target for cancer chemotherapeutic agents. J Clin Oncol, 1986; 4:994-1012.
53. Orosz F, Horváth I, Ovádi J. New anti-mitotic drugs with distinct anti-calmodulin activity. Mini Rev Med Chem, 2006; 6:1145-1157.
54. Mayur YC, Jagadeesh S, Thimmaiah KN. Targeting calmodulin in reversing multi drug resistance in cancer cells. Mini Rev Med Chem, 2006; 6:1383-1389.
55. Weiss B, Prozialeck WC, Wallace TL. Interaction of drugs with calmodulin: biochemical, pharmacological and clinical implications. Biochem Pharmacol, 1982; 31:2217-2226.
56. Roufogalis BD, Minocherhomjee AM, Al-Jobore A. Pharmacological antagonism of calmodulin. Can J Biochem Cell Biol, 1983; 61:927-933.
57. Walsh MP. Calmodulin: structure-function relations and inhibitors. Rev Clin Basic Pharm, 1985; 5:35-69.
58. Veigl ML, Klevit RE, Sedwick WD. The use and limitations of calmodulin antagonists. Pharmacol Ther, 1989; 44:181-239.
59. Hidaka H, Ishikawa T. Molecular pharmacology of calmodulin pathways in the cell functions. Cell Calcium, 1992; 13:465-472.
60. Martínez-Luis S, Pérez-Vásquez A, Mata R. Natural products with calmodulin inhibitor properties. Phytochemistry, 2007; 68:1882-1903.
61. Takuwa N, Zhow W, Takuwa Y. Calcium, calmodulin and cell cycle progression. Cell Signal, 1995; 7:93-104.
62. Sánchez-González P, Jellali K, Villalobo A. Calmodulin-mediated regulation of the epidermal growth factor receptor. FEBS J, 2010; 277:327-342.
63. San José E, Benguría A, Geller P, Villalobo A. Calmodulin inhibits the epidermal growth factor receptor tyrosine kinase. J Biol Chem, 1992; 267:15237-15245.
64. Martín-Nieto J, Villalobo A. The human epidermal growth factor receptor contains a juxtamembrane calmodulin-binding site. Biochemistry, 1998; 37:227-236.
65. Aifa S, Johansen K, Nilsson UK, Liedberg B, Lundström I, Svensson SPS. Interactions between the juxtamembrane domain of the EGFR and calmodulin measured by surface plasmon resonance. Cell Signal, 2002; 14:1005-1013.
66. Li H, Villalobo A. Evidence for the direct interaction between calmodulin and the human epidermal growth factor receptor. Biochem J, 2002; 362:499-505.
67. Li H, Ruano MJ, Villalobo A. Endogenous calmodulin interacts with the epidermal growth factor receptor in living cells. FEBS Lett, 2004; 559:175-180.
68. McLaughlin S, Smith SO, Hayman MJ, Murray D. An electrostatic engine model for autoinhibition and activation of the epidermal growth factor receptor (EGFR/ErbB) family. J Gen Physiol, 2005; 126:41-53.
69. Aifa S, Aydin J, Nordvall G, Lundström I, Svensson SPS, Hermanson O. A basic peptide within the juxtamembrane region is required for EGF receptor dimerization. Exp Cell Res, 2005; 302:108-114.
70. Sato T, Pallavi P, Golebiewska U, McLaughlin S, Smith SO. Structure of the membrane reconstituted transmembrane-juxtamembrane peptide EGFR(622-660) and its interaction with Ca^{2+}/calmodulin. Biochemistry, 2006; 45:12704-12714.
71. Sengupta P, Ruano MJ, Tebar F, Golebiewska U, Zaitseva I, Enrich C, McLaughlin S, Villalobo A. Membrane-permeable calmodulin inhibitors (e.g., W-7/W-13) bind to membranes, changing the electrostatic surface potential: dual effect of W-13 on EGFR activation. J Biol Chem, 2007; 282:8474-8486.
72. Panina S, Stephan A, La Cour JM, Jacobsen K, Kallerup LK, Bumbuleviciute R, Knudsen KVK, Sánchez-González P, Villalobo A, Olesen UH,

Berchtold MW. Significance of calcium binding, tyrosine phosphorylation, and lysine trimethylation for the essential function of calmodulin in vertebrate cells analyzed in a novel gene replacement system. J Biol Chem, 2012; 287:18173-18181.

73. Li H, Panina S, Kaur A, Ruano MJ, Sánchez-González P, La Cour JM, Stephan A, Olesen UH, Berchtold MW, Villalobo A. Regulation of the ligand-dependent activation of the epidermal growth factor receptor by calmodulin. J Biol Chem, 2012; 287:3273-3281.
74. Martín-Nieto J, Cusidó-Hita DM, Li H, Benguría A, Villalobo A, Regulation of ErbB receptors by calmodulin, in Pandalai SG (ed), Recent Research Developments in Biochemistry vol. 3, Research Signpost, Trivandrum, pp. 41-58, 2002.
75. Li H, Sánchez-Torres J, del Carpio A, Salas V, Villalobo A. The ErbB2/Neu/HER2 receptor is a new calmodulin-binding protein. Biochem J, 2004; 381:257-266.
76. White CD, Li Z, Sacks DB. Calmodulin binds HER2 and modulates HER2 signaling. Biochim Biophys Acta, 2011; 1813:1074-1082.
77. Villalobo A, García-Andrés C, Molina-Ortiz P. Translocation of ErbB receptors into the nucleus. Rev Oncol, 2003; 5:381-389.
78. Brand TM, Iida M, Li C, Wheeler DL. The nuclear epidermal growth factor receptor signaling network and its role in cancer. Discov Med, 2011; 12:419-432.
79. Wang Y-N, Hung M-C. Nuclear functions and subcellular trafficking mechanisms of the epidermal growth factor receptor family. Cell Biosci, 2012; 2:13.
80. Lin S-Y, Makino K, Xia WY, Matin A, Wen Y, Kwong KY, Bourguignon L, Hung MC. Nuclear localization of EGF receptor and its potential new role as a transcription factor. Nat Cell Biol, 2001; 3:802-808.
81. Schlessinger J, Lemmon MA. Nuclear signaling by receptor tyrosine kinases: the first robin of spring. Cell, 2006; 127:45-48.
82. Kim H, Muller WJ. The role of the epidermal growth factor receptor family in mammary tumorigenesis and metastasis. Exp Cell Res, 1999; 253:78-87.
83. Yu D, Hung MC. Overexpression of ErbB2 in cancer and ErbB2-targeting strategies. Oncogene, 2000; 19:6115-6121.
84. Pedersen MW, Meltorn M, Damstrup L, Poulsen HS. The type III epidermal growth factor receptor mutation: biological significance and potential target for anti-cancer therapy. Ann Oncol, 2001; 12:745-760.
85. Roskoski RJr. The ErbB/HER receptor protein-tyrosine kinases and cancer. Biochem Biophys Res Commun, 2004; 319:1-11.
86. Stephens P, Hunter C, Bignell G, Edkins S, Davies H, Teague J, Stevens C, O'Meara S, Smith R, Parker A, Barthorpe A, Blow M, Brackenbury L, Butler A, Clarke O, Cole J, Dicks E, Dike A, Drozd A, Edwards K, Forbes S, Foster R, Gray K, Greenman C, Halliday K, Hills K, Kosmidou V, Lugg R, Menzies A, Perry J, Petty R, Raine K, Ratford L, Shepherd R, Small A, Stephens Y, Tofts C, Varian J, West S, Widaa S, Yates A, Brasseur F, Cooper CS, Flanagan AM, Knowles M, Leung SY, Louis DN, Looijenga LH, Malkowicz B, Pierotti MA, Teh B, Chenevix-Trench G, Weber BL, Yuen ST, Harris G, Goldstraw P, Nicholson AG, Futreal PA, Wooster R, Stratton MR. Lung cancer: intragenic ERBB2 kinase mutations in tumours. Nature, 2004; 431:525-526.
87. Arjona D, Bello MJ, Alonso ME, González-Gómez P, Aminoso C, Isla A, de Campos JM, Vaquero J, Gutierrez M, Villalobo A, Rey JA. Molecular analysis of the EGFR gene in astrocytic gliomas: mRNA expression, quantitative-PCR analysis of non homogeneous gene amplification and DNA sequence alterations. Neuropathol Appl Neurobiol, 2005; 31:384-394.
88. Sharma SV, Bell DW, Settleman J, Haber DA. Epidermal growth factor receptor mutations in lung cancer. Nat Rev Cancer, 2007; 7:169-181.
89. Gan HK, Kave AH, Luwor RB. The EGFRvIII variant in glioblastoma multiforme. J Clin Neurosci, 2009; 16:748-754.
90. Pines G, Köstler WJ, Yarden Y. Oncogenic mutant forms of EGFR: lessons in signal transduction and targets for cancer therapy. FEBS Lett, 2010; 584:2699-2706.
91. Da Cunha Santos G, Shepherd FA, Tsao MS. EGFR mutations and lung cancer. Annu Rev Pathol, 2011; 6:49-69.
92. Arcila ME, Chaft JE, Nafa K, Roy-Chowdhuri S, Lau C, Zaidinski M, Paik PK, Zakowski MF, Kris MG, Ladanyi M. Prevalence, clinicopathologic associations, and molecular spectrum of ERBB2 (HER2) tyrosine kinase mutations in lung adenocarcinomas. Clin Cancer Res, 2012; 18:4910-4918.
93. Grossmann AH, Samowitz WS. Epidermal growth factor receptor pathway mutations and colorectal cancer therapy. Arch Pathol Lab Med, 2011; 135:1278-1282.
94. Anderson NG, Ahmad T. ErbB receptor tyrosine kinase inhibitors as therapeutic agents. Front Biosci, 2002; 7:d1926-d1940.
95. Normanno N, Maiello MR, De Luca A. Epidermal growth factor receptor tyrosine kinase inhibitors (EGFR-TKIs): simple drugs with a complex mechanism of action? J Cell Physiol, 2002; 194:13-19.
96. Normanno N, Maiello MR, Mancino M, De Luca A. Small molecule epidermal growth factor receptor tyrosine kinase inhibitors: an overview. J Chemother, 2004; 16 Suppl4:36-40.
97. Ranson M. Epidermal growth factor receptor

tyrosine kinase inhibitors. Br J Cancer, 2004; 90:2250-2255.
98. Mendelson J, Baselga J. Epidermal growth factor receptor targeting in cancer. Semin Oncol, 2006; 33:369-385.
99. Sequist LV. Second-generation epidermal growth factor receptor tyrosine kinase inhibitors in non-small cell lung cancer. Oncologist, 2007; 12:325-330.
100. Jamal-Hanjani M, Spicer J. Epidermal growth factor receptor tyrosine kinase inhibitors in the treatment of epidermal growth factor receptor-mutant non-small cell lung cancer metastatic to the brain. Clin Cancer Res, 2012; 18:938-944.
101. Sawatdichaikul O, Hannongbua S, Sangma C, Wolschann P, Choowongkomon K. *In silico* screening of epidermal growth factor receptor (EGFR) in the tyrosine kinase domain through a medicinal plant compound database. J Mol Model, 2012; 18:1241-1254.
102. Lipton A, Villalobo A. EGFR-targeted cancer research: continuing progress and changing views (Editorial). Signal, 2001; 2:2-3.
103. Baselga J, Arteaga CL. Critical update and emerging trends in epidermal growth factor receptor targeting in cancer. J Clin Oncol, 2005; 23:2445-2459.
104. De Lorenzo C, D'Alessio G. Human anti-ErbB2 immunoagents - immunoRNases and compact antibodies. FEBS J, 2009; 276:1527-1535.
105. Markman B, Capdevilla J, Elez E, Tabernero J. New trends in epidermal growth factor receptor-directed monoclonal antibodies. Immunotherapy, 2009; 1:965-982.
106. Elloumi J, Jellali K, Jemel I, Aifa S. Monoclonal antibodies as cancer therapeutics. Rec Pat Biotechnol, 2012; 6:45-56.
107. Omidfar K, Shirvani Z. Single domain antibodies: a new concept for epidermal growth factor receptor and EGFRvIII targeting. DNA Cell Biol, 2012; 1015-1026.
108. King CR, Kasprzyk PG, Fischer PH, Bird RE, Turner NA. Preclinical testing of an anti-erbB-2 recombinant toxin. Breast Cancer Res Treat, 1996; 38:19-25.
109. Altintas I, Kok RJ, Schiffelers RM. Targeting epidermal growth factor receptor in tumors: from conventional antibodies via heavy chain-only antibodies to nanobodies. Eur J Pharm Sci, 2012; 45:399-407.
110. Mellinghoff IK, Cloughesy TF, Mischel PS. PTEN-mediated resistance to epidermal growth factor receptor kinase inhibitors. Clin Cancer Res, 2007; 13:378-381.
111. Engelman JA, Jänne PA. Mechanisms of acquired resistance to epidermal growth factor receptor tyrosine kinase inhibitors in non-small cell lung cancer. Clin Cancer Res, 2008; 14:2895-2899.
112. Mukohara T. Mechanisms of resistance to anti-human epidermal growth factor receptor 2 agents in breast cancer. Cancer Sci, 2011; 102:1-8.
113. Ayoola A, Barochia A, Belani K, Belani CP. Primary and acquired resistance to epidermal growth factor receptor tyrosine kinase inhibitors in non-small cell lung cancer: an update. Cancer Invest, 2012; 30:433-446.
114. Schneider JW, Chang AY, Rocco TP. Cardiotoxicity in signal transduction therapeutics: erbB2 antibodies and the heart. Semin Oncol, 2001; 28:18-26.
115. Chaudhary P, Gaira A. Cardiovascular effects of EGFR (epidermal growth factor receptor) monoclonal antibodies. Cardiovasc Hematol Agents Med Chem, 2010; 8:156-163.
116. Yamane K, Toyoshima C, Nishimura S. Ligand-induced functions of the epidermal growth factor receptor require the positively charged region asymmetrically distributed across plasma membrane. Biochem Biophys Res Commun, 1992; 184:1301–1310.
117. Red Brewer M, Choi SH, Alvarado D, Moravcevic K, Pozzi A, Lemmon MA, Carpenter G. The juxtamembrane region of the EGF receptor functions as an activation domain. Mol Cell, 2009; 34:641–651.
118. He L, Hristova K. Consequences of replacing EGFR juxtamembrane domain with an unstructured sequence. Sci Rep, 2012; 2:854.
119. Jura N, Endres NF, Engel K, Deindl S, Das R, Lamers MH, Wemmer DE, Zhang X, Kuriyan J. Mechanism for activation of the EGF receptor catalytic domain by the juxtamembrane segment. Cell, 2009; 137:1293-1307.
120. Park SW, Chung NG, Han JY, Eom HS, Yoo NJ, Lee SH. Somatic mutations of EGFR, ERBB2, ERBB3 and ERBB4 in juxtamembrane activating domains are rare in non-small cell lung cancers. Acta Pathol Microbiol Immunol Scand, 2009; 118:83-84.
121. Arjona D, Bello MJ, Alonso ME, González-Gómez P, Lomas J, Aminoso C, López-Marín I, Isla A, de Campos JM, Vaquero J, Villalobo A, Rey JA. Molecular analysis of the *erb*B gene family calmodulin-binding domain and calmodulin-like domain in astrocytic gliomas. Int J Oncol, 2004; 25:1489-1494.
122. Boran ADW, Seco J, Jayaraman V, Jayaraman G, Zhao S, Reddy S, Chen Y, Iyengar R. A potential peptide therapeutic derived from the juxtamembrane domain of the epidermal growth factor receptor. PLoS One, 2012; 7:e49702.
123. Ward NE, Gravitt KR, O'Brian CA. Irreversible inactivation of protein kinase C by a peptide-substrate analog. J Biol Chem, 1995; 270:8056-8060.
124. Hunter T, Ling N, Cooper JA. (1984) Protein kinase C phosphorylation of the EGF receptor at threonine residue close to the cytoplasmic face of

the plasma membrane. Nature, 1984; 311:480-483.
125. von Heijne G. The signal peptide. J Membr Biol, 1990; 115:195-201.
126. Lin Y-Z, Yao SY, Veach RA, Torgerson TR, Hawiger J. Inhibition of nuclear translocation of transcription factor NF-□B by a synthetic peptide containing a cell membrane-permeable motif and nuclear localization sequence. J Biol Chem, 1995; 270:14255-14258.
127. Rojas M, Yao SY, Lin Y-Z. Controlling epidermal growth factor (EGF)-stimulated Ras activation in intact cells by a cell-permeable peptide mimicking phosphorylated EGF receptor. J Biol Chem, 1996; 271:27456-27461.
128. Hsu SC, Hung MC. Characterization of a novel tripartite nuclear localization sequence in the EGFR family. J Biol Chem, 2007; 282:10432-10440.
129. Liccardi G, Hartley JA, Hochhauser D. EGFR nuclear translocation modulates DNA repair following cisplatin and ionizing radiation. Cancer Res, 2011; 71:1103-1114.
130. García-Palmero I, Villalobo A. Calmodulin regulates the translocation of Grb7 into the nucleus. FEBS Lett, 2012; 586:1533-1539.
131. Chan DW, Hui WW, Cai PC, Liu MX, Yung MM, Mak CS, Leung TH, Chan KK, Ngan HY. Targeting GRB7/ERK/FOXM1 signaling pathway impairs aggressiveness of ovarian cancer cells. PLoS One, 2012; 7:e52578.
132. Pero SC, Daly RJ, Krag DN. Grb7-based molecular therapeutics in cancer. Expert Rev Mol Med, 2003; 5:1-11.
133. Pero SC, Oligino L, Daly RJ, Soden AL, Liu C, Roller PP, Li P, Krag DN. Identification of novel non-phosphorylated ligands, which bind selectively to the SH2 domain of Grb7. J Biol Chem, 2002; 277:11918-11926.
134. Tanaka S, Pero SC, Taguchi K, Shimada M, Mori M, Krag DN, Arii S. Specific peptide ligand for Grb7 signal transduction protein and pancreatic cancer metastasis. J Natl Cancer Inst, 2006; 98:491-498.
135. Ambaye ND, Gunzburg MJ, Lim RCC, Price JT, Wilce MCJ, Wilce JA. Benzopyrazine derivatives: a novel class of growth factor receptor bound protein 7 antagonists. Bioorg Med Chem, 2011; 19:693-701.
136. Ambaye ND, Gunzburg MJ, Lim RCC, Price JT, Wilce MCJ, Wilce JA. The discovery of phenylbenzamide derivatives as grb7-based antitumor agents. ChemMedChem, 2013; 8:280-288.

PLOS | ONE

RESEARCH ARTICLE

Characterization of Phospho-(Tyrosine)-Mimetic Calmodulin Mutants

Silviya R. Stateva[1], Valentina Salas[1,2], Gustavo Benaim[2,3], Margarita Menéndez[4], Dolores Solís[4], Antonio Villalobo[1]*

1 Instituto de Investigaciones Biomédicas, Consejo Superior de Investigaciones Científicas and Universidad Autónoma de Madrid, Madrid, Spain, **2** Universidad Central de Venezuela, Facultad de Ciencias, Instituto de Biología Experimental, Caracas, Venezuela, **3** Instituto de Estudios Avanzados (IDEA), Caracas, Venezuela, **4** Instituto de Química Física Rocasolano, Consejo Superior de Investigaciones Científicas, Madrid, Spain

* antonio.villalobo@iib.uam.es

OPEN ACCESS

Citation: Stateva SR, Salas V, Benaim G, Menéndez M, Solís D, Villalobo A (2015) Characterization of Phospho-(Tyrosine)-Mimetic Calmodulin Mutants. PLoS ONE 10(4): e0120798. doi:10.1371/journal.pone.0120798

Academic Editor: Keiko Abe, The University of Tokyo, JAPAN

Received: September 29, 2014

Accepted: February 6, 2015

Published: April 1, 2015

Data Availability Statement: All relevant data are within the paper.

Funding: This work was funded by grants to AV from the Secretaría de Estado de Investigación, Desarrollo e Innovación (SAF2011-23494) and the Consejería de Educación de la Comunidad de Madrid (S2011/BMD-2349), and grant to AV and DS from the European Commission (contract PITN-GA-2011-289033 DYNANO). Additional funding to DS and MM was provided by the Centro de Investigación Biomédica en Red de Enfermedades Respiratorias. SRS was funded by a Marie Curie contract from the European Commission and VS and GB were

Abstract

Calmodulin (CaM) phosphorylated at different serine/threonine and tyrosine residues is known to exert differential regulatory effects on a variety of CaM-binding enzymes as compared to non-phosphorylated CaM. In this report we describe the preparation and characterization of a series of phospho-(Y)-mimetic CaM mutants in which either one or the two tyrosine residues present in CaM (Y99 and Y138) were substituted to aspartic acid or glutamic acid. It was expected that the negative charge of the respective carboxyl group of these amino acids mimics the negative charge of phosphate and reproduce the effects that distinct phospho-(Y)-CaM species may have on target proteins. We describe some physicochemical properties of these CaM mutants as compared to wild type CaM, after their expression in *Escherichia coli* and purification to homogeneity, including: i) changes in their electrophoretic mobility in the absence and presence of Ca^{2+}; ii) ultraviolet (UV) light absorption spectra, far- and near-UV circular dichroism data; iii) thermal stability in the absence and presence of Ca^{2+}; and iv) Tb^{3+}-emitted fluorescence upon tyrosine excitation. We also describe some biochemical properties of these CaM mutants, such as their differential phosphorylation by the tyrosine kinase c-Src, and their action as compared to wild type CaM, on the activity of two CaM-dependent enzymes: cyclic nucleotide phosphodiesterase 1 (PDE1) and endothelial nitric oxide synthase (eNOS) assayed *in vitro*.

Introduction

Calmodulin (CaM) is a highly conserved Ca^{2+}-receptor protein, ubiquitous in all eukaryotic organisms, implicated in the regulation of many cellular systems by transducing changes in the concentration of free Ca^{2+} in the cytosol and other intracellular compartments and structures (reviewed in [1]). CaM is multifunctional and controls a myriad of cellular processes ranging from egg fertilization, muscle contraction, osmotic control and ions transport, metabolism, gene expression, cell migration, proliferation, autophagy and programmed cell death, among

supported by fellowship and grants (03-00-6057-2005 and PG-03-8728-2013) from the Consejo de Desarrollo Científico y Humanístico de la Universidad Central de Venezuela.

Competing Interests: The authors have declared that no competing interests exist.

many others, and plays a significant role in functions that are deregulated in pathological processes such as cancer (reviewed in [2]), arrhythmias and infant cardiac arrest [3, 4], and other ailments such asthma or chronic obstructive pulmonary disease (reviewed in [5]) among others. By interacting with close to three hundred target proteins, with and without enzymatic activity, and regulating their functions in a temporo-spatial fashion, CaM achieves this feast. Distinct mechanisms of interaction between the Ca^{2+}/CaM complex and CaM-binding proteins have been described [6, 7]. In addition to the Ca^{2+}-mediated modulation of CaM action, apocalmodulin (Ca^{2+}-free CaM) also interacts with and regulates the activity of a variety of CaM-binding proteins [8, 9].

An assortment of serine/threonine- and tyrosine-protein kinases have been shown to phosphorylate CaM *in vitro* and in living cells. The distinct phospho-CaM species differentially regulate the activity of many target proteins as compared to non-phosphorylated CaM (reviewed in [10]). This suggests that this posttranslational modification could play additional and/or complementary roles to Ca^{2+} binding in the modulation of CaM activity.

The non-receptor tyrosine kinase Src [11], the insulin receptor [12], and the epidermal growth factor receptor (EGFR) [13], are prominent kinases implicated in the phosphorylation of CaM at both Y99 and Y138, the only two tyrosine residues present in vertebrate CaM. It seems likely that the dynamic identification of distinct phosphorylated forms of CaM at a given time acting on specific targets could be difficult to observe in living cells due in part to the short half-life of phospho-(Y)-CaM. An alternative to explore these events could be to use recombinant phospho-(Y)-mimetic CaM mutants.

In order to understand the implication of distinct phospho-(Y)-CaM species on the activity of different CaM-binding target proteins, we have prepared a set of recombinant phospho-(Y)-mimetic CaM mutants by substituting either one or the two tyrosine residues to aspartic acid or glutamic acid. Here we characterized their physico-chemical properties and tested *in vitro* their action on the activity of two CaM-dependent enzymes: the 3',5'-cyclic nucleotide phosphodiesterase 1 (CaM-dependent isoform) (PDE1) (EC 3.1.4.17) and endothelial nitric oxide synthase (eNOS) (EC 1.14.13.39).

Materials and Methods

Reagents

Phenyl-Sepharose 6 (fast flow), (6R)-5,6,7,8-tetrahydrobiopterin dihydrochloride, FMN, FAD, cAMP, 3',5'-cyclic nucleotide phosphodiesterase 1 (CaM-dependent isoform) (PDE1) (from bovine brain), 5'-nucleotidase (EC 3.1.3.5) (from *Crotalus atrox* venom), eNOS (bovine recombinant baculovirus-expressed in Sf9 cells), histone (type II-A), and anti-mouse IgG (Fc specific) peroxidase-conjugated secondary antibody were obtained from Sigma-Aldrich Co. (St. Louis, MO). The ultrasensitive colorimetric assay kit for eNOS was purchased from Oxford Biomedical Research (Rochester Hills, MI). Rabbit monoclonal anti-Src antibody (clone 36D10, isotype IgG) was purchased from Cell Signaling Technology Inc. (Danvers, MA). Mouse monoclonal anti-phosphotyrosine antibody (clone 4G10, isotype $IgG_{2b\kappa}$), recombinant c-Src (human) and mouse monoclonal anti-CaM antibody (isotype IgG_1) were obtained from Millipore (Billerica, MA). Anti-rabbit IgG horseradish peroxidase-linked secondary antibody was purchased from Invitrogen (Eugene, OR). The QuickChange XL site-directed mutagenesis kit was acquired from Agilent Technology (Santa Clara, CA), and the QIAprep plasmid preparation kit from Quiagen Ltd. (Manchester, UK). The Slide-A-Lyzer dialysis cassettes were purchased from Thermo Scientific-Pierce (Rockford, IL). Competent *Escherichia coli* BL21(DE3)pLysS was purchased from Stratagene (La Jolla, CA), and the BugBuster protein extraction reagent kit was from Merck/Millipore (Darmstadt, Germany). The pETCM vector was kindly provided by

Prof. Nobuhiro Hayashi from the Institute for Comprehensive Medical Science, Fujita Health University, Japan.

Generation of calmodulin mutants

Polymerase chain reaction-aided site-directed mutagenesis was performed in the pETCM vector containing the coding sequence of *Rattus norvegicus* CaM gene II [14] as template using the QuickChange XL Site-Directed Mutagenesis kit and the following set of complementary oligos: 5'-GGCAATGGCGACATCAGTGCAGCA-3' and 5'-TGCTGCACTGATGTCGCCATT GCC-3' for the Y99D substitution; 5'-GGGGATGGTCAGGTAAACGACGAAGAGTTTGTA CAAATG-3' and 5'-CATTTGTACAAACTCTTCGTCGTCGTTTACCTGACCATCCCC-3' for the Y138D substitution; 5'-GGCAATGGCGAGATCAGTGCAG-3' and 5'CTGCACT GATCTCGCCATTGCC-3' for the Y99E substitution; and 5'-GGGGATGGTCAGGTAAAC GAGGAAGAGTTTGTACAAATG-3' and 5'-CATTTGTACAAACTCTTCCTCGTCGTTTA CCTGACCATCCCC-3' for the Y138E substitution. Sequential mutagenesis was carried out to obtain the double substitutions Y99D/Y138D and Y99E/Y138E using the Y99D and Y99E mutated vectors, respectively, as template. *Escherichia coli* DH5α was transformed with the pETCM, pETCM(Y99D), pETCM(Y138D), pETCM(Y99D/Y138D), pETCM(Y99E), pETCM (Y138E) or pETCM(Y99E/Y138E) vectors for their replication, and purification by the alkaline lysis method [15] using the QIAprep plasmid preparation kit. The correctness of the mutagenesis procedures was ascertained by sequencing the vectors using an oligo annealing to the T7 promoter.

Expression and purification of recombinant calmodulin mutants

E. coli BL21(DE3)pLysS was transformed with the vectors indicated above using a thermic-shock protocol. Single colonies grown in solid medium in the presence of 100 μg/ml ampicillin were collected and seeded in 5 ml of Luria´s broth containing the same concentration of ampicillin. Larger cultures (500 ml) were seeded with the pre-culture and grown in the same conditions until they reached an OD_{600nm} = 0.7 ± 0.1. The expression of the recombinant proteins was induced with 0.5 mM isopropyl-1-thio-β-D-galactopyranoside (IPTG) during 4 hours at 37°C. Control cultures in the absence of IPTG were included. The bacteria were collected by centrifugation at 6,000 x g for 20 min and frozen at -70°C until used. The bacteria were lysed using the BugBuster protein extraction reagent kit, centrifuged at 11,000 x g during 10 min at 4°C and the supernatant collected, heated at 95°C for 5 min and centrifuged again as above. Heat-resistant CaM present in the new supernatant was purified as previously described [14]. Briefly, phenyl-Sepharose 6 Fast Flow was prepacked in a column and equilibrated with a buffer containing 50 mM 2-amino-2-hydroxymethyl-propane-1,3-diol (Tris)-HCl (pH 7.5) and 1 mM $CaCl_2$. The sample was applied to the column and washed with four column volumes of a buffer containing 50 mM Tris-HCl (pH 7.5), 1 mM $CaCl_2$ and 100 mM NaCl. CaM was eluted with a buffer containing 50 mM Tris-HCl (pH 7.5) and 2 mM EGTA in fractions of 10 ml. The fractions containing CaM were desalted using Slide-A-Lyzer dialysis cassettes with membranes of 3.5 kDa cut-off against a buffer containing 10 mM 4-(2-hydroxyethyl)-1-piperazineethanesulfonic acid (Hepes)-NaOH (pH 7.5) or 20 mM Tris-HCl (pH 7.5) and kept at a concentration of 1–2 mg/ml at -70°C. Protein concentration was determined by the bicinchoninic acid method [16] using bovine serum albumin as standard. The purity of the samples was confirmed by polyacrylamide gel electrophoresis in the presence of sodium dodecyl sulfate (SDS-PAGE) [17] in a 5–20% (w/v) continuous gradient slab gel adding 5 mM EGTA or 1 mM $CaCl_2$ in the loading buffer to attain the characteristic Ca^{2+}-induced electrophoretic mobility shift of CaM [18], and staining the gel with Coomassie Brilliant Blue R-250.

Absorption spectra

The absorption spectra in the range 240–340 nm of the different species of CaM (120 μM) were measured in 20 mM Tris-HCl (pH 7.5) using a CARY/1E/UV-Visible spectrophotometer (Varian) equipped with Cary winUV software.

Circular dichroism

Far-UV (200–260 nm) and near-UV (250–320 nm) circular dichroism spectra of the different CaM species were measured at 20°C in the presence of either 1 mM EGTA or 1 mM $CaCl_2$ in a buffer containing 20 mM Tris-HCl (pH 7.5) and 0.1 M KCl using a JASCO J-810 spectropolarimeter (Cremelia, Italy) equipped with a Peltier type temperature control system (Model PTC-423S/L), a bandwidth of 0.2 nm and a response time of 4 s. Far-UV spectra were recorded in 0.1 cm path-length quartz cells at a protein concentration of 0.2 mg/ml, and near-UV spectra in 1 cm path-length cuvettes at a protein concentration of 2 mg/ml as previously described [19]. The Spectra Manager software (JASCO, v 1.52.01) was used for data collection and analysis. Routinely, the corresponding buffer baseline was subtracted and the corrected data were normalized per mole of amino acid. Thermal denaturation experiments were carried out in the same system by increasing the temperature from 20 to 90°C at a scanning rate of 0.66°C/min. Variations in ellipticity at 222 nm were monitored at steps of 0.2°C.

Tb^{3+} fluorescence

The emission fluorescence spectra in the range 520–580 nm of the different species of CaM (10 μM) upon excitation of tyrosine (if present) at 280 nm were measured in 10 mM 1,4-piperazinediethanesulfonic acid (Pipes)-HCl (pH 6.5), 100 mM KCl, and increasing concentrations of $TbCl_3$ (0–200 μM) using a Photon Technology International Inc. spectrofluorometer system (Birmingham, NJ). The Tb^{3+} emission fluorescence peak at 543 nm upon tyrosine excitation at 280 nm was quantified as previously described [20].

Isothermal titration calorimetry (ITC)

Determination of the kinetics parameters of PDE1 in the absence and presence of wild type CaM and CaM(Y99D/Y138D) were done in a VP-ITC instrument (GE-Healthcare). The reaction cell (1.4619 ml) was filled with degassed protein solutions and equilibrated at 37°C. Stirring speed was 307 rpm and thermal power was registered every 2 seconds with an instrumental reference power of 20 μcal/s. Enzyme reaction rates were determined by measuring the change in the instrumental power supplied to the sample cell after addition of the substrate [21]. At least three independent measurements were carried out in each experimental condition. Serial injections of 4.7 mM cAMP were made every 2 min into the sample cell loaded with (0.01–0.04 U) phosphodiesterase solutions containing or not either wild type CaM or the Y99D/Y138D mutant (3.8 μM). To avoid distortions associated with dilution events, the power change associated with substrate addition at injection i was averaged over the 30 s immediately before the injection i+1. Reaction rates under steady-state conditions were then calculated dividing the power change for each injection, $(dQ/dt)_i$, by the cell volume and the apparent reaction enthalpy (ΔH_{app}) using the software provided by the manufacturer (Origin ITC 7.0). The complete enthalpy of reaction was determined in separate experiments where 15 μl of 4.7 mM cAMP were injected into the cell filled with a solution of (0.1 units) PDE1 and 3.8 μM CaM wild type and the hydrolysis was monitored until position of the initial base was recovered. Integration of the area under the peak gave the total heat of hydrolysis that was corrected by the heat of cAMP dilution, measured independently by injecting the substrate

solution in the sample cell loaded with buffer. Very similar values of ΔH_{app} (-19.9 ± 0.5 kcal/mol) were obtained with subsequent injections, indicative of no product inhibition.

Phosphorylation of calmodulin

Phosphorylation of CaM was carried out at 37°C for 30 min in a total volume of 0.1 ml in a buffer containing 15 mM Hepes-NaOH (pH 7.4), 5 mM $MgCl_2$, 1 mM EGTA, 1 mM dithiothreitol, 1.2 μM histone, 1.2 μM CaM (different species), and 0.02 μg of recombinant c-Src. The reaction was started upon addition of 2 mM ATP and stopped upon addition of Laemmli sample buffer and heating the sample at 100°C for 5 min. Tyrosine-phosphorylated CaM and auto-phosphorylated c-Src were detected by standard Western blot technique using the anti-phospho-tyrosine 4G10 antibody. Membrane segments were stripped at 50°C for 45 min in a buffer containing 2% (w/v) SDS, 60 mM Tris-HCl (pH 6.8) and 0.1% (v/v) β-mercaptoethanol, extensively washed with water, incubated in TBST buffer (0.1% (w/v) Tween-20, 100 mM Tris-HCl (pH 8.8), 500 mM NaCl and 0.25 mM KCl) for 30 min and reprobed with either anti-Src or anti-CaM antibodies as loading controls. Alternatively, the phosphorylation assay was performed in 0.1 ml of medium containing 15 mM Hepes–NaOH (pH 7.4), 5 mM $MgCl_2$, 1 mM EGTA, 1 mM dithiothreitol, 1.2 μM histone, 1.2 μM CaM, 10 μM (2 μCi) [γ-^{32}P]ATP, and 2 units c-Src at 37°C for 30 min, and detection of ^{32}P-labeled phospho-(Y)-CaM was done by autoradiography as previously described [22]. One unit of c-Src activity corresponds to the incorporation of 1 nmol of phosphate into 250 μM cdc2 substrate peptide per min at 30°C using 100 μM ATP according to the manufacture's datasheet. When larger amounts of phospho-(Y)-CaM was required to assay its action on target proteins, CaM (1 mg) was phosphorylated in a 1 ml reaction mixture containing 400 mM NaCl, 50 mM Tris-HCl (pH 7.5), 5 mM $MgCl_2$, 5 mM ATP, 2 mM EGTA, 1 mM dithiothreitol, 1 mg histone, and 8 μg c-Src at 37°C overnight as described [23]. Tyrosine-phosphorylated CaM, free of non-phosphorylated CaM, was obtained by affinity-purification using an immobilized anti-phospho-tyrosine antibody as previously described [24].

Phosphodiesterase assay

The CaM-dependent cyclic nucleotide PDE1 was assayed as previously described [24] at 37°C for 15 min in 250 μl of a medium containing 50 mM imidazole-HCl (pH 7.5), 10 mM Hepes-NaOH (pH 7.4), 0.2 M NaCl, 0.4 mM β-mercaptoethanol, 5 mM $MgCl_2$, 0.4 mM EGTA, 0.5 mM $CaCl_2$ (0.1 mM free Ca^{2+}), 2.5 mM cAMP, 0.01 units of cyclic nucleotide PDE1, 2 units of 5'-nucleotidase, and the concentrations of the different CaM species indicated in the legend to the figures. One unit of cyclic nucleotide PDE1 transforms 1 μmol of cAMP to AMP per min at 30°C and pH 7.5. One unit of 5'-nucleotidase releases 1 μmol of inorganic phosphate from AMP per min at 37°C and pH 9. The inorganic phosphate released from AMP was determined colorimetrically based in the method of Fiske and Subbarow [25].

Nitric oxide synthase assay

Recombinant eNOS was assayed determining the accumulation of nitrite as by-product of NO oxidation using a nitrate reductase/colorimetric assay kit (Oxford Biomedical Research, UK) exogenously supplemented with 25 μM FAD, 25 μM FMN, 12 μM tetrahydrobiopterin and the concentrations of the different CaM species indicated in the legends to the figures following the recommendation of the supplier. One unit of eNOS produces 1 nmol/min of NO from arginine at 37°C and pH 7.4.

Determination of free Ca^{2+} concentrations

The concentrations of free Ca^{2+} in the PDE1 and eNOS assay systems were determined using established algorithms of the Maxchelator program. This program is freely available at http://maxchelator.stamford.edu.

Statistical analysis

The paired Student's t test was performed using the Microsoft Excel (Microsoft Co., Redmon, WA) and GraphPad Prism (GraphPad Software Inc., La Jolla, CA) software programs. Data were expressed as the mean μ SEM and differences were considered significant at $p \leq 0.05$ as indicated in the legends to the figures.

Results

Physicochemical characterization of the phospho-(Y)-mimetic CaM mutants

The expression of wild type and the different CaM mutants in *E. coli* BL21(DE3)pLysS was very efficient and their purification yielded an average ± SEM (n = 12) of 13 ± 2 mg CaM per 500 ml of bacterial culture. Fig 1A shows an example of the expression of the mutants CaM (Y99E), CaM(Y138E) and CaM(Y99E/Y138E) induced by IPTG addition, and the material obtained in the supernatant after heating the extracted proteins at 95°C for 5 min. It can be seen that CaM is the majoritarian heat-resistant protein. After Ca^{2+}-dependent phenyl-Sepharose chromatography all purified CaM species were homogeneous in SDS-PAGE (Fig 1B). The CaM variants presented a single band (≈ 18 kDa) when electrophoretically separated in the presence of EGTA. In the presence of Ca^{2+}, however, wild type CaM and both CaM(Y99D) and CaM(Y99E) mutants presented the typical Ca^{2+}-induced electrophoretic mobility shift [18], yielding a major band at ≈ 15 kDa and a minor one with lower mobility. The electrophoretic mobility shift was less apparent in the single mutants CaM(Y138D) and CaM(Y138E), and in the double mutants CaM(Y99D/Y138D) and CaM(Y99E/Y138E) (Fig 1B).

Fig 2 shows the UV absorption spectra (240–340 nm) of wild type CaM and the single and double Y/D (*panel A*) and Y/E (*panel B*) CaM mutants. Wild type CaM showed the characteristic absorption peaks at 252, 258, 265, 269 and 276 nm [26], the latter due to the presence of tyrosine residues. As expected, the single Y/D and Y/E CaM mutants presented a drastic reduction of the 276 nm peak, while this peak totally disappeared in the double mutants CaM (Y99D/Y138D) and CaM(Y99E/Y138E). The Y99D and Y99E substitutions yielded a slightly higher decrease in the 270–285 nm region of the absorption spectrum than identical substitutions at Y138, unveiling a higher contribution of Y99 to the spectrum. No significant spectral differences between the respective Y/D and Y/E CaM mutants were found.

Circular dichroism (CD) is a very useful tool to study conformational features of proteins in solution [27]. In the absence of Ca^{2+} (presence of EGTA), the far-UV (200–260 nm) CD spectra of wild type and double Y/D and Y/E CaM mutants showed the characteristic negative maxima at 207/208 and 222 nm (Fig 3, *top panels*), typical of proteins with a high proportion of α-helical content. The same was observed for the single mutants (*not shown*). However, the ratio of molar ellipticity at 208 and 222 nm, a sensitive gauge of possible alterations in interactions between neighboring helices [19, 28], was slightly higher for the mutants (*not shown*), pointing to subtle differences in helix packing compared to wild type CaM. For all the samples, there was a significant, mutant-specific, deepening of the far-UV signals in the presence of Ca^{2+} that may reflect a differential increase in α-helical content and/or reorientation of existing α -helices [29, 30]. Also,

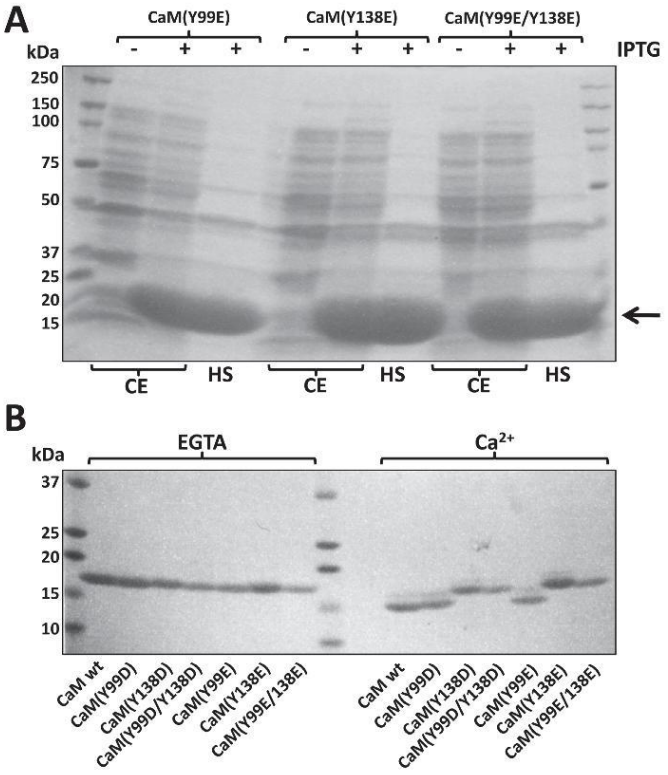

Fig 1. Expression and purification of the different CaM species. (*A*) The figure shows the pattern of proteins of the bacterial cell extract (CE) and the corresponding heated supernatant (HS) from *E. coli* BL21 (DE3)pLysS transformed with plasmids encoding CaM(Y99E), CaM(Y138E) and CaM(Y99E/Y138E) in the absence (-) and presence (+) of 0.5 mM IPTG for 4 h as described in Materials and Methods. The arrow points to the band of CaM induced by IPTG. (*B*) The different recombinant CaM species (≈ 1–2 μg) purified as described in Materials and Methods were separated by SDS-PAGE in the presence of 5 mM EGTA or 1 mM $CaCl_2$ (Ca^{2+}) in the loading buffer, to observe the Ca^{2+}-induced mobility shift.

doi:10.1371/journal.pone.0120798.g001

both CaM(Y99D/Y138D) and CaM(Y99E/Y138) mutants presented a slight blue-shift of the 208 nm minimum in the absence of Ca^{2+} (presence of EGTA) as compared to wild type CaM.

As shown in Fig 3 (*panel A*), the ellipticity at 222 nm increased in the presence of Ca^{2+} 22 ± 3% for wild type CaM, while for the Y138D and Y138E mutants the increase was of 32–35%, and for the Y99D, Y99E, and double Y/E mutants it reached values of 50% and above, the only exception being the CaM(Y99D/Y138D) mutant where no significant change was observed. Interestingly, the magnitude of the increase in ellipticity at 222 nm is directly correlated to the value of the $\Theta_{208}/\Theta_{222}$ ratio. On the other hand, percentage increases in ellipticity at 208 nm and variations among CaM species were noticeably smaller, going from 14% to 29% (Fig 3, *panel B*). As a result, no significant differences in the $\Theta_{208}/\Theta_{222}$ ratio were observed in the presence of calcium, again with the only exception of the CaM(Y99D/Y138D) mutant (*not*

shown), revealing a similar overall structure of the holo forms. Above all, far-UV data clearly show that all the single and double Y/D and Y/E CaM mutants bind Ca^{2+}.

It is known that Ca^{2+} binding induces a remarkable increase in the thermal stability of wild type CaM [29, 31]. In order to examine whether the same is true for the single and double Y/D and Y/E mutants, we carried out thermal denaturation experiments by measuring changes in ellipticity at 222 nm at increasing temperature. Fig 4 shows a quasi-sigmoidal decrease in

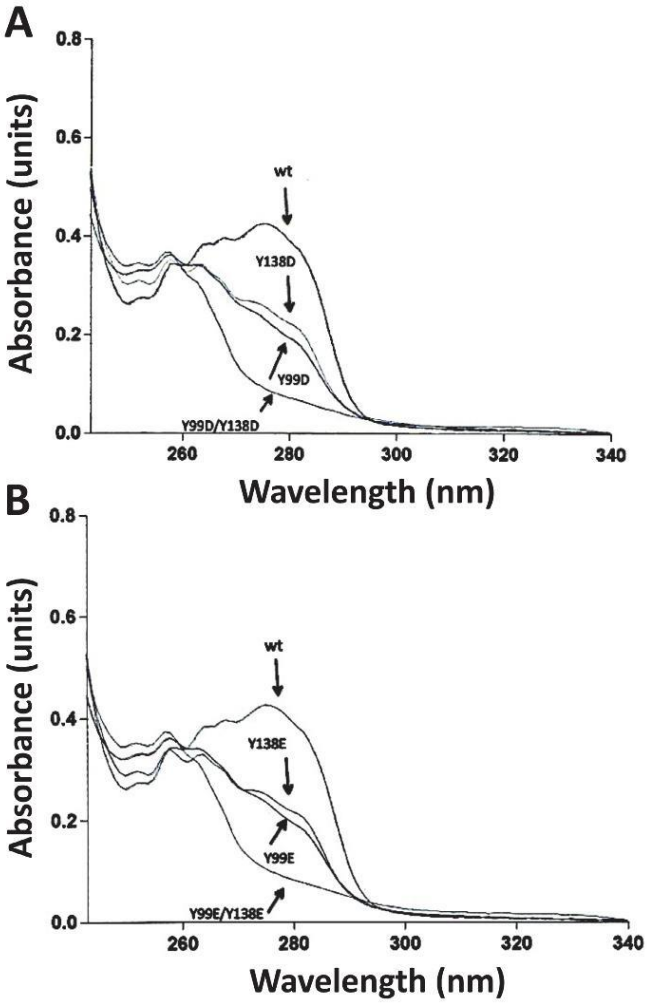

Fig 2. Absorption spectra of the different CaM species. The plots show UV-light absorption spectra of recombinant wild type (*wt*) and the indicated Y/D (*panel A*) and Y/E (*panel B*) CaM mutants (2 mg/ml) purified as described in Materials and Methods and dialyzed against 20 mM Tris-HCl (pH 7.5).

doi:10.1371/journal.pone.0120798.g002

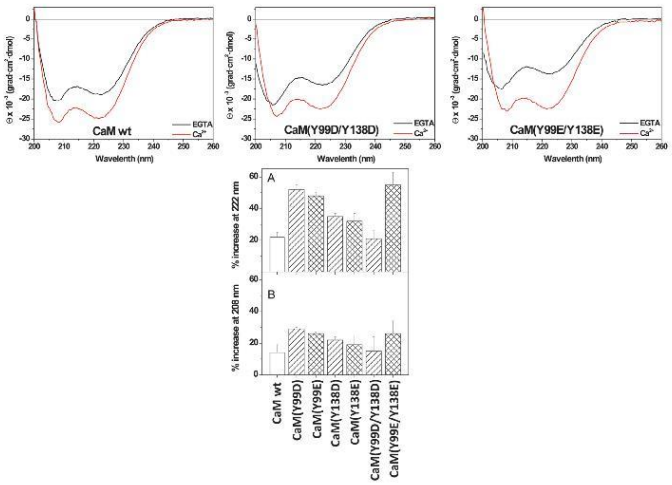

Fig 3. Ca^{2+}-induced changes in the far-UV circular dichroism spectra of the different CaM species. (*Top panels*) Far-UV CD spectra for wild type (*wt*) and the double Y/D and Y/E CaM mutants (118 μM) were recorded *at 20°C in* 20 mM Tris-HCl (pH 7.5), 0.1 M KCl, containing 1 mM EGTA (black lines) or 1 mM $CaCl_2$ (red lines). (*Bottom panels*) The mean ± SEM (n = 3) increase in ellipticity in the far-UV circular dichroism signals at 222 nm (*A*) and 208 nm (*B*) of the indicated CaM species is represented as percentage taking as 100% the ellipticity of each CaM species in the presence of EGTA. Measurements were carried out at 20°C in 20 mM Tris-HCl (pH 7.5), 0.1 M KCl, containing 1 mM EGTA or 1 mM $CaCl_2$, respectively. The concentration of CaM was 12 μM (*A*) and 118 μM (*B*).

doi:10.1371/journal.pone.0120798.g003

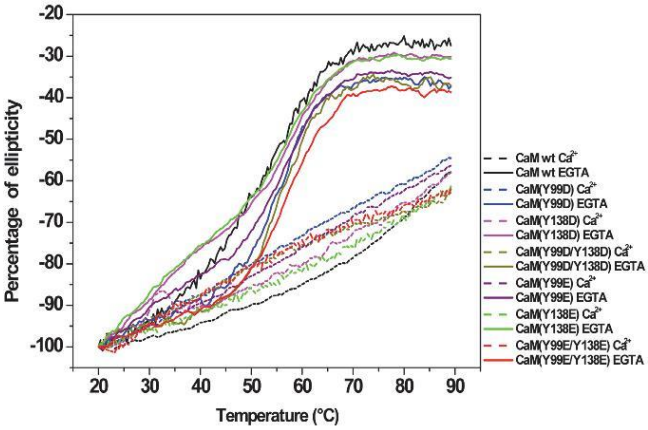

Fig 4. Thermal stability of the different CaM species in the absence and presence of Ca^{2+}. The plots present the decrease in the CD signal at 222 nm, expressed as percentage of the ellipticity at 20°C, for wild type (*wt*) and the single and double Y/D and Y/E CaM mutants (12 μM) in 20 mM Tris-HCl (pH 7.5), 0.1 M KCl, in the presence of 1 mM EGTA (*solid lines*) and 1 mM $CaCl_2$ (*dashed lines*) as described in Materials and Methods.

doi:10.1371/journal.pone.0120798.g004

ellipticity of wild type and all CaM mutants in the absence of Ca^{2+} (presence of EGTA), indicating the occurrence of at least one intermediate state, as previously described for wild type CaM [19, 29]. In the case of the CaM(Y138D) and CaM(Y138E) mutants, the temperature-dependent unfolding was clearly biphasic, showing a notable deviation of sigmoidicity at temperatures below 50°C. Of note, the shape of the CaM(Y138D/E) denaturation curves is remarkably similar to that reported for a CaM Y138Q mutant [19]. Although fitting the data to a two- or three-state model did not yield acceptable clear-cut information, it is clear from the denaturation profiles that a major thermal unfolding for the different CaM species occurred at ≈ 50–55°C, all of them being completely unfolded above 70°C. In addition, lower temperature transitions and/or discontinuities, also reported for wild type CaM [31–34] were observed in the ≈ 20–40°C region, both in the absence and presence of Ca^{2+}. The binding of Ca^{2+}, however, had a profound impact on the stability of wild type CaM and the mutants above 40°C. Thus, the major unfolding transition occurring at ≈ 50–55°C in the presence of EGTA was not observed when Ca^{2+} is present, and more than 54% of the initial ellipticity signal was still preserved at 90°C (Fig 4), confirming that Ca^{2+} binding to the single and double Y/D and Y/E CaM mutants also causes remarkable thermal stabilization.

Ca^{2+}-binding also induces noticeable changes in the near-UV spectrum of wild type CaM [19, 26, 32], which is sensitive to the environment of phenylalanines and the two tyrosine residues in the molecule (please, notice that CaM does not contain tryptophan residues). As shown in Fig 5, in the presence of EGTA the spectrum is characterized by two well-defined negative bands at 262 and 269 nm, attributed to phenylalanine residues, and a broad negative region centered at 280 nm arising from the tyrosine residues. Addition of Ca^{2+} results in an increase of these ellipticity signals, what has been interpreted as a change in the environment of both phenylalanine and tyrosine residues. Having confirmed by far-UV CD and thermal denaturation experiments that all single and double Y/D and Y/E mutants bind Ca^{2+}, we also examined the near-UV CD spectra of their apo and holo forms. In the absence of Ca^{2+} (presence of EGTA), the ellipticity around 280 nm of the mutants diminished noticeably or even became positive (Fig 5B–5D), confirming a predominant contribution of the two tyrosine residues to this region. In addition, there was a significant decrease in the intensity of the bands at 262 and 269 nm compared to wild type CaM, pointing to a partial contribution of both tyrosine residues to these signals. However, addition of Ca^{2+} induced different changes in the spectra depending on the mutant. While the Y99D and Y99E mutants showed a small decrease in positive ellipticity at 280 nm, for the respective Y138 mutants the ellipticity became almost zero (Fig 5). Differences related to the 262/269 nm bands were even more apparent. Here, there was a manifest increase in ellipticity for the Y99 mutants upon Ca^{2+} binding, whereas little or no change was observed for the Y138 and double mutants (Fig 5), clearly revealing that the Ca^{2+}-induced alterations observed for wild type CaM in this region are mostly due to changes in the environment of Y138. This conclusion fully explains the small effect of Ca^{2+} on the near-UV CD spectrum of the separate CaM N-terminal half (residues 1–77) reported by Martin and Bayley [32], a result considered surprising by the authors in view of the similar distribution of phenylalanine residues in the N- and C-terminal halves of the protein. Indeed, the spectra with/without Ca^{2+} of the Y138 and double mutants (Fig 5) are very similar to those published for the N-terminal half [32].

We also studied the fluorescence energy transfer from excited tyrosine residues to Tb^{3+}, a surrogate ion that binds CaM at the Ca^{2+}-binding sites, in wild type CaM and the different CaM mutants by measuring the fluorescence emitted by Tb^{3+} in the 535–550 nm region upon exciting at 280 nm the tyrosine residues (if present) located at sites III and IV of CaM. The spectrum obtained for wild type CaM presented a distinctive emission peak at 543 nm upon addition of increasing concentrations of Tb^{3+} to the medium (Fig 6A). Interestingly, the

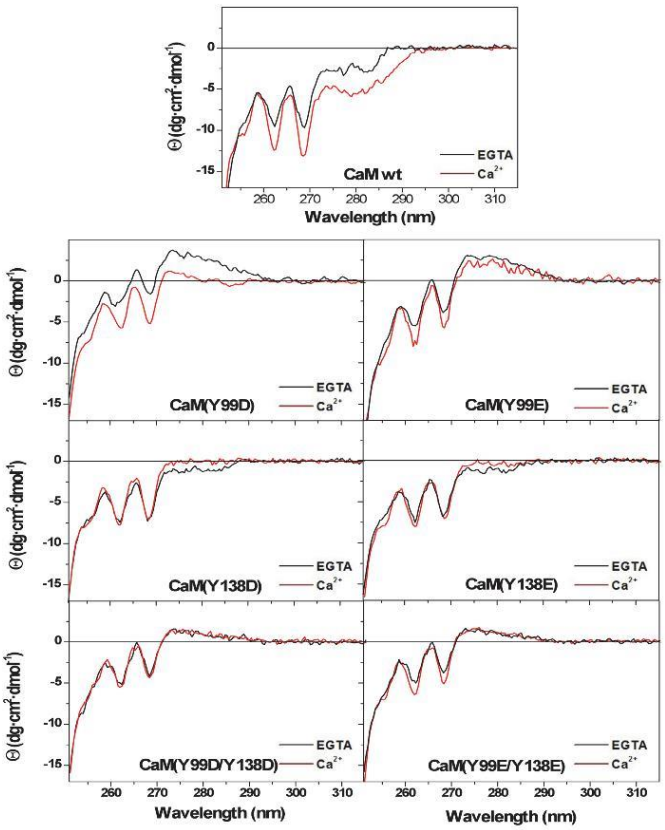

Fig 5. Ca^{2+}-induced changes in the near-UV circular dichroism spectra of the different CaM species. Near-UV CD spectra for wild type (*wt*) and the single and double Y/D and Y/E CaM mutants (118 μM) were recorded at 20°C in 20 mM Tris-HCl (pH 7.5), 0.1 M KCl, containing 1 mM EGTA (black lines) or 1 mM $CaCl_2$ (red lines). Ellipticity values were normalized per mole of residue.

doi:10.1371/journal.pone.0120798.g005

absence of Y99 induced an almost complete loss of the Tb^{3+} emission peak at 543 nm, while the absence of Y138 did not (Fig 6A). A similar behavior was observed for the Y/D and Y/E mutants. The Tb^{3+} titration curves shown in Fig 6B and 6C demonstrated that the apparent binding affinity of the lanthanide ion to wild type CaM was slightly higher ($K'_d \approx 20$ μM) than for the CaM(Y138D) or CaM(Y138E) mutants ($K'_d \approx 50$ and 75 μM, respectively). Only trace fluorescence emission of Tb^{3+} was detected in the CaM(Y99D) or CaM(Y99E) mutants, and no significant fluorescence was detected in the double Y/D or Y/E mutants as expected.

Biological activity of the phospho-(Y)-mimetic CaM mutants

We first tested the capacity of the non-receptor tyrosine kinase c-Src to phosphorylate the different CaM species. Fig 7 shows that both CaM(Y99D) and CaM(Y99E) were phosphorylated

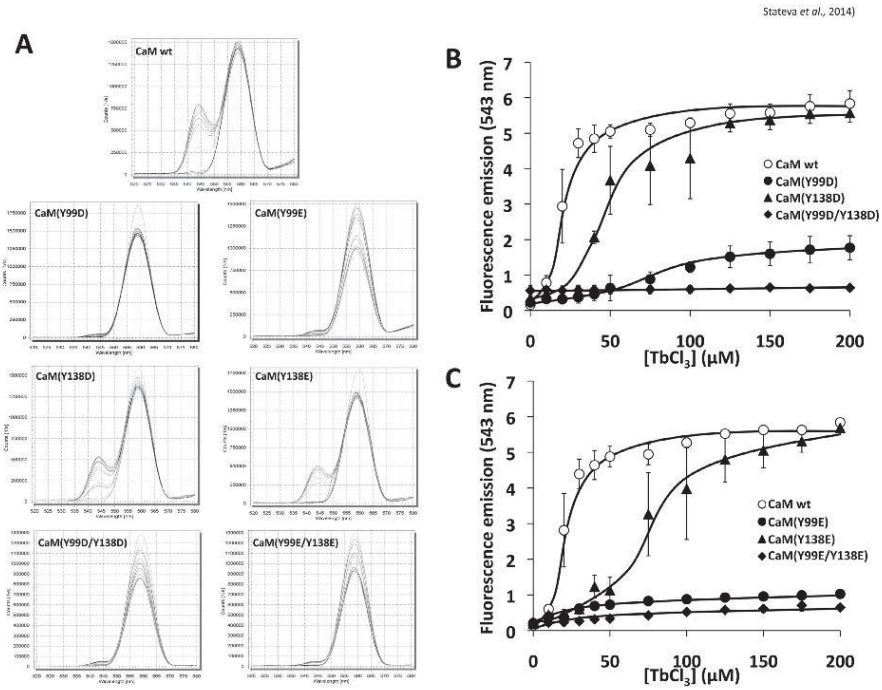

Fig 6. Tb^{3+}-induced fluorescence emission spectra of the different CaM species. (*A*) The fluorescence emission spectra (520–580 nm) of wild type (*wt*) CaM and the indicated CaM mutants (10 μM) was recorded in a buffer containing 10 mM Pipes-HCl (pH 6.5) and 100 mM KCl in the absence and presence of increasing concentrations of $TbCl_3$ (10–200 μM) as described in Materials and Methods. (*B*, *C*) The plots present the emission fluorescence at 543 nm of wild type (*wt*) CaM and the indicated CaM mutants (10 μM) at increasing concentrations of $TbCl_3$ in the conditions described in *A*.

doi:10.1371/journal.pone.0120798.g006

in vitro by recombinant c-Src with similar efficiency than wild type CaM. However, the CaM (Y138D) and CaM(Y138E) mutants were phosphorylated with far lower efficiency than wild type CaM. As expected, no phosphorylation of the double mutants CaM(Y99D/Y138D) and CaM(Y99E/Y138E) was detected.

We next tested two CaM-dependent enzymes, cyclic nucleotide PDE1 and eNOS, to assess whether the different Y/D and Y/E CaM mutants have biological activity, and whether they present any differential effects on the target enzyme as compared to wild type CaM mimicking the action of phospho-(Y)-CaM.

Fig 8A shows that all the Y/D and Y/E CaM mutants were able to activate PDE1 in the presence of Ca^{2+} as it does wild type CaM. However, the CaM-dependent activity attained with CaM(Y99D/Y138D) was consistently lower (≈ 20%) than with the other CaM species, including the CaM(Y99E/Y138E) mutant. PDE1 assays performed at increasing concentrations of CaM(Y99D/Y138D), as compared to wild type CaM, showed no significant differences in the K_{act} (≈ 5–10 nM), but a small decrease (≈ 20%) in the V_{max} of the enzyme was noticeable (Fig 8B). The lower activatory effect of this mutant was of the same magnitude that the one observed when purified bovine brain phospho-(Y)-CaM (phosphorylated by c-Src and free of non-phosphorylated CaM) was assayed on the PDE1 (Fig 8C). When the assays were

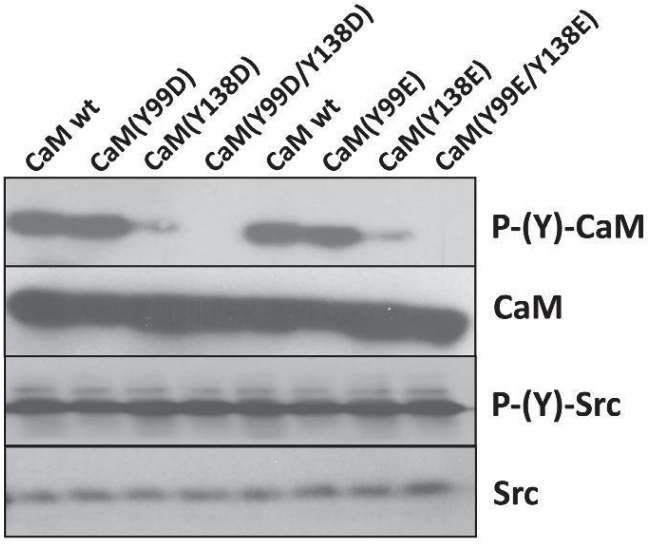

Fig 7. Phosphorylation of different CaM species by c-Src. The different CaM species (2 μg) were assayed for phosphorylation by recombinant c-Src as described in Materials and Methods. The samples were probed with an anti-phospho-tyrosine antibody to detect the tyrosine-phosphorylated CaM species (*P-(Y)-CaM*) and auto-phosphorylated c-Src (*P-(Y)-Src*). The membranes were striped and reprobed with anti-CaM and anti-Src antibodies as loading controls.

doi:10.1371/journal.pone.0120798.g007

performed at increasing concentrations of free Ca^{2+} no significant changes in the apparent affinity for free Ca^{2+} (≈ 5 μM) between wild type and the double Y/D CaM mutant was noticed. And again a decrease (≈ 20–30%) in the CaM-dependent activity of PDE1 at saturating concentrations of free Ca^{2+} was observed with CaM(Y99D/Y138D), as compared to wild type CaM (Fig 8D). Moreover, assays performed at increasing concentrations of free Ca^{2+} in the presence of no-phosphorylated CaM and phospho-(Y)-CaM showed no significant differences in the apparent affinity for free Ca^{2+} (Fig 8E).

We also determined additional kinetics parameters of PDE1 by ITC using increasing concentrations of cAMP in the absence and presence of wild type CaM and CaM(Y99D/Y138D). Fig 9 shows a typical experiment where the presence of wild type CaM greatly enhanced PDE1 activity, while CaM(Y99D/Y138D) had a lesser effect. We determined in a series of similar experiments that the PDE1 activity increased 2.61 ± 0.22 and 1.94 ± 0.09 folds ($n = 3$, $p < 0.05$) upon addition of wild type CaM and CaM(Y99D/Y138D), respectively. Moreover, the V_{max} was determined to be 7.4 ± 2.8 and 5.5 ± 2.3 nmoles/s ($n = 3$, $p < 0.05$) in the presence of wild type CaM and CaM(Y99D/Y138D), respectively, while the K_m of the enzyme for cAMP was the same (221 ± 27 μM) in the presence of both CaM species.

We finally tested the comparative action of wild type CaM, CaM(Y99D/Y138D) and CaM (Y99E/Y138E) on the activation of recombinant eNOS. Fig 10A shows that both CaM mutants strongly activate eNOS in assays performed in the presence of Ca^{2+}, and this activation was slightly more efficient than when wild type CaM was used. When eNOS was assayed at increasing concentrations of the different CaM species (Fig 10B), no significant differences in the K_{act}

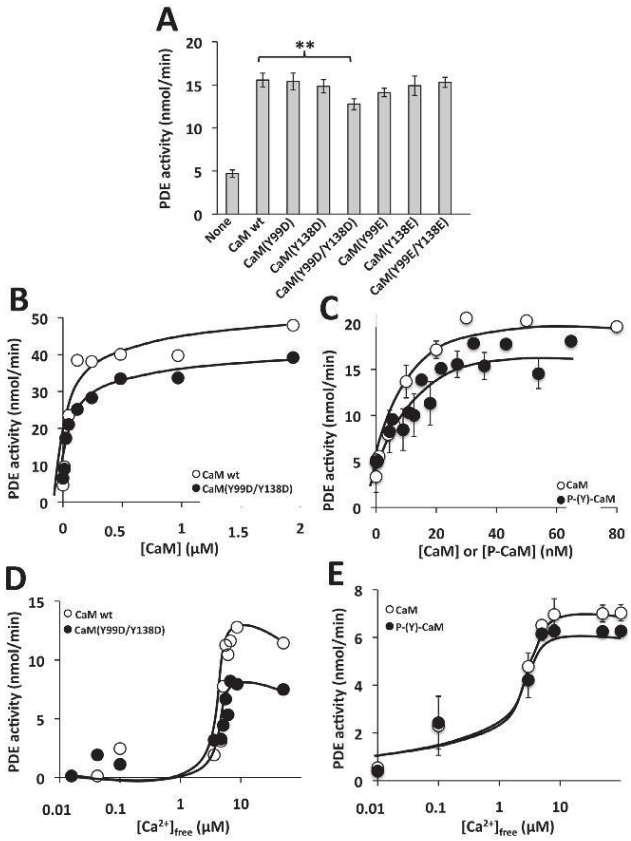

Fig 8. Effect of different CaM species on the activity of PDE1. (*A*) The cyclic nucleotide PDE1 activity was assayed in the absence (*None*) and presence of the indicated CaM species (1.9 μM) in the presence of 100 μM free Ca^{2+} as described in Materials and Methods. The plot presents the average ± SEM of triplicate samples from three separate experiments (** p = 0.02 using the Student's t test). (*B*) The plots present the PDE1 activity assayed as in *A* but using increasing concentrations of the indicated CaM species. (*C*) The plot presents the average ± SEM activity of PDE1 of three independent experiments assayed at increasing concentrations of non-phosphorylated CaM (*open symbols*) or phospho-(Y)-CaM (*filled symbols*) prepared as described in Materials and Methods. (*D*) The plot presents the PDE1 activity assayed as in *A* in the presence of the indicated CaM species (1.9 μM) at increasing concentrations of free Ca^{2+} using an EGTA/Ca^{2+} buffer as described in Materials and Methods. (*E*) The plot presents the average ± range activity of PDE1 assayed in the presence of non-phosphorylated CaM (*open symbols*) and phospho-(Y)-CaM (*filled symbols*) (0.97 μM) of two independent experiments assayed at increasing concentrations of free Ca^{2+} using an EGTA/Ca^{2+} buffer as described in Materials and Methods.

doi:10.1371/journal.pone.0120798.g008

(≈ 0.1 μM) were observed between wild type and the double Y/E CaM mutant. In contrast, a slight increment in the V_{max} (≈ 30%) with respect to wild type CaM was noticeable with CaM (Y99E/Y138E). Similarly, phospho-(Y)-CaM increased the activity of eNOS more efficiently (≈ 30%) than non-phosphorylated CaM (Fig 10C). When the assays were performed at

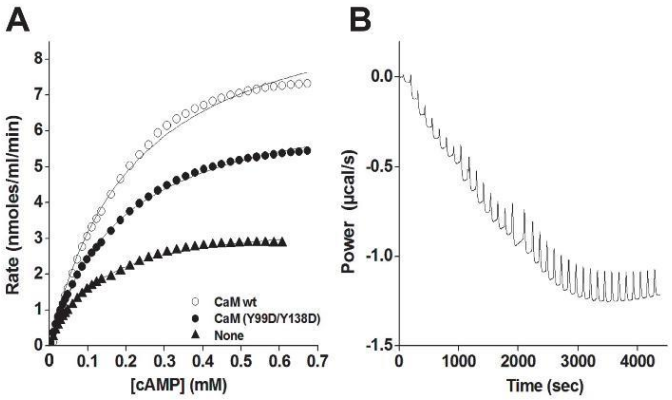

Fig 9. Effect of different CaM species on the kinetics of PDE1 determined by isothermal titration calorimetry. (*A*) The plot presents the PDE1 activity (normalized for 0.04 units of enzyme) at increasing concentrations of cAMP in the absence (*filled triangles*) and presence of wild type CaM (*open circles*) or CaM (Y99D/Y138D) (*filled circles*) (3.8 μM) in a buffer containing 50 mM imidazol-HCl (pH 7.5), 200 mM NaCl, 5 mM $MgCl_2$, 0.4 mM EGTA, and 0.5 mM $CaCl_2$ using ITC as described in Materials and Methods setting the micro-calorimeter chamber 37°C. (*B*) The trace corresponds to a typical experiment showing the rate of heat produced by PDE1 over time after injections of different pulses of cAMP from which the activity of the enzyme can be derived as described in Materials and Methods. This particular trace corresponds to an experiment performed in the absence of CaM using 0.04 units of PDE1. Similar traces were obtained in other conditions tested.

doi:10.1371/journal.pone.0120798.g009

increasing concentrations of free Ca^{2+} no significant changes in the apparent affinity for free Ca^{2+} (≈ 4–6 μM) when compared wild type CaM and the double Y/E CaM mutant (Fig 10D). Moreover, no differences in the apparent affinity for free Ca^{2+} for non-phosphorylated CaM and phospho-(Y)-CaM were detected (Fig 10E).

Discussion

In contrast to the homogeneous electrophoretic migration (≈ 18 kDa) of the single or double Y/D and Y/E CaM mutants in the absence of Ca^{2+} (presence of EGTA), and the near absence of Ca^{2+}-induced electrophoretic mobility shift of the single or double CaM mutants where Y138 was substituted by acidic residues (D or E) observed in this work, the non-phosphorylatable Y/F CaM mutants previously described presented a different behavior [22]. Thus, the CaM (Y138F) and CaM(Y99F/Y138F) mutants presented in the absence of Ca^{2+} (presence of EGTA) higher electrophoretic mobility than wild type CaM and CaM(Y99F), and even higher Ca^{2+}-induced mobility shift [22]. This suggests that the substitution of Y138 either by an acidic or a hydrophobic residue exerts distinct effects on the conformation of CaM. Our results are in agreement with previous findings in which a differential behavior was observed when Y138 or Y99 were substituted by diverse amino acids, suggesting that mutation of Y138 disrupts the structural coupling between the N and C lobular halves of CaM potentially mimicking the collapse that CaM undergoes when binding to target proteins [19, 35]. The central position of Y138 in the Ca^{2+}-induced conformational change of CaM is also evidenced by the modification of the chiroptical properties of this residue, here revealed to be the culprit for the well-known changes in the near-UV CD spectrum of CaM. Of note, the spectrum of Ca^{2+}-bound CaM is

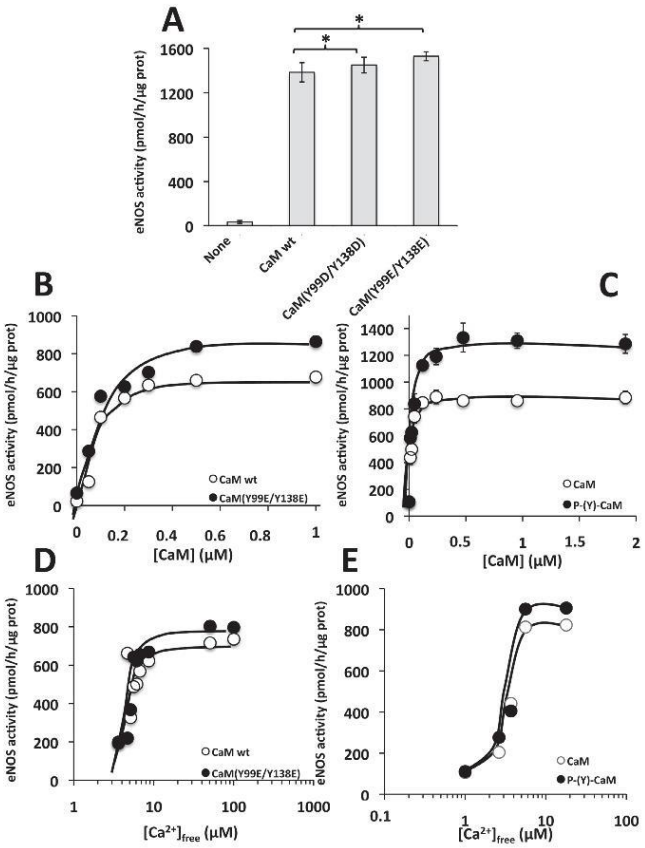

Fig 10. Effect of different CaM species on the activity of eNOS. (*A*) The activity of eNOS was assayed in the absence (*None*) and presence of the indicated CaM species (4.7 µM) in the presence of 1 mM free Ca^{2+} as described in Materials and Methods. The plot presents the average ± SEM of triplicate samples from three separate experiments (* $p \leq 0.05$ using the Student's t test). (*B*) The plot presents the eNOS activity assayed as in *A* but using increasing concentrations of the indicated CaM species. (*C*) The plot presents the average ± range activity of eNOS of two independent experiments assayed at increasing concentrations of non-phosphorylated CaM (*open symbols*) or phospho-(Y)-CaM (*filled symbols*) prepared as described in Materials and Methods. (*D*) The plot presents the eNOS activity assayed as in *A* in the presence of the indicated CaM species (4.7 µM) at increasing concentrations of free Ca^{2+} using an EGTA/Ca^{2+} buffer as described in Materials and Methods. (*E*) The plot presents the activity of eNOS assayed as in *A* in the presence of non-phosphorylated CaM (*open symbol*) and phospho-(Y)-CaM (*filled symbols*) (0.6 µM) assayed at increasing concentrations of free Ca^{2+} using an EGTA/Ca^{2+} buffer as described in Materials and Methods.

doi:10.1371/journal.pone.0120798.g010

very similar to that of *Drosophila melanogaster* calmodulin [36], which only contains this tyrosine residue but not that at position 99, further substantiating this conclusion.

The far-UV CD spectra of the different phosphomimetic CaM mutants as compared to wild type CaM in the absence and presence of Ca^{2+} suggest that the substitution of either one or the

two tyrosine residues does not impair Ca^{2+} binding, as the presence of Ca^{2+} induces a similar conformational change in the molecules. Furthermore, the thermal stability of all the mutants is remarkably increased in the presence of Ca^{2+}, showing that Ca^{2+} binding has a similar stabilizing effect on wild type and the mutant CaM species. This conclusion is also supported by the fact that all the Y/D CaM mutants required Ca^{2+} to stimulate the activities of PDE1 and eNOS, as it was the case for wild type CaM. Therefore, the absence of a significant Ca^{2+}-induced electrophoretic mobility shift in the Y138D and Y138E CaM mutants is not a valid criterion to propose absence of Ca^{2+}-binding capability.

The near loss of fluorescence emission by Tb^{3+} upon tyrosine excitation in the single mutant lacking Y99, but not the single mutant lacking Y138, suggests that Tb^{3+} is closer to tyrosine 99 located at the III Ca^{2+}-binding site of CaM than to tyrosine 138 located at its IV Ca^{2+}-binding site. This is in full agreement with the crystallographic structure of CaM, where the carbonyl group of Y99 participates in the coordination of Ca^{2+}, while Y138 has a rather outward projecting conformation unable to coordinate Ca^{2+} [37].

In agreement with the distinct spatial projection and accessibility to kinases of the two tyrosine-residues of CaM, our c-Src phosphorylation experiments show that Y99 was phosphorylated with lower efficiency than Y138 by this kinase. The inward projection of Y99 within the III Ca^{2+}-binding pocket as compared to a more outward projection of Y138 within the IV Ca^{2+}-binding pocket [37] may explain these results. Although both tyrosine residues in CaM are phosphorylated by both c-Src and EGFR, as demonstrated using Y99F and Y138F CaM mutants [22], the substitution of the tyrosine residue at position 138 by a non-phosphorylatable amino acid somehow disturbs in part the accessibility of these kinases to Y99. This is remarkable as it was previously suggested that the phosphorylation of Y99 by several tyrosine kinases was more efficient than the phosphorylation of Y138 with the same kinases (reviewed in [10]). Thus, the phosphorylation of single-tyrosine CaM mutants may not reflect the comparative efficiency of phosphorylation of both tyrosine residues of CaM in living cells. This may be related to the fact that substituting Y138 by other amino acids disrupts the structural coupling between the N- and C-globular domains of CaM [19], as previously mentioned.

Our results also show that the single and double Y/D and Y/E CaM mutants all retain biological activity, as they were able to activate distinct CaM-binding enzymes including PDE1, eNOS, and the plasma membrane Ca^{2+}-ATPase (*not shown*). Moreover, we have shown a differential action of wild type CaM and some of the phospho-(Y)-mimetic CaM mutants under study on the activity of PDE1 and eNOS.

The double mutant CaM(Y99D/Y138D), but not CaM(Y99E/Y138E), exerts a lower activatory effect on the V_{max} of the CaM-dependent cyclic nucleotide PDE1 isolated from bovine brain, as compared to wild type CaM, but it does not significantly change the apparent affinity for Ca^{2+} or the activation constant (K_{act}) of CaM for the enzyme. Other studies on the effect of phospho-(Y)-CaM versus non-phosphorylated CaM on the cyclic nucleotide PDE1 of different origin yielded divergent results. Thus, both an increase [38] and a decrease [23] in the K_{act}, without affecting the V_{max}, has been reported for phospho-(Y)-CaM (phosphorylated by the insulin receptor) and a phospho-(Y99)-CaM species, respectively, on the PDE1 from bovine brain in comparison to non-phosphorylated CaM. In contrast, phospho-Y-CaM (phosphorylated by the insulin receptor, preferably at Y99) presented similar K_{act} and V_{max} than with non-phosphorylated CaM when assayed on the PDE1 from rat hepatocytes, although the phosphorylated form increased the IC_{50} of CaM antagonists inhibiting the PDE1 activity [39]. In radical contrast, phospho-(Y)-CaM (phosphorylated by the EGFR) inhibited by 90% the activity of the PDE1 from bovine heart [24].

These discrepancies may be due to the fact that at least eleven families of distinct cyclic nucleotide PDEs, including different isoforms of the CaM-dependent PDE1, with distinct

affinities for cAMP and/or cGMP and diverse regulatory properties may coexist and/or being differentially expressed at distinct ratios in various tissues and/or cell types in diverse organisms [40]. Alternatively, distinct phospho-Y99/phospho-Y138 ratios in phospho-(Y)-CaM may account for the observed discrepancies. Nevertheless, it is likely that the negative charges of the extra aspartic acids present in CaM(Y99D/Y138D) may exert a similar action that phospho-(Y99/Y138)-CaM in some PDE1 isoform(s). Furthermore, the absence of effect of the single Y/D mutants suggests that the phosphorylation of both tyrosine residues may be necessary for the lower activatory action of phospho-(Y)-CaM on PDE1. The absence of significant effect of the CaM(Y99E/Y138E) mutant also suggests that the length of the side chain of glutamic acid, longer than the one of aspartic acid (3.39 Å and 2.56 Å, respectively, from the carboxylic to the C-α) [41], may be unfitted to interact with the PDE1 site where phospho-(Y)-CaM exerts its regulatory action on the enzyme.

We show that the mutant CaM(Y99D/Y138D), and most prominently CaM(Y99E/Y138E), slightly increase (≈ 20–30%) the V_{max} of eNOS as compared to wild type CaM. Other studies, however, have shown that the single mutant CaM(Y99E) slightly increase (16%) the activity of recombinant inducible nitric oxide synthase (iNOS), has no significant effect on neuronal nitric oxide synthase (nNOS), and significantly inhibited (40%) the activity of eNOS [42]. This suggests that the different NOS isoforms may be regulated differently and that the phosphorylation of either one or the two tyrosine residues of CaM may exert significant differential effects on its activity. Nevertheless, our results are qualitatively, but not quantitatively, in agreement with the stimulatory action that phospho-(Y99)-CaM exerts on the V_{max} of nNOS, where a 3.4-fold higher V_{max} than with non-phosphorylated CaM was reported [23]. These authors also reported a two-fold higher K_{act} of phospho-(Y99)-CaM with respect to non-phosphorylated CaM, and a 4-fold lower K_d for a peptide corresponding to the CaM-binding domain of nNOS [23]. The different NOS isoforms used in these studies could explain the lower phospho-mimetic capacity of CaM(Y99D/Y138D) and CaM(Y99E/Y138E) when compared to tyrosine-phosphorylated CaM.

It is intriguing that CaM(Y99D/Y138D), but not CaM(Y99E/Y138E), exerts a differential action on PDE1, as compared to wild type CaM; while in the case of eNOS this differential action was exerted by both CaM(Y99D/Y138D) and CaM(Y99E/Y138E), albeit the latter with better efficiency. This could be related to the different length of the side chain of glutamic and aspartic acids as mentioned above. Thus, although the actual reason for these distinct effects is unknown, we could speculate that each enzyme may have pockets or clefts of distinct depths were the negative charge of the carboxyl group of the acidic amino acid must adapt in a proper conformation in order to exert its differential action, and that this pocket/cleft may be deeper in PDE1 than in eNOS.

Although the phospho-(Y)-mimetic CaM mutants described in this work exert small differential effects with respect to wild type CaM on the two CaM-binding enzymes tested, the observed effects are qualitative consistent with those exerted by phospho-(Y)-CaM. Therefore, these mutants might be useful tools to study the differential regulation exerted by phospho-(Y)-CaM in a wide variety of CaM-binding proteins with and without enzymatic activity in living cells. This could be achieved by the stable expression of these phospho-(Y)-mimetic CaM mutants in a conditional CaM knockout DT40 cell line recently described, after the down-regulation of endogenous CaM by tetracycline, where the action of distinct Ca^{2+}-null and other CaM mutants on the viability and proliferation capacity of these cells was tested [43].

Author Contributions

Conceived and designed the experiments: AV DS GB. Performed the experiments: SRS VS MM. Analyzed the data: AV DS SRS MM. Contributed reagents/materials/analysis tools: AV DS. Wrote the paper: AV DS SRS.

References

1. Chin D, Means AR. Calmodulin: a prototypical calcium sensor. Trends Cell Biol. 2000; 10: 322–328. PMID: 10884684
2. Berchtold MW, Villalobo A. The many faces of calmodulin in cell proliferation, programmed cell death, autophagy, and cancer. Biochim Biophys Acta. 2014; 1843: 398–435. doi: 10.1016/j.bbamcr.2013.10.021 PMID: 24188867
3. Crotti L, Johnson CN, Graf E, De Ferrari GM, Cuneo BF, Ovadia M, et al. Calmodulin mutations associated with recurrent cardiac arrest in infants. Circulation. 2013; 127: 1009–1017. doi: 10.1161/CIRCULATIONAHA.112.001216 PMID: 23388215
4. Yin G, Hassan F, Haroun AR, Murphy LL, Crotti L, Schwartz PJ, et al. Arrhythmogenic calmodulin mutations disrupt intracellular cardiomyocyte Ca^{2+} regulation by distinct mechanisms J Am Heart Assoc. 2014; 3: e000996. doi: 10.1161/JAHA.114.000996 PMID: 24958779
5. Ten Broeke R, Blalock JE, Nijkamp FP, Folkerts G. Calcium sensors as new therapeutic targets for asthma and chronic obstructive pulmonary disease. Clin Exp Allergy. 2004; 34: 170–176. PMID: 14987293
6. Hoeflich KP, Ikura M. Calmodulin in action: diversity in target recognition and activation mechanisms. Cell. 2002; 108: 739–742. PMID: 11955428
7. Vetter SW, Leclerc E. Novel aspects of calmodulin target recognition and activation. Eur J Biochem. 2003; 270: 404–414. PMID: 12542690
8. Jurado LA, Chockalingam PS, Jarrett HW. Apocalmodulin. Physiol Rev. 1999; 79: 661–682. PMID: 10390515
9. Bähler M, Rhoads A. Calmodulin signaling via the IQ motif. FEBS Lett. 2002; 513: 107–113. PMID: 11911888
10. Benaim G, Villalobo A. Phosphorylation of calmodulin. Functional implications. Eur J Biochem. 2002; 269: 3619–3631. PMID: 12153558
11. Fukami Y, Nakamura T, Nakayama A, Kanehisa T. Phosphorylation of tyrosine residues of calmodulin in Rous sarcoma virus-transformed cells. Proc Natl Acad Sci U S A. 1986; 83: 4190–4193. PMID: 2424020
12. Graves CB, Gale RD, Laurino JP, McDonald JM. The insulin receptor and calmodulin. Calmodulin enhances insulin-mediated receptor kinase activity and insulin stimulates phosphorylation of calmodulin. J Biol Chem. 1986; 261: 10429–10438. PMID: 3525545
13. Benguría A, Hernández-Perera O, Martínez-Pastor MT, Sacks DB, Villalobo A. Phosphorylation of calmodulin by the epidermal-growth-factor-receptor tyrosine kinase. Eur J Biochem. 1994; 224: 909–916. PMID: 7925415
14. Hayashi N, Matsubara M, Takasaki A, Titani K, Taniguchi H. An expression system of rat calmodulin using T7 phage promoter in Escherichia coli. Protein Expr Purif. 1998; 12: 25–28. PMID: 9473453
15. Birnboim HC, Doly J. A rapid alkaline extraction procedure for screening recombinant plasmid DNA. Nucleic Acids Res. 1979; 7: 1513–1523. PMID: 388356
16. Stoscheck CM. Quantitation of protein. Methods Enzymol. 1990; 182: 50–68. PMID: 2314256
17. Laemmli UK. Cleavage of structural proteins during the assembly of the head of bacteriophage T4. Nature. 1970; 227: 680–685. PMID: 5432063
18. Burgess WH, Jemiolo DK, Kretsinger RH. Interaction of calcium and calmodulin in the presence of sodium dodecyl sulfate. Biochim Biophys Acta. 1980; 623: 257–270. PMID: 7397213
19. Sun H, Yin D, Coffeen LA, Shea MA, Squier TC. Mutation of Tyr138 disrupts the structural coupling between the opposing domains in vertebrate calmodulin. Biochemistry. 2001; 40: 9605–9617. PMID: 11583160
20. Wallace RW, Tallant EA, Dockter ME, Cheung WY. Calcium binding domains of calmodulin. Sequence of fill as determined with terbium luminescence. J Biol Chem. 1982; 257: 1845–1854. PMID: 6276400
21. Todd MJ, Gomez J. Enzyme kinetics determined using calorimetry: a general assay for enzyme activity? Anal Biochem. 2001; 296: 179–187. PMID: 11554713

22. Salas V, Sánchez-Torres J, Cusidó-Hita DM, García-Marchan Y, Sojo F, Benaim G, et al. Characterisation of tyrosine-phosphorylation-defective calmodulin mutants. Protein Expr Purif. 2005; 41: 384–392. PMID: 15866726

23. Corti C, Leclerc L'Hostis E, Quadroni M, Schmid H, Durussel I, et al. Tyrosine phosphorylation modulates the interaction of calmodulin with its target proteins. Eur J Biochem. 1999; 262: 790–802. PMID: 10411641

24. Palomo-Jiménez PI, Hernández-Hernando S, García-Nieto RM, Villalobo A. A method for the purification of phospho(Tyr)calmodulin free of nonphosphorylated calmodulin. Protein Expr Purif. 1999; 16: 388–395. PMID: 10425159

25. Fiske CH, Subbarow Y. The colorimetric determination of phosphorus. J Biol Chem. 1925; 66: 375–400.

26. Wolff DJ, Poirier PG, Brostrom CO, Brostrom MA. Divalent cation binding properties of bovine brain Ca^{2+}-dependent regulator protein. J Biol Chem. 1977; 252: 4108–4117. PMID: 193856

27. Kelly SM, Jess TJ, Price NC. How to study proteins by circular dichroism. Biochim Biophys Acta. 2005; 1751: 19–139. PMID: 15894523

28. Fasman GD. Differentiation between transmembrane helices and peripheral helices by the deconvolution of circular dichroism spectra of membrane proteins. In: Fasman G. D., editor. Circular dichroism and the conformational analysis of biomolecules. Plenum Press, New York; 1996. pp. 381–412.

29. Wang Q, Liang KC, Czader A, Waxham MN, Cheung MS. The effect of macromolecular crowding, ionic strength and calcium binding on calmodulin dynamics. PLoS Comput Biol. 2011; 7: e1002114. doi: 10.1371/journal.pcbi.1002114 PMID: 21829336

30. Protasevich I, Ranjbar B, Lobachov V, Makarov A, Gilli R, Briand C, et al. Conformation and thermal denaturation of apocalmodulin: role of electrostatic mutations. Biochemistry. 1997; 36: 2017–2024. PMID: 9047299

31. Brzeska H, Venyaminov S, Grabarek Z, Drabikowski W. Comparative studies on thermostability of calmodulin, skeletal muscle troponin C and their tryptic fragments. FEBS Lett. 1983; 153: 169–173. PMID: 6825857

32. Martin SR, Bayley PM. The effects of Ca^{2+} and Cd^{2+} on the secondary and tertiary structure of bovine testis calmodulin. A circular-dichroism study. Biochem J. 1986; 238: 485–490. PMID: 3800949

33. Kilhoffer MC, Demaille JG, Gerard D. Tyrosine fluorescence of ram testis and octopus calmodulins. Effects of calcium, magnesium, and ionic strength. Biochemistry. 1981; 20: 4407–4414. PMID: 7284330

34. Gangola P, Pant HC. Temperature dependent conformational changes in calmodulin. Biochem Biophys Res Commun. 1983; 111: 301–305. PMID: 6830594

35. Sun H, Yin D, Squier TC. Calcium-dependent structural coupling between opposing globular domains of calmodulin involves the central helix, Biochemistry. 1999; 38: 12266–12279. PMID: 10493794

36. Maune JF, Beckingham K, Martin SR, Bayley PM. Circular dichroism studies on calcium binding to two series of Ca^{2+} binding site mutants of Drosophila melanogaster calmodulin. Biochemistry. 1992; 31: 7779–7786. PMID: 1510964

37. Strynadka NC, James MN. Crystal structures of the helix-loop-helix calcium-binding proteins. Annu Rev Biochem. 1989; 58: 951–998. PMID: 2673026

38. Williams JP, Jo H, Sacks DB, Crimmins DL, Thoma RS, Hunnicutt RE, et al. Tyrosine-phosphorylated calmodulin has reduced biological activity. Arch Biochem Biophys. 1994; 315: 119–126. PMID: 7526800

39. Saville MK, Houslay MD. Phosphorylation of calmodulin on Tyr99 selectively attenuates the action of calmodulin antagonists on type-I cyclic nucleotide phosphodiesterase activity. Biochem J. 1994; 299: 863–868. PMID: 8192677

40. Francis SH, Blount MA, Corbin JD. Mammalian cyclic nucleotide phosphodiesterases: molecular mechanisms and physiological functions. Physiol Rev. 2011; 91: 651–690. doi: 10.1152/physrev.00030.2010 PMID: 21527734

41. Allen FH. The Cambridge Structural Database: a quarter of a million crystal structures and rising. Acta Crystallogr B. 2002; 58: 380–388. PMID: 12037359

42. Piazza M, Futrega K, Spratt DE, Dieckmann T, Guillemette JG. Structure and dynamics of calmodulin (CaM) bound to nitric oxide synthase peptides: effects of a phosphomimetic CaM mutation. Biochemistry. 2012; 51: 3651–3661. doi: 10.1021/bi300327z PMID: 22486744

43. Panina S, Stephan A, la Cour JM, Jacobsen K, Kallerup LK, Bumbuleviciute R, et al. Significance of calcium binding, tyrosine phosphorylation, and lysine trimethylation for the essential function of calmodulin in vertebrate cells analyzed in a novel gene replacement system. J Biol Chem. 2012; 287: 18173–18181. doi: 10.1074/jbc.M112.339382 PMID: 22493455

Erratum

1. **On Page 51, 5. Material and Methods section, 5.1 Antibodies: the following antibody should be included: Anti-EGFR Mouse Anti-EGF Receptor antibody obtained from BD Biosciences (New Jersey, U.S.) used for determining the total EGFR in the experiment presented in Figure 35, Panel B.**

2. **On page 87, Result section, Legend of Figure 30: the concentration of the EGF used to activate the EGFR was 1 µM instead of 10 nM.**

3. **Page 108, Discussion section. "And the EGFR phosphorylates Src (Parks and Ceresa, 2014)" should be substituted by "And EGFR activates Src (Parks and Ceresa, 2014)"**